Coden: JPLPAY
Volume 9, Part A-2, No. 11, November 1971

Journal of Polymer Science

Part A-2: Polymer Physics

Contents

Published by INTERSCIENCE PUBLISHERS a division of John Wiley & Sons, Inc.

Journal of Polymer Science **Part A-2: Polymer Physics**

The Journal of Polymer Science is published in four sections as follows: Part A-1, Polymer Chemistry, monthly; Part A-2, Polymer Physics, monthly; Part B, Polymer Letters, monthly; Part C, Polymer Symposia, irregular.

Published monthly by Interscience Publishers, a Division of John Wiley & Sons, Inc., covering one volume annually. Publication, Executive, Editorial, and Circulation Offices at 605 Third Avenue, New York, N.Y. 10016. Second-class postage paid at New York, New York, and additional mailing offices. Subscription price, $325.00 per volume (including Parts A-1, B, and C). Foreign postage $15.00 per volume (including Parts A-1, B, and C).

JOURNAL OF POLYMER SCIENCE: PART A-2 VOL. 9, 1919–1933 (1971)

Self-Oscillation Mechanism of Necking on Extension of Polymers*

G. P. ANDRIANOVA, A. S. KECHEKYAN, and V. A. KARGIN,†
A. V. Topchiev Institute of Petrochemical Synthesis, Academy of Sciences of the USSR, Moscow, USSR

Synopsis

A new phenomenon in necking of some polymers, including poly(ethylene terephthalate) (PETP) was detected. It was found that extension of PETP films under certain conditions results in periodic stress oscillations and a periodic change in appearance of the sample. The conditions at which self-oscillations appear have been determined, and the principal regularities of this regime of deformation are described. The following factors are critical for the appearance of self-oscillation: speed of straining and compliance of the sample. The self-oscillation of stress and formation of the periodic transverse bands is attributed to heat dissipation during necking corresponding to local temperature jumps and periodic strong variation of elasticity modulus due to poor heat conductivity of the polymer. Changing the external conditions of heat transfer influences the possibility and development of the effect. The phenomenon is common for various crystallizing polymers, being dependent on physical properties of the polymer and conditions of deformation.

Extension of poly(ethylene terephthalate) (PETP) under certain conditions gives rise to periodic stress oscillation and a periodic change in appearance of the sample.

The nature of this phenomenon is closely associated not only with the mechanics of deformation, but also with such structural changes as crystallization and necking. The stress oscillation and attendant changes in appearance of the sample on extension occur in PETP within a convenient time scale and extension rate. However, as will be shown below, the physical phenomena are of a general nature and are caused by properties inherent in any polymeric material. Indeed, analogous effects were observed by us on extension of other polymers, polyethylene and polypropylene, for example.

It should be noted that the appearance of longitudinal periodicity of various types on extension of polymers has been described.[1–4]

* Presented in part as a short communication at the International Symposium on Macromolecules, Leiden, 1970.

† Deceased.

Experimental

Experiments were conducted on samples of amorphous PETP. Samples of commercial films, 250–300 μ thick were selected. From these films were cut out either rectangular strips of various lengths (ranging from 20 to 400 mm) and 10 mm wide or standard spatulas 5 mm wide with a working base of 10 mm.

The samples were extended in a testing machine, one clamp being connected to a tensometric force transducer and the other was fixed rigidly to a drive frame which moved at an assigned constant speed. With this unit tests could be made at a series of extension rates varying, in steps of 1:10, from 0.00435 to 435 mm/min. Some of the tests were carried out on an FM-1000 testing machine where speed can be varied continuously from 10 to 90 mm/min. The change of stress with time was recorded as a function of extension by means of an electronic recording potentiometer or a bifilar oscillograph. During tests the temperature of the samples could be controlled in air, vacuum, or a liquid bath over the temperature interval 10 to 100°C.

For the purposes of this work it was important to measure the true rate of neck formation, which generally does not coincide with the average speed of clamp movement. This true rate is determined by the relative speed of

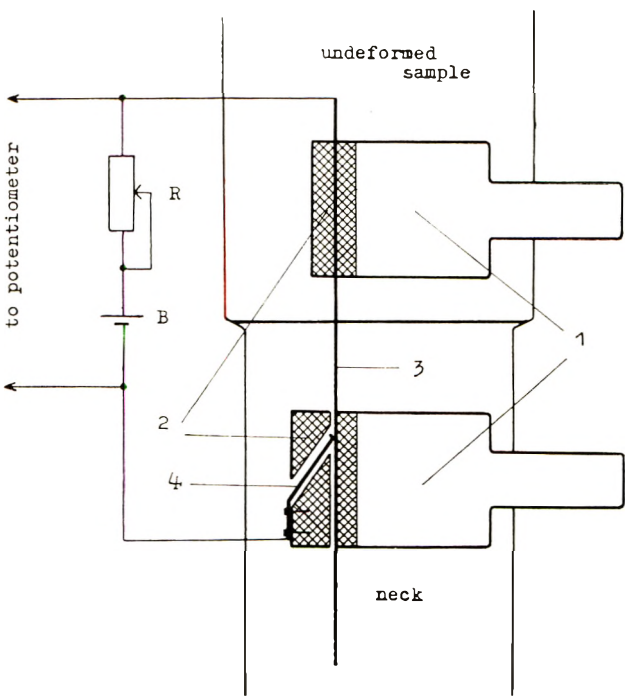

Fig. 1. Scheme used for measuring of the true rate of neck formation: (1) spring clamps; (2) insulator (3) rheostat, nichrome wire, diameter 0.07 mm (4) brush; (R) resistance; (B) battery.

separation of two points in the immediate vicinity of the line along which the neck is forming. To measure this speed, a simple circuit was set up (Fig. 1), consisting of two clamps, one with a nichrome wire, and the other with a brush fixed in it. The clamps were fastened on the two sides of the neck boundary. The wire served as a simple rheostat to which a constant voltage was fed. The voltage across the fixed clamp and brush was measured. This voltage is related linearly to the movement of the neck front and makes it possible to follow the rate of its formation. The measured voltage was fed to a multichannel oscillograph, the signal from the tensometric transducer measuring the stress being fed simultaneously to another channel. This circuit enables comparison of the voltage change in time with the rate of neck formation.

Results

Under definite conditions of deformation, the range of which will be established below, periodic oscillations appear. Their nature can be judged from Figure 2, which presents a typical record of the variation of stress with time, and Figure 3, which illustrates the external appearance of the deformed sample. (Fig. 3*a* shows the appearance of a film with many periods, and Fig. 3*b* the typical change in appearance of the sample during several periods in enlarged scale.) An examination of the appearance of the sample reveals that the repeat period consists of three distinct sections with definite boundaries: (I) a region where the film remains transparent; (II) a region of marked whitening (clouding)of the neck, where the film is completely opaque, and (III) a region in which the film has become cloudy, but not yet opaque. These regions cover the entire neck in this sequence. The boundaries between regions I and II and between III and I are very distinct, but that between II and III is somewhat arbitrary.

This type of deformation is observed most simply for samples which already have a neck, or at least a weak point favoring neck formation. On extension of a "fresh" (undeformed) sample, the stress has to pass through a

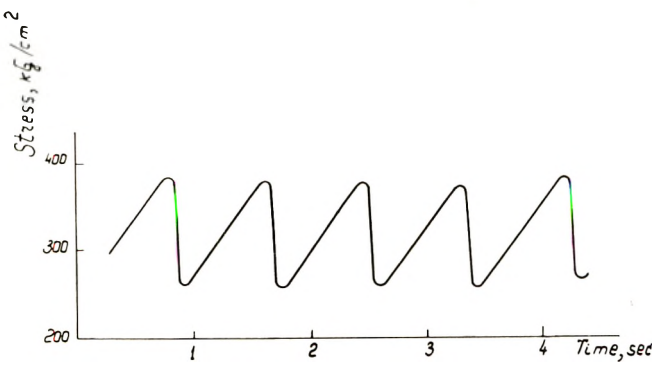

Fig. 2. Stress vs. time under conditions of steady self-oscillations during extension of PETP (oscillographic recording). Rate of extension, 43.5 mm/min.

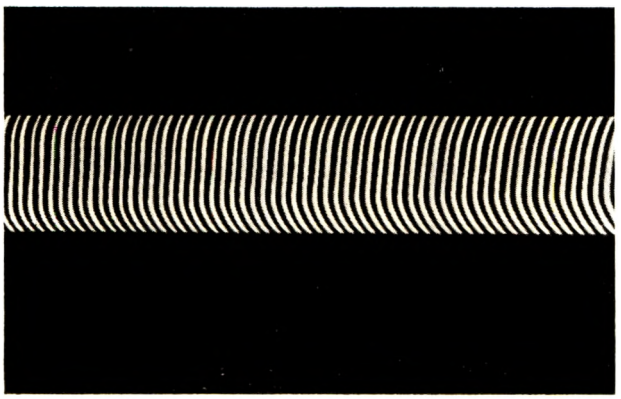

(*a*)

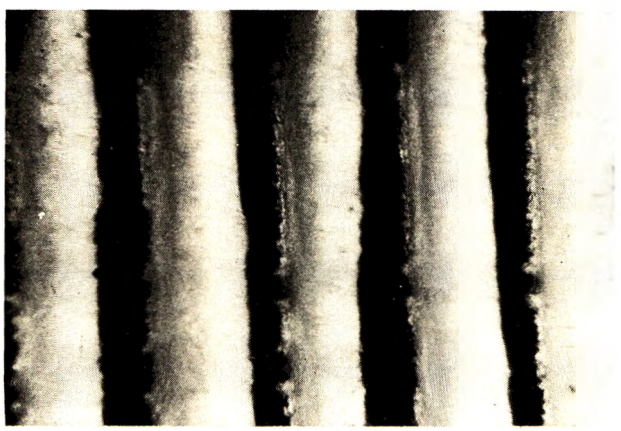

(*b*)

Fig. 3. Photomicrographs of a PETP specimen strained under self-oscillation conditions; (*a*) general view of specimen; (*b*) several bands greatly enlarged.

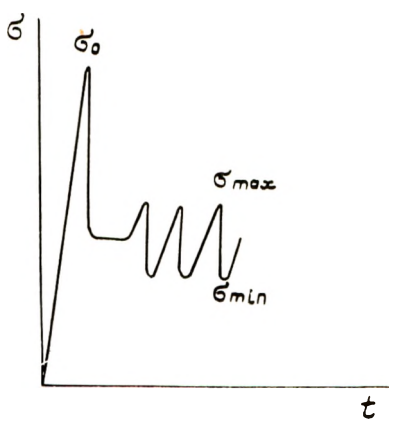

Fig. 4. Diagram of stress development in time at an imposed constant rate of deformation.

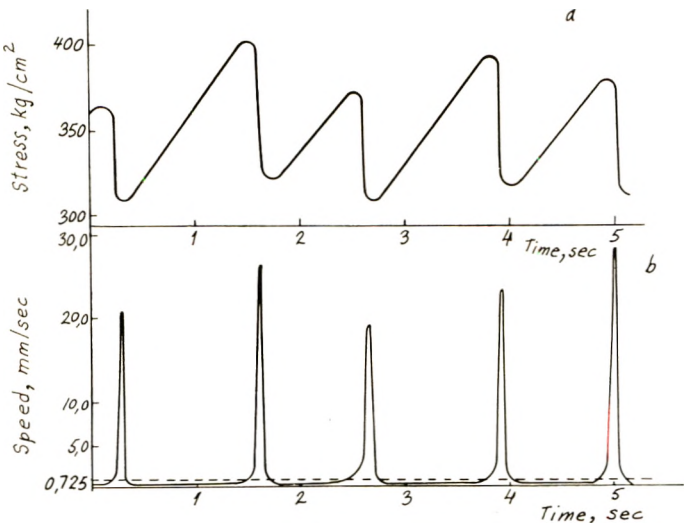

Fig. 5. Variation of (*a*) stress with time and (*b*) accompanying change in true rate of deformation in the region of passage of polymer into the neck. The broken line shows the imposed "average" rate of deformation calculated from relative speed of clamp movement.

maximum (σ_0 in Fig. 4) before the regime corresponding to necking (change in stress between the limits σ_{max} and σ_{min} on the diagram on Fig. 4) can be reached. In the range of the amorphous PETP under study, at room temperature, σ_0 exceeds the stress range σ_{max} to σ_{min} very greatly. For this reason, the sample fails, as a rule, before the steady-extension regime can be attained, except for very low (<0.435 mm/min) speeds.

But if there is a defective region in the polymer—and it is quite sufficient to bend ("crumple") the sample at one point a few times for one to appear—the stress σ_0 decreases sharply, approaching σ_{max}. If there already is a neck in the sample, then σ_0 is approximately equal to σ_{max} and stable oscillations occur with the corresponding periodic changes in appearance of the sample.

We shall now establish relations between changes in stress σ, the rate of movement of the neck front, and the change in appearance of the sample. Figure 5 shows, on an enlarged scale, (*a*) several periods of stress variations and (*b*) the corresponding changes in rate of necking. It is evident from this figure that two regions of stress change correspond to the three structural regions shown in Figure 4: one region where the stress increases slowly (on the order of 50 kgf/cm²-sec at an extension rate of 43.5 mm/min) and another region where there is a very sharp drop of the stress (at least one order of magnitude greater than the rate of increase). The region of increasing stresses corresponds to very slow necking (Fig. 5*b*). Thus, in the example under consideration, at an average extension rate of 43.5 mm/min, the rate of necking is not more than 12 mm/min, i.e., roughly speaking, practically no neck is formed in this case. Necking occurs almost entirely in the region of declining stresses, so that all three regions described above

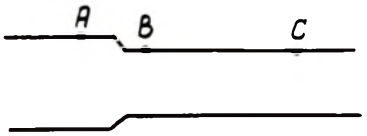

Fig. 6. Diagram showing points marked on the specimen for measuring rate of necking.

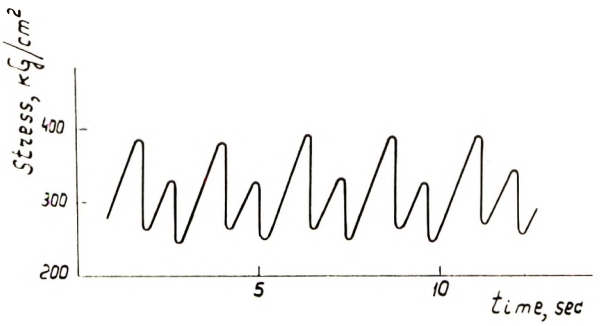

Fig. 7. Double periodicity in self-oscillations during necking.

form successively in a time of less than 0.1 sec. The rate of extension thereupon increases very sharply (Fig. 5*b*), exceeding the average extension rate by an order of magnitude. Hence, in the example under consideration, ca. 0.1 mm of neck length forms per cycle during growth of the stress, and up to 1 mm on the declining branch. Thus, the entire cycle shown in Figure 3 occurs almost entirely in the region of declining stresses.

The relations among the nature of stress change , rate of necking, and extension–contraction of the neck already formed is clear from the diagram in Figure 6. The velocity V_C of point C can be considered as the sum of the velocity $V_{C/B}$ of point C relative to B plus the velocity $V_{B/A}$ of point B relative to A plus the velocity $V_{A/0}$ of point A relative to the fixed clamp, i.e.:

$$V_C = V_{C/B} + V_{B/A} + V_{A/0}$$

Obviously, $V_{A/0} \approx 0$, the since initial part of the sample is much more rigid than the long neck already formed and deforms a negligible amount and hence $V_{B/A} = V_B$.

The value V_C = constant is equal to the imposed velocity of the movable clamp. The value of $V_{C/B}$ determines the rate of deformation $\dot{\epsilon}$ of the neck already formed of length l since $\dot{\epsilon} = V_{C/B}/l$. Therefore we may write:

$$V_C = V_{B/A} + \dot{\epsilon} l = \text{constant}$$

The example shown in Figure 5*b* illustrates the relation between V_C and $V_{B/A}$. In the region of increasing stresses $V_{B/A} \approx 0$, and hence the rate of extension of the neck is $\dot{\epsilon} = V_C/l$. In the region of decreasing stresses we have $V_{B/A} \gg V_C$; therefore, the neck contracts at the rate $\dot{\epsilon} = -V_{B/A}/l$ and a new part of the neck forms from the initial material.

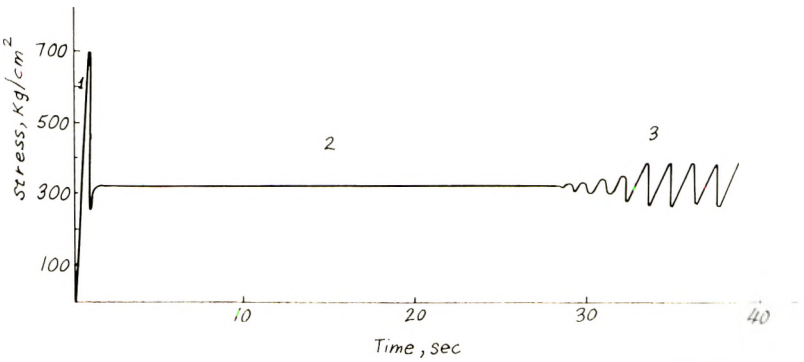

Fig. 8. Actual nature of stress development and growth of self-oscillations during extension of PETP at a constant rate.

In the simplest behavior, the oscillations described above may be regarded as strictly periodic, of constant amplitude and period and with a stress–time curve of constant shape. But with increasing compliance* of the sample the change in stress becomes more complex and a "double" periodicity appears, where the stress pattern is repeated every other period in such a way that a very pronounced stress maximum is followed by a somewhat smaller one.

This is illustrated, for example, in Figure 7, while the oscillogram in Figure 1 exhibits strictly periodic stress oscillations. But these effects most probably are due to secondary causes; the key problem is, strictly speaking, the self-oscillation of the deformation process, which is the point of main interest in this study.

First of all, let us determine the conditions under which the periodic oscillations arise. Obviously, if the sample fails because of brittleness before the neck is formed, no periodic oscillations will ever arise. The initial length of the samples and the length of the preformed neck are of great importance. As a matter of fact, self-oscillations arise only when the length of the neck already formed exceeds a certain critical value characteristic of given rate of extension and the initial length of the sample. The lower the extension rate, the higher should be the compliance of the sample (e.g., the length of the preformed neck or the initial length of sample) for oscillations to arise.

Usually the process develops in the following manner: necking begins suddenly at a certain strain, after which steady neck formation continues at constant stress. At this stage the process of necking is stable, since, as experiment has shown, weak external influences (a stream of cold air, weak mechanical influences, etc.) do not cause undamped oscillation. But after critical conditions are reached (these being the critical length of preformed

* Here and in the following, by compliance we mean the change in length of the sample divided by the stress causing the change; the dimensions of this quantity are cm^3/kgf. If the neck length is large compared to the rest of the sample, the length of the neck already formed may be taken as the measure of compliance.

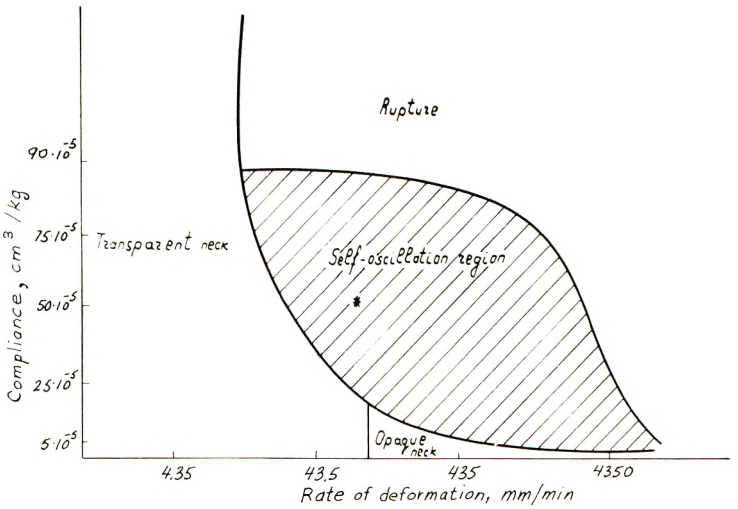

Fig. 9. Regions of deformation conditions corresponding to different regimes of extension of a PETP specimen.

neck in the sample under consideration) the process becomes unstable. Hence any weak accidental action can give rise to periodic stress oscillation and to corresponding periodic changes in appearance of the sample. This can be seen clearly in Figure 8, where 1 indicates the region before neck formation, 2, the region of steady neck formation, and 3, the region of self-oscillations. Finally, there is a velocity of any arbitrary order of smallness, at which, under the conditions of the experiment no oscillations can be induced.

All this is illustrated in Figure 9, where the lower line determines the critical conditions for appearance of self-oscillation. However, even at very high compliance, self-oscillations will not arise since the stresses developed exceed the ultimate strength of the sample. This is denoted in Figure 9 by the upper line which separates the region of self-oscillations from that of failure.

Thus, oscillations arise only within a relatively narrow region of experimental conditions, shown for the material under study as a shaded field in Figure 9. It is obvious that location of this region depends on the properties of the material and on experimental conditions. Figure 9 indeed represents a plane section of a three-dimensional diagram, the temperature of extension being the third coordinate axis.

The compliance of the sample, which determines the conditions under which self-oscillations occur, can be imitated by the compliance of a spring connected in series with the sample. This spring may be, for example, the transducer spring, from the deformation of which the stresses acting in the sample are calculated (measured).

In the experiments described above, very rigid dynamometers were used, whose strain could be neglected compared to the extension of the sample.

We also carried out a model experiment, which in the compliance of the sample was insufficient (according to Fig. 9) for self-oscillations to appear, but a soft spring was connected in series with the sample so that the total compliance (of sample plus spring) corresponded to the point marked by an asterisk in Figure 9. This point was selected to fall in the self-oscillation region. In this model experiment, the periodicity described above was indeed realized, whereas without the soft spring the sample deformed under steady necking conditions. It is clear that in samples with a sufficiently long neck, i.e., possessing high compliance, it assumes role of the soft spring. It stretches during the period of gradual stress growth, in parallel with very insignificant neck formation, and contracts at the moment of sharp drop of the stress and necking of the main part of the polymer (see Fig. 5 and relevant discussion).

Now we shall try to account for the appearance of self-oscillations. A possible mechanism of this process could be temperature fluctuations and the corresponding change in mechanical properties of PETP. For this mechanism to be realized one would expect the temperature rise to be a few decades of degrees. It is usually thought that the glass transition temperature of PETP is close to 70 or 80°C; but it will be shown below that a fairly abrupt change in properties of the PETP sample studied by us begins at approximately 50°C.

We estimated the true temperatures of the samples in the course of deformation by means of organic crystals with melting points within the temperature intervals of interest. For greater contrast these crystals were colored with nigrosine dye, and the melting point of the organic crystal–nigrosine eutectic was determined in a capillary in the usual way. We used mixtures of benzotriazole with nigrosine (mixed melting point 90°C) and of benzoic acid with nigrosine (mixed melting point, 110°C). A thin layer of temperature indicators was dusted onto the surface of the film studied. After extension the film was subjected to a weak current of air. Where crystals had melted the dye remained on the surface, while the unmelted crystals were blown away. Then the film was photographed on a black background. Figure 10 is a typical photograph obtained in this way, the dark band corresponding to the transparent section of the film (I in Fig. 3); the light band with numerous black spots is the opaque white section of the sample (II) with the resolidified temperature-indicator crystals adhering to it; the grey band without spots is the cloudy region (III in Fig. 3) which completes the cycle.

Direct measurement with a copper–constantan thermocouple showed the temperature to be about 90°C. Thus, in some sections of the deforming sample the temperature may rise by many tens of degrees. At slow extension rates this does not occur. In the example under consideration at an extension rate of the order of 43.5 mm/min the maximum temperature may be up to 90°C. At an extension rate of 435 mm/min it exceeds 110°C, and on further increase of the rate the maximum temperature reaches 140°C. It is quite clear from Figure 10 that the region of maximum temperature in-

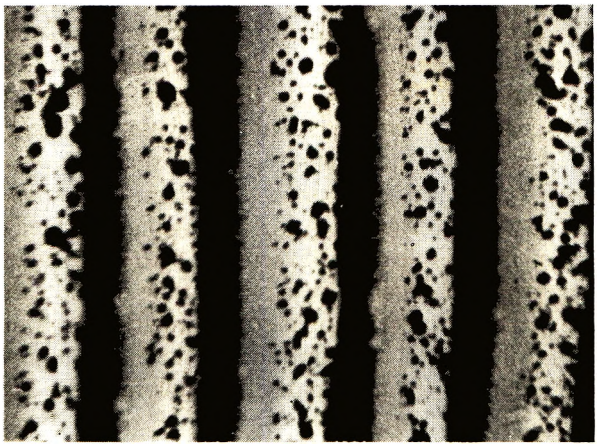

Fig. 10. Photomicrograph of PETP film strained with a temperature indicator in a self-oscillation regime.

crease coincides with the very opaque band (II). The highest temperatures develop beginning immediately from the boundary between the transparent and opaque regions and fall off on passing from region II to region III of the cycle.

To show how such a change in temperature affects the properties of the films, the stress σ_n at which necking occurs is plotted in Figure 11 against temperature under isothermal conditions at an extension rate of 435 mm/-

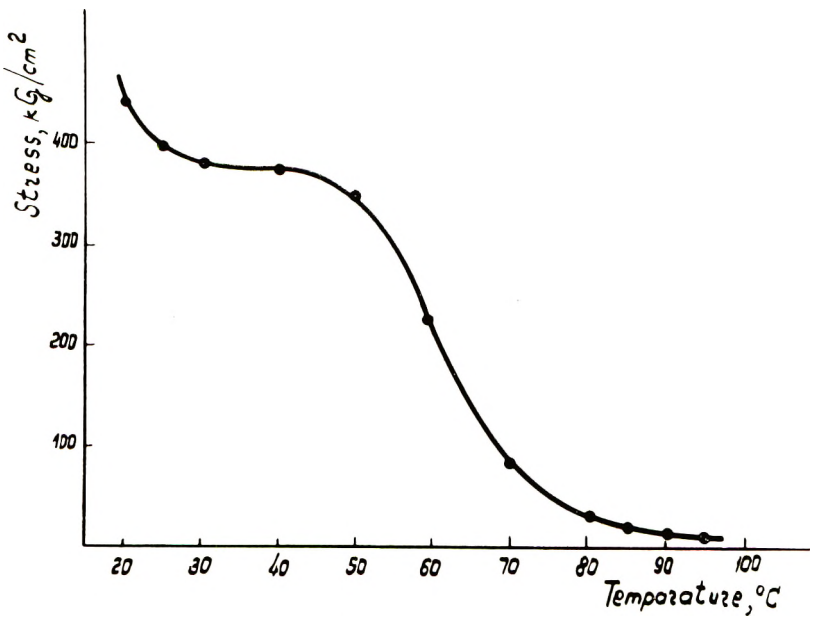

Fig. 11. Temperature dependence of stress during steady necking on extension of PETP.

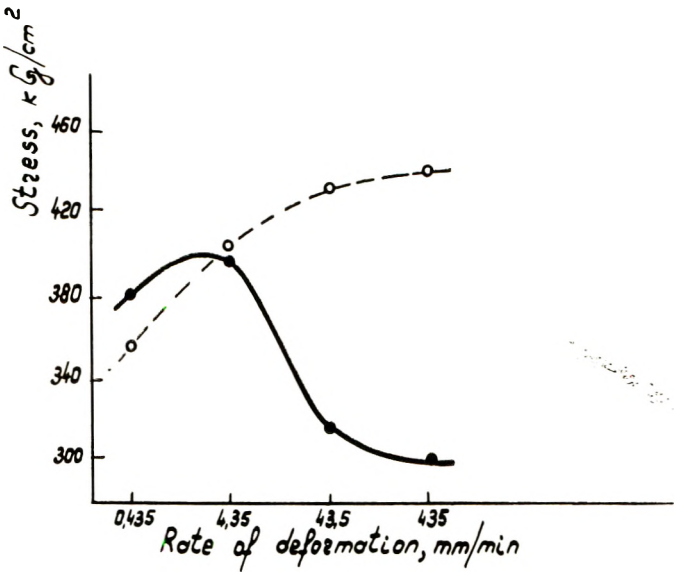

Fig. 12. Dependence of necking stress σ_n on rate of deformation of PETP, measured (——) in air and (- -) under water.

min. In contrast to the experiments described above, the data of Figure 11 were obtained for extension of the film under water, which prevented any substantial local heating of the film owing to the high heat conductivity of water as compared to air.

It is clear from the material described above that the local increase in temperature is related to the rate of extension, namely, the higher the deformation rate, the greater is the temperature jump. Hence, one would expect an increase in extension rate to have the same effect as an increase of temperature on the stress at which necking occurs. That this is actually the case is confirmed by the experimental data shown in Figure 12 as a solid line. At low extension rates, σ_n increases with the rate because the temperature effects are as yet of no importance. On further increase of the extension rate, σ_n decreases in a manner analogous to the decrease in σ_n in Figure 11 with increasing temperature. That this effect is actually due to changes in temperature and not to the effect of extension rate itself is proved by determining the dependence of σ_n on the rate under isothermal conditions. As indicated above, conditions of efficient heat removal could be attained by stretching under water. The results of such measurements are represented in Figure 12 by the broken line. The obvious contrast between the shapes of the solid and broken lines is due to the effect of temperature.

The effect of heat dissipation to the surrounding medium can be eliminated completely by stretching in a high vacuum. We performed such experiments at a gauge pressure of 10^{-5} mm Hg. Though the general picture of the self-oscillation process remained unchanged, the bands became narrower and sharper as the gauge pressure decreased.

An interesting confirmation of the difference in mechanism of formation of the "transparent" and "turbid" sections of the strained sample is offered by a study of film shrinkage on heating. Experiment shows that only the transparent section shrinks, whereas the width of the opaque bands remains unchanged. This means that the formation of transparent sections is related to imposed elastic strains which develop below the glass transition temperature, while the opaque bands form by plastic deformation, which is possible only above the glass temperature.

The transparent and opaque sections of strained PETP samples also have different structures, the macromolecules in these regions being oriented to different extents.

Thus, the experiments described above show that the appearance of self-oscillations on extension of PETP is actually related to local temperature jumps in the sample, which substantially change tne mechanical properties of the polymer.

The experimental facts described above suggest the following scheme in the self-oscillation regime of necking. With one end of the sample moving at a constant speed, its most compliant part deforms. This compliant part may be a preformed fairly long neck (or soft dynamometric spring). The strain is elastic and is accompanied by an increase of stress. This is accompanied by insignificant neck formation, which may be neglected in the approximate scheme under consideration. When the stress reaches a certain limiting (maximum) value, it becomes possible for unoriented material to pass abruptly into the neck. This moment is similar to attainment of the yield point in elastic-plastic media. Hence, on attainment of the maximum stress, necking begins to develop intensively. This corresponds to abrupt formation of a transparent band in the neck. The very rapid deformation is due to rapid liberation of heat which results in the local temperature jump described above. Therefore neck formation actually occurs nonisothermally, and a turbid band appears beyond the transparent band. But the temperature jump causes a drop in stress whereupon necking occurs (see Fig. 11 and Fig. 12). This is what determines the interrelation between the turbid band formation, the temperature jump, and the drop in stress. Since the polymer possesses very low heat conductivity, the temperature jump is of a local nature and the region in which the glass temperature is exceeded extends only over the narrow opaque band. Then, owing to the fact that the temperature of the polymer at some distance from the region of local heating drops below the glass temperature, necking there requires much higher stresses than are actually present in the material. This causes a pause in necking, during which the stress slowly increases again and the most compliant part of the sample is deformed. The process then repeats itself and becomes self-oscillatory.

Thus, the following factors are critical to formation of periodic oscillations: rate of deformation, compliance of the sample, and conditions of heat removal. At a very low rate of deformation the value of σ is small and therefore heating is insufficient for the glass temperature to be exceeded and

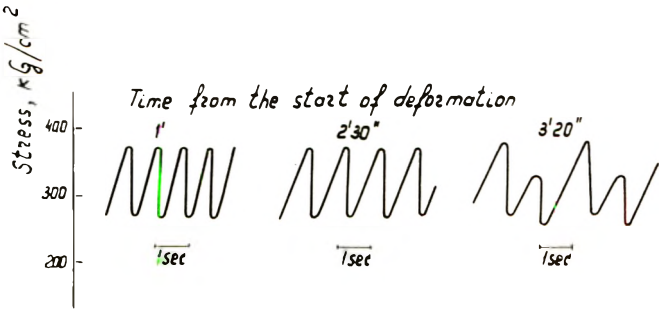

Fig. 13. Variation of frequency and nature of self-oscillation with increase of compliance of specimen, showing (*a*) high frequency oscillations, 1 min after start of deformation; (*b*) relatively low-frequency oscillations, 2½ min after start of deformation; (*c*) double periodicity, 3⅓ min after start of deformation.

self-oscillation is impossible. The higher the rate, the more rapid is the liberation of heat, and the shorter the time required for the minimum temperature jump needed. Hence, beginning from a certain rate, periodic oscillations become possible, and their frequency increases with increasing rate.

The rigidity of the strained part of the sample determines the possibility of the stress increasing without the sample failing. If the rigidity is very high, either a steady process becomes possible with a rate of necking equal to the imposed rate of extension, or the sample may fail on increase of the stress. But if there is a soft element in the system slow increase in the stress becomes possible, and the softer this element is, the more time will be taken up by the region of stress increase. The latter is due to the fact that in the elastic region σ is proportional to ϵ, and the rate of increase of stress is given by $\dot{\sigma} \sim V_c/l$.

The higher l is (i.e., the greater the compliance), the lower will be the rate of stress increase. The most obvious manifestation of this relationship is that the oscillation cycle becomes longer as the sample is extended. This effect is obviously due to the increase in compliance as the neck grows longer with developing strain (Fig. 13).

Finally, concerning the role of heat conductivity, according to the scheme outlined above, self-oscillations become possible because of local temperature jumps and the abrupt change in properties of polymer on passing through the glass temperature. If the temperature jump is eliminated, no self-oscillation can develop. This can be confirmed most vividly by extension under water to ensure rapid (compared to air) cooling and prevent a sudden temperature increase. Indeed, when PETP was stretched under water, no self-oscillation could be induced under any conditions. Even a weaker influence is sufficient to eliminate periodic oscillation. For example, oscillations are usually prevented if the sample is exposed to a stream of cold air. In this case the critical factor is usually the strength of specimen, because the film fails owing to the increase in stress as the preformed

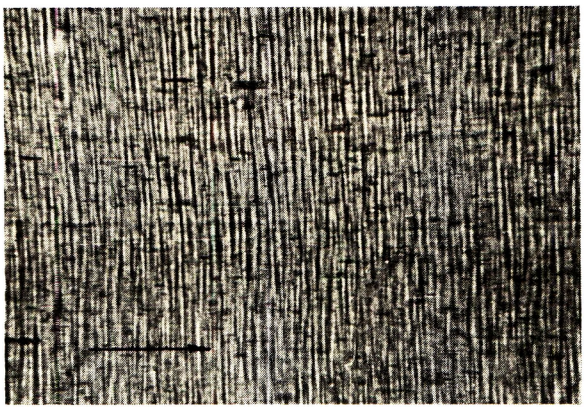

Fig. 14. Photomicrograph of transverse banding of the types described previously[1] in PETP specimens.

neck is being extended. The role of heat conductivity can readily be illustrated by the following simple experiment. A thin strip of filter paper moistened with water was laid on the specimen in the initial state at right angles to the direction of tensile stress at a point sufficiently remote from the line of transition to the neck. Then deformation was begun in the self-oscillation regime. Passage of the polymer into the neck occurred periodically, as described above, but continued only up to the point where the strip lay. Here the specimen always failed. This experiment shows vividly that if local temperature jumps are eliminated, self-oscillation in necking becomes impossible.

The mechanism described gives only a general scheme of the self-oscillation process without allowance for such details as slow passage into the neck in the region of increasing stress and more complex structure of the stress–time dependence than described above. Evidently, these details are secondary and do not play a decisive part in this phenomenon.

The self-oscillation mechanism of necking was also observed by us on extension of quenched samples of polypropylene and high-density polyethylene. The development of the process for these polymers occurs quite analogously to that of PETP. In the case of polyolefins, however, self-oscillations can be realized only at temperatures below 0°C and at extremely high rates of deformation.

The self-oscillation regime of necking discussed in this paper should not be confused with other instances of periodicity arising during deformation, described in the literature. Thus, a previous paper[1] describes in detail the occurrence of transverse banding of polypropylene and polyethylene at large strains, just before the specimens failed. The transverse bands had a period of 1.7–3 μ and were due to morphological formations whose origin had nothing to do with the deformation regime. Therefore neither the conditions of extension nor the temperature were critical for this phenomenon. We obtained similar transverse banding of approximately the same periodicity

in the PETP specimens studied. However, certain special conditions are required for such periodicity to occur; it is easier to obtain, as a rule, upon further deformation of a previously strained transparent section I of PETP at right angles to the axis of the first extension (Fig. 14).

Still more profound structural features of polymers are responsible for the periodicity detected at the electron-microscopic level[2–4] (relating to structural elements about 150–230 Å in size.) In both cases the periodicity is primarily morphological in nature and unrelated to the self-oscillation regime of deformation. The same can be said of periodicity at a definite angle to the direction of extension,[5] which appears as a result of plastic slippage in the direction of the maximum shear stresses. Though all these effects give rise to periodicity, they develop over the entire sample simultaneously and have no relation to self-oscillation on extension. They therefore differ essentially from the periodicities studied in this work.

We suggest that this new phenomenon is connected with the effect of necking of polymers in general. The experiments described are analyzed theoretically by Barenblatt.[6] Starting from the equations of motion and thermal equilibrium, and adding the relation between stress and temperature and rate of necking, he showed that at certain values of essential constants the solution of these equations leads to a self-oscillating regime of neck formation, as it is described above.

Conclusions

The self-oscillation regime observed on extension of polymers, consisting in periodic variations of stress in the polymer and of its appearance, has been studied for poly(ethylene terephthalate).

The conditions at which self-oscillations appear on extension have been determined, and the principal regularities for this regime of deformation are described. It is established that self-oscillation is related to the effect of local heating associated with passage of the polymer into the neck. A mechanism is suggested and studied.

References

1. G. P. Andrianova, G. G. Kardash, A. S. Kechekyan, and V. A. Kargin, *Vysokomol. Soedin. A*, **10**, 1990 (1968).
2. E. H. Andrews, *J. Polym. Sci. A-2*, **4**, 668 (1966).
3. A. Peterlin and K. Sakuoku, *Kolloid-Z.*, **212**, 51 (1966).
4. G. A. Bassett and A. Keller, *Phil. Mag.*, **9**, 817 (1964).
5. T. Hitton and J. G. Rider, *J. Appl. Phys.*, **39**, 4932 (1968).
6. G. I. Barenblatt, *Isvest. Acad. Nauk. S.S.S.R. Mech. Tverologo Tela.* No. 5, 121 (1970).

Received December 3, 1970
Revised April 21, 1971

JOURNAL OF POLYMER SCIENCE: PART A-2 VOL. 9, 1935–1954 (1971)

Diffusion Mechanisms in Solid and Molten Polyethylene

P. N. LOWELL* and N. G. McCRUM, *Department of Engineering Science, University of Oxford, Oxford, England*

Synopsis

The diffusion coefficient D and solubility coefficient k of small molecules [C_3H_8, C_4H_{10}, $(CH_3)_4C$] are determined at very low solute concentrations in annealed linear polyethylene over a wide range of temperature above and below the melting point T_m. For measurements above T_m the specimen was lightly crosslinked by irradiation from a ^{60}Co source. The diffusion data fit equations of the form $D = D_0 \exp\{-\Delta H_D/RT\}$. An abrupt change in ΔH_D occurs at T_m: representative values (for C_4H_{10}) are 4.53 and 14.9 kcal/mole above and below T_m. At T_m, D_0 also changes abruptly: representative values (for C_4H_{10}) are $\log D_0 = -2.65$ above T_m and $\log D_0 = +2.70$ below T_m. The mechanism of diffusion therefore changes at the melting point. The melt exhibits typical liquidlike characteristics (negative values of activation entropy ΔS_D). The ratio $\Delta S_D/\Delta H_D = 4\beta$ (β denoting the isobaric coefficient of volume expansion) holds below but not above T_m. Equations of the form $k = k_0 \exp\{-\Delta H_k/RT\}$ fit the solubility data. The $\log k$ versus T^{-1} plots above and below T_m are parallel but separated by a step at T_m. If crystallization followed by annealing is assumed to leave a weight fraction of polymer α_k (the amorphous fraction) in which the solute can absorb and if the specific solubility coefficient of the amorphous fraction is identical to that of the melt, then $\log \alpha_k$ equals the magnitude of the step at T_m. Values of α_k determined from the observed step are very close to values of amorphous fraction determined by measurement of density. The solubility experiments support the concept of polyethylene as a two-phase solid with the amorphous fraction of specific volume equal to the extrapolated specific volume of the melt. The passage of a solute molecule from one potential well to another, however, occurs by processes in the melt and the amorphous fraction which are entirely different.

INTRODUCTION

The study of the absorption of small molecules in polyethylene is a powerful technique for probing the properties of the amorphous fraction. It is well known that the solubility coefficient k decreases with increasing density, which leads to the relation

$$k = \alpha k^* \tag{1}$$

in which α is the weight fraction of amorphous material and k^* the specific solubility coefficient of amorphous polyethylene. The implication of this

* Present address: Royal Military College of Science, Shrivenham, Swindon, Wiltshire, England.

statement is that the crystalline fraction does not absorb small molecules, a conclusion in complete accord with experimental evidence.[1-4]

Since the solute absorbs in the amorphous fraction alone, the lines of flow of the diffusing molecules are determined by the geometrical arrangement of the crystals. This problem is analogous to the problem of impermeable fillers in rubber, which has received much attention.[5-9] The theory of the diffusion coefficient D and solubility coefficient of pure rubbers is well advanced due to the pioneer experiments of Barrer,[10] van Amerongen,[11] Meares,[12] Ryskin,[13] and others. In filled rubbers, therefore, the several theories formulated to describe the flow of solute are, in principle, easily tested by experiment. For a crystalline and spherulitic polymer such as polyethylene understanding of the diffusion coefficient is inhibited for two reasons. First, amorphous polyethylene does not exist in bulk and therefore cannot be studied in the pure state. Second, the morphology of the solid is extremely complex: the amorphous fraction lies in thin lamellae, tens of Ångstroms thick, sandwiched between the lamellar crystals which are of the order of 100 Å thick. In the spherulite this layered structure is twisted about the spherulite radius. A realistic calculation of the geometrical impedance to flow is obviously extremely difficult. Nevertheless, a formal statement of the problem in terms of a structure or transmission factor has been of considerable conceptual if not quantitative assistance. The relationship between the diffusion constant of the semicrystalline polymer D and the intrinsic diffusion constant of the amorphous fraction D^* is[2,3,14-16]

$$D = \kappa D^* \tag{2}$$

in which κ is the structure factor ($\kappa \leq 1$). The utility of eq. (2) depends on two hypotheses. First, D^* is independent of the crystal volume fraction; that is to say, D^* is truly the intrinsic diffusion coefficient of the amorphous fraction and is independent of the size of the amorphous layers and of thermal history. Second, for a particular morphology which is determined by crystallization conditions and subsequent annealing, κ is independent of temperature. The slender experimental evidence, fully supported by the experiments described in this paper, supports both hypotheses, and we accept eq. (2) as a basis for the following molecular interpretation.

The coefficient D^* is related to the jump-length a of the diffusing molecule and to τ, the mean time-of-stay between jumps, by

$$D^* = \lambda a^2 \tau^{-1} \tag{3a}$$

in which λ is a constant of order 10^{-1} which depends on the geometry of the diffusion step. In the derivation of this elementary equation it is assumed *inter alia* that there is no correlation between jumps; that the probability of a jump occurring in a particular direction is independent of the directions of the preceeding jumps. It is apparent, however, that in many solids this is not true. For instance, if the atomic jump takes place through a vacancy mechanism the diffusing atom may be more likely to return to the

previous site than to move in any of the other possible directions. This is taken into account by writing,[17]

$$D^* = \lambda a^2 \tau^{-1} f \tag{3b}$$

in which f is the correlation factor. For solids, $f \leq 1$.

According to the theory of reaction rates as applied to diffusion and ammended by Wert and Zener,[18] the temperature dependence of D^* is controlled by the temperature dependence of τ^{-1}:

$$\tau^{-1} = \tau_0^{-1} \exp\{-\Delta H_D/RT\} \tag{4}$$

in which

$$\tau_0^{-1} = n\nu \exp\{\Delta S_D/RT\}$$

where ν is the linear vibrational frequency of the diffusing molecule in its potential well, n the number of nearest-neighbor potential wells, and ΔS_D and ΔH_D are the entropy and enthalpy of activation for diffusion. Hence

$$D^* = D_0^* \exp\{-\Delta H_D/RT\} \tag{5}$$

$$D_0^* = \lambda a^2 n\nu f \exp\{\Delta S_D/R\} \tag{6}$$

The mechanism of diffusion is best defined in terms of D_0^* and ΔH_D. From eqs. (2) and (5):

$$\Delta H_D = -R \frac{d \ln D^*}{d(1/T)} = -R \frac{d \ln D}{d(1/T)} \tag{7}$$

assuming κ and f to be independent of temperature. Thus ΔH_D is determined by measuring the temperature dependence of D. Unfortunately, D_0^* cannot be determined. Extrapolation of the log D versus T^{-1} plot to $T^{-1} = 0$ yields log D_0. Since $\kappa \leq 1$, it follows from eq. (2) that

$$D_0^* \geq D_0 \tag{8}$$

Thus a determination of D_0 is useful in the limited sense that it provides information on the lower bound of D_0^*.

The objective of the experiments described in this paper was to seek differences between the properties of the two noncrystalline phases; the melt at temperatures above the melting point T_m and the amorphous fraction at temperatures below T_m. Although the amorphous fraction of the solid cannot be studied in the pure state, the melt can. In developing the theory of two-phase (crystalline–amorphous) polymers the classical hypothesis is that the amorphous fraction is a supercooled liquid. The value of the amorphous weight fraction α is usually obtained by measuring the specific volume of the specimen v and then, on the assumption that the crystalline and amorphous phases are of volume v_c and v_a,

$$\alpha = (v - v_c)/(v_a - v_c) \tag{9}$$

In the estimation of v_a the classical hypothesis assumes a linear relation between specific volume and temperature above T_m to extrapolate linearly to 25°C to yield v_a. That the procedure is extremely successful cannot be doubted. That is to say, many diverse pieces of experimental evidence are fully rationalized on this assumption. Yet, there are grounds for hesitation in accepting the model completely. To be specific, is it reasonable for the interlamellar, amorphous material to possess properties identical to those of the supercooled liquid? In this sense the model may be seen to be fairly presumptuous. One way of testing this point is to study properties of the solid which are dominated by the amorphous fraction. In the experiments described in this paper this is done by studying the diffusion and solubility of small molecules in linear polyethylene at temperatures above and below the melting point. The molecules selected for study were hydrocarbon gases (e.g., n-C_4H_{10}) for which the solubilities obey Henry's Law.

The experiments were performed at very small concentrations of solute, of the order of 1 part in 10^3 by weight. At such small concentrations it is possible to neglect several complicating factors (such as the interaction of solute atoms with one another, plasticization, and the dissolution of crystals) which become important at high concentrations.

EXPERIMENTAL

Apparatus

A Sartorius vacuum microbalance was employed to obtain solubility and diffusion measurements. The solubility coefficient was determined from the total weight of gas absorbed by the polymer and the diffusion coefficient D was determined from the rate at which the gas was absorbed. Specimens of rectangular cross section of varying thickness were studied.

Both the weighing technique for determining D and k[13] and also the principles of the Sartorius vacuum microbalance are well known.[19] In this section we emphasize certain experimental problems which were encountered and do not present a detailed description of the experimental arrangements.

Figure 1 shown a schematic diagram of the microbalance. The quartz arm A holds at one end the specimen B (weight approximately 0.5 g) and at the other end a counterbalance C. The balance is sealed in glass. Both the specimen tube (D) and the counterbalance tube (E) are coated with a colloidal suspension of carbon and earthed to prevent the buildup of electrostatic charge. On the most sensitive scale a change in weight of 1 μg induces a change in current of 1 μA. Measurements were made with a chart recorder with full-scale deflection (10 in.) equal to 100 μg.

The specimen tube is immersed in an oil bath F having a thermal fluctuation of ± 0.1°C. In order to suppress temperature surges due to the heaters switching on and off the specimen tube is surrounded by a metal baffle G which has its own stirred oil supply heated by conduction from the main bath. Small temperature surges must be eliminated since they cause

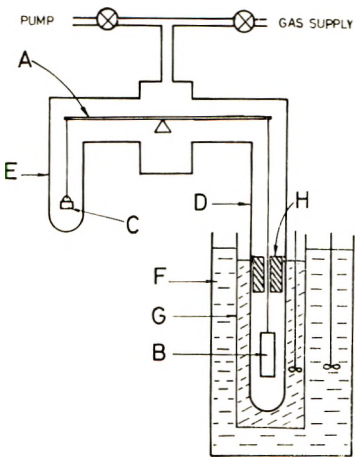

Fig. 1. Schematic diagram of microbalance.

fluctuations in the density of the gas and hence in the buoyancy, thereby causing an apparent oscillation in the weight of the specimen.

Convection currents in the specimen tube presented a serious problem. They were reduced to negligible proportions by inserting a long copper ferrule H (Fig. 1) which extended below the oil level. Paper-thin copper fins within the ferrule restricted the flow of gas and thereby suppressed convection currents. The wire carrying the specimen passed through a close-fitting hole in the ferrule. Mounting of specimen and ferrule was achieved by means of a cone and socket joint (not shown in Fig. 1) in the specimen tube just above the ferrule.

To reduce the time required to desorb gases from the specimen in the microbalance several desorption chambers were added to the vacuum line. The specimens could then be desorbed at ambient temperature for several weeks before use thereby reducing the desorption time required in the microbalance.

After removal from the desorption chamber the specimen was transferred to the microbalance and degassed at temperatures up to 95°C. The speci-

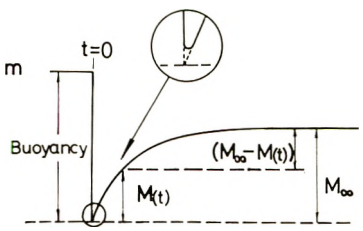

Fig. 2. Illustration of the course of an absorption experiment: a plot of recorded weight against time. At $t = 0$, gas is admitted causing an apparent loss in weight due to buoyancy. The time-dependent absorption process than commences. The experiment is terminated when the equilibrium weight of gas, M_∞, is absorbed.

men was considered to be degassed when the desorption rate was less than 1 μg/hr. The specimen was then maintained at the required temperature and measurements of D and k obtained. This was done by admitting gas to the microbalance to the required pressure, usually 400 torr (mm Hg). The course of an experiment is illustrated in Figure 2. From the weight in vacuum m there is an instantaneous weight drop due to increased buoyancy (of the order of 0.2 mg) The recorded absorption process yields a time-dependent weight increase $M(t)$ which finally comes to an equilibrium value M_∞. The specimen is then desorbed under vacuum in preparation for the next experiment.

The solubility coefficient k is calculated from M_∞ by using the relationship

$$k = M_\infty/pm \tag{10}$$

where m is the mass of specimen and p is the gas pressure. In obtaining M_∞ it is necessary to calculate the buoyant force. The buoyant force cannot be measured accurately since absorption commences as soon as the gas is admitted. This leads to a "rounding off" of the recorded weight (see inset Fig. 2) which inhibits an accurate determination of the buoyant force. It is therefore necessary to calculate the buoyant force with some precision, since it is often larger than the weight of absorbed gas. This means that the volumes of the components on both sides of the balance must be known. Gas densities were obtained by using Boyle's law. Temperature-induced changes in the specific volume of polyethylene were taken into account since they lead to a buoyancy correction as high as 5% at 100°C.

The diffusion coefficient is calculated by using the standard equations for absorption of solute into a thin flat strip of thickness L,

$$\frac{M(t)}{M_\infty} = 1 - \sum_{n=0}^{\infty} \frac{8}{(2n+1)^2\pi^2} \exp\left\{-\frac{t}{\theta/(2n+1)^2}\right\} \tag{11}$$

$$\theta = L^2/\pi^2 D \tag{12}$$

Consideration of eq. (11) shows that for $t > 0.3\,\theta$ all terms other than $n = 0$ may be neglected in comparison with experimental error. Hence, for $t > 0.3\theta$, we write

$$\frac{1}{\theta} = -\frac{d}{dt} \ln\left(\frac{M_\infty - M(t)}{M_\infty}\right)$$

The major random error in the determination of D lies in the determination of the specimen relaxation time θ from the measurement of the slope. The relaxation time was calculated by plotting $\log\{[M_\infty - M(t)]/M_\infty\}$ against t and determining the slope. Then D was calculated from θ by using eq. (12). The calculation of D is sensitive to the measurement of specimen thickness since it appears as a squared value. Thicknesses were measured with a micrometer to within 0.0002 cm; the mean of ten squared readings was taken for L^2. The specimen thickness was not corrected for thermal

expansion; this accounted for an error of approximately 3% at 100°C. The thickness was so chosen that an experiment could be completed within 2 hr.

Materials and Specimen Preparation

Sheets of the linear polyethylene (LPE) resins described in Table I were compression-molded to a thickness of 60 mils (60×10^{-3} in.). The specimens were then machined to the required thickness. The major problem in machining was in holding the specimens true and flat. Down to a thickness of 10 mil the specimen could be held on a vacuum plate. With the thickness under 10 mils, specimens were warped by the vacuum in a pattern corresponding to the holes in the vacuum plate. Specimens under 10 mil thick were held with double-sided adhesive tape.

TABLE I
Properties of Linear Polyethylenes

Polyethylene	Manufacturer	Melt index	M_w	$\frac{CH_3}{10^3C}$
PE-85	E.I. duPont de Nemours	2.92	1.44×10^5	1
Rigidex Type 2	B.P. Plastics.	0.2	1.7×10^5	1

Measurements in the melt were made with specimens crosslinked by radiation from a ^{60}Co source to a dose of 6 Mrad. These specimens were 60 mils thick. Measurenents of D and k in the melt were found to be independent of radiation dose for the doses studied (below 20 Mrad).

The amorphous fraction α was determined from measurements of density by Archimedes method at room temperature. Values of $v_a = 1.171$ cc/g and $v_c = 1.001$ cc/g were used to obtain α[2,3,15] [eq. (9)].

The gases used in the study were ethane, cyclopropane, butane, and neopentane and were supplied by Air Products Ltd. The stated purities were 99%, 99.9%, 99.99%, and 99.87%, respectively. The ethane, which was relatively impure, was used only in the preliminary experiments outlined in the next section.

RESULTS

It was necessary early in the experimental program to establish a standardized procedure for preparing the specimen surface. According to Eby,[20] specimens as-molded yield higher values of D than specimens whose surfaces have been machined. Eby attributes this fact to the existence of an oriented surface layer in the specimen as-molded, through which the solute passes more rapidly than in the bulk. On the other hand, Michaels et al.[21] report that permeabilities in films having oriented surface layers ranging from 4 to 25% of the total film thickness were the same. The machining of thin specimens of polyethylene is an awkward procedure, and we were relu-

tant to undertake it lightly. Nevertheless it seemed essential to do so if Eby's findings were correct and so the preliminary experiments described in the following section were initiated.

Surface Orientation

Four specimens were compression-molded from resin PE85 (see Table I): two of thickness 15 mil and two of 30 mil. One specimen of each thickness was quenched from the melt and one cooled at a moderate rate. The densities of the four specimens are given in Table II together with the fractional thickness of the surface layer. The fractional thickness is equal to the sum of the two surface layers divided by the total thickness of the specimen. The thickness of the surface layer was obtained by the study of microtomed sections using a microscope with crossed polaroids. Since the thickness of the surface layer varied along the film, an average of ten readings was used to determine the fractional thicknesses given in Table II. Specimens were cut from each sheet and annealed in a nitrogen atmosphere at 124°C to essentially equal densities. Specimens were not studied in these experiments in the unannealed state.

TABLE II
Specimen Densities and Fractional Thicknesses of Surface Layer

Specimen[a]	Initial density, g/cc	Annealed density, g/cc	Surface layer[b]
15Q	0.939	0.964	0.42
35Q	0.948	0.964	0.26
15MC	0.954	0.966	0.13
35MC	0.961	0.965	0.18

[a] The specimen code numbers indicate roughly the thickness of the specimen (in mils) and the crystallization procedure (quenching or cooling from the melt at a moderate rate).

[b] The thickness of the surface layer is taken as the average of ten measurements along the surface.

The experimental procedure was as follows. (1) The temperature dependence of D to ethane gas at 400 torr was measured for each of the four films. A higher temperature range was used for the thicker specimens to keep the experimental time to periods of the order of 1 hr. (2) The specimen was removed from the microbalance and a layer greater than the thickness of the largest surface layer (4 mils) was removed from each side of the specimen by machining. (3) The density of the specimen was measured. A negligible increase of 0.001 g/cc over that of the total film was normally observed: density values in Table II are prior to machining. (4) D was again measured for each of the films.

The results of the investigation are plotted in Figure 3 as log D against $1/T$. The most important result is that the diffusion coefficient is reduced (by $\sim$10%) in all cases when the surface film is removed. Other results of

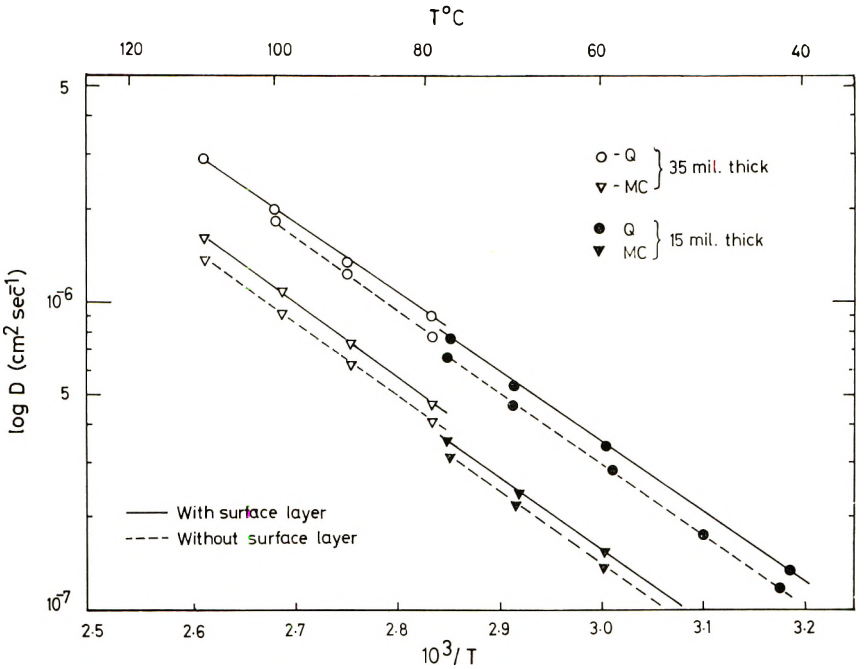

Fig. 3. Dependence on T^{-1} of diffusion constant D for C_2H_6 in linear polyethylene showing effect of removal of the surface layer: (——) specimens with surface layer; (- -) specimens with surface layer removed by machining. All specimens annealed to essentially constant density (see Table II). Quoted thickness values for as-molded specimens prior to removal of surface film.

interest are: the values of D for quenched and annealed specimens exceed (by ca. 100%) those for slow-cooled and annealed specimens, despite the fact that the densities are essentially equal; also, the activation energy for diffusion both before and after removal of the surface layer is 10.6 kcal/mole.

It is clear from the results that the surface layer affects the measured D: in the following experiments care was taken in all cases to machine the surface of the specimen to remove the oriented surface layer.

Sorption in Molten and Solid Polyethylene

The intention in these experiments was to study the absorption and diffusion of three different gases in polyethylene from room temperature up to temperatures well above T_m. Preliminary experiments showed that between 100°C and T_m the time required for the specimen to reach thermal equilibrium was quite long. We studied, therefore, the absorption of a single gas, (C_3H_6) in LPE up to 160°C leaving the specimen at each temperature for the time necessary to achieve equilibrium, (in some instances in excess of 4 hr). Having established the general pattern of behavior it was then possible to confine measurements on the solid to temperatures between

20 and 90°C: that is to say, to avoid taking measurements between 100°C and T_m, in which range the attainment of thermal equilibrium was extremely time-consuming due presumably to crystal premelting. Equilibrium above T_m was achieved rapidly.

Figure 4 shows a plot of log k versus T^{-1} for the absorption of C_3H_6 in LPE. Below T_m, measurements were made on an annealed specimen (ρ = 0.965 g/cc), 35 mils thick and irradiated to a dose of 12 Mrad. Measurements were begun at the lowest temperature and then at successively higher temperatures. The specimen was held at temperature before commencing

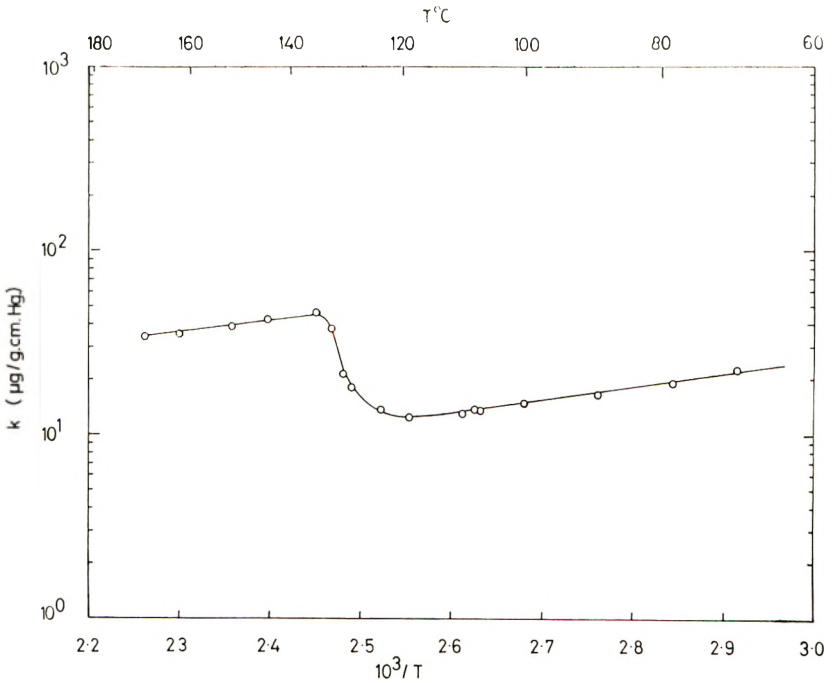

Fig. 4. Temperature dependence of the solubility constant k for C_3H_6 in linear polyethylene above and below the melting point. Measurements taken at successively increasing temperature.

the experiment for sufficient time to attain thermal equilibrium. Equilibrium was judged by agreement (or lack of agreement) between repetitive measurements of k. Measurements of log D versus T^{-1} are plotted in Figure 5. From these results it is apparent that the pattern of behavior of both D and k can be obtained by measuring from T_m up to 160°C and, for the solid, in the range 20–90°C. Measurements for the other gases studied were confined to these ranges of temperature.

Figure 6 shows a plot of log k versus T^{-1} for the absorption of C_3H_6, C_4H_{10}, and $C(CH_3)_4$ in LPE. Below T_m, measurements were made on irradiated, annealed specimens 20 mils thick machined from a 60-mil compression molding. The density of the specimen used for C_3H_6 and $C(CH_3)_4$ was

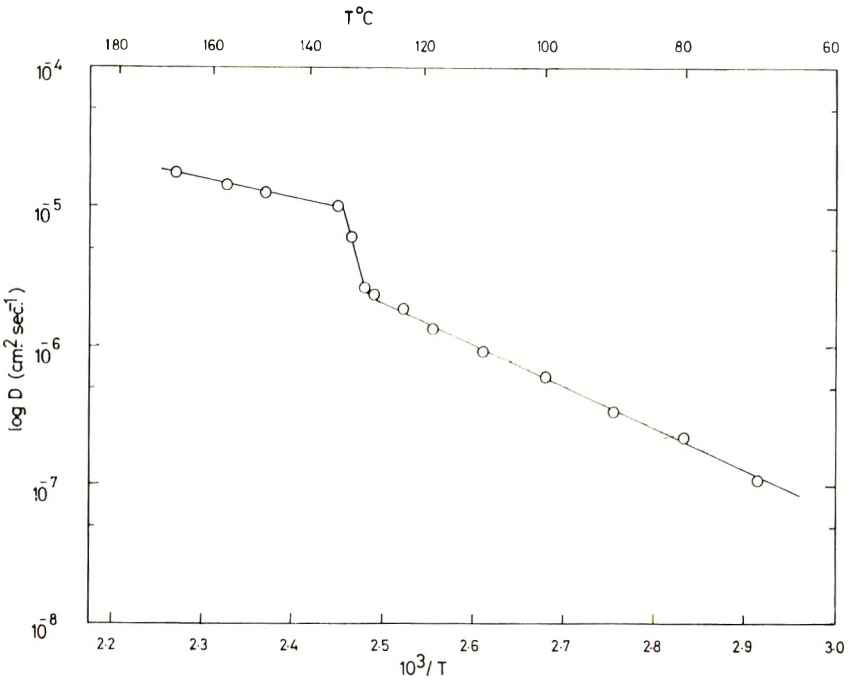

Fig. 5. Temperature dependence of the diffusion constant D for C_3H_6 in linear polyethylene above and below the melting point. Measurements taken at successively increasing temperature.

$\rho = 0.967$ g/cc and for C_4H_{10}, $\rho = 0.965$ g/cc. Values of the heat of solution ΔH_k,

$$\Delta H_k = -R \frac{d \ln k}{d (1/T)}$$

were obtained from the data of Figure 6 and appear in Table III. Up to a pressure of 300 torr the solubility was found to obey Henry's law.

Figure 7 shows a plot of log D versus T^{-1} for the diffusion of the three gases in LPE. The temperature dependence of log D is taken to be given by eq. (5). Values of ΔH_D are listed in Table IV together with the constant term D_0. Diffusion was found to obey Fick's first law at all temperatures;

TABLE III
Heats of Solution of Hydrocarbon Gases in Molten and Solid Linear Polyethylene

Gas	Molten polymer		Solid polymer	
	ΔH_k^m (± std. deviation), kcal/mole	log k_0	ΔH_k^s (± std. deviation), kcal/mole	log k_0
C_3H_6	−3.53 ± 0.03	−0.2154	−3.89 ± 0.03	−1.194
n-C_4H_{10}	−4.38 ± 0.06	−0.4092	−4.77 ± 0.09	−1.418
$(CH_3)_4C$	−4.30 ± 0.32	−0.2538	−4.49 ± 0.10	−1.187

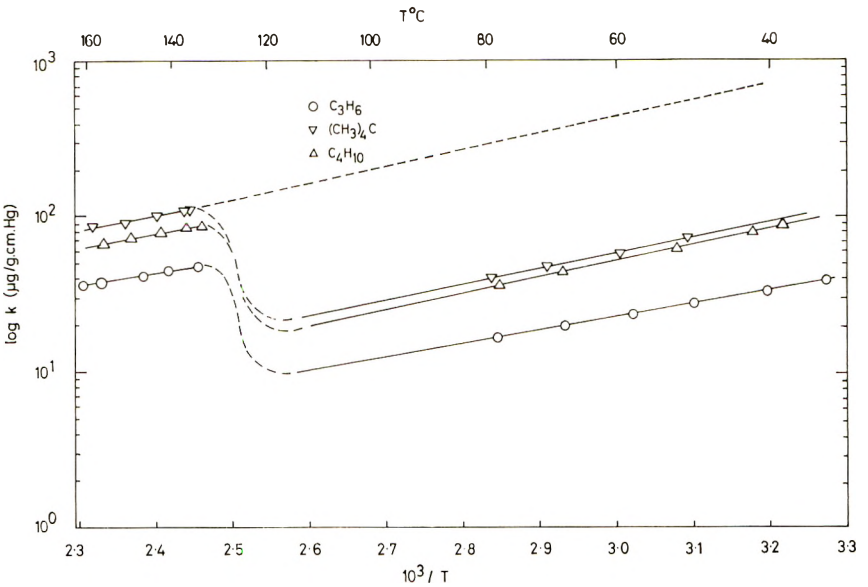

Fig. 6. Temperature dependence of the solubility constant k of C_3H_6, C_4H_{10}, and $(CH_3)_4C$ in linear polyethylene above and below the melting point.

D was independent of pressure up to 300 torr. In both Figures 6 and 7, although measurements were not taken just below T_m, the log k and log D versus T^{-1} plots are drawn to exhibit steps in accordance with the experiments described in Figures 4 and 5.

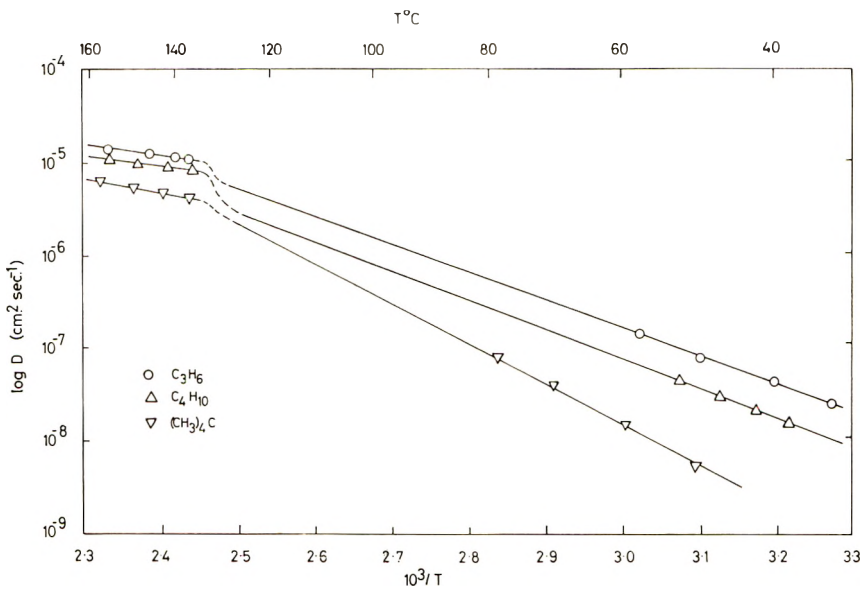

Fig. 7. Temperature dependence of the diffusion constant D of C_3H_6, C_4H_{10}, and $(CH_3)_4C$ in linear polyethylene above and below the melting point.

TABLE IV
Activation Enthalpies and Values of log D_0 for Molten and Solid Linear Polyethylene

Gas	Molten polymer		Solid polymer		
	ΔH_D^m (± std. deviation), kcal/mole	log D_0	ΔH_D^s (± deviation), kcal/mole	log D_0	$\frac{\Delta H_D^m}{\Delta H_D^s}$
C_3H_6	4.03 ± 0.39	−2.79	13.7 ± 0.24	2.26	0.29
n-C_4H_{10}	4.53 ± 0.50	−2.65	14.9 ± 0.05	2.70	0.30
$(CH_3)_4C$	6.43 ± 0.29	−1.93	20.9 ± 0.77	5.90	0.31

The log k versus T^{-1} plot exhibits a strikingly simple pattern. Both solid and liquid states yield negative values of ΔH_k which, for a particular gas, are essentially equal (Table III). A simple explanation of the course of melting follows at once. Take the solubility constant of the polyethylene melt, k_m to be equal to the specific solubility of constant amorphous polyethylene k^*. More precisely, take the value of $k_m(T)$ extrapolated to temperature T below T_m [see Fig. 6, data for $(CH_3)_4C$] to be equal to $k^*(T)$:

Hypothesis I:

$$k_m(T) = k^*(T)$$

It follows from eq. (1) and Hypothesis I that,

$$\log \alpha_k = \log k(T) - \log k_m(T) \tag{15}$$

so that the magnitude of the drop in log k on crystallization is equal to the amorphous fraction. Values of α_k obtained from eq. (15) are compared in Table V with values of amorphous fraction determined by density, (henceforth designated α_ρ). The extrapolation of the k_m data below the melting point was performed using computer techniques. The 95% confidence limits of α_k are also shown in Table V. Normally, density values may be reproduced to ±0.0005 which leads to a scatter in α_ρ of ca. ±0.003.

It will be seen from Table V that α_ρ is very close to but systematically greater than α_k. The origin of this small discrepancy is discussed below in the Discussion.

TABLE V
Values of Amorphous Fraction Determined by Solubility Technique (α_k) and Density (α_ρ) for v_a = 1.171 cc/g, v_c = 1.001 cc/g

Gas molecule	Specimen density ρ (at 25°C), g/cc	α_ρ	α_k
C_3H_6	0.967	0.195	0.177 ± 0.002
n-C_4H_{10}	0.965	0.207	0.172 ± 0.010
$(CH_3)_4C$	0.967	0.195	0.161 ± 0.024

Dependence of k on Amorphous Fraction

In the previous section the plot of log k versus T^{-1} was found to exhibit a step at T_m^{-1} of magnitude approximately equal to the amorphous fraction. This result is based on Hypothesis I. A second check in the validity of Hypothesis I may be performed by measuring the effect on k of variations in α_ρ produced by annealing and then obtaining k^* by using eq. 1.

A quenched specimen of LPE (Rigidex 2) was degassed in the microbalance at 90°C, and measurements of k were made between 90 and 60°C for the gases C_3H_6 and C_4H_{10}. The specimen was removed from the microbalance for a density determination at room temperature, replaced in the microbalance, and annealed at 95°C for 10 hr, after which k was measured between 90 and 60°C. The specimen was removed from the microbalance for a density determination and then replaced. The sequence of annealing in 5–10° increments, measurements of k between 90 and 60°C, and density determination at room temperature was continued until the specimen had had a final annealing at 130°C.

In Figure 8, k determined at 80°C is plotted against α_ρ for the gases C_3H_6 and C_4H_{10}. The lines drawn in Figure 8 were obtained from the data by the least squares method, as were the values of k^* (80°C) recorded in Table VI.

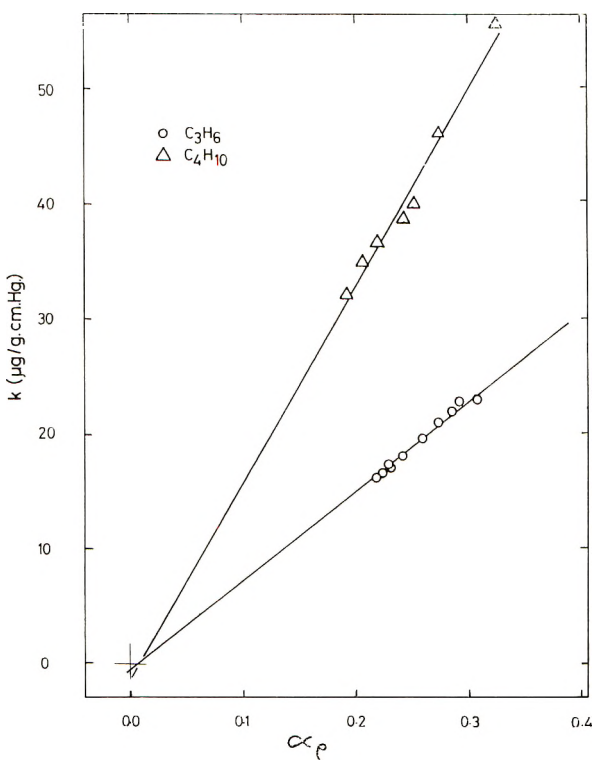

Fig. 8. Dependence of the solubility constant k (determined at 80°C) on amorphous fraction α_ρ for C_3H_6 and n-C_4H_{10}.

TABLE VI
Values of k^* and k_m at 80°C

Gas	k^*, μg/g cm Hg[a]	k_m, μg/g cm Hg[b]
C_3H_6	80.7 ± 3.5	93 ± 2
n-C_4H_{10}	176.5 ± 37.8	201 ± 11

[a] Determined by extrapolation.
[b] Extrapolated to 80°C from data above T_m.

Values of k_m extrapolated down to 80°C are also given in Table VI. It will be seen that k_m slightly exceeds k^* for both C_3H_6 and C_4H_{10}. The origin of this systematic difference is also discussed below.

DISCUSSION

Surface Orientation

It is clear from the results above that the removal of the oriented surface layer lowers the observed diffusion coefficient of a specimen. This result is in agreement with the conclusions of Eby.[20] The contrary conclusions of Michaels et al.[21] are probably due to the use of the time-lag technique which has a larger experimental error than the microbalance technique.

The result that the values of D for quenched and annealed specimens exceed those for slow-cooled and annealed specimens is in agreement with earlier observations which, stated briefly, are as follows.[21,22] (1) If a series of specimens is prepared with regularly decreasing density (by regularly increasing rate of crystallization) then D will be found to increase with decreasing density. Clearly, in the molded specimen, the greater the amorphous fraction, the greater the value of D. (2) If this series of specimens is then annealed to achieve equal density, the measured values of D for all specimens increase. The values of D after annealing are not equal: the greater the value of D prior to annealing, the greater the value of D after annealing. The amorphous fraction in the annealed specimens is not now the determining parameter. The best explanation is that annealing causes recrystallization which increases the structure factor κ, D^* in eq. (2) remaining constant.

The result that the activation energy for diffusion, both before and after removal of the surface layer, is 10.6 kcal/mole is of considerable interest, since it shows beyond doubt that the basic diffusion act, at the molecular level, occurs independent of crystal geometry and amorphous fraction. According to the two-phase model this result is observed because a change in crystal geometry changes the structure factor but not the character of the amorphous polyethylene through which the flow occurs. That is to say, D^* is independent of crystal volume fraction whereas κ is a complex function of the initial conditions of crystallization and of subsequent recrystallization. In drawn polyethylene this is not true; annealing changes both D^* and κ.[23]

Absorption

The difference between the heat of solution of melt (ΔH_k^m) and solid (ΔH_k^s) is small (Table III). For the gases, C_3H_6, C_4H_{10}, and $(CH_3)_4C$, the difference between ΔH_k^m and ΔH_k^s amounts to 9, 8, and 4%, respectively. These values are taken to be in accord with the prediction for dilute solutions that the heats of solution for ideal mixtures should be controlled by the heat of condensation of the solute and independent of the physical state of the solvent.

It will be seen in Table V that the values of amorphous fraction determined from density α_ρ exceed slightly the values obtained from solubility α_k. The amorphous fractions determined by density exceed those determined by solubility by 1.8, 3.5, and 3.4% for the gases C_3H_6, C_4H_{10}, and $(CH_3)_4C$, respectively.

The simplest explanation of this discrepancy is that the specimens contained a small void content.[24] The effect of a small void content is to decrease the apparent ρ (and hence increase α_ρ) with no effect on k (and hence no effect on α_k).

A second explanation is that the values of the constants v_c and v_a are incorrect. The most suspect constant is of course v_a.

A third explanation is that Hypothesis I, which is the basis for the determination of α_k, is not exact. It is clear from the approximate agreement shown in Table V that Hypothesis I is at least qualitatively correct. It could well be, however, that quantitative examination of Hypothesis I will show it to be systematically in error so that the derived α_k values are too low.

Of these three explanations we favor the first. A void content of ca. 0.3% would lower the apparent α_ρ from 19.5% to a value of 17.7% (the latter being the value of α_k determined for C_3H_6 for which the 95% confidence limits are tightest). The second explanation would imply v_a to be greater than 1.171 cc/g. The third explanation (lack of precision in Hypothesis I) we do not reject. Nevertheless, in our opinion it seems more likely that a small void content in the polyethylene specimens is the major factor causing the systematic difference between α_ρ and α_k.

The presence of a small void content also explains satisfactorily the systematic differences shown in Table VI between k^* determined at 80°C (by extrapolation of the k versus α_ρ data, Fig. 8) and k_m determined at 80°C (by extrapolation of the k versus T^{-1} data for the melt, Fig. 6).

The linear extrapolation of the volume-temperature curve of the melt to room temperature has been questioned by Swan,[25] Mandelkern et al.,[26] and by Schultz and Kavesh.[27,28] At room temperature the specific volumes quoted are $v_c = 0.994$[27,25] and 1.00 cc/g[26] and $v_a = 1.12$[27,28] and 1.11 cc/g.[26] The amorphous fractions obtained by using these values of v_c and v_a are considerably larger (approximately 50%) than the α_k and α_ρ values shown in Table V.

The solubility determination of amorphous fraction is of course entirely based on Hypothesis I and to this extent, it is not possible to attack the

specific volumes given by Kavesh and Schultz and by Mandelkern et al. Thus it could be argued (to gain agreement with Kavesh and Schultz or Mandelkern et al.) that the absorption coefficient of the amorphous fraction of the solid k^* is less than the extrapolated melt value k_m. Values of k^* equal to approximately 0.7 k_m would bring the solubility determination into agreement with the density determination based on the specific volumes of Kavesh and Schultz and of Mandelkern et al. There is no *a priori* evidence which would lead us to accept a value for k^* equal to k_m as being more likely than a value for k^* equal to 0.7 k_m. Nevertheless the acceptance of k^* equal to k_m is the simplest assumption and is certainly in satisfactory agreement with the accepted value of the specific volume.

Diffusion

An empirical relationship between log D_0 and ΔH_D has been found to hold for many rubbers and diffusing gases by Barrer,[10] Barrer and Skirrow,[29] and van Amerongen.[30] Self-diffusion in inorganic systems obeys an analogous relationship derived from an elastic continuum model by Keyes.[31]

$$\Delta S_D/\Delta H_D = 4\beta \tag{16}$$

in which β is the isobaric coefficient of volume expansion. Lawson[32] has applied this equation to the diffusion of small solute molecules in organic amorphous polymers with considerable success. In calculating ΔS_D, Lawson assumed essentially $\lambda n \nu f = 10^{12}$ sec^{-1} and $a = 10$ Å. To facilitate comparison we accept these values and calculate the values of ΔS_D and $(\Delta S_D/\Delta H_D)$ shown in Table VII. For the solid, the values of $(\Delta S_D/\Delta H_D)$ are in excellent agreement with a measured value of $4\beta = 1.4 \times 10^{-3}$ °C^{-1}.* For the melt there is no agreement whatsoever: the entropies are in fact negative in two cases. It is of course an assumption that a simple reaction-rate equation, eq. (5), is applicable above T_m. There are theories of diffusion in low molecular weight liquids which lead to temperature dependence different from eq. (5).[34,35] None of these theories however, has found support and we have therefore confined discussion to the application of eq. (5) to the results above as well as below T_m. We were unable to make use in analysis of the theory of Cohen and Turnbull[36] owing to imprecision in the definition of free volume in molten polyethylene.

There is no doubt that the mechanism of diffusion changes radically at the melting point. This change is seen both in the abrupt changes in ΔH_D and in D_0 as well as in the ratio $(\Delta S_D/\Delta H_D)$. It is clear that the parameters affecting the movement of the diffusing molecule in the melt are entirely different from those in the amorphous fraction of the solid.

For the gases studied in these experiments the ratio of the activation enthalpies for diffusion above and below T_m vary from 0.29 to 0.31 (Table IV).

* Eby has found reasonable agreement between this value of 4β and values of $(\Delta S/\Delta H)$ for the mechanical γ relaxation.[33] For the purposes of this comparison we choose β to be the coefficient of the bulk specimen and thus bypass the finer question whether or not β for the amorphous fraction alone is the more appropriate parameter.

TABLE VII
Comparison of Entropies and Enthalpies of Activation for Diffusion between Solid and Melt

Gas	Melt at 150°C		Solid at 50°C	
	ΔS_D, cal/mole-°C	$\Delta S_D/\Delta H_D$, $°C^{-1} \times 10^3$	ΔS_D, cal/mole-°C	$\Delta S_D/\Delta H_D$, $°C^{-1} \times 10^3$
C_3H_6	−3.6	−0.91	19	1.4
n-C_4H_{10}	−3.0	−0.66	21	1.4
$(CH_3)_4C$	0.3	0.05	36	1.7

VanAmerongen[16] observed ratios of activation enthalpies above and below T_m for the diffusion of hydrogen, nitrogen, oxygen and carbon dioxide in gutta-percha which ranged from 0.68 to 0.83. The explanation of the departure of the ratio from unity[37] is that as the specimen is cooled below T_m (ca. 50°C), the specimen continues to crystallize thus contributing a large term to the apparent enthalpy of activation. This may well be true in gutta-percha but cannot hold for linear polyethylene under the experimental conditions described in this paper. All the specimens were annealed, typically at 124°C for 10 hr, and then cooled slowly to room temperature. The measurements of D and k were made in the range 30–80°C and were repeatable. Other considerations, such as volumetric studies, make it certain that for these annealed specimens and in the temperature range 30–80°C there was no additional recrystallization or annealing.

It will be shown elsewhere[38] by an adaption of the theory of Wert and Zener[18] that the measurements of D for n-C_4H_{10} support the hypothesis that the γ mechanism in linear polyethylene is a platzwechsel mechanism involving the passage of small groups of atoms across a potential barrier from one equilibrium position to another. The best available evidence for the γ relaxation is that it occurs in the amorphous fraction[39–41] and is a cooperative mechanism involving the correlation of molecular segment rotation[42] and free volume.[43] If this is so, the process must be similar to the diffusion of a small n-paraffin molecule of size equal to the size of the relaxing group. The energy required to create a hole and to bring the n-paraffin molecule to the saddle point should be close to that required to create a hole and to bring the polymer relaxing group to the saddle point. It will be shown that the activation energy of the γ relaxation (11–15 kcal/mole) is very close to ΔH_D for C_2, C_3, and C_4 n-paraffins in linear polyethylene (12.5, 13.6,[15] and 14.9 kcal/mole). The argument is also supported by comparison of measured values of log D for n-C_4H_{10} and values of log ω_{max} (ω_{max} value of frequency of maximum mechanical tan δ).

CONCLUSIONS

The diffusion characteristics of small molecules in molten polyethylene and in the amorphous fraction of the solid are quite different. The amorphous fraction exhibits higher activation enthalpy and higher D_0 than the

melt: that is to say the melt shows liquidlike characteristics when compared with the amorphous fraction. It is clear that the properties of the solute molecule at the saddle point between potential wells are entirely different in melt and amorphous fraction. The equilibrium propertes of the absorbed molecule in its potential well in both melt and amorphous fraction are identical. This is shown by the close agreement between the solubility coefficient of the melt and the specific solubility coefficient of the amorphous fraction. The solubility experiments support the concept of polyethylene as a two phase solid with the amorphous fraction of specific volume approximately equal to the extrapolated specific volume of the melt.

The authors wish to thank Professor A. Charlesby and Mr. P. J. Fydelor for irradiating specimens, Professor J. M. Schultz for the communication of results before publication and Mr. A. D. LeClaire for comments on the manuscript. The work was supported by the Science Research Council.

References

1. C. E. Rogers, V. Stannett, and M. Szwarc, *J. Phys. Chem.*, **63**, 1406 (1959).
2. A. S. Michaels and R. B. Parker, *J. Polym. Sci.*, **41**, 53 (1959).
3. A. S. Michaels and H. J. Bixler, *J. Polym. Sci.*, **50**, 393 (1961).
4. P. N. Lowell and N. G. McCrum, *J. Polym. Sci. B*, **5**, 1145 (1967).
5. Lord Rayleigh, *Phil. Mag.*, [5], **34**, 481 (1892).
6. I. Runge, *Z. Tech. Phys.*, **6**, 61 (1925).
7. P. Thirion, *Proc. 3rd Rubber Technol. Conf. London*, **1954**, 334.
8. R. E. Meredith and C. W. Tobias, *J. Appl. Phys.*, **31**, 1270 (1960).
9. M. Fricke, *Physics*, **1**, 106 (1931).
10. R. M. Barrer, *Trans. Faraday Soc.*, **38**, 322 (1942).
11. G. J. van Amerongen, *J. Polym. Sci.*, **5**, 307 (1950).
12. P. Meares, *J. Amer. Chem. Soc.*, **76**, 3415 (1954).
13. G. Y. Ryskin, *Zhur Tekh. Fiz.*, **25**, 458 (1955).
14. C. H. Klute, *J. Polym. Sci.*, **41**, 307 (1959).
15. A. S. Michaels and H. J. Bixler, *J. Polym. Sci.*, **50**, 413 (1961).
16. G. J. van Amerongen, *J. Polym. Sci.*, **2**, 281 (1947).
17. A. D. LeClaire, in *Physical Chemistry, An Advanced Treatise*, W. Jost, Ed., Vol. X, Academic Press, New York, 1970.
18. G. Wert and C. Zener, *Phys. Rev.*, **76**, 1169 (1949).
19. G. Sanstede and E. Robens, *Chem. Eng. Tech.*, **32**, 413 (1960).
20. R. K. Eby, *J. Appl. Phys.*, **35**, 2720 (1964).
21. A. S. Michaels, H. J. Bixler, H. L. Fein, *J. Appl. Phys.*, **35**, 3165 (1964).
22. N. G. McCrum, *Polymer*, **5**, 319 (1964).
23. A. Peterlin, J. L. Williams, and V. Stannett, *J. Polym. Sci. A-2*, **5**, 957 (1967).
24. S. Matsuoka, *J. Appl. Phys.*, **32**, 2334 (1961).
25. P. R. Swan, *J. Polym. Sci.*, **42**, 525 (1960).
26. L. Mandelkern, J. G. Fatou, R. Denison, and J. Justin, *J. Polym. Sci. B*, *3*, 803 (1965).
27. S. Kavesh and J. M. Schultz, *J. Polymer Sci. A-2*, **9**, 85 (1971).
28. J. M. Schultz, private communication.
29. R. M. Barrer and G. Skirrow, *J. Polym. Sci.*, **3**, 549 (1948).
30. G. J. van Amerongen, *J. Appl. Phys.*, **17**, 978 (1946).
31. R. W. Keyes, *J. Chem. Phys.*, **29**, 467 (1958).
32. A. W. Lawson, *J. Chem. Phys.*, **32**, 131 (1960).
33. R. K. Eby, *J. Chem. Phys.*, **37**, 2785 (1962).

34. G. Carere, A. Paoletti, and M. Vincentini, *Nuovo Cimento*, **10**, 1088 (1958).
35. B. N. Brockhouse, and N. K. Pope, *Phys. Rev. Letters*, **3**, 259 (1959).
36. M. H. Cohen and D. Turnbull, *J. Chem. Phys.*, **31**, 1164 (1959).
37. G. J. van Amerongen, *Rubber Chem. Technol.*, **37**, 1065 (1964).
38. P. N. Lowell and N. G. McCrum, *Polymer Letters*, **9**, 477 (1971).
39. R. W. Gray and N. G. McCrum, *J. Polym. Sci. A-2*, **7**, 1929 (1969).
40. H. G. Olf and A. Peterlin, *Kolloid-Z.*, **215**, 97 (1967).
41. K. Bergmann and K. Nawotki, *Kolloid-Z.*, **219**, 132 (1967).
42. H. G. Olf and A. Peterlin, *J. Polym. Sci. A-2*, **8**, 771 (1970).
43. F. C. Stehling and L. Manderlkern, *Macromolecules*, **3**, 242 (1970)

Received December 7, 1970

JOURNAL OF POLYMER SCIENCE: PART A-2 VOL. 9, 1955–1976 (1971)

Emulsion Polymerization of Styrene in a Single Continuous Stirred-Tank Reactor

ANDREW W. DeGRAFF* and GARY W. POEHLEIN,† *Department of Chemical Engineering, Lehigh University, Bethlehem, Pennsylvania 18015*

Synopsis

The effects of mean residence time, initiation rate, and emulsifier concentration on particle formation, particle growth, and polymerization rate are examined for the emulsion polymerization of styrene in a completely mixed continuous stirred-tank reactor. Experimental measurements of number of particles, particle size distribution, polymerization rate, and molecular weights are compared with theoretical predictions. A theoretical model which incorporates Stockmayer's modification of the Smith-Ewart theory into the particle growth equation allows reasonably accurate prediction of polymerization rate, particle formation rate, and particle size distribution. Agreement between experimental measurements of number-average and weight-average molecular weights and a theory based on Smith-Ewart case 2 kinetics is also reasonable.

INTRODUCTION

A continuous stirred-tank reactor (CSTR) consists of a single vessel equipped with a mechanical agitator to provide rapid mixing of the inflowing reagent streams. Polymerization studies in a CSTR can be useful for two reasons. First, the results can be applied to the design of commercial systems. Second, the data can be more discriminatory than batch data for the elucidation of some process mechanisms.

Large-scale continuous systems have been used in polymer production for more than twenty years. Early papers describe the synthesis of rubbers[1–3] and poly(vinyl chloride).[4] More recent work has involved styrene,[5] methyl acrylate,[5] ethylene,[6] vinyl chloride,[7] and copolymers of ethylene and vinyl chloride.[8]

Continuous processes are destined to become more important in the future.[9] Growing production rates will provide economic incentives. Other factors, such as reduced product quality fluctuations and the ability to manufacture products difficult to produce in batch reactors will provide additional impetus toward continuous operation.

The potential differences in product characteristics can be extremely important for reactor designers who may face the task of designing commercial

* Present address: Jackson Laboratories, E. I. duPont de Nemours & Co., Deepwater, New Jersey 08023.

† To whom correspondence should be addressed.

continuous systems on the basis of laboratory data obtained from batch reactors. For example, Wall and co-workers[10] have shown that differences in molecular composition heterogeneity can be expected between copolymer products from batch reactors and CSTR's. Graessley and Nagasubramanian[11] have demonstrated that molecular size characteristics of the products of the two kinds of reactors can be different if branching reactions are important. We have found that the latex particle-size distribution in the product of a CSTR is different from a batch reactor product.

The second motivation for the use of continuous tank reactors in laboratory studies results from the ease and accuracy of analyzing a steady-state process. As early as 1947 Denbigh[12] discussed the advantages of using a "homocontinuous" reactor for polymerization studies. The differences between a single CSTR and a batch reactor are significant in emulsion systems. The theory proposed by Harkins[13] and Smith and Ewart[14] for batch reactions includes three intervals: the first that of particle formation, the second the growth of particles swollen at equilibrium with monomer, and the third that of polymerization of the remaining monomer in the partially swollen particles. In a CSTR operating at steady state, particles are formed continuously in the presence of many existing particles. The data obtained from such a system includes the rate of particle formation along with a rather complete knowledge of the state of the reaction mixture which yields this rate. Possibly a more complete understanding of particle formation rates can be obtained from such data.

A second major difference between batch reactors and CSTR's is the time for particle growth. In a batch reactor almost all particles are formed at low conversions, and they grow rather uniformly until all the monomer is polymerized. The particles formed in a CSTR, however, leave the reactor with broadly distributed ages. This, of course, leads to a different latex product.

The theoretical model for a CSTR presented in this paper is an attempt to explain the performance of such a reactor for the emulsion polymerization of styrene. Studies are continuing with other, more water-soluble, monomers.

THEORY

The mathematical model presented in this paper was, to a large extent, given by Gershberg and Longfield[15] in a paper which has not been published in the open literature. We have altered the original derivation by removing an unnecessary assumption, by expanding the particle-size distribution theory, and by including consideration of molecular weights. The framework of the theory is rather general. Some of the specific relationships, however, will probably require modification as more experimental data become available, especially for monomer systems more water soluble than styrene.

The theory is applicable only when the mean residence time is much

larger than the average time between the entry of free radicals into a particle. All of the data presented meet this criterion.

Particle Generation

Polymer particles could conceivably be formed by several mechanisms. Free-radical oligomers in the aqueous phase could diffuse into micelles as Harkins suggested. Also, the growing oligomer chains might become stabilized by adsorbed surfactant before or after coalescence or termination with similar chains in the aqueous phase. Many of the free radicals initiated in the water phase, however, will eventually be absorbed by existing particles instead of forming new particles. The particle formation relationship in eq. (1) is equivalent to Smith and Ewart's model, which assumes that the free radicals would be divided between particles and micelles in direct proportion to surface area:

$$N = R_i \theta N_A (A_f / a_s S N_A) \tag{1}$$

where N is the particle concentration, R_i is the rate of free radical initiation, θ is the mean residence time of reagents and particles in the reactor, N_A is Avogadro's number, S is the total surfactant concentration, a_s is the area occupied by one molecule of adsorbed surfactant, and A_f is the area that could be covered by the unadsorbed surfactant, which may exist in the form of micelles or as molecularly dissolved species.

The simple relation given in eq. (1) will probably not account for all the foregoing particle initiation mechanisms. As will be demonstrated later, however, it does provide a reasonable model for styrene polymerization.

Particle Growth

The growth of emulsion polymer particles, at least for styrene, is quite well understood. Early experimental studies by Roe and Brass[16] and Vanderhoff and co-workers[17] and subsequent theoretical treatments by Stockmayer[18] and O'Toole[19] make eq. (2) a widely accepted growth relation:

$$dV/dt = 4\pi r^2 dr/dt = K_1[\mathrm{M}]\bar{n} \tag{2}$$

where V is the particle volume, r is the radius, t is time, [M] is monomer concentration in the monomer-swollen polymer particle, K_1 is a constant dependent on the monomer, the amount of monomer swelling of the polymer particles, and reaction conditions, and $\bar{n}$ is the average (in a time sense) number of free radicals in the particle.

If the particles are small, corresponding to Smith and Ewart's case 2 model, $\bar{n}$ is 0.5, and the volumetric growth rate dV/dt is constant. When the particles become larger, $\bar{n}$ increases above 0.5 and the growth rate accelerates; $\bar{n}$ might also be greater than 0.5 during the very early stages of growth. If particles are formed according to the Harkins mechanism they would contain one free radical from the instant of formation until the second enters with subsequent termination.

Equation (3) was derived by Stockmayer for the case in which free radicals do not desorb from the growing particle:

$$\bar{n} = (a/4)[I_0(a)/I_1(a)] \tag{3}$$

where

$$a = (8V/k_t\tau)^{1/2}$$

k_t is the termination rate constant, $I_0(a)$ and $I_1(a)$ are Bessel functions of the first kind, and τ is the average time between successive entries of free radicals into the particle. This equation does not account for $\bar{n} > 0.5$ during the early stages of growth but it does predict the accelerating growth for large particles.

Residence Time Distribution

The distribution of residence times in a completely mixed stirred-tank reactor is given by:

$$g(t) = \theta^{-1}e^{-t/\theta} \tag{4}$$

If one assumes that particles are formed uniformly throughout the reactor, eq. (4) also describes the age distribution of the particles in the latex product. Zwietering[20] gives a more complete discussion of the relations between residence time and age distributions.

Particle Size Distribution

The distribution of particle sizes can be derived from eqs. (2) and (4). A simplified solution is obtained for the ideal case in which $\bar{n} = 0.5$. In this case, eq. (2) can be integrated analytically to give particle size as a function of age:

$$r^3 = r_0^3 + (3K_1[\mathrm{M}]/8\pi)t \tag{5}$$

where r_0 is the particle size at $t = 0$, the instant of particle formation. For those who prefer the Harkins model, r_0 may be considered the micelle size, or it could represent a critical nucleus size. In either case r_0 will be small relative to r and it can safely be neglected for all but small values of particle age t.

The distribution of particle radii $U(r)$ can be obtained by combining eqs. (2) and (4) to obtain:

$$\begin{aligned} U(r) &= \frac{g(t)}{|dr/dt|} \\ &= \theta^{-1}e^{-t/\theta}(4\pi r^2/K_1[\mathrm{M}]\bar{n}) \end{aligned} \tag{6}$$

If eqs. (5) and (6) are combined and $\bar{n}$ is assumed to be 0.5, the following relation is obtained for $U(r)$:

$$U(r) = (8\pi r^2/K_1[\mathrm{M}]\theta)\exp\{-8\pi(r^3 - r_0^3)/3K_1[\mathrm{M}]\theta\} \tag{7}$$

or if

$$r_0 \approx 0$$

$$U(r) = K_2 r^2 \exp\left\{-K_2 r^3/3\right\} \tag{8}$$

where

$$K_2 = 8\pi/K_1[\mathrm{M}]\theta.$$

The cumulative distribution function which is the usual quantity employed for plotting experimental data is given by eq. (9).

$$\mathfrak{U}(r) = \int_0^r U(r')dr' = 1.0 - \exp\left\{-K_2 r_3/3\right\} \tag{9}$$

If the particles grow large enough for $\bar{n} > 0.5$, Stockmayer's relation, eq. (3), must be used to determine the relation between r and t. This calculation is straightforward when numerical techniques are employed on a digital computer. Details are given by DeGraff[21]

Number of Particles and Polymerization Rate

Equation (1) for the number of particles has one undetermined parameter, A_f. This free surfactant is the difference between the surfactant charged and the surfactant adsorbed on the surface of the polymer particles as given by:

$$A_f = a_s S N_A - A_p \tag{10}$$

where A_p, the area of the polymer particles can be evaluated from a knowledge of the particle size distribution as given by:

$$A_p = N \int_0^\infty 4\pi r^2 U(r)dr \tag{11}$$

Substituting the relation for $U(r)$ of eq. (8) into this expression and carrying out the integration gives the following expression for A_p:

$$A_p = 3.61\pi(3/K_2)^{2/3}N \tag{12}$$

Combining eqs. (12), (10), and (1) and evaluating the parameter K_2, gives a final equation relating N to the reactor variables:

$$\frac{R_i\theta N_A}{N} = 1.0 + (\alpha_0 R_i\theta/a_s S)\left\{k_p[\mathrm{M}]\theta/(1 - \alpha_1[\mathrm{M}])\right\}^{2/3} \tag{13}$$

where k_p is the propagation rate constant, $\alpha_0 = 3.85\ (M_0 V_p)^{2/3}$, $\alpha_1 = M_0 V_m \times 10^{-3}$, M_0 is the monomer molecular weight, and V_p and V_m are the specific volumes of polymer and monomer, respectively. Equation (13) is written in dimensionless form. The quantity, $1 - \alpha_1[\mathrm{M}]$, is the volume fraction of polymer in the particles swollen with monomer.

The rate of polymerization R_p for a Smith-Ewart (S-E) case 2 system is given by:

$$R_p = k_p[\mathrm{M}]N/2N_A \tag{14}$$

Combining eqs. (13) and (14), therefore, yields a dimensionless rate equation:

$$R_i\theta k_p[\mathrm{M}]/2R_p = 1 + (\alpha_0 R_i\theta/a_s S)\{k_p[\mathrm{M}]\theta/(1 - \alpha_1[\mathrm{M}])\}^{2/3} \tag{15}$$

As was true in earlier developments, if some particles grow large enough for $\bar{n} > 0.5$, a numerical solution which incorporates Stockmayer's equation can be obtained on a digital computer.

Molecular Weight Properties

Two major factors contribute to the distribution of molecular weight in the latex product from a CSTR. First, the stochastic process for the entry of free radicals into particles leads to molecular size variations among particles of similar size. Second, the distribution of particle sizes leads to large predicted differences in average arrival rates of free radicals, with the larger particles capturing free radicals at a faster rate than small particles. This fact causes an added broadening of the molecular weight distribution.

Katz et al.[22] considered the problem of molecular size distribution of polymer being formed in a monodisperse particle system. They showed that the ratio X_w/X_n, of the weight-average to number-average degree of polymerization, for the case of coupling termination, varies from 2.0 for small particles (Smith-Ewart case 2 polymerization) to 1.5 for large particles (bulk polymerization). Their derivations assumed that the mean arrival rate of free radicals and the mean rate of chain growth were not time variant. Thus, in a batch reactor the predictions of Katz et al. would only apply to the polymer formed in the midconversion ranges. Such is not the case, however, with a steady-state stirred-tank reactor, where the conditions assumed by Katz et al., with the exception of particle monodispersity, do exist.

In the derivation which follows, the results of Katz et al.[22] for Smith-Ewart case 2 polymerization will be expanded to include the polydisperse latex product of a CSTR. We begin with eq. (16), which describes the size distribution of the polymer being formed in a particle of radius r:

$$f(x) = (B/G) \exp\{-Bx/G\} \tag{16}$$

where x is the degree of polymerization, B is the mean rate of free radical arrival, and G is the mean rate of radical propagation. We note that X_w/X_n is 2.0 for this distribution and that B would be equal to R_iN_A/N for a monodisperse latex.

If the latex is polydisperse, B becomes a function of particle size (i.e., of r). The nature of this functionality depends on the model chosen for the

movement of free radicals into particles. If one assumes a uniform radical uptake per unit of surface area eq. (17) applies.

$$B = (R_i N_A/N)(r^2/\langle r^2\rangle) \tag{17}$$

where $\langle r^2\rangle$ is the expectation of r^2.

If, on the other hand, one applies continuum diffusion theory, which predicts diffusion flux proportional to $1/r$, B is given by:

$$B = (R_i N_A/N)(r/\langle r\rangle) \tag{18}$$

The basis for eq. (18) was presented by Flory.[23] The derivation given by Flory assumes a steady-state concentration gradient with spherical symmetry within an infinite container. Gardon[24] suggested that these assumptions are not valid and used a model based on Brownian motion to predict that particles absorb radicals at a rate proportional to their surface, i.e., as predicted by eq. (17).

In order to determine the overall distribution of molecular sizes in polydisperse systems one must "weight" the contributions of all particles. Such a weighting is given by:

$$\overline{f(x)} = (R_i N_A/N) \int_0^\infty Bf(x)U(r)dr \tag{19}$$

This relation assumes that the rate of polymer production (on a mass basis) is not a function of particle size; i.e. as in Smith-Ewart case 2 polymerization. We note that $\overline{f(x)}$ is a number distribution and that, on a number basis, those particles with the higher radical-arrival rates are producing polymer molecules at a faster rate. These molecules, however, have a smaller mean size. Thus the polymer produced in the larger particles should have the lowest molecular weight.

Although the concept of some sort of distribution of free radical flux according to particle size is widely accepted in the literature, molecular weight data are somewhat confusing. Morton et al.[25] found that 400 and 800 Å particles fractionated from the same latex had the same molecular weight. Williams and Grancio[26] found that molecular weight increased substantially during periods of constant growth rate for monodisperse polystyrene latexes. They suggest that radical utilization efficiencies of less than 100% may be responsible for such observations.

In contrast to batch reactors, the steady-state nature of a completely mixed CSTR will eliminate extraneous effects due to possible changes in the reaction mixture. Thus the distribution described by eq. (19) should characterize the latex product from a CSTR unless our mechanistic concepts are incorrect.

If a specific model is chosen for the free-radical arrival rate B, the distribution $\overline{f(x)}$ can be used to calculate X_n and X_w via the standard tech-

niques of probability theory. The use of eq. (17) for B leads to the following results:

$$X_n = \langle x \rangle = NG/R_iN_n = G/\langle B \rangle \tag{20}$$

$$X_w = \langle x^2 \rangle / \langle x \rangle = 4.84G/\langle B \rangle \tag{21}$$

Thus $X_w/X_n = 4.84$, considerably larger than the value 2.0 predicted for monodisperse systems. If the diffusion model as represented by eq. (18) is used for B, the number-average degree of polymerization is the same, as given by eq. (20). The weight-average however is different and is given by:

$$X_w = 1.88K_2^{1/3} \tag{22}$$

Thus X_w/X_n for this model is not a single numerical value, but a function of the variables K_2, G, and B. A qualitative comparison of the two models, however, shows that the following relation will exist for all operating conditions.

$$\begin{array}{ccccc} 2.0 & < & X_w/X_n & < & 4.84 \\ \text{Monodisperse latex} & & \text{Continuum diffusion model} & & \text{Equal flux model} \end{array} \tag{23}$$

Equation (23) follows directly from the fact that in the diffusion model, smaller particles are more efficient, on an area basis, as collectors of free radicals. This difference in efficiency will, in a relative sense, decrease the average molecular size differences between particles of different sizes.

EXPERIMENTAL

Reactor System

A flow diagram of the experimental apparatus is shown in Figure 1. Two separate feed streams, monomer and a water solution of initiator and surfactant, were fed at a constant rate by Milton-Roy duplex volumetric pumps. These pumps maintained a set volumetric feed-rate ratio* for water solution and monomer. The reactor had 480 ml working capacity and was stirred by a flat-blade paddle rotating at about 190 rpm. The feed tubes, temperature controller, and nitrogen purge line provided adequate baffles to insure good mixing. The assumed exponential distribution of residence times was confirmed with experimental salt-tracer studies.

The reactor and raw material storage tanks were blanketed with nitrogen to prevent oxygen retardation. The effluent emulsion was collected and continuously stirred in a vessel containing the inhibitor hydroquinone. Experimental runs were continued for at least eight mean residence times to assure steady-state operation. The polymerization rate, as measured by monomer conversion, had reached a steady-value well before this time;

* Monomer/water ratios in the reactor feeds varied from 0.43 to 0.67 but in most runs were around 0.54.

normally between two and three mean residence times. The conversion in all runs was below 50%; low enough to assure the presence of a free monomer phase in the latex product and therefore an equilibrium monomer concentration in the growing latex particles.

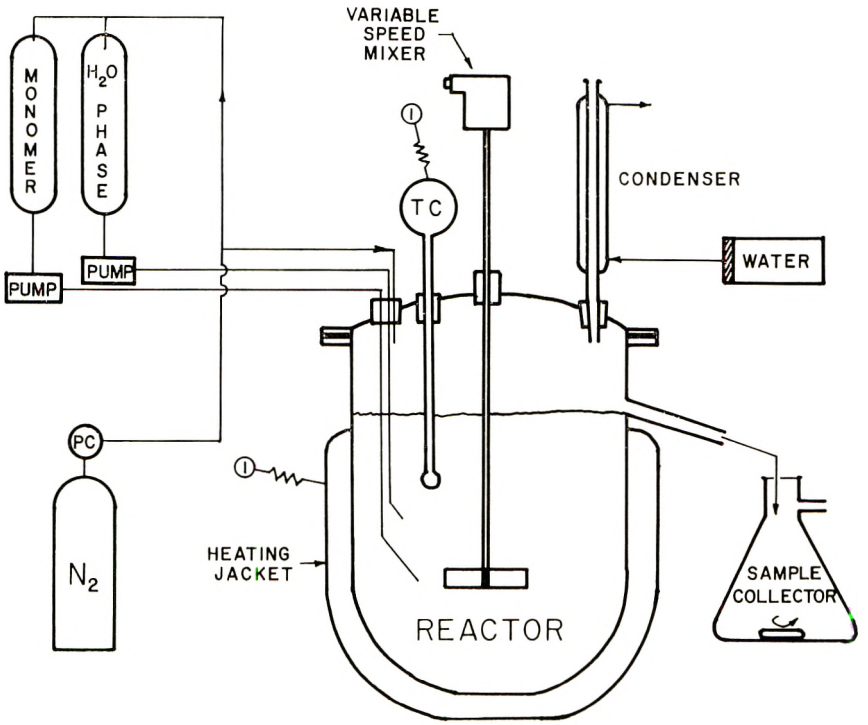

Figure 1. Flow diagram.

Raw Materials

Styrene was supplied, with inhibitor, by the Dow Chemical Company. The inhibitor was removed by multiple washing with 5% caustic as outlined by Boundy and Boyer.[27] The initiator, ammonium persulfate, and the surfactant, sodium lauryl sulfate, were supplied by Fisher Scientific Co. Numerical values for the rate constants and other independently measured variables are listed in Table I. These values were used for all theoretical calculations. The experimental data obtained in this work were not used to determine the value of any of the variables appearing in the theoretical equations.

The experimental studies of Gerrens and Kuchner,[5] and of Gershberg and Longfield[5] which are discussed below involved the same raw materials except for the surfactant. Gershberg and Longfield used a GR-S type emulsifier, and Gerrens and Kuchner used a Mesolate emulsifier. Values for the adsorption areas of these materials are also given in Table I.

TABLE I
Experimental Constants

Constant	
V_p, cm³/g	0.95
V_m, cm³/g	1.139
a_s, Å²/molecule	
Sodium lauryl sulfate[a]	61
GR-S type emulsifier[b]	28
Mersolate emulsifier[c]	42
[M], mole/l.[d]	5.2
k_p, l./mole-sec[d]	
At 50°C	125
At 70°C	265
At 100°C	975
k_t, l./mole-sec[d]	
At 50°C	2.1×10^5
At 70°C	7.2×10^6
Initiation rate $R_i = 2k_d[I]$[e]	
k_d, l./sec[f]	
At 40°C	2.2×10^{-7}
At 50°C	1×10^{-6}
At 70°C	2.33×10^{-5}
At 100°C	1.4×10^{-3}

[a] Data of Brodnyan and Brown.[28]
[b] Data of Gershberg and Longfield.[15]
[c] Data of Gerrens and Kuchner.[5]
[d] Data of Van Der Hoff.[29]
[e] [I] is in units of mole/l.
[f] Data of Miller and Kolthoff.[30]

Measurement Techniques

Particle number, particle size distribution, rate of polymerization, and the number-average and weight-average molecular weights were measured as outlined below.

Particle size distribution and particle concentration were measured with an electron microscope. The samples were prepared by the technique suggested by Maron et al.[31] The resolution of the electron microscope was limited to particles larger than 80–100 Å. This measurement is somewhat inaccurate for experimental runs at low residence times because theory predicts a number of particles below 100 Å in diameter. Light-scattering measurements were used to check the electron microscope values for more than 30 samples. A light-scattering diameter was calculated from the distribution function obtained from the electron microscope measurements. These diameters were then compared with the measured light-scattering diameters. The average percentage difference (absolute value) was 9%. One must remember, however, that light scattering places more weight on the large particles. Thus, this comparison does not assure accuracy of the electron microscope measurements in the small size range.

Rate of polymerization was measured by gravimetric analysis. The polymer product was coagulated, dried in a vacuum oven and weighed.

Number-average and weight-average molecular weights were determined with a calibrated gel-permeation chromatograph unit (Air Products and Chemicals Inc.). The results from GPC were checked by light-scattering measurements in our laboratories for three samples. The light-scattering values were higher with an average deviation of +6.7%.

RESULTS AND DISCUSSION

Particle Size Distribution

The prediction of particle size distribution in the product from a CSTR requires less knowledge about the process than is necessary for the theoretical calculation of any of the other dependent variables such as: rate of polymerization, number of particles formed, molecular weights, etc. If stochastic variations and particle coalescence do not substantially influence the distribution, it may be calculated from a knowledge of the distribution

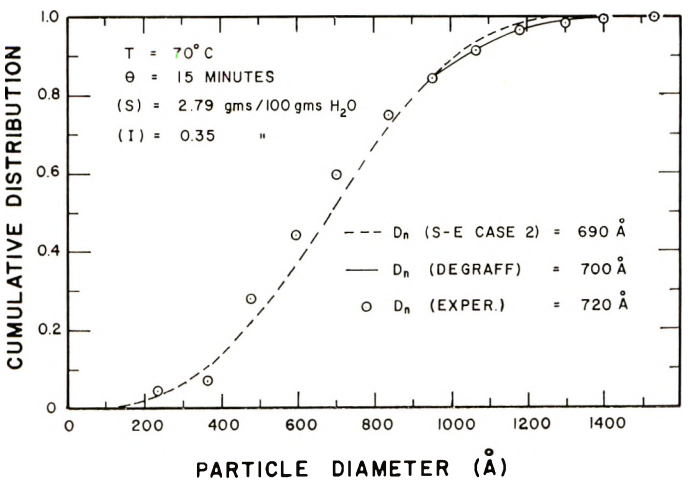

Fig. 2. Particle size distribution.

of residence times and a particle growth equation. Equations (8) and (9) for the differential and cumulative distributions result from a theory based on the Smith-Ewart case 2 assumptions: that is, $\bar{n} = 0.5$, and thus the volumetric growth rate of all particles is constant and equal.

If some particles in the latex grow large enough for $\bar{n}$ to become greater than 0.5, Stockmayer's relation can be incorporated into the particle-growth equation. Stockmayer's model predicts that $\bar{n}$ will increase with particle size and thus the volumetric growth rate of a particle will also increase with size. For the limiting case of very large particles (bulk kinetics) Stock-

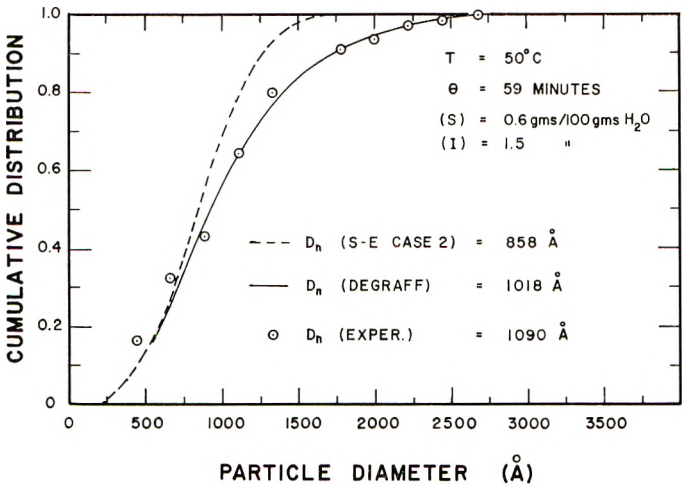

Fig. 3. Particle size distribution.

mayer's modification predicts that volumetric growth will be directly proportional to particle volume, i.e.,

$$dV/dt \propto V$$

or

$$dr/dt \propto r \tag{24}$$

We were not able to obtain a closed solution for the particle size distributions similar to eqs. (8) and (9) for the modified particle-growth theory. These distribution functions were, however, evaluated numerically on a digital computer. The procedure for obtaining the numerical solution involved first assuming values for N and $\langle r \rangle$, the number of particles, and the average radius. Then Stockmayer's relation was used in eq. (6) to calculate the particle size distribution. This was followed by the calculation of N and $\langle r \rangle$ with the use of eqs. (1), (10), and (11). If the calculated values of $\langle r \rangle$ and N did not agree with the previously assumed values, the assumptions were altered and the procedure repeated until convergence was obtained.

Figures 2 and 3 show a comparison between the experimental cumulative particle distribution and the predictions of the two theories, i.e., eq. (9) for the S-E case 2 theory and the numerical solution for the Stockmayer modification. Both theories show good agreement with the experimental data for the run with the short (15 min) mean residence time, as is shown in Figure 2. The difference between the two theories is more pronounced at the longer (59 min) mean residence time (Fig. 3) because larger particles are formed. Since these larger particles contain, on the average, a higher number of free radicals and thus experience more rapid growth, the experimental particle size distribution is skewed toward the large end. The

model based on S-E case 2 kinetics does not predict this behavior but the model which includes Stockmayer's modification does agree with the data.

Figure 4 shows the influence of mean residence time on the breadth of the distribution. The breadth increases at larger mean residence times because of the broader distribution of residence times and because of the production of larger particles with $\bar{n} > 0.5$. The use of the modified theory for particle growth would be even more important for prediction of particle

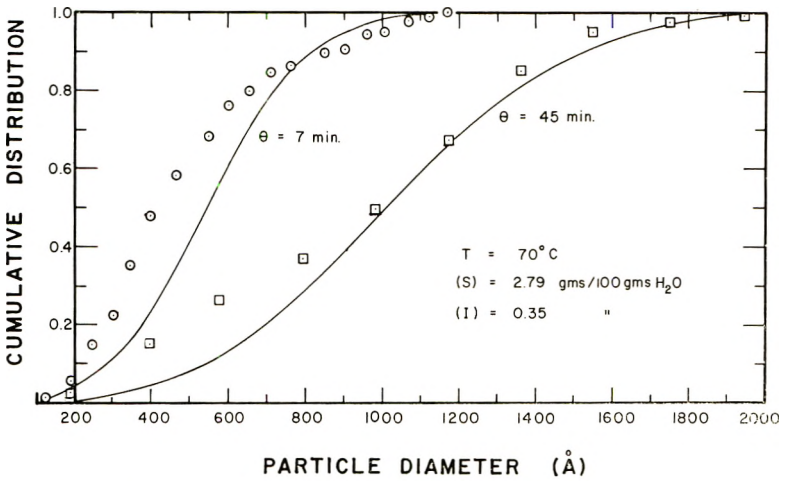

Fig. 4. Influence of mean residence time on particle size distribution.

size distributions in processes involving several stirred tanks in series. Continued particle growth after the first reactor could lead to particles with even larger values of $\bar{n}$.

Particle Formation and Polymerization Rate

Rate of polymerization and particle-number predictions of the S-E case 2 model are given by eqs. (13) and (15). The relation assumed for particle formation, eq. (1), can be rearranged to a dimensionless form similar to eqs. (13) and (15) as follows:

$$R_i \theta N_A / N = 1 + (A_p / A_f) \tag{25}$$

Gershberg and Longfield (15) suggested a comparison of this equation with eqs. (13) and (15) to show that the second term on the right side of eqs. (13) and (15) has simple physical significance. It represents the ratio of surfactant adsorbed on the monomer-polymer particles to the unadsorbed surfactant. If this ratio is small ($\ll 1.0$), the number of particles formed and the rate of polymerization are directly proportional to both initiation rate and mean residence time. The emulsifier concentration has no effect under such conditions because all initiated free radicals become stabilized particles.

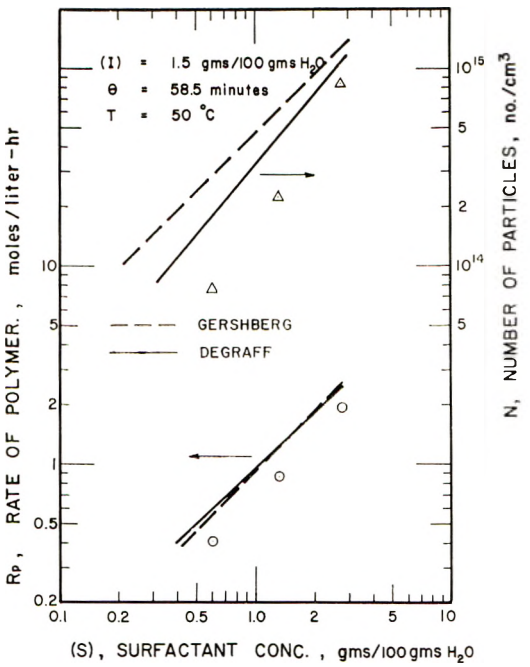

Fig. 5. Emulsifier effects on particle formation and polymerization rate.

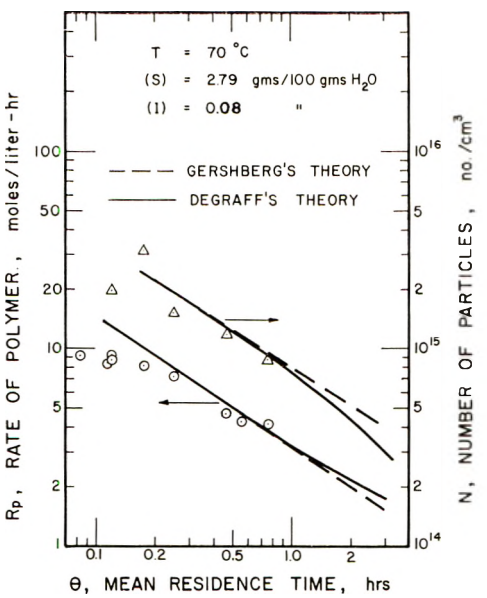

Fig. 6. Influence of mean residence time on particle formation and polymerization rate.

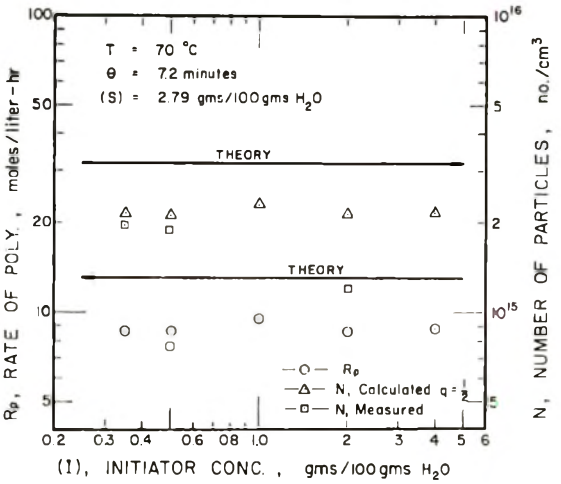

Fig. 7. Initiation effects on particle formation and polymerization rate.

The conditions necessary to maintain $A_p/A_f \gg 1$ are usually so impractical that just the opposite is normally true; that is:

$$A_p/A_f \gg 1$$

In this case eq. (13) reduces to:

$$N = (a_s S N_A/\alpha_0)\{k_p[M]\theta/(1 - \alpha_1[M])\}^{-2/3} \tag{26}$$

Thus polymerization rate and number of particles formed are directly proportional to surfactant concentration and to the $-2/3$ power of the mean residence time. Initiation rate has no influence.

If the polymerization conditions are outside the S-E case 2 range, the above equation will be somewhat inaccurate. Particles for which $\bar{n} > 0.5$ will grow larger than predicted and thus consume more adsorbed soap than predicted. Under these conditions, the theory of DeGraff,[21] which includes the Stockmayer growth relation, will predict the formation of fewer particles than is in accord with the S-E case 2 theory. The total rate of polymerization can be expressed as:

$$R_p = (k_p[M]/N_A)\bar{n}N \tag{27}$$

Since decreases in N result from increases in $\bar{n}$, the rate of polymerization may not decrease.

Figures 5, 6, and 7 show the influence of surfactant concentration, mean residence time, and initiation rate on particle formation and polymerization rate. Experimental measurements follow the trends of both theories but quantitative agreement is not always good.

Differences between theory and experiment can be due to several factors. First, the model for particle formation based on area ratios might be inaccurate. Second, the parameters such as rate constants, surfactant area

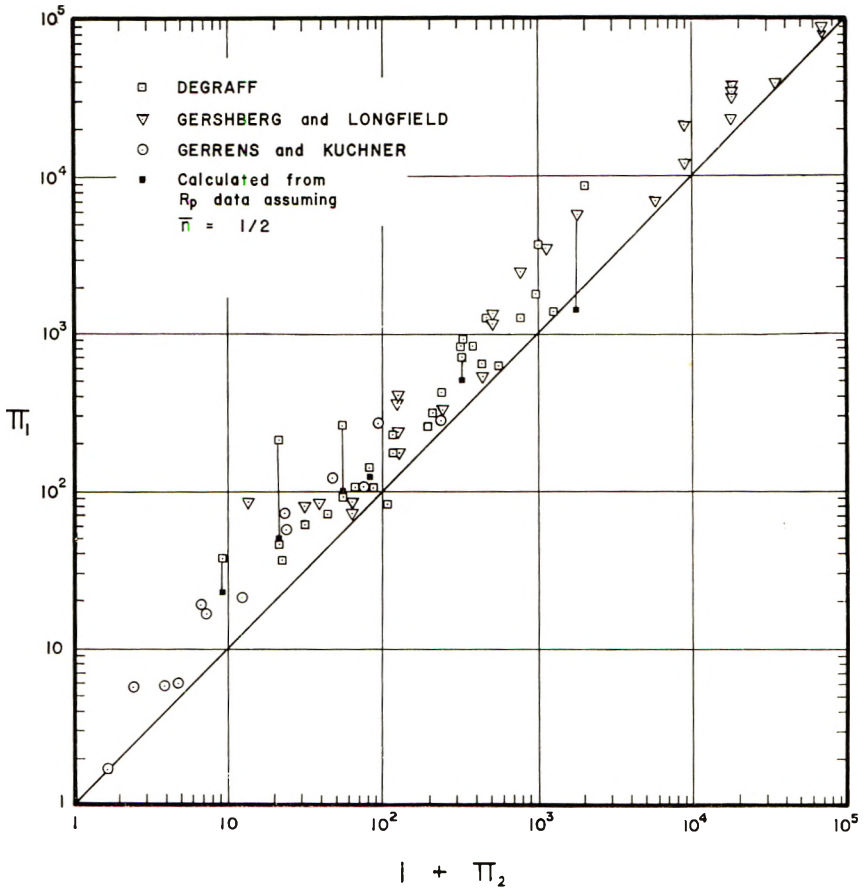

Fig. 8. Particle number correlation.

coverage, monomer concentration, etc., used in the theoretical equations might be incorrect. Third, experimental errors could be significant in some measurements, especially those involving particle numbers and size distributions at small values of the mean residence time.

Equations (13) and (15) are written in dimensionless form and thus suggest a convenient method of comparing experimental results obtained by different investigators over a wide range of experimental conditions. Figures 8 and 9 show experimental data from this work, those of Gerrens and Kuchner,[5] and those of Gershberg and Longfield[15] compared with the S-E case 2 theory which is represented by the 45° solid line. The dimensionless groups used are defined by eqs. (28)–(30).

$$\pi_1 = R_i\theta N_A/N \tag{28}$$

$$\pi_2 = (\alpha_0 R_i\theta/a_s S)^{\frac{1}{2}} k_p[\mathrm{M}]\theta_i/(1 - \alpha_i[\mathrm{M}])^{\frac{1}{2}} \tag{29}$$

$$\pi_3 = R_i\theta k_p[\mathrm{M}]/2R_p \tag{30}$$

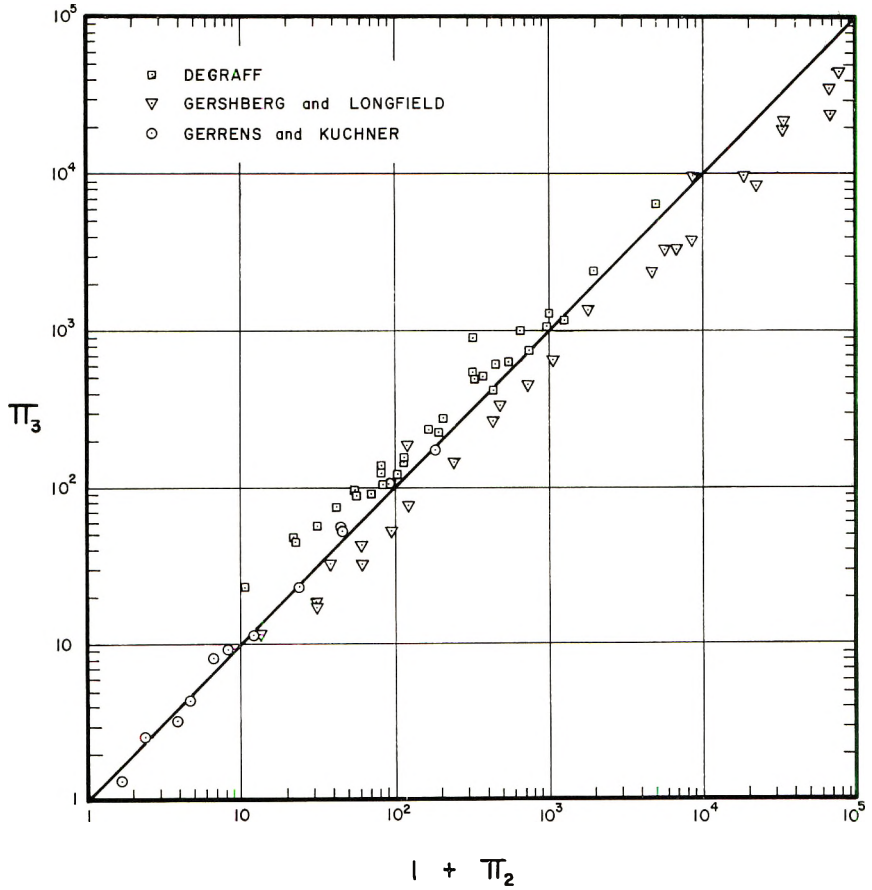

Fig. 9. Polymerization rate correlation.

Nearly all the data points in Figure 8 fall above the 45° line of the S-E case 2 theory, indicating that fewer particles are measured than predicted. Both experimental errors and deviations from the theory cause changes in this direction. Data on rate of polymerization (Fig. 9) fit the theory better because the experimental measurements are more accurate and because deviations from S-E case 2 kinetics involving smaller N and larger $\bar{n}$ tend to cancel, as eq. (27) suggests.

Considering the numerous possibilities for errors in components of the theoretical calculations and in the experimental measurements, the agreement theory and experiment is acceptable. Certainly the expanded theory is adequate for reactor design calculations.

Molecular Weight

The number-average molecular weight can be evaluated from eq. (20). The weight-average molecular weight, however, depends on the free-radical diffusion model [eq. (17) or eq. (18)], the size of the particles, and the significance of the $\bar{n} > 0.5$ phenomena at and shortly after particle initiation.

The weight-average molecular weight could be as large as $4.84\bar{M}_n$ if S-E case 2 conditions prevail and the radical diffusion flux is constant [eq. (17)]. A number of factors, however, will tend to reduce $\bar{M}_w$ below $4.84\bar{M}_n$. First, the diffusion flux may be as described by continuum theory,

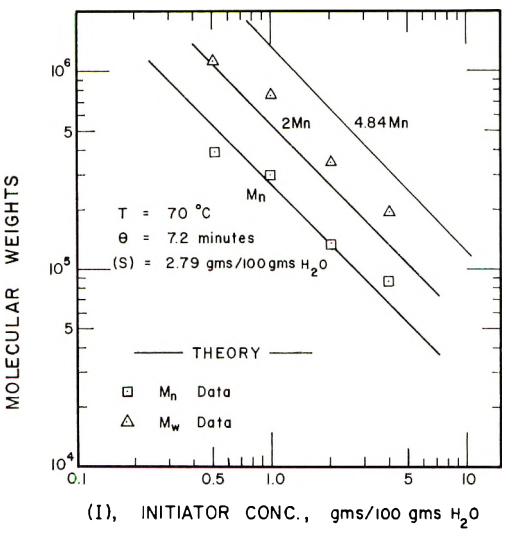

Fig. 10. Influence of initiation rate on molecular weights.

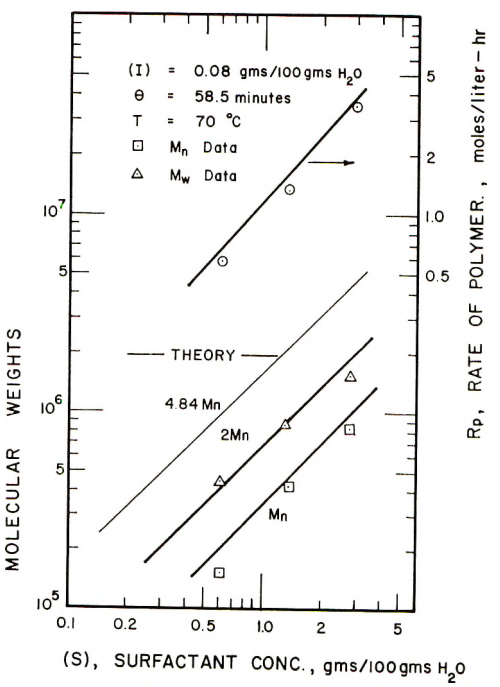

Fig. 11. Influence of surfactant concentration on molecular weights and rate of polymerization.

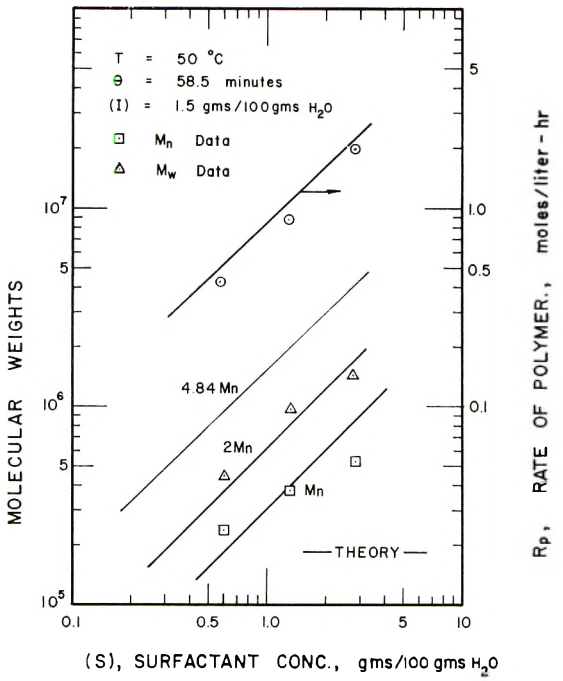

Fig. 12. Influence of surfactant concentration of molecular weights and rate of polymerization.

eq. (18). Second, the distribution of polymer being formed in particles large enough for $n > 0.5$ will be narrower than that being formed when $n \approx 0.5$ as indicated by Katz et al.[22] Third, the theoretical development includes particles down to $r = 0$. Experimental work indicates that a newly formed particle is substantially larger than $r = 0$. Thus the high molecular weight material which theory predicts for extremely small particles will not be present in the product.

Figures 10–13 show the influence of initiation rate, surfactant concentration, and mean residence time on molecular weight. The theoretical predictions were computed completely from the equations derived. Predicted, not measured, value of N, R_p etc. were used in the molecular weight equations.

Since R_i does not exert an influence on the number of particles formed or on the rate of polymerization, one would expect a linear decrease in $\bar{M}_n$ with increasing R_i. The agreement shown in Figure 10 supports this expectation. $\bar{M}_n$ and $\bar{M}_w$ increase with surfactant because more particles are formed to share the free radicals being generated. Figures 11 and 12 show this effect for two polymerization temperatures (50 and 70°C).

Figure 13 shows the effect of mean residence time on molecular weight. The agreement between experiment and theory is reasonable at large values of θ but poor for low values. This type of behavior is not restricted to molecular weight but is also observed for particle concentration and polym-

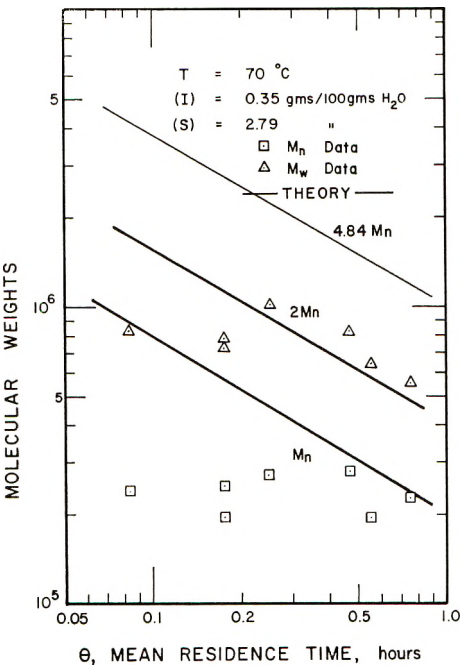

Fig. 13. Influence of mean residence time on molecular weights.

erization rate (see Figs. 6 and 7). Molecular weight predictions are high, however, even if experimental values of N are used for the calculation. Thus errors in molecular weight cannot be solely attributed to incorrect predictions of N.

Differences between measured values of particle concentration N and theoretical predictions could, in the absence of other data, be attributed to experimental errors in counting small particles. Such should not be the case, however, for polymerization rate or molecular weight measurements. The explanation of the low predictions for small mean residence times probably lies in a better understanding of particle formation phenomena and reaction conditions in newly formed particles and in the water phase.

The experimental values of the ratio $\bar{M}_w/\bar{M}_n$ averaged 3.07 for 37 runs. This value is considerably less than 4.84 and suggests that the constant-flux flux model [eq. (17)] may not describe free radical movement into polymer particles.

The kinetic and physical-chemical parameters listed in Table I were obtained from the sources indicated. The values given for several of these parameters can be questioned. The theory presented is based on the assumption that a_s, the adsorption area per surfactant molecule, is independent of particle size. While this assumption is probably valid for most particles it could be questioned for micelles and very small particles.

The k_t value taken from Van Der Hoff[29] may be too high. Gardon[32] discusses this point in some detail. He recommends a k_t value about ten

times lower. A lower k_t would make the differences between DeGraff's theory and S-E case 2 theory even more pronounced than those reported. That is, fewer particles would be formed but they would be larger. The rate of polymerization would not be greatly effected but the $\bar{M}_w/\bar{M}_n$ ratio would become smaller.

CONCLUSIONS

The expanded theory of DeGraff can be used for prediction of particle size, particle formation, and rate of polymerization for emulsion polymerization of styrene in a CSTR at moderate to large values of mean residence time, if conversion is low enough to assure equilibrium swelling of the polymer particles. Although the number-average molecular weight can be predicted with reasonable accuracy the ratio $\bar{M}_w/\bar{M}_n$ was not as high as predicted. The present work does not provide enough information to pinpoint the reason for this difference between theory and experiment.

Acknowledgment is made to the donors of the Petroleum Research Fund, administered by the American Chemical Society, for support of this reasearch. Andrew DeGraff also acknowledges the support of Lehigh University and an NSF Fellowship.

The styrene monomer provided by the Dow Chemical Company and the analytical services provided by Air Products and Chemicals, Inc. is appreciated.

References

1. R. W. Laundrie and R. F. McCann, *Ind. Eng. Chem.*, **41**, 1568 (1949).
2. M. Fledon, R. F. McCann, and R. W. Laundrie, *India Rubber World*, **128**, 51 (1953).
3. P. Baumann, *Chimia*, **12**, 233 (1958).
4. B. Jacobi, *Angew. Chem.*, **64**, 539 (1952).
5. H. Gerrens and K. Kuchner, *Brit. Polym. J.*, **2**, 18 (1970).
6. Spencer Chemical Co., Belg. Pat. 621,386 (1963).
7. V. M. Soldatov, A. I. Kirillov, and P. G. Vekslyarskii, *Plast. Massy*, **1969**, No. 1, 5.
8. Monsanto Co., U.S. Pat. 3,403,147 (1968).
9. N. Platzer, *Ind. Eng. Chem.*, **62**, 6 (1970).
10. F. T. Wall, C. J. Delberg, and R. E. Florin, *J. Polym. Sci.*, **9**, 177 (1952).
11. W. W. Graessley and K. Nagasubramanian, *Chem. Eng. Sci.*, **25**, 1559 (1970).
12. K. G. Denbigh, *Trans. Faraday Soc.*, **43**, 648 (1947).
13. W. D. Harkins, *J. Amer. Chem. Soc.*, **69**, 1428 (1947).
14. W. V. Smith and R. H. Ewart, *J. Chem. Phys.*, **16**, 592 (1948).
15. D. B. Gershberg and J. E. Longfield, paper presented at Symposium on Polymerization Kinetics and Catalyst Systems, 45th A.I.Ch.E. Meeting, New York (1961); *Preprints*, No. 10.
16. C. P. Roe and P. D. Brass, *J. Polym. Sci.*, **24**, 401 (1957).
17. J. W. Vanderhoff, J. F. Vituske, E. B. Bradford, and T. Alfrey, Jr., *J. Polym. Sci.*, **20**, 225 (1956).
18. W. H. Stockmayer, *J. Polym. Sci.*, **24**, 314 (1957).
19. J. T. O'Toole, *J. Appl. Polym. Sci.*, **9**, 1291 (1965).
20. N. Zwietering, *Chem. Eng. Sci.*, **11**, 1 (1959).
21. A. W. DeGraff, Ph.D. Dissertation, Department of Chemical Engineering, Lehigh University, 1970.

22. S. Katz, R. Shinnar, and G. Saidel, in *Addition and Condensation Polymerization Processes*, (*Advan. Chem. Ser.*, **91**), ACS, Washington, D. C., 1969, Chap. 8.
23. P. J. Flory, *Principles of Polymer Chemistry*, Cornell Univ. Press, Ithaca, N. Y., 1953.
24. J. L. Gardon, *J. Polym. Sci. A-1*, **6**, 623, (1968).
25. M. Morton, S. Kaizerman, and M. W. Altier, *J. Colloid Sci.*, **9**, 300 (1954).
26. D. J. Williams and M. R. Grancio, *J. Polym. Sci. A-1*, **8**, 2733 (1970).
27. R. H. Boundy and R. F. Boyer, *Styrene, Its Polymers, Co-polymers and Derivatives*, Reinhold, New York, 1952.
28. J. G. Brodynan and G. L. Brown, *J. Colloid Sci.*, **15**, 76 (1950).
29. B. M. F. Van Der Hoff, *Polymerization and Polycondensation Processes* (*Advan. Chem. Ser.*, **34**), ACS, Washington, D. C., 1962.
30. I. K. Miller and I. M. Kolthoff, *J. Amer. Chem. Soc.*, **73**, 3055 (1951).
31. S. H. Maron, M. E. Elder, and I. M. Ulevetch, *J. Colloid Sci.*, **9**, 89 (1954).
32. J. L. Gardon, *J. Polym. Sci. A-1*, **6**, 687 (1968).

Received February 9, 1970
Revised April 28, 1971

JOURNAL OF POLYMER SCIENCE: PART A-2 VOL. 9, 1977–1989 (1971)

Crystallinity and Conformational Changes in Poly(β-benzyl L-Aspartate)

HIROKO OBATA and HISAAKI KANETSUNA, *Research Institute for Polymers and Textiles, Kanagawa-ku, Yokohama, Japan*

Synopsis

The crystallinity of poly(β-benzyl L-aspartate) is highly variable, in a series of specimens prepared under various conditions: films cast from chloroform solutions at various evaporation rates, films cast comparatively slowly from chloroform–trifluoroacetic acid solutions, films prepared from dichloroacetic acid solution by treatment with ethyl alcohol, precipitates formed from trifluoroacetic acid solution by addition of ether. Film cast slowly from chloroform is in the highly crystalline ω form. In contrast, the conformation of the benzene rings in the ω helix obtained from the α helix by heating is distorted to some extent in comparison with the structure of the highly crystalline ω form. Crystallization and conformational changes from the α to the ω form, and from the ω to the β form upon heating, are correlated with the dispositions of the side chains, the packing of the benzene rings, and the motion of the side chains. The main chain of the α helix is distorted into the ω form when its side chains are in a favorable conformation. The α helix is stable in the disordered conformation, and it is distorted to some extent at high temperature.

INTRODUCTION

It is well known that poly(β-benzyl L-aspartate) (PBLAsp) forms a left-handed α helix,[1,2] which is converted into the ω helix by heating. According to conformational studies,[3] the ω helix is characterized by tetragonal stacking of benzyl groups around the helical core, and the conformation of the side chains is more ordered than in the α helix, but varies a little from one sample to another. Moreover the coexistence of the tetragonal phase with the hexagonal one in a concentrated solution in *m*-cresol suggests that intermolecular interaction, especially the packing of benzyl groups, is an important factor in the transition from the α form to the ω form.[4]

On the other hand, since a similar transition has been observed in poly(β-methyl L-aspartate)[5] and some of its copolymers with PBLAsp, it has been suggested that the α helix is destabilized by the interaction of the side-chain ester group with the main chain, and thus is readily distorted by close packing of the benzene rings into tetragonal stacks.[6]

The variability of the conformation of PBLAsp is of great interest in view of questions of structure and molecular motion in polypeptides. In this study, conformational changes of the main chain and the side chain were examined by means of infrared spectroscopy. Most of the samples

were films prepared by casting from chloroform solution at various evaporation rates. A discussion of the interrelations among conformation, crystallinity, and molecular motion is based, in addition, on the results of DSC thermograms, dielectric measurements, x-ray diffractometry, and dilatometry.

EXPERIMENTAL

PBLAsp was obtained from Pilot Chemicals Inc. The molecular weights of samples used were in the range 1.8×10^5 to 2.5×10^5. The following types of specimens were prepared: (1) films cast from chloroform solutions at various evaporation rates, (2) films cast from chloroform–trifluoroacetic acid solutions, (3) films prepared from dichloroacetic acid solutions by treatment with ethyl alcohol, (4) precipitates formed by adding ether to solutions in trifluoroacetic acid.

Infrared spectra were measured with films (or KBr disks for precipitates). The x-ray photographs were obtained with Ni-filtered CuKα radiation. Spacings were calibrated by aluminum powder. The DSC thermograms were measured under nitrogen, at a heating rate of 8°C/min and a sensitivity of 2 mcal full scale, and corrected to correspond to 4 mg specimens. The dielectric measurements were carried out in the range of -50 to 150°C at 1 kcps. The dilatometric measurements were carried out with about 1 g of film.

PREPARATION OF SPECIMENS: CONFORMATIONS

Films Cast from Chloroform Solution

Films, a few microns thick, were prepared by casting from dilute chloroform solutions at room temperature (25–30°C). Evaporation was

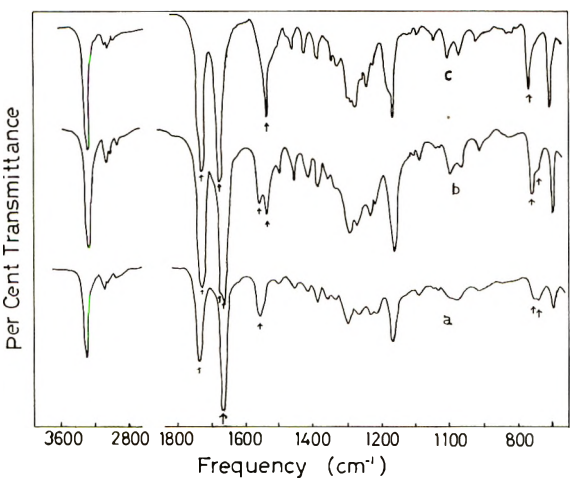

Fig. 1. Infared spectra of films cast from chloroform solutions: (*a*) quick-dried film; (*b*) moderately slow-dried film; (*c*) slow-dried film.

controlled in evaporating dishes at various rates from the most rapid (allowing the solution to stand in the open) to slow drying for about 10 hr (covering the dish with a Kre-Wrap film). Infrared spectra of the films are shown in Figure 1. The amide I and II bands for quick-dried film are at 1667 and 1557 cm^{-1}, respectively, indicating the α conformation.

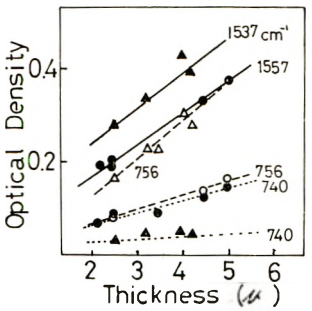

Fig. 2. Intensities of absorption bands vs. thickness for the α and the ω standard films prepared from chloroform solutions by quick drying and slow drying: (○) α film; (●) ω film.

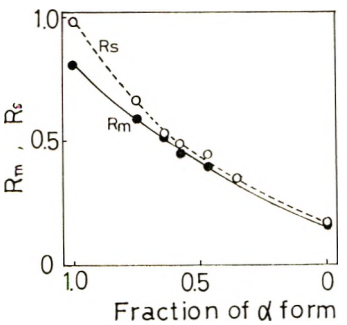

Fig. 3. Variation of R_m and R_s with fraction of the α form for superimposed α and ω standard films.

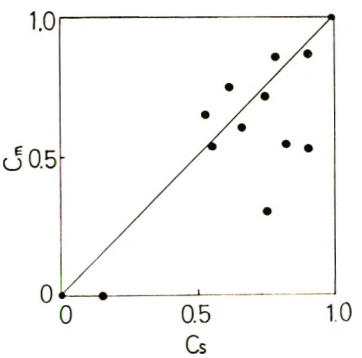

Fig. 4. Relation between C_m and C_s for films cast at various rates from chloroform solutions.

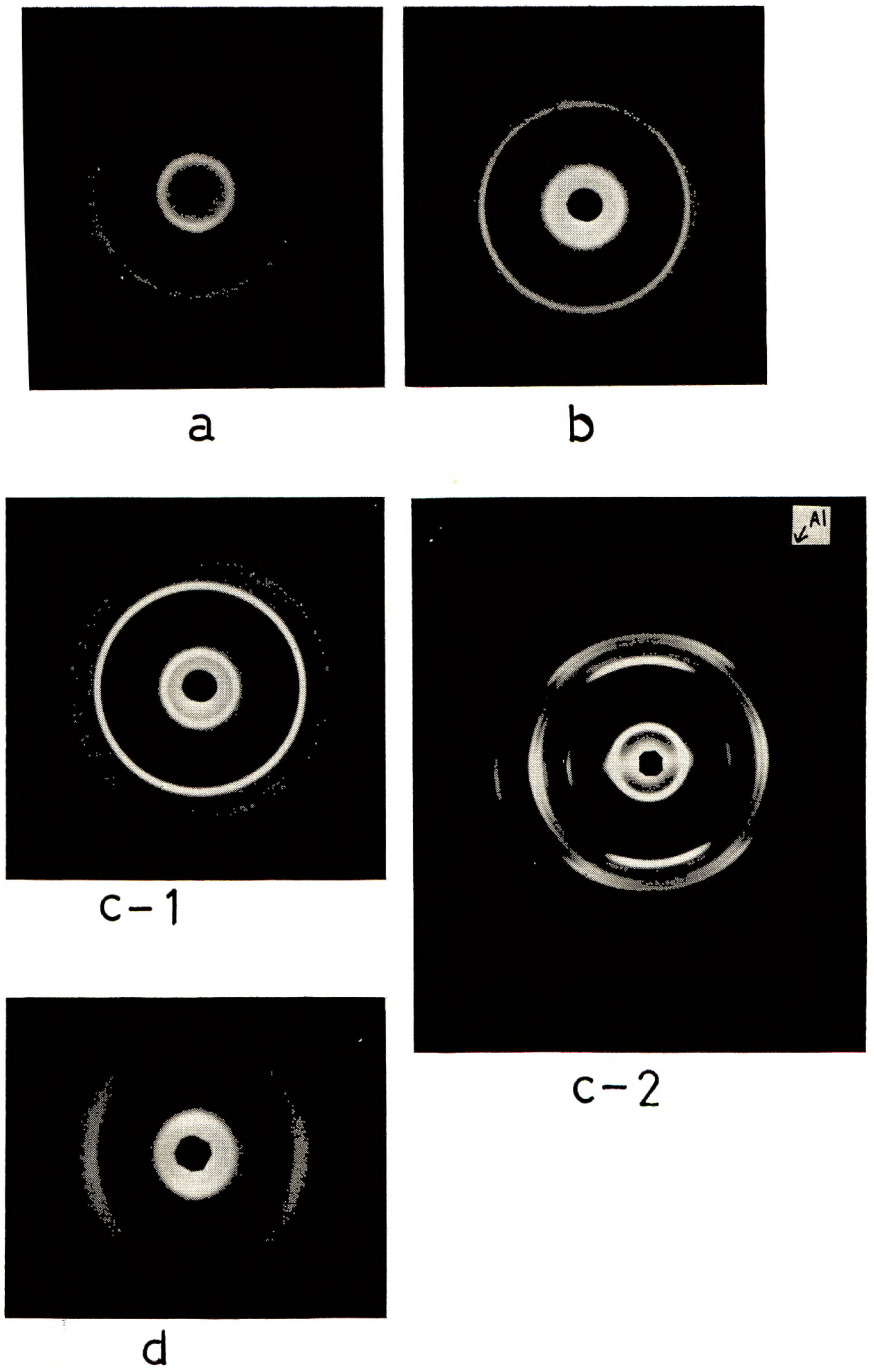

Fig. 5. X-ray diffraction patterns of films prepared from chloroform solutions by (*a*) quick drying, (*b*) moderately slow drying, and (*c*) slow drying and (*d*) a film cast from the mixed solvent system 1:1 TFA–chloroform. Flat camera, with beam normal to the film (*a*, *b*, *c*-1, and *d*) and beam parallel to the film (*c*-2).

TABLE I
X-Ray Reflections from Poly(β-benzyl L-Aspartate) Films Cast Slowly from Chloroform

	$l = 0$	$l = 1$
hk	d	d
10	13.83	4.97
11	9.79	4.67
20	6.90	4.27
21	6.19	3.99
22	4.91	3.42
30	4.63	3.42
31	4.35	3.42
32	3.82	3.11
40	3.45	2.91
41	3.34	
42	3.07	2.66
43	2.76	
50		2.44

For film dried under intermediate conditions (dish covered with a perforated film), the bands corresponding to the ω conformation appear at 1677 and 1537 cm^{-1} together with the α bands, while only the ω bands are observed in a slow-dried film. Other interesting changes are observed in the bands associated with the benzene ring at 756 and 740 cm^{-1}. The intensity at 740 cm^{-1} decreases, and the intensity at 756 cm^{-1} increases as a result of slower drying, until the latter band is virtually alone in the slow-dried case. The extent of conformational change of the main chain and the side chain were estimated from the band intensities for the amide II and the benzene ring in the following way. The quick-dried and the slow-dried films were used as standards for the α and the ω forms. The intensities of these bands vary linearly with the thickness of the film (Fig. 2). The band peak intensities at 1557, 1537, 756, and 740 cm^{-1} were measured for pairs of standard films by laying the α film over the ω film. From the results, intensity ratios R_m and R_s were calculated.

$$R_m = I_{1557}/(I_{1557} + I_{1537}) \quad (1)$$

$$R_s = I_{740}/I_{756} \quad (2)$$

The ratio R_m corresponds to the apparent fraction of the α form, and R_s to the change in the conformation of the benzene rings. Both R_m and R_s were plotted against the fraction C of the α form (Fig. 3). Apparent values of C corresponding to R_m and R_s are represented respectively by C_m and C_s, which were used as conformational parameters of the main chain and the side chain to characterize the structure of films.

The correlation between C_m and C_s for films cast from chloroform at various evaporation rates is shown in Figure 4. The corresponding x-ray diffraction patterns in Figure 5 become sharper as evaporation is carried out more slowly. When the photographs were taken with the beam parallel to the surface of the films, a meridional 1.5 Å reflection was ob-

served for both the quick-dried and the moderately slow-dried films, although it was weaker in the latter case. However, a 1.3 Å reflection was observed in the slow-dried film. Table I gives the reflections of the diffraction photograph shown in Figure 5*c*–2 for the slow-dried film. Within experimental error, the spacings are in accord with ω patterns studied by Bradbury *et al.*[3] The corresponding dimensions are given in Table I.

Films Cast from Chloroform Solutions Containing Trifluoroacetic Acid

Casting is more complicated in the mixed-solvent system. When the amount of trifluoroacetic acid (TFA) is very small, at least below 1%, the films resemble those cast from pure chloroform, except that the molecules tend to aggregate to form locally oriented films. Large amounts of TFA, however, prevent crystallization. According to the broad amide bands in the infrared spectra, a film cast quickly from chloroform containing 2% TFA is composed of a mixture of α, β, and random conformations, but a large fraction of the material changes into the α helical form during moderately slow evaporation. When the amount of TFA is large, the solvated molecules aggregate readily to form locally oriented and nonuniform films. The x-ray patterns of these films, especially the reflections corresponding to the 5.4 Å layer line, are very diffuse. An x-ray photograph of film cast from 1:1 TFA–chloroform (by volume) is shown in Figure 5*d*.

Films Prepared from Dichloroacetic Acid Solution by Treatment with Ethyl Alcohol (DCA–Alcohol Film)

A dichloroacetic acid solution spread on glass was immersed in ethyl alcohol to form a film, which was then washed several times with fresh alcohol. Most of the film is in the α form, although a small amount of the β form was detected by means of the infrared spectra. The x-ray diffraction pattern is very diffuse, like that in Figure 5*d*, although in this case it is not oriented.

Precipitates Formed by Addition of Ether to Dilute TFA Solution (TFA–Ether Precipitate)

Very broad amide bands in the infrared spectrum and very diffuse Debye rings, especially around 17–13 Å, were observed, indicating a mixture of various conformations.

CONFORMATIONAL CHANGES AND CRYSTALLIZATION BY HEATING

Infrared Spectra

Figure 6 shows the variations of C_m and C_s for heated films. Films A and B were cast from chloroform solutions by quick drying, and film

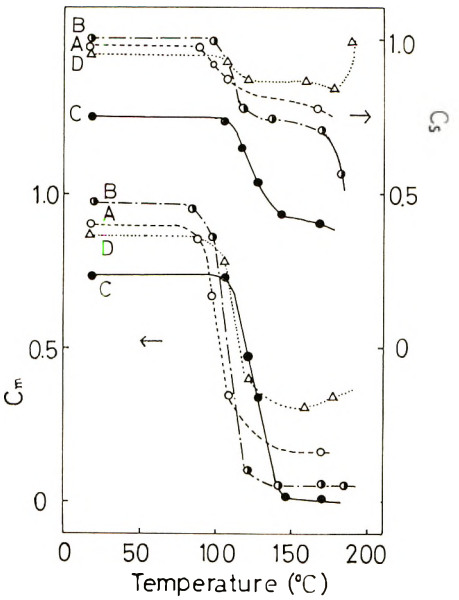

Fig. 6. Variation of C_m and C_s for heated films at various temperatures. A, B and C denote chloroform-cast films heated for 15 min. Films A, B, were prepared by quick drying and C by moderately slow drying. D is the DCA–alcohol film heated for 5 min.

C by moderately slow drying. Films A and B are about 1 and 5 μ thick, respectively, and the former was rather quickly dried. Values of C_m fall off sharply in the region of 90–110, 100–120, and 110–140°C for films A, B, and C, respectively. Values of C_s decrease in the same regions and begin to drop further at about 170°C. These values decrease to smaller values in the slowly dried films. Another conformational change was evidenced in the infrared spectra. The bands of the β form are distinguishable at 180°C and become stronger with increasing temperature, until the β conformation prevails above 210°C.

The decreases in C_m and C_s for the DCA–alcohol film D occur mainly at 110–130°C and are smaller than those noted above. In comparison with films cast from chloroform, the conversion to the β form begins at lower temperature, about 160°C, and C_s begins correspondingly to increase near 200°C.

X-Ray Diffraction

Figure 7 indicates the effect of heating on the x-ray patterns. For the quick-dried film from chloroform, the diffraction patterns are not particularly sharp at 140°C (Fig. 7*a*–1). However, the spacings of the Debye rings change from 5.15 to 5.00 Å and from 13.7 to 13.85 Å, and the meridional 1.5 Å reflection is replaced by the weak 1.3 Å reflection in this temperature region. The diffraction patterns are considerably sharpened after heating at 190°C (Fig. 7*a*–3).

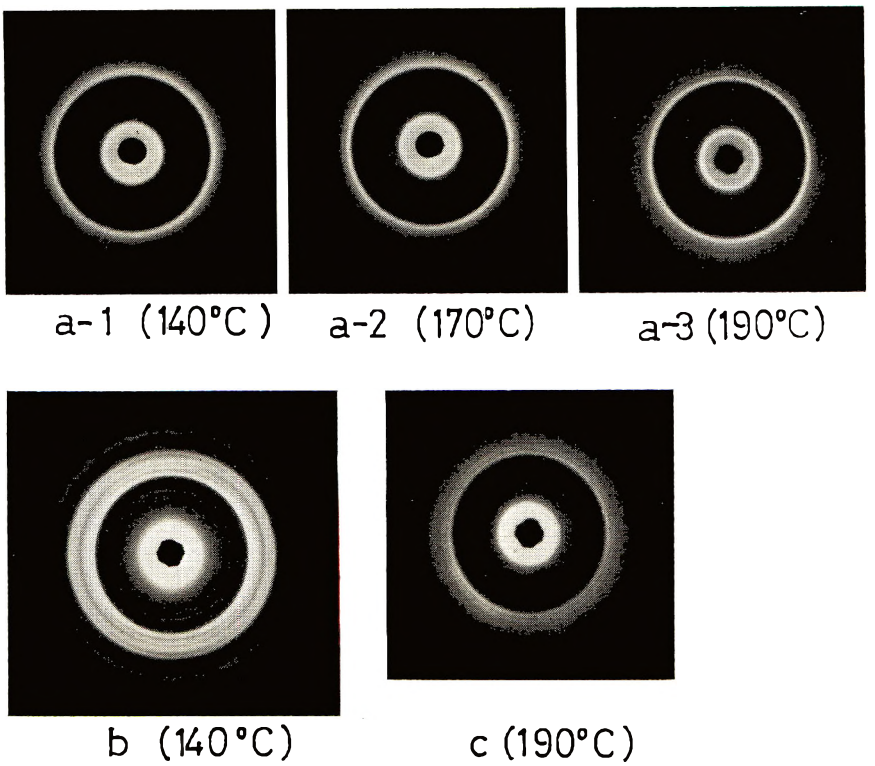

Fig. 7. X-ray diffraction patterns of heated films at various temperatures for 15 min, (flat camera, with beam normal to the films): (*a*) film cast quickly from chloroform, (*b*) film cast from 1:1 TFA–chloroform, (*c*) DCA–alcohol film. (Samples in *a* and *b* are the same respectively as in *a*, *d* in Fig. 5).

In a film cast from the TFA–chloroform system, the diffuse x-ray patterns become sharper at lower temperature than in the pure chloroform system; for instance, they are considerably sharpened at 140°C for the 1:1 cast film (Fig. 7*b*). The diffraction patterns of DCA–alcohol film (Fig. 7*c*) become slightly sharper after heating at 170°C, but even more sharp at 190°C, although still not so sharp as those of the film cast from chloroform. The x-ray patterns of TFA–ether precipitates do not change upon heating at 130°C, but become slightly sharper at 170°C, and still more sharp at 190°C. The diffuse ring at 13–17 Å splits into two rings, 17.6 and 13.7 Å, at 170°C.

DSC Curves

In the DSC curves of the films cast from chloroform (Fig. 8), an exothermic peak is observed at 110°C for the quick-dried film (Fig. 8*a*), and it broadens and shifts to higher temperature with progressively slower drying. This peak is followed by a broad exothermic peak at 170–200°C. Both exothermic peaks are not detected clearly in the slow-

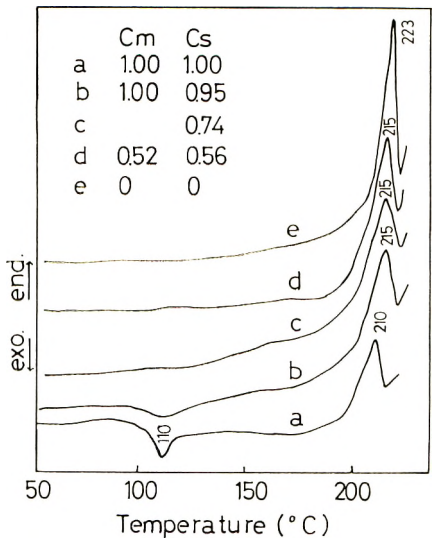

Fig. 8. DSC curves of chloroform-cast film. Evaporation is slow on going from *a* to *e*, and parameters C_m and C_s are given in the figure.

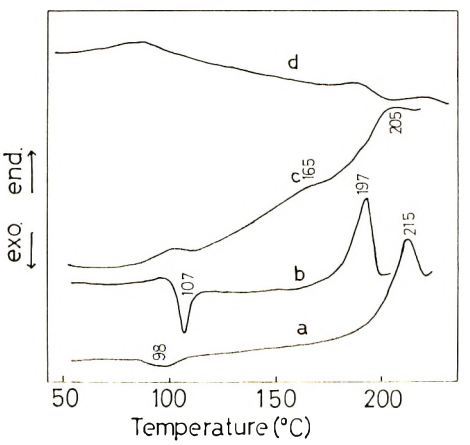

Fig. 9. DSC curves: (*a*) film cast from the 1:1 TFA–chloroform system, (*b*) film cast very slowly from chloroform solution containing 2% TFA; (*c*) DCA–alcohol film; (*d*) TFA–ether precipitate.

dried film (Fig. 8*e*). An endothermic peak at 210°C for the quick-dried film shifts to higher temperature and becomes sharper for slow drying. In the case of the film cast from 1:1 TFA–chloroform by volume (Fig. 9*a*), the temperature of the exothermic peak is lowered to 98°C. When a mixed solution containing TFA is evaporated for a long period, DSC curves change irregularly. For instance, with 2% TFA and drying for about three days, the exothermic peak at 107°C is rather sharp and the endothermic peak shifts to lower temperature at 197°C (Fig. 9*b*). The

DSC curves of both the DCA–alcohol and the TFA–ether precipitates (Fig. 9*c*, 9*d*), show an endotherm around 90–100°C. This is followed by very broad exotherm and endotherm.

Dielectric Measurements

Figures 10 and 11 show tan δ at 1 kcps for films cast from chloroform with quick and slow drying. The behavior of the dielectric dispersion depends upon the evaporation rate and heat treatment. The tan δ maximum is at 50°C for the quick-dried film, and its height decreases after heating to 150°C. The corresponding dispersion maximum appears at 30°C for the slow-dried film, and becomes very small upon heating to 150°C.

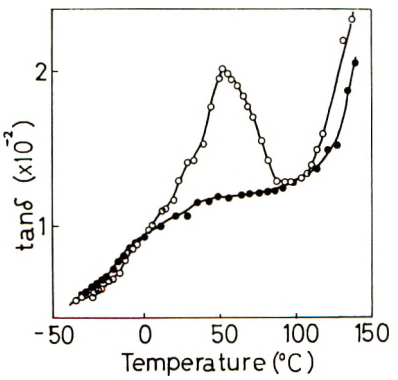

Fig. 10. Dielectric dispersion (at 1 kcps) for film cast quickly from chloroform: (○) first run; (●) second run.

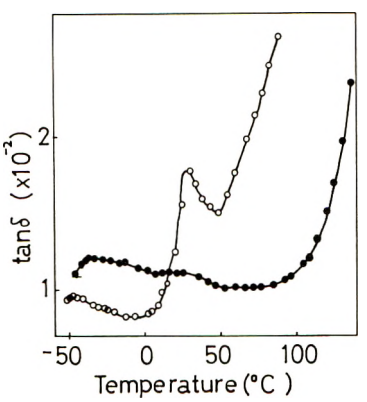

Fig. 11. Dielectric dispersion (at 1 kcps) for film cast slowly from chloroform: (○) first run; (●) second run.

Specific Volume

Figure 12 shows curves of specific volume versus temperature for the ω film cast from chloroform. The measurement was repeated after the

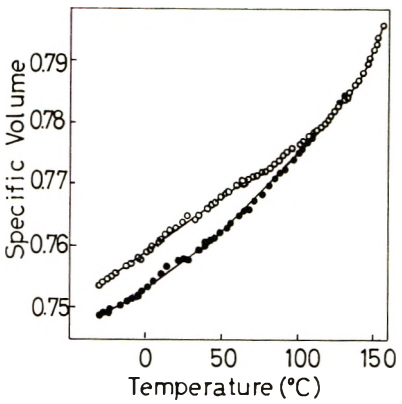

Fig. 12. Curves of specific volume vs. temperature for ω form cast relatively slowly from chloroform: (○) first run; (●) second run.

sample had been raised to 150°C in the first run. A large inflection is observed around 130°C in both curves, and small inflections at 0 and 50°C in the second run.

DISCUSSION

The structure of films cast from chloroform depends upon the temperature and the rate of evaporation. Although the temperature dependence has not been studied in detail, the conversion from the α to the ω helix by slow evaporation was found to be rather difficult at 5–10°C. According to the infrared spectra and x-ray photographs, the quick-dried film is in poorly crystallized α form, but the α helices are converted into ω helices by slower evaporation, and for the slowest rate, into highly crystalline ω helices. The conformational changes of the main chain and the side chains in this process can be estimated by the parameters C_m and C_s which indicate the extent of distortion of the main chain and of the orientation of the benzene rings.

According to a study[7] of a blend of poly(γ-benzyl L-glutamate) with poly(γ-benzyl D-glutamate), the 740 cm^{-1} band due to the benzene ring shifts to higher frequency when the interaction between benzene rings becomes strong and nearly merges with another band at 756 cm^{-1} attributable to the benzene ring. This frequency shift was also observed in PBLAsp films, as shown in Figure 1. The parameters C_m and C_s for films cast from chloroform at various evaporation rates are in an almost 1:1 relation, indicating that the orientation of the side chains corresponds to the distortion of the main chains. The changes in some values of C_s, however, are considerably smaller than those of C_m, suggesting that extensive orientation of the benzene rings is not strictly necessary for this distortion.

For the film cast from chloroform, crystallization by heating is divided largely into two processes, reflected by exothermic regions at about

90–170°C and 170–200°C in DSC curves. The dielectric dispersion at 50°C is evidently caused by the thermal motion of poorly crystallized side chains. According to the values of C_m and C_s, and the x-ray patterns, the main chain is distorted with the change in the packing of the benzene rings at about 90–140°C. The increase in the tan δ corresponds to the large inflection around 130°C in the specific volume curves. In NMR measurements,[8] the decrease in the second moment above 350°K was explained as due to the onset of motion involving the rotation of whole side chains. As the side chains gradually crystallize near 170°C with an increase in the motion in this case, it is expected that the restricted motion of the bulky side chains in close packing continues, and the rearrangement becomes more ordered in the region above 170°C, in which C_s decreases further and the x-ray patterns become considerably sharper. However, C_s is still larger than C_m in this region. Thus, the benzene rings are partly disordered, and this disorder depends upon the original crystallinity. Although the behavior of the dielectric dispersion of the slow-dried film has not been studied in detail, close packing may be incomplete when the solvent has evaporated, but heating may permit improved packing without further conformational changes. This effect of heating is observed in the specific volume curves.

On the other hand, the β form is detected increasingly from 180°C on, and the conformation is entirely in the β form above the endothermic peak at 210–223°C. As the height of this endothermic peak depends upon the crystallinity, it is reasonable to conclude that the endotherm is due to the release of the restricted motion of the side chain and the formation of the β form, although thermal degradation also occurs. The sharpness of the endothermic peak for the slow-dried film suggests that the side chains are in highly ordered conformation with respect to close-packed benzene rings, in contrast with the ω form as converted from the α form by heating.

Since TFA is a polar solvent, mixing it with chloroform prevents the side chains of PBLAsp from crystallizing, as is indicated by the diffuse x-ray patterns in Figure 5*d*, but does not prevent the α helices from aggregating side by side. The side chains will be in a relatively favorable arrangement, i.e., less restricted than those of the film cast from chloroform, and consequently the α helix will be converted to a crystalline ω form at lower temperature. The irregular DSC curve for the film evaporated very slowly from solvent containing TFA is probably due to the effect of depolymerization or partial cleavage of the benzyl groups. The endothermic peak was observed at 180°C in the DTA curve of PBLAsp of molecular weight 5000.[9]

The DCA–alcohol film is in a somewhat disordered α form, and TFA–ether precipitates are in still more disordered and mixed conformations. In the disordered α form, the α helix is more stable against heating than in the more ordered state such as exists in the film cast from chloroform. There is considerable main-chain distortion at 110–130°C in the DCA–

alcohol film, but not in the TFA–ether precipitates. In the latter case, however, the distortion is permitted in part at high temperature. Considerable motional freedom of the side chains is expected in the disordered form, and thus the endotherm around 90–100°C may be caused by some rearrangement of the side chains. However, the large motion of the side chains required to improve this partial order will be allowed at high temperature. On the other hand, the conformational change to the β form is allowed at lower temperature in the disordered structure. Because of this balance between the exotherm and endotherm, two very broad endothermic peaks are observed in the DSC curve of the DCA–alcohol film.

As described above, the conformation and the crystallinity of PBLAsp are very variable and characterized largely by three factors: the relative disposition of the side chains, the packing of the benzene rings, and the motion of the side chains. From observations of the processes occurring in specimens variously cast and heated, however, it was found that the benzene rings are not necessarily in a highly ordered orientation in the region of the distortion of the main chain. If the interaction of the side-chain C=O group with the main-chain N—H group is involved in the transition from the α to the ω form, arrangement of the benzene rings probably takes precedence over this interaction for the quick-dried film from chloroform. In slow-dried film, however, the main chain may be distorted by the interaction and then the side chains may develop into a more ordered conformation. The frequency shift of the side-chain C=O group from 1735 to 1730 cm^{-1} in the transition (see Fig. 1) is consistent with this interaction.

The authors would like to thank Mr. Kanji Sasaki of the Research Institute for Polymers and Textiles for help with dielectric measurements.

References

1. E. M. Bradbury, A. R. Downie, A. Elliott, and W. E. Hanby, *Proc. Roy. Soc. (London)*, **A259**, 110 (1960).
2. R. H. Carson, K. S. Norland, G. D. Fasman, and E. R. Blout, *J. Amer. Chem. Soc.*, **82**, 2268 (1960).
3. E. M. Bradbury, L. Brown, A. R. Downie, A. Elliott, R. D. B. Fraser, and W. E. Hanby, *J. Mol. Biol.*, **5**, 320 (1962).
4. P. Saludjian, C. de Lozé, and V. Luzzati, C. R. Acad. Sci. (Paris), **256**, 4297 (1967).
5. M. Goodman, F. Boardman, and I. Listowsky, *J. Amer. Chem. Soc.*, **85**, 2491 (1963).
6. E. M. Bradbury, B. G. Carpenter, and R. M. Stephens, *Biopolymers*, **6**, 905 (1968).
7. M. Tsuboi, *Biopolymers Symp.*, **1**, 527 (1964).
8. K. Hikichi, *J. Phys. Soc. Japan*, **19**, 2169 (1964).
9. B. M. Watson, D. B. Green, and F. Happey, *Nature*, **211**, 1394 (1966).

Received August 17, 1970
Revised March 22, 1971

JOURNAL OF POLYMER SCIENCE: PART A-2 VOL. 9, 1991–2007 (1971)

Crystal Orientation in a Semicrystalline Polymer in Relation to Deformation of Spherulites*

SHUNJI NOMURA, AKIRA ASANUMA,† SHOJI SUEHIRO, and HIROMICHI KAWAI, *Department of Polymer Chemistry, Faculty of Engineering, Kyoto University, Kyoto, Japan*

Synopsis

A mathematical development interrelating the orientation distribution functions of three kinds of orientation units for a polymer spherulite (i.e., a crystal lamella, a crystallite, and a given reciprocal lattice vector of the crystallite) is formulated on the basis of series expansions of the distribution functions in generalized spherical harmonics. Two types of uniaxial deformation models of a polyethylene spherulite, taking account of micronecking and untwisting of crystal lamellae, and of chain tilting and untwisting of crystal lamellae, respectively, both in addition to affine deformation of the lamellae are discussed. The models are tested by comparison of the theoretical orientation distribution functions of some reciprocal lattice vectors of the crystallite with the results of x-ray diffraction experiments.

Introduction

The deformation mechanism of polymer spherulites has been studied by many authors.[1–13] Quantitative investigations have been made by Stein et al.,[3,4] Kawai et al.,[6,8] and Moore[10] by using essentially very similar models for a polyethylene spherulite. The deformation of the spherulite was compared with that of the models in terms of the second-order orientation factors of the orientation distribution functions of the principal crystallographic axes of the crystallite; $F_{20}{}^{j}$ (j denoting a, b, and c axes). The second-order orientation factors provide, however, only limited knowledge of the orientation distribution,[14,15] and one cannot discuss the crystalline orientation in detail on this basis.

In this paper, it is intended, first, to represent mathematically the relations between the orientation distribution functions for the crystal lamellae within the spherulite, the crystallites, and its reciprocal lattice vectors in terms of the series expansions of the functions in generalized spherical harmonics.[14,15]

* Presented at the 17th Symposium on Polymer Chemistry, Japan, Ehime University, Matsuyama, Ehime-ken, Japan, October 22, 1968.

† Present address: Development Research Laboratories, Teijin Ltd., Iwakuni, Yamaguchi-ken, Japan.

Second, one of the simplest applications of the mathematical treatment, to a uniaxially deformed polyethylene spherulite, will be discussed mainly with respect to the principal axes of the crystallite and the reciprocal lattice vector of the (110) crystal plane, which gives the strongest x-ray diffraction.

Relation between Orientation Distribution Functions for Crystal Lamellae, Crystallites, and Reciprocal Lattice Vectors

The orientation of a crystallite, which is represented by Cartesian coordinates 0–$u_1u_2u_3$, with respect to the specimen coordinates 0–$x_1x_2x_3$, may be specified by three Euler angles, ϕ, θ, and η, as shown in Figure 1. Similarly, the orientation of a crystallite within the crystal lamella, which is also represented by other Cartesian coordinates 0–$v_1v_2v_3$, may be specified by three Euler angles, α, β, and γ. The Cartesian coordinates 0–$u_1u_2u_3$ can be arbitrarily fixed within the crystallite, but for the polyethylene crystal, it is convenient to take the u_1, u_2, and u_3 axes as the principal axes, a, b, and c of the crystal, respectively. The specimen coordinate system 0–$x_1x_2x_3$ is so fixed that the x_3 axis is along the direction of stretching of the specimen and the x_2x_3 plane is parallel to the film surface. In the Cartesian coordinates 0–$v_1v_2v_3$, the v_3 axis may be taken along the lamellar axis (or radial direction of the spherulite) the v_2v_3 plane being parallel to the lamellar surface. The angles θ and ϕ (or β and α), which define the orientation of the u_3 axis of the crystallite within the specimen (or crystal lamella), are the polar and azimuthal angles, respectively, and η (or γ) specifies the rotation of the crystallite around its own u_3 axis. The orientation of the crystal lamellae, 0–$v_1v_2v_3$, with respect to the specimen coordinates may be also specified by three Euler angles, ϕ', θ', and η'.

Let us consider a given jth reciprocal lattice vector $\mathbf{r}_j$ fixed within the crystallite. The orientation of the vector $\mathbf{r}_j$ may also be specified by three sets of polar and azimuthal angles, (θ_j,ϕ_j), (Θ_j,Φ_j), and (Θ_j',Φ_j')

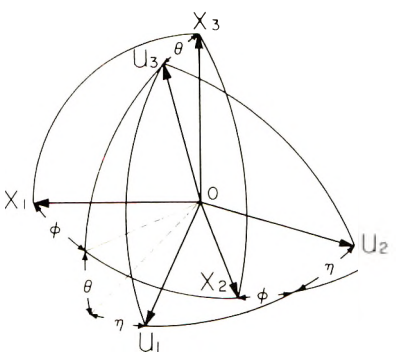

Fig. 1. Euler angles, ϕ, θ, and η, specifying the orientation of Cartesian coordinates O–$u_1u_2u_3$ fixed within a crystallite with respect to other Cartesian coordinates O–$x_1x_2x_3$ oriented with respect to the geometry of the film specimen.

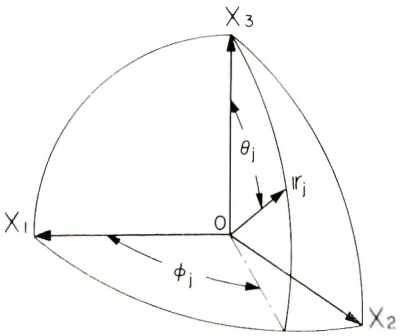

Fig. 2. Polar and azimuthal angles θ_j and ϕ_j specifying the orientation of a reciprocal lattice vector of the crystallite with respect to the Cartesian coordinates 0–$x_1x_2x_3$.

with respect to the coordinates, 0–$x_1x_2x_3$, 0–$u_1u_2u_3$, and 0–$v_1v_2v_3$, respectively. Figure 2 shows one such illustration of the orientation of an $\mathbf{r}_j$ vector with 0–$x_1x_2x_3$ as the reference coordinates.

These sets of angles can be related through linear transformations of the Cartesian coordinates accompanied by rotations of the coordinate axes:

$$\begin{bmatrix} \sin\theta_j\cos\phi_j \\ \sin\theta_j\sin\phi_j \\ \cos\theta_j \end{bmatrix} = T(\phi, \theta, \eta) \begin{bmatrix} \sin\Theta_j\cos\Phi_j \\ \sin\Theta_j\sin\Phi_j \\ \cos\Theta_j \end{bmatrix} \tag{1}$$

$$\begin{bmatrix} \sin\theta_j\cos\phi_j \\ \sin\theta_j\sin\phi_j \\ \cos\theta_j \end{bmatrix} = T(\phi', \theta', \eta') \begin{bmatrix} \sin\Theta_j'\cos\Phi_j' \\ \sin\Theta_j'\sin\Phi_j' \\ \cos\Theta_j' \end{bmatrix} \tag{2}$$

$$\begin{bmatrix} \sin\Theta_j'\cos\Phi_j' \\ \sin\Theta_j'\sin\Phi_j' \\ \cos\Theta_j' \end{bmatrix} = T(\alpha, \beta, \gamma) \begin{bmatrix} \sin\Theta_j\cos\Phi_j \\ \sin\Theta_j\sin\Phi_j \\ \cos\Theta_j \end{bmatrix} \tag{3}$$

where, for example,

$$T(\alpha, \beta, \gamma) = \begin{bmatrix} \cos\alpha\cos\beta\cos\gamma - \sin\alpha\sin\gamma, & -\cos\alpha\cos\beta\sin\gamma - \sin\alpha\cos\gamma, & \cos\alpha\sin\beta \\ \sin\alpha\cos\beta\cos\gamma + \cos\alpha\sin\gamma, & -\sin\alpha\cos\beta\sin\gamma + \cos\alpha\cos\gamma, & \sin\alpha\sin\beta \\ -\sin\beta\cos\gamma, & \sin\beta\sin\gamma, & \cos\beta \end{bmatrix} \tag{4}$$

With eqs. (1)–(3), a generalization of the Legendre addition theorem gives the following relations:[14]

$$\Pi_l^m(\zeta_j)\exp\{im\phi_j\} = \left(\frac{2}{2l+1}\right)^{1/2} \sum_{n=-l}^{l} Z_{lmn}(\xi)\exp\{i(m\phi + n\eta)\} \times \Pi_l^n(\cos\Theta_j)\exp\{in\Phi_j\} \tag{5}$$

$$\Pi_l^m(\zeta_j)\exp\{im\phi_j\} = \left(\frac{2}{2l+1}\right)^{1/2} \sum_{s=-l}^{l} Z_{lms}(\xi')\exp\{i(m\phi' + s\eta')\} \times \Pi_l^s(\cos\Theta_j')\exp\{is\Phi_j'\} \tag{6}$$

$$\Pi_l^s(\cos\Theta_j')\exp\{is\Phi_j'\} = \left(\frac{2}{2l+1}\right)^{1/2}\sum_{n=-l}^{l} Z_{lsn}(\cos\beta) \times \exp\{i(s\alpha + n\gamma)\}\,\Pi_l^n(\cos\Theta_j)\exp\{in\Phi_j\} \quad (7)$$

where $\zeta_j = \cos\theta_j$, $\xi = \cos\theta$, and $\xi' = \cos\theta'$.

The normalized orientation distribution functions of the crystal lamella, the crystallite, and the jth reciprocal lattice vector within the bulk specimen, i.e., $w'(\xi', \phi', \eta')$, $w(\xi, \phi, \eta)$, and $q_j(\zeta_j, \phi_j)$, respectively, can be defined by

$$\int_{\eta'=0}^{2\pi}\int_{\phi'=0}^{2\pi}\int_{\xi'=-1}^{1} w'(\xi', \phi', \eta')d\xi' d\phi' d\eta' = 1 \quad (8)$$

etc.

For orthogonally biaxial orientation of the orthotropic unit, the three kinds of distribution function, $w'(\xi', \phi', \eta')$, $w(\xi, \phi, \eta)$, and $q_j(\zeta_j, \phi_j)$ may be expanded in series of generalized spherical harmonics for even l, m, and n, as follows:

$$w'(\xi', \phi', \eta') = \sum_{l=0}^{\infty} A'_{l00}\,\Pi_l(\xi') + 2\sum_{l=2}^{\infty}\sum_{m=2}^{l}(A'_{lm0}\cos m\phi' + A'_{l0m}\cos m\eta')\,\Pi_l^m(\xi') + 2\sum_{l=2}^{\infty}\sum_{m=2}^{l}\sum_{n=2}^{l} A'_{lmn}\{Z_{lmn}(\xi')\cos(m\phi' + n\eta') + Z_{lm\bar{n}}(\xi')\cos(m\phi' - n\eta')\} \quad (9)$$

Orientations of the crystallites within a lamella may be described for three cases: (I) the crystallites are fixed within the lamella with given angles, α, β, and γ independent of ξ', ϕ', and η'; (II) the angles α, β, and γ are functions of ξ' and ϕ'; (III) the orientation of the crystallites is given by the distribution function, $q(\cos\beta, \alpha, \gamma)$, which is also dependent on ξ' and ϕ'.

In case I, multiplying both sides of eq. (6) by $w(\xi', \phi', \eta')\cdot q_j(\zeta_j, \phi_j)$ and integrating over all angles, ξ', ϕ', η', ζ_j, ϕ_j, one can obtain the following relation for even l, m, and n:

$$A_{lm}^{\,j} = 2\pi\left(\frac{2}{2l+1}\right)^{1/2}\left\{A'_{lm0}\,\Pi_l(\cos\Theta_j') + 2\sum_{n=2}^{l} A'_{lmn}\,\Pi_l^n(\cos\Theta_j')\cos n\Phi_j'\right\} \quad (10)$$

where $\Pi_l^n(\cos\Theta_j')\cos n\Phi_j'$ may be derived from eq. (7), in which Θ_j and Φ_j must be calculated from lattice constants of the crystallite. Thus,

the orientation distribution function of a given reciprocal lattice vector $\mathbf{r}_j$ can be calculated from

$$q_j(\zeta_j, \phi_j) = \sum_{l=0}^{\infty} A_{l0}{}^j \, \Pi_l(\zeta_j) + 2 \sum_{l=2}^{\infty} \sum_{m=2}^{l} A_{lm}{}^j \Pi_l{}^m(\zeta_j) \cos m\phi_j \qquad (11)$$

In case II, substituting eq. (7) into eq. (6) and comparing the result with eq. (5), one may obtain the following relation:

$$Z_{lmn}(\xi) \exp\{i(m\phi + n\eta)\} = \left(\frac{2}{2l+1}\right)^{1/2} \sum_{s=-l}^{l} Z_{lms}(\xi') \times \exp\{i(m\phi' + s\eta')\} Z_{lsn}(\cos\beta) \exp\{i(s\alpha + n\gamma)\} \qquad (12)$$

Again, substituting

$$Q_{lsn}(\xi', \phi') = Z_{lsn}(\cos\beta) \exp\{i(s\alpha + n\gamma)\} \qquad (13)$$

into eq. (12), multiplying both sides of eq. (12) by $w(\xi, \phi, \eta)\, w'(\xi', \phi', \eta')$, and integrating over all angles, one obtains the coefficients A_{lmn}:

$$A_{lmn} = \left\{\left(\frac{2}{2l+1}\right)^{1/2} \Big/ 4\pi^2\right\} \sum_{s=-l}^{l} \int_{\eta'=0}^{2\pi} \int_{\phi'=0}^{2\pi} \int_{\xi'=-1}^{1} w'(\xi', \phi', \eta') \times Z_{lms}(\xi') Q_{lsn}(\xi', \phi') \exp\{i(m\phi' + s\eta')\} d\xi' d\phi' d\eta' \qquad (14)$$

Thus, the orientation distribution function of a reciprocal lattice vector, $q_j(\zeta_j, \phi_j)$, may be calculated from eqs. (11) and (14) and from the relation:

$$A_{lm}{}^j = 2\pi\left(\frac{2}{2l+1}\right)^{1/2} \left\{A_{lm0}\, \Pi_l(\cos\Theta_j) + 2 \sum_{n=2}^{l} A_{lmn}\, \Pi_l{}^n(\cos\Theta_j) \cos n\Phi_j\right\} \qquad (15)$$

which can be obtained similarly to eq. (10).

In case III, multiplying both sides of eq. (12) by $w(\xi, \phi, \eta) w'(\xi', \phi', \eta') \cdot q(\cos\beta, \alpha, \gamma)$ and integrating over all angles, one can obtain the same form as eq. (14), with $Q_{lsn}(\xi', \phi')$ now denoting:

$$Q_{lsn}(\xi', \phi') = \int_{\gamma=0}^{2\pi} \int_{\alpha=0}^{2\pi} \int_{\beta=0}^{\pi} q(\cos\beta, \alpha, \gamma) Z_{lsn}(\cos\beta) \times \exp\{i(s\alpha + n\gamma)\} \sin\beta d\beta d\alpha d\gamma \qquad (16)$$

For uniaxial deformation, the orientation distribution functions contain no terms dependent on the angles ϕ, ϕ', and ϕ_j. Therefore, eqs. (10), (11), (14), and (15) may be rewritten as follows:

$$A_{l0}{}^j = 2\pi\left(\frac{2}{2l+1}\right)^{1/2} \left\{A'_{l00}\, \Pi_l(\cos\Theta_j') + 2 \sum_{n=2}^{l} A_{l0n}\, \Pi_l{}^n(\cos\Theta_j') \cos n\Phi_j'\right\} \qquad (10')$$

$$q_j(\zeta_j) = \sum_{l=0}^{\infty} A_{l0^j} \, \mathrm{II}_l(\zeta_j) \tag{11'}$$

$$A_{l0n} = \left\{\left(\frac{2}{2l+1}\right)^{1/2} \Big/ 2\pi\right\} \sum_{s=-l}^{l} (-1)^s \int_{\eta'=0}^{2\pi} \int_{\xi'=-1}^{1} w'(\xi', \eta') \times \mathrm{II}_l^s(\xi') Q_{lsn}(\xi') \exp(is\eta') d\xi' d\eta' \tag{14'}$$

and

$$A_{l0^j} = 2\pi \left(\frac{2}{2l+1}\right)^{1/2} \left\{A_{l00} \, \mathrm{II}_l(\cos \Theta_j) + 2 \sum_{n=2}^{l} A_{l0n} \, \mathrm{II}_l^n(\cos \Theta_j) \cos n\Phi_j\right\} \tag{15'}$$

Deformation of a Spherulite and the Distribution Function for Orientation of the Lamellar Axis

Whether or not the deformation of a spherulite is affine depends on the conditions of deformation of the bulk specimen, the perfection of the spherulite, and the state of the amorphous material. Hay and Keller[5] extensively studied the deformation mechanism of a spherulite in a relatively thin film and classified the possible mechanisms as homogeneous deformation and several types of inhomogeneous deformation. Oda et al.[12,13] examined dimensional changes of spherulites by optical microscopic as well as small-angle light-scattering techniques and concluded that the spherulite deformation is affine and occurs at constant volume, provided the thickness of film specimen is large compared with the size of the spherulite. Thus, the extension ratio of a spherulite may be assumed to correspond to the macroscopic deformation of a relatively thick specimen.

On the basis of the affine transformation which was assumed, first, by Kuhn and Grün[16] in their calculation of the birefringence of rubber networks and then by Wilchinsky,[2] Stein et al.,[3,4] Kawai et al.,[6,8] and Moore[10] in investigations of deformation of polymer spherulites, the orientation distribution function $w''(\xi', \phi')$ of the lamellar axis v_3 for the orthogonal biaxial deformation of a spherulite is given by

$$w''(\xi', \phi') = \frac{(\lambda_1\lambda_2\lambda_3)^2}{4\pi} [(\lambda_1\lambda_2\xi')^2 + (\lambda_3)^2(1 - \xi'^2) \times \{(\lambda_2 \cos \phi')^2 + (\lambda_1 \sin \phi')^2\}]^{-3/2} \tag{17}$$

where λ_i is the extension ratio along the x_i axis.

For uniaxial deformation of the spherulite along the x_3 axis at constant volume, eq. (17) can be reduced to:

$$w''(\xi') = \frac{\lambda^3}{4\pi} \{\lambda^3 - (\lambda^3 - 1)\xi'^2\}^{-3/2} \tag{18}$$

where $\lambda = \lambda_3$.

For the polyethylene spherulite, the polymer chain lies along the c axis (u_3 axis) within the crystallite and is perpendicular to the lamellar surface, i.e., parallel to the v_2 axis of the lamella. Therefore, it is reasonable that the u_3 axis should reorient toward the stretching direction, owing to strain of tie-chains which connect adjacent lamellae. In other words, this forced reorientation results in tilting of the crystal c axis within lamellae in the polar zone of spherulite, and untwisting of lamellae in the equatorial zone of the spherulite about their v_3 axes.[6] In addition, transformation from a crystalline to an amorphous phase, transition from the folded-chain crystals to fringed-micellar crystals due to micronecking of lamellae, crystal twinning, and cracking of lamellae, may be taken into consideration.[3–8]

In the following two sections, two models of spherulite deformation, model I, taking into account the untwisting and micronecking of lamellae, and model II, taking into account the untwisting of lamellae and the chain tilting, will be checked by using the simplest calculation in the previous section, i.e., case I, in terms of the orientation distribution functions of reciprocal lattice vectors of the crystallite.

Modified Sasaguri-Yamada-Stein Model of Spherulite Deformation (Model I)*

Sasaguri et al.[4] take the crystal lamellae grown radially within a spherulite as the orientation units, and assume the orientation distribution function of the lamellae for uniaxial deformation of the spherulite to be given by eq. (18). The crystal lamellae are assumed to be composed of two types of crystals, i.e., the folded-chain crystal (b axis parallel to the v_3 axis) and the fringed-micellar crystal (c axis parallel to the v_3 axis), as shown schematically in Figure 3. Transformation from the folded-chain

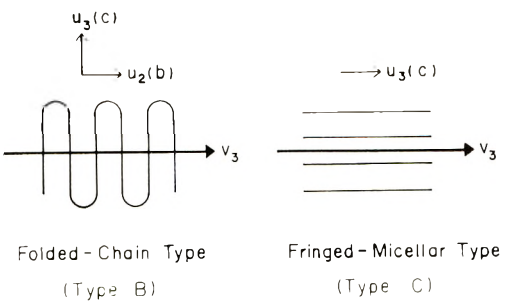

Fig. 3. Schematic representation of the folded-chain crystal (type B), in which the u_1 (a), u_2 (b), and u_3 (c) axes are parallel to the v_2, v_3, and v_1 axes of a crystal lamella, respectively, and the fringed-micellar type crystal (type C), in which the u_3 (c) axis is parallel to the v_3 axis and the u_1 (a) and u_2 (b) axes are randomly oriented around the v_3 axis.

* The model was proposed by Sasaguri et al.[4] for two-dimensional spherulites and modified by Oda et al.[6] for three-dimensional spherulites.

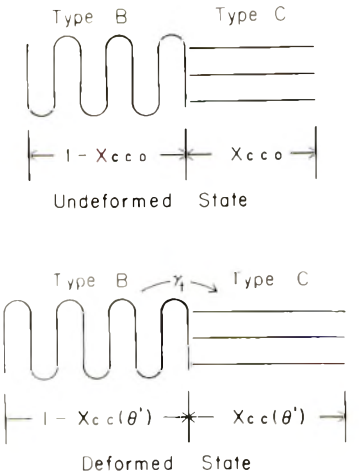

Fig. 4. Representation of weight fractions of type B and type C crystals within a lamella.

crystal to the fringed micelle due to micronecking of the lamella occurs only when the length $R(\theta')$ of a lamella in the deformed state is larger than the initial length R_0 in the undeformed state.

By a modification of the affine transformation, the length of the lamella is given, as a function of λ and θ', by

$$R(\theta) = R_0\lambda\{\lambda^3 - (\lambda^3 - 1)\cos^2\theta'\}^{-1/2} \tag{19}$$

The crystal transition from the folded-chain type to the fringed-micellar type has been represented by[3,4]

$$\begin{aligned} X_{cc}(\theta') &= X_{cc0} && \text{for} \quad R(\theta') \leqq R_0 \\ X_{cc}(\theta') &= X_{cc0} + \gamma_t\{R(\theta')/R_0 - 1\} && \text{for} \quad R(\theta') \geqq R_0 \end{aligned} \tag{20}$$

where $X_{cc}(\theta')$ is weight fraction of fringed-micellar (type C) crystals, and the parameter γ_t is a measure of the easiness of the crystal transition, illustrated schematically in Figure 4.

For a type C crystal, the u_1 axis (a axis) and the u_2 axis (b axis) are randomly oriented around its u_3 axis (the c axis which is parallel to the v_3 axis). Thus, the orientation distribution function of the type C crystal is given by

$$w^C(\xi, \eta) = w''(\cos\theta)X_{cc}(\theta)/2\pi \tag{21}$$

where $\xi' = \cos\theta'$ is interchangable with $\xi = \cos\theta$, because of coincidence of the v_3 axis with the u_3 axis, and $w^C(\xi, \eta)$ contains no term with η.

For a type B crystal, the a (u_1), b (u_2), and c (u_3) axes are parallel to v_2, v_3 (lamellar axis), and v_1 (lamellar normal), respectively. In uniaxial deformation of the spherulite, the lamellar surface may tend to untwist perpendicular to the plane containing the stretching axis (x_3 axis) and lamellar axis (v_3 axis). Therefore, on adding the effect of untwisting of

the lamella to eq. (18), the orientation distribution function of the type B crystal is given by

$$w'^{B}(\xi', \eta') = \{1 + \sigma(\lambda - 1)\sin^2\theta' \cos 2\eta'\} \times w''(\cos\theta')\{1 - X_{cc}(\theta')\}/2\pi \quad (22)$$

where σ is a measure of the easiness of untwisting of the lamella. This also corresponds to case I, where $\alpha = 0$ and $\beta = \gamma = \pi/2$. Thus, by using eq. (3), Θ_j' and Φ_j' are related to Θ_j and Φ_j:

$$\begin{bmatrix} \sin\Theta_j' \cos\Phi_j' \\ \sin\Theta_j' \sin\Phi_j' \\ \cos\Theta_j' \end{bmatrix} = \begin{bmatrix} 0, & 0, & 1 \\ 1, & 0, & 0 \\ 0, & 1, & 0 \end{bmatrix} \begin{bmatrix} \sin\Theta_j \cos\Phi_j \\ \sin\Theta_j \sin\Phi_j \\ \cos\Theta_j \end{bmatrix} \quad (23)$$

With eq. (7), the following relation may be obtained:

$$\Pi_l^s(\cos\Theta_j') \cos s\Phi_j' = \left(\frac{2}{2l+1}\right)^{1/2} \sum_{n=-l}^{l} Z_{lsn}(0)(-1)^{n/2} \times \Pi_l^n(\cos\Theta_j) \cos n\Phi_j \quad (24)$$

The coefficients of the series for $w^C(\xi, \eta)$ and $w'^B(\xi,' \eta')$ can be calculated from the following relations:

$$A^C_{l00} = \int_0^\pi w''(\cos\theta) X_{cc}(\theta)\, \Pi_l(\cos\theta) \sin\theta d\theta/2\pi \quad (25)$$

where

$$A^C_{lmn} = 0 \qquad (m \neq 0, \text{ or } n \neq 0)$$

$$A'^B_{l00} = \int_0^\pi w''(\cos\theta')\{1 - X_{cc}(\theta')\}\, \Pi_l(\cos\theta') \sin\theta' d\theta'/2\pi \quad (26)$$

$$A'^B_{l02} = \frac{\sigma(\lambda - 1)}{4\pi} \int_0^\pi w''(\cos\theta')\{1 - X_{cc}(\theta')\}\, \Pi_l^2(\cos\theta') \sin^3\theta' d\theta' \quad (27)$$

where

$$A'^B_{lmn} = 0 \qquad (m \neq 0, \text{ or } n \neq 0, 2)$$

Therefore, the coefficients of the series expansion of the orientation distribution function of a reciprocal lattice vector are given by

$$A_{l0}{}^j = A^B{}_{l0}{}^j + A^C{}_{l0}{}^j \quad (28)$$

where

$$A^B{}_{l0}{}^j = 2\pi\left(\frac{2}{2l+1}\right)^{1/2} \{A'^B_{l00}\, \Pi_l(\cos\Theta_j') + 2A'^B_{l02}\, \Pi_l^2(\cos\Theta_j') \cos 2\Phi_j'\} \quad (29)$$

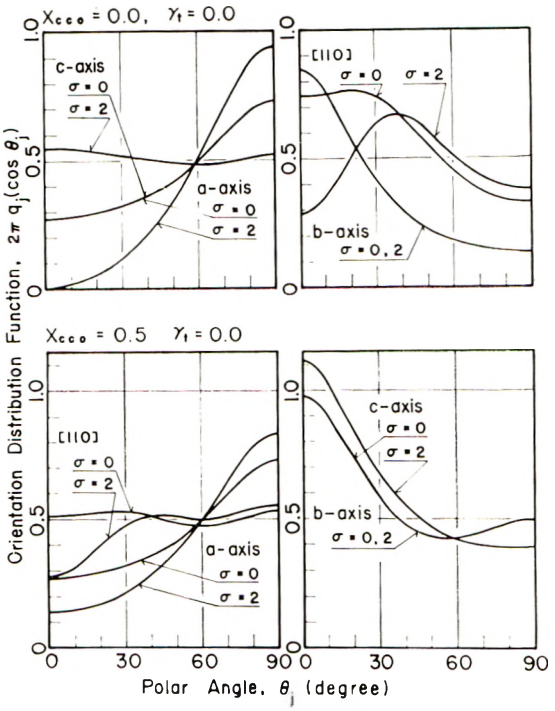

Fig. 5. Orientation distribution functions of the crystal axes and the reciprocal lattice vector of the (110) plane for spherulite deformation ($\lambda = 1.5$), model I.

and

$$A^{C}{}_{l0}{}^{j} = 2\pi\left(\frac{2}{2l+1}\right)^{1/2} A^{C}_{l00}\, \Pi_l(\cos\Theta_j) \tag{30}$$

Thus, the orientation distribution function of a reciprocal lattice vector can be calculated from eq. (11′).

Figures 5 and 6 show the calculated results for orientation distribution functions of a reciprocal lattice vector at an extension ratio $\lambda = 1.5$. In Figure 5, γ_t is assumed to be zero, i.e., the crystal transition is not taken into account, while the other two parameters, X_{cc0} and σ are changed. The orientation of the crystal b axis is, as recognized from the model, independent of the parameter σ. The a and b axes of the crystal orient preferentially perpendicular and parallel to the stretching direction, respectively. The c axis tends toward the stretching direction with increase of X_{cc0} and σ. In contrast, the reciprocal lattice vector of the (110) crystal plane orients away from the stretching direction with increasing of X_{cc0} and σ.

Figure 6 shows results with fixed values $X_{cc0} = 0.5$ and $\sigma = 2$ but with varying γ_t. Variation of γ_t has the strongest effect on the orientation of the crystal b axis, which changes from parallel to perpendicular with respect to the stretching direction as γ_t increases. On the other hand,

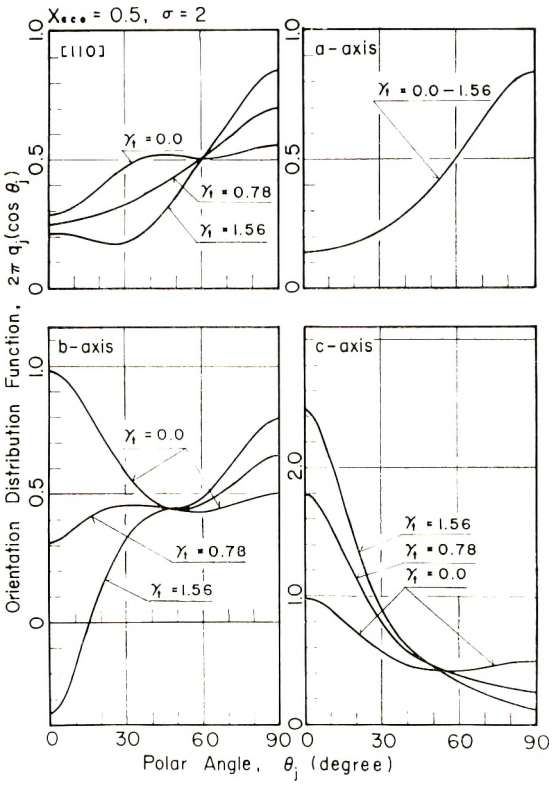

Fig. 6. Orientation distribution functions of the crystal axes and of the reciprocal lattice vector of the (110) plane for spherulite deformation ($\lambda = 1.5$), model I.

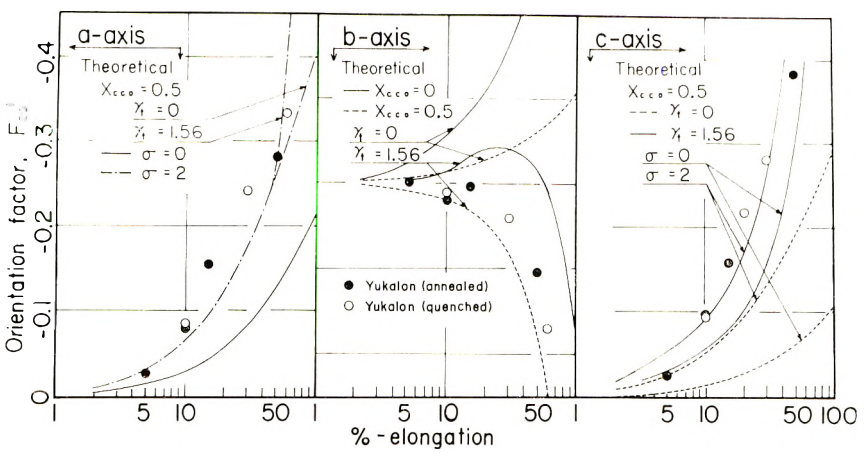

Fig. 7. Comparison of crystal orientation in uniaxially stretched polyethylene with behavior calculated from model I for spherulite deformation: orientation factors $F_{20}{}^{j}$.

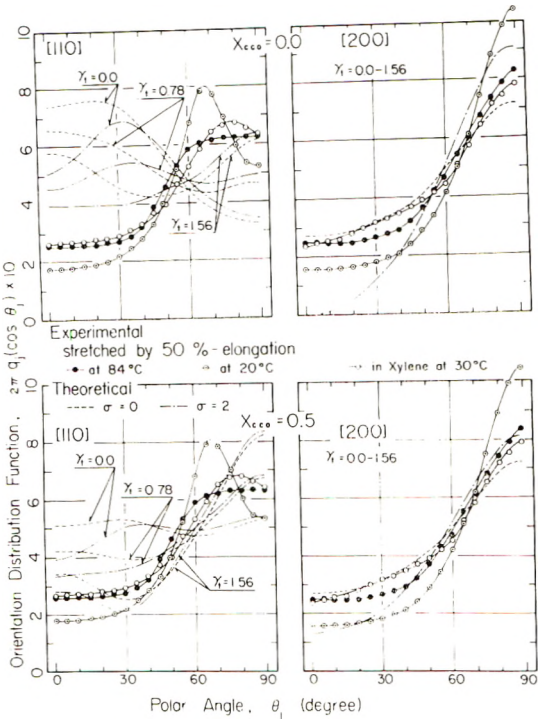

Fig. 8. Comparison of crystal orientation of uniaxially stretched polyethylene under various conditions with behavior calculated from model I for spherulite deformation: orientation distribution functions of reciprocal lattice vectors.

the orientation of the crystal c axis and that of the reciprocal lattice vector of the (110) crystal plane change gradually to become parallel and perpendicular to the stretching direction, respectively, as γ_t increases.

Figure 7 shows a comparison of uniaxial orientation behavior of crystalline polyethylene in terms of the second-order orientation factors, F_{20}^j, observed experimentally for quenched and annealed low-density polyethylene, Yukalon YK-3200, near 20°C with that calculated theoretically from the above SYS model of spherulite deformation.[6] As can be seen, fairly good agreement of the calculated results with the experimental ones for both samples is obtained, when the parameters, X_{cc0}, γ_t, and σ are chosen as 0.5, 1.56, and 2, respectively.

However, in contrast, Figure 8 shows another comparison of the orientation behavior in terms of the orientation distribution functions of the reciprocal lattice vectors of the (110) and (200) crystal plane observed experimentally for the same quenched Yukalon specimen at a fixed extension ratio $\lambda = 1.5$, but under various conditions, with that calculated theoretically from the above model. Rather good agreement of the calculated and experimental results is achieved only for swollen samples and at high temperature. At room temperature, very poor agreement is

realized between the calculated and experimental results (especially for the distribution function of the reciprocal lattice vector of the (110) crystal plane, which experimentally gives a peak at a polar angle $\theta_{110} \approx 70°$), even when the proper values of parameters are taken. This discrepancy suggests some insufficiency of the SYS model, probably due to the extreme crystal transition mechanism, and also that the investigation of orientation behavior in terms of such a limited number of orientation factors $F_{lm}{}^{j}$ (e.g., for $l = 2$) may be very misleading, giving no detailed information on the orientation behavior.[14,15]

Spherulite Deformation Model Taking into Account Lamellar Untwisting and Chain Tilting (Model II)

In the previous section, the crystal transition due to unfolding of folded chains within the crystal lamella was taken into account in addition to untwisting of the lamella. Here, instead of unfolding, chain tilting within the lamella due to shearing deformation of crystallites along a crystal plane will be considered. The orientation mechanism for crystal lamellae is taken to be the same as that described in the previous section; i.e., the deformation is affine and the orientation distribution function, like eq. (22), is given by

$$w'(\xi', \eta') = w''(\xi')\{1 + \sigma(\lambda - 1)(1 - \xi'^2)\cos 2\eta'\}/2\pi \qquad (31)$$

The direction of chain tilt may not be confined to the v_1v_3 plane, i.e., it is not necessarily toward the 010 direction of the crystallite as shown in Figure 9. The chain tilt may be associated with slippage of some particular crystal plane of the crystallite, and the geometrical relation between the coordinates $0\text{-}v_1v_2v_3$ and $0\text{-}u_1u_2u_3$ must change with each type of chain tilt. However, the principle of the calculation is not

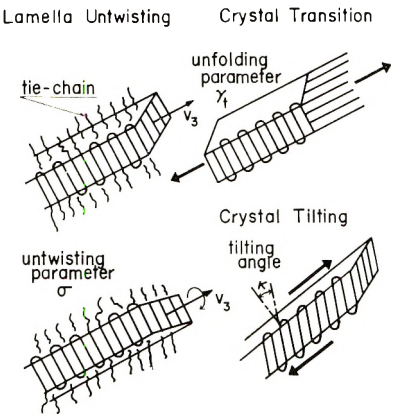

Fig. 9. Schematic illustrations of deformation of crystal lamellae: (above) model I taking account of the crystal transition and untwisting of lamella; (lower) model II taking account of the chain tilting and untwisting of lamella.

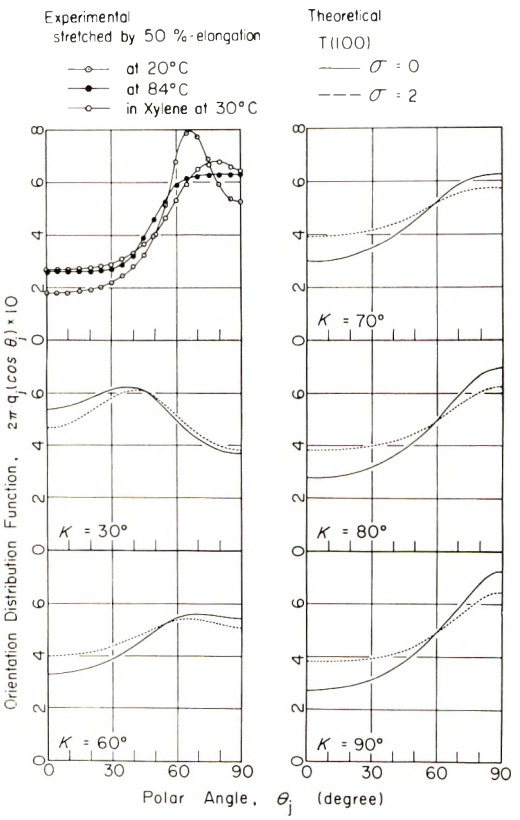

Fig. 10. Comparison of orientation distribution functions of reciprocal lattice vectors for the (110) crystal plane observed for uniaxially stretched polyethylene at $\lambda = 1.5$, with those calculated from model II for spherulite deformation.

changed: the calculation still follows Case I, and α, β, and γ are not functions of ξ' and ϕ'.

As in the previous model, the distribution function, eq. (31), can be expanded in a series of spherical harmonics. The coefficients A'_{lmn}, as in eqs. (26) and (27), may be obtained, and reduced to zero except when m is zero and n is zero or 2. Then, for each type of chain tilting, the relations given by eq. (7) may be calculated, and the coefficients $A_{lm}{}^{j}$ for each reciprocal lattice vector may be calculated from eq. (10′). Thus, the orientation distribution function of a given reciprocal lattice vector can be obtained from eq. (11′).

Comparisons of the orientation distribution function observed for the reciprocal lattice vector of the crystal (110) plane with those calculated by varying the tilt angle and tilt direction, are illustrated in Figures 10–12. In Figure 10, the polymer chain, i.e., the crystal c axis is assumed to be tilted toward the 010 direction within the (100) crystal plane, and the tilt angle κ and the untwisting parameter σ are varied. As can be seen in the figure, variation of σ causes only a slight shift of peak position of

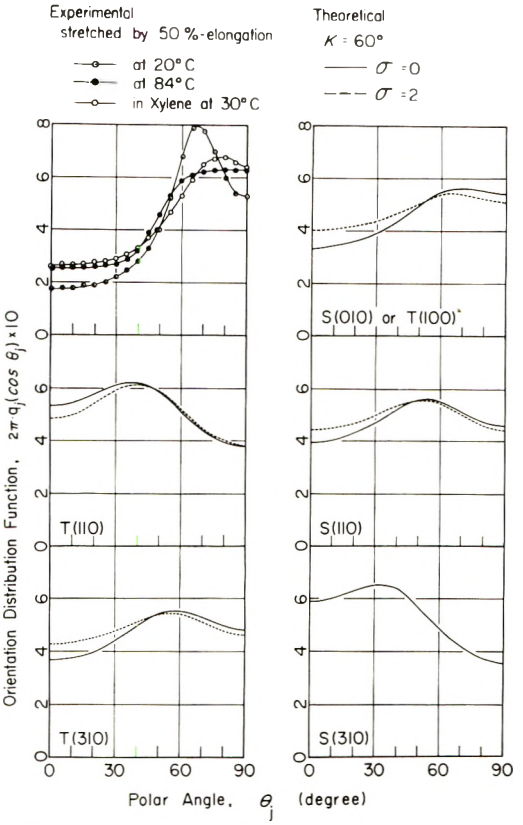

Fig. 11. Comparison of observed orientation distribution function of reciprocal lattice vectors of the (110) crystal plane for uniaxially stretched polyethylene ($\lambda = 1.5$) with functions calculated from model II with $\kappa = 60°$.

the distribution function, but, in contrast, the variation of κ gives a definite change in the distribution function, shifting the peak position toward higher angles θ_j with increasing κ. By comparing the results for $\kappa = 60°$ and $\kappa = 70°$ in Figure 10 with those in Figure 8, considerable improvement may be seen, though some discrepancies still remain. That is, the result for $\kappa = 70°$ and $\sigma = 0$ is in fairly good agreement with the experimental result at 84°C; and the result for $\kappa = 60°$ and $\sigma = 2$ exhibits a peak in the distribution function, whose sharpness is, however, still less than that of the experimental peak at room temperature, at $\theta_j \approx 70°$.

Figures 11 and 12 show the comparison of observed results with calculated ones when the tilting angle is taken as 60° and 90°, and the tilt direction is varied. In these figures, $S(hk0)$ designates the tilt of the c axis toward the normal of the $(hk0)$ crystal plane owing to the slip of the $(hk0)$ plane, and $T(hk0)$ designates the tilt of the c axis within the $(hk0)$ plane. As is shown in the figures, the variation of the untwisting parameter σ has a somewhat smaller effect on the distribution function than variation of the tilt direction. Comparing the results in Figure 10 with

those in Figure 12, we note that the result for $\kappa = 30°$ in Figure 10 corresponds to the results for $S(310)$ and $T(110)$ and $T(310)$; i.e., the changes of the tilt angle κ and tilt direction $(\pi/2 - \delta)$ have similar effects on the distribution function [δ is the angle between the v_3 axis and the projection of the tilted c axis to the v_2v_3 plane as shown in Figure 13 and listed in Table I in terms of $S(hk0)$ and $T(hk0)$]. From the calculated results in Figures 10–12, it may be concluded that, when the value of $(\sin \kappa \cos \delta)$

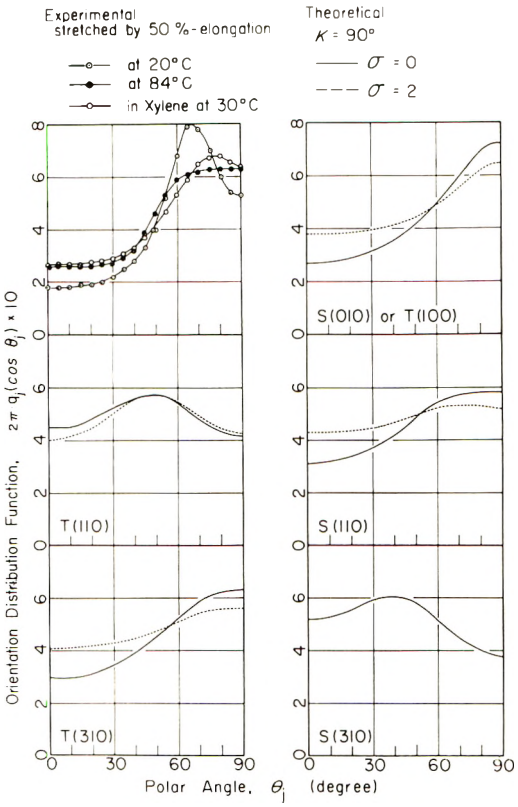

Fig. 12. Orientation distribution functions of the reciprocal lattice vectors of the (110) crystal plane: as in Fig. 11 but with $\kappa = 90°$.

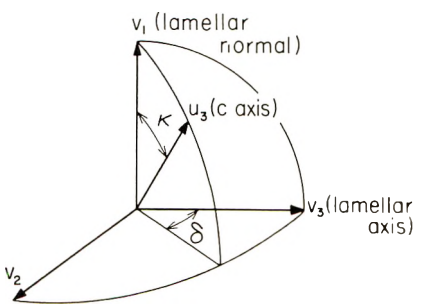

Fig. 13. Illustrations of tilt direction (δ) and tilt angle κ of the u_3 axis in a crystal lamella.

TABLE I
Values of δ

Notation	δ
$S(010)$	0.0°
$T(100)$	0.0°
$T(310)$	26.57°
$S(110)$	33.69°
$T(110)$	56.31°
$S(310)$	63.43°

is larger than $\sqrt{3}/2$, good agreement with the experimental results at elevated temperature and in the swollen state is achieved.

In view of imperfections in crystal lamella and/or the so-called mosaic structure of lamellae,[17,18] our conclusion favoring the chain tilting mechanism rather than untwisting of crystal lamella, is reasonable. More detailed calculations based on cases II and III taking α, β, and γ as functions of θ' and ϕ' will be discussed elsewhere.

The authors are indebted to the Toray Industries Ltd., the Nippon Gosei Kagaku Co. Ltd., and the Dai-Nippon Cellophane Mfg. Co. Ltd., for financial support through a scientific research grant.

References

1. H. D. Keith and J. Paddon, *J. Polym. Sci.*, **41**, 525 (1959).
2. Z. W. Wilchinsky, *Polymer*, **5**, 271 (1964).
3. K. Sasaguri, S. Hoshino, and R. S. Stein, *J. Appl. Phys.*, **35**, 47 (1964).
4. K. Sasaguri, R. Yamada, and R. S. Stein, *J. Appl. Phys.*, **35**, 3188 (1964).
5. I. L. Hay and A. Keller, *Kolloid-Z. Z. Polym.*, **204**, 43 (1965).
6. T. Oda, S. Nomura, and H. Kawai, *J. Polym. Sci. A*, **3**, 1993 (1965).
7. K. Kobayashi and T. Nagasawa, in *U.S.–Japan Seminar in Polymer Physics* (*J. Polym. Sci. C*, **15**), R. S. Stein and S. Onogi, Eds., Interscience, New York, 1966, p. 163.
8. T. Oda, N. Sakaguchi, and H. Kawai, *U.S.–Japan Seminar in Polymer Physics* (*J. Polym. Sci. C*, **15**), R. S. Stein and S. Onogi, Eds., Interscience, New York, 1966, p. 223.
9. R. J. Samuels, in *Supramolecular Structure in Polymers* (*J. Polym. Sci. C*, **20**), P. H. Lindenmeyer, Ed., Interscience, New York, 1967, p. 253; *J. Polym. Sci. A-2*, **6**, 1101 (1968).
10. R. S. Moore, *J. Polym. Sci. A-2*, **5**, 711 (1967).
11. R. G. Crystal and D. Hansen, *J. Polym. Sci. A-2*, **6**, 981 (1968).
12. T. Oda, N. Sakaguchi, and H. Kawai, *Kobunshi Kagaku*, **25**, 588 (1968).
13. T. Oda, M. Motegi, M. Moritani, and H. Kawai, *Kobunshi Kagaku*, **25**, 639 (1968).
14. R. J. Roe, *J. Appl. Phys.*, **36**, 2024 (1965).
15. S. Nomura, H. Kawai, I. Kimura, and M. Kagiyama, *J. Polym. Sci. A-2*, **8**, 383 (1970).
16. W. Kuhn and F. Grün, *Kolloid-Z.*, **101**, 248 (1942).
17. V. F. Holland and P. H. Lindenmeyer, *J. Appl. Phys.*, **36**, 3049 (1965).
18. M. Takayanagi and T. Matsuo, *J. Macromol. Sci.-Phys.*, **B1**, 407 (1967).

Received December 3, 1970
Revised April 28, 1971

JOURNAL OF POLYMER SCIENCE: PART A-2 VOL. 9, 2009–2021 (1971)

Dynamic Mechanical Properties of Moderately Concentrated Polystyrene Solutions

LARRY A. HOLMES,* SUMIO KUSAMIZU,† KUNIHIRO OSAKI,‡ and JOHN D. FERRY, *Department of Chemistry, University of Wisconsin, Madison, Wisconsin 53706*

Synopsis

The storage (G') and loss (G'') shear moduli have been measured in the frequency range from 0.04 to 630 Hz for solutions of narrow distribution polystyrenes with molecular weights (M) 19,800 to 860,000, and a few of poly(vinyl acetate), M = 240,000. The concentration (c) range was 0.014–0.40 g/ml and the viscosities of the solvents (diethyl phthalate and chlorinated diphenyls) ranged from 0.12 to 70 poise. Data at different temperatures (0–40°C) were combined by the method of reduced variables. Two types of behavior departing from the usual frequency dependence describable by the Rouse-Zimm-Tschoegl theories were observed. First, for $M \cong 20{,}000$, the ratio $(G'' - \omega\eta_s)/G'$ in the neighborhood of $\omega\tau_1 = 1$ was abnormally large and the steady-state compliance J_e^0 was abnormally small, especially at the lowest concentrations studied. Here ω is circular frequency, η_s solvent viscosity, and τ_1 terminal relaxation time. Related anomalies have been observed by others in undiluted polymers at still lower molecular weights. Second, at the highest concentrations and molecular weights, a "crossover" region of the logarithmic frequency scale appeared in which $G'' - \omega\eta_s < G'$. The width of this region is a linear function of log c; the frequency dependence under these conditions can be represented by a sequence of Rouse relaxation times grafted on to a sequence of Zimm relaxation times. For each molecular weight, the terminal relaxation time τ_1 was approximately a single function of c for different solvents of widely different η_s. At lower concentrations, τ_1 was close to the Rouse prediction of $6\eta M/\pi^2 cRT$, where η is the steady-flow viscosity; but at higher concentrations, τ_1 was proportional to η/c^2 and corresponded, according to a recent theory of Graessley, to an average molecular weight of 20,000 between entanglement coupling points in the undiluted polymer.

INTRODUCTION

Extensive measurements have been reported previously for dynamic mechanical properties of rather dilute solutions of narrow-distribution polystyrenes, in the molecular weight range from 8.2×10^4 to 1.7×10^6, in solvents of high viscosity, obtained with the Birnboim transducer apparatus in its original form.[1] Subsequent low-frequency measurements at higher concentrations provided steady-state compliances over wide ranges of concentration and molecular weight, which have also been

* Present address: Esso Research and Engineering Company, Baytown, Texas.
† Present address: Japan Synthetic Rubber Company, Kawasaki, Japan.
‡ Present address: Kyoto University, Kyoto, Japan.

published,[2-4] but the data obtained at higher frequencies in these studies have not yet been reported. Recently, modifications in the Birnboim apparatus by Massa and Schrag[5-7] have permitted more precise measurements at higher concentrations and in solvents of higher viscosity. In the present paper, some results are described which cover an extended range of reduced frequency, obtained partly before and partly after the apparatus modifications made by Massa and Schrag. They provide some information about anomalies at lower molecular weights, effects of entanglement coupling at higher concentrations, and the dependence of terminal relaxation times on concentration and molecular weight. Some fragmentary data on poly(vinyl acetate) solutions are included.

MATERIALS AND METHODS

The sources and characteristics of the polystyrene and polyvinyl acetate samples have been described previously;[2-4] their identifications are summarized in Table I.

The solvents used were three Aroclors (partially chlorinated diphenyls), with viscosities at 25°C as follows: A1232, 0.119 or 0.143 poise (depending on the lot); A1248, 2.62 poise; A1254, 69.1 poise; also diethyl phthalate, 0.73 poise. Additional information on the temperature dependence of viscosity and density of these liquids is reported elsewhere.[1-4,8,9] Solutions were made up by weight; to calculate concentrations in grams per milliliter, the solution densities were estimated with sufficient accuracy by assuming additivity of the volumes of polymer and solvent.

The Birnboim-Ferry apparatus[10] with minor modifications previously described[2,11] was used in the frequency range from 0.06 to 400 Hz ("old apparatus"). As modified by Massa and Schrag, with computerized data acquisition and processing system and open-ended geometry for solutions of high viscosity,[5-7] it was used in the frequency range from 0.04 to 630 Hz ("new apparatus"). Measurements of the storage and loss shear moduli, G' and G'', were usually made at two temperatures (sometimes one or three) and reduced to a single reference temperature, usually 25°C., by multiplying the frequency by[11] $(\eta - \eta_s)T_0c_0/(\eta - \eta_s)_0Tc$, where η is the steady-flow viscosity of the solution and η_s the solvent viscosity, T the absolute temperature and c the concentration in g/ml; the subscript 0 refers to the reference temperature. (The values of c and c_0 differ only

TABLE I
Characteristics of Polymer Samples

Polymer	Sample code	$\bar{M}_w \times 10^{-3}$	$\bar{M}_w/\bar{M}_n$
Polystyrene	2a	19.8	1.06
	2b	21.0	1.06
	S-108	267	1.08
	6a	860	1.15
Poly(vinyl acetate)	3-9	240	1.04

because of thermal expansion.) The storage and loss moduli G' and G'' are multiplied by T_0c_0/Tc for temperature reduction. In some previous publications,[1,2] η_s in the above expression has been multiplied by v_1, the volume fraction of solvent, but this factor is now abandoned because its effect is always negligible in practice.

RESULTS

Frequency Dependence of the Complex Shear Modulus

Logarithmic plots of G' and $G'' - \omega\eta_s$ against the radian frequency ω, for polystyrene of $M = 267{,}000$ at concentrations up to 0.1 g/ml and $M = 860{,}000$ up to 0.05 g/ml, displayed the familiar shapes previously found for many dilute polymer solutions,[11–16] with frequency dependence ranging between the characteristic predictions of the Rouse theory[17] and the Zimm theory with dominant hydrodynamic interaction.[18] For the former, $G' = G'' - \omega\eta_s$ at higher frequencies; for the latter, $\log(G'' - \omega\eta_s)/G' = 0.24$. However, two departures from this standard behavior were seen in some of the other solutions.

At the lowest molecular weight (21,000), $G'' - \omega\eta_s$ and G' are separated by more than 0.24 on the logarithmic scale, as illustrated in Figure 1.

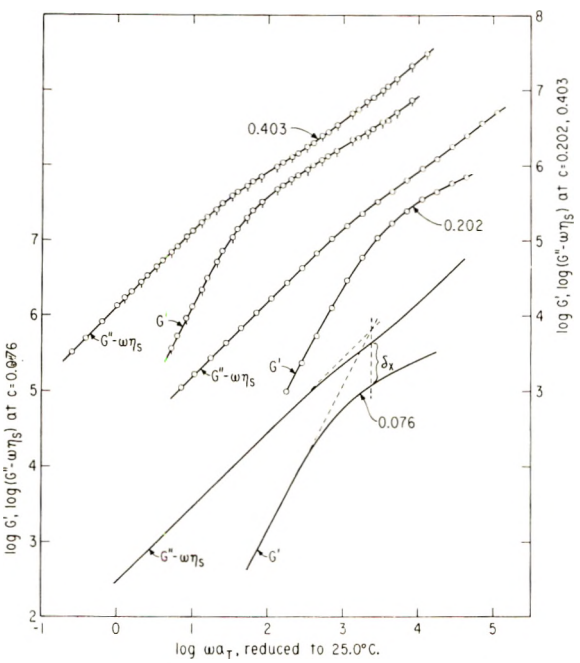

Fig. 1. Logarithmic plots of G' and G''-$\omega\eta_s$ against radian frequency for polystyrene of low molecular weight at concentrations (c) in g/ml as shown. All data reduced to 25.0°C. Lowest concentration: $M = 19{,}800$ in Aroclor 1254 (data of Massa[6,7]); upper two concentrations, $M = 21{,}000$ in Aroclor 1248. Temperatures of measurement at $c = 0.403$: (○) 24.9°C; (♀) 18.9°C. All measurements with new apparatus. See text for explanation of δ_x.

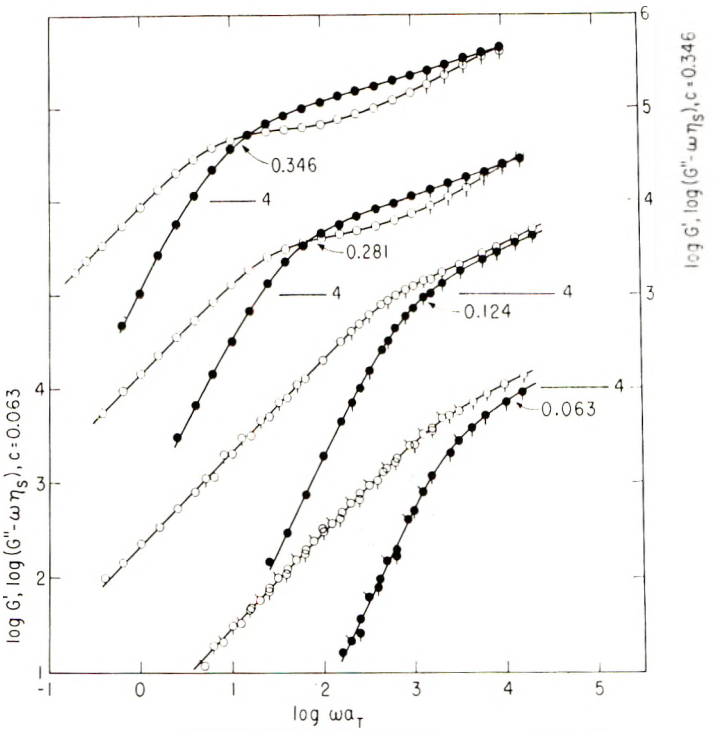

Fig. 2. Logarithmic plots of (●, ◔, ◕,) G' and (○,◔,◑) $G'' - \omega\eta_s$ against radian frequency for polystyrene with $M = 267{,}000$, at various concentrations in g/ml as shown, in Aroclor 1232. Ordinates displaced as shown by respective locations of 4 on the scale. Lower two concentrations with old apparatus, upper two with new. Temperatures as follows: $c = 0.063$, (◔,◔) 0.2°C, (◑,◕) 15.2°C, (○,●) 25.1°C; $c = 0.124$, (◔,◔) 0.1°C, (○,●) 25.1°C; $c = 0.281$, (◔,◔) 0.6°C, (○,●) 25.0°C; $c = 0.346$, (◔,◔) 15.0°C, (○,●) 24.9°C. All reduced to 25.0°C.

This behavior has already been reported for a polystyrene of similar molecular weight by Massa[6,7] (data included in Fig. 1); it is associated with a truncated "power-law" region of frequency dependence and the early onset, with increasing frequency, of behavior reflecting backbone immobility.

On the other hand, for higher molecular weights at higher concentrations, a crossover region develops in which $G' > G'' - \omega\eta_s$; and the width of this region on the logarithmic frequency scale increases progressively with concentration, as illustrated in Figure 2. This is, of course, the familiar pattern seen in undiluted polymers,[19] corresponding to the plateau zone of viscoelastic behavior which is attributed to entanglement coupling.

To characterize the low molecular weight anomaly empirically, we have adopted an arbitrary measure of the separation between $G'' - \omega\eta_s$ and G' by taking the logarithm of their ratio at the frequency where the linear low-frequency segments of G' and $G'' - \omega\eta_s$ would cross, as shown by the construction in Figure 1 for the bottom pair of curves. This character-

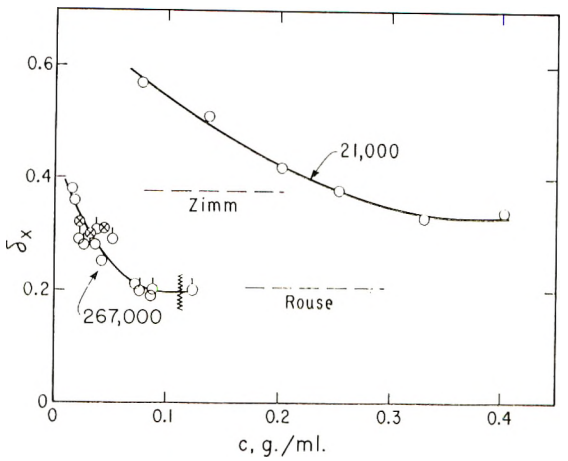

Fig. 3. Plot of δ_x (= log $(G'' - \omega\eta_s)/G'$ at the terminal zone cross frequency) against concentration for polystyrenes of two molecular weights as indicated (except that lowest concentration for upper curve is M = 19,800): (Ô) in A1232, (○) in A1248; and for poly(vinyl acetate), M = 240,000, (⊗) in diethyl phthalate and (⊗) A1248. Wavy line denotes onset of entanglement coupling.

istic frequency is given by $(\eta - \eta_s)/A_G$, where A_G is the limiting ratio G'/ω^2 at low frequencies (often used for calculating the steady-state compliance J_e^0). The values of $\log(G'' - \omega\eta_s)/G'$ here (denoted by δ_x) corresponding to the Rouse and Zimm theories are 0.21 and 0.35 respectively.

Values of δ_x for a number of polystyrene solutions and a few of poly(vinyl acetate) are summarized in Table II. Those for M = 21,000 and 267,000 are plotted against concentration in Figure 3. With increasing concentration, δ_x for M = 267,000 falls from a value characteristic of dominant hydrodynamic interaction (Zimm, $h = \infty$) to a value characteristic of vanishing hydrodynamic interaction (Rouse, h = 0); this behavior is consistent with the previously reported apparent dependence of h on concentration and molecular weight.[1,12] It may be noted that the points for poly(vinyl acetate) with M = 240,000 fall quite close to those for polystyrene with M = 267,000. This would be expected if the change in effective hydrodynamic interaction with concentration is associated with overlapping of the peripheries of the random coils;[1] the unperturbed coil dimensions of these two polymers are quite similar,[20] so equal molecular weights correspond to equal effective coil volumes. However, for M = 21,000, δ_x is higher than the Zimm value of 0.35 at lower concentrations, and it does not drop to the Rouse value at high concentrations. This behavior is associated with an abnormally small steady-state compliance as previously reported for a sample of similar molecular weight,[3,4] although the anomaly then seen was exaggerated by errors due to compliance of the apparatus.[6,7] Reliable data for the steady-state compliance obtained with the new modified apparatus are included in Table II, expressed as J_{eR}^0 =

TABLE II
Parameter δ_x, Nominal Terminal Relaxation Time, and j^0_{eR}

$M \times 10^{-3}$	Solvent[a]	$c \times 10^2$, g/ml	Temp, °C	δ_x	log τ_1	log τ_1/η_s	j^0_{eR}	App.[b]
			Polystyrene					
19.8[c]	A1254	7.6	25.0[d]	0.57	−3.15	−4.97	0.16	N
21.0	A1248	13.6	10.0	0.51	−2.67	−4.13	0.24	N
	1248	20.2	10.0	0.42	−2.08	−3.62	0.29	N
	1248	25.4	10.0	0.38	−1.70	−3.24	0.27	N
	1248	33.0	24.9	0.33	−2.51	−2.91	0.32	N
	1248	40.3	24.9[d]	0.34	−1.81	−2.21	0.36	N
267	A1248	1.53	25.0	0.38	−2.91	−3.32	e	O
	1248	1.84	25.0	0.36	−2.84	−3.25	e	O
	1248	2.2	22.8	0.29	−2.61	−3.24	e	O
	1232	2.5	0.6	0.28	−3.19	−3.09	e	O
	1248	3.6	25.0	0.28	−2.60	−3.01	e	O
	1232	3.8	0.0	0.31	−2.94	−2.87	e	O
	1248	4.3	25.1	0.25	−2.46	−2.87	e	O

	1232	5.0	0.0	0.29	−2.67	−2.60	e	O
	1232	6.3	25.1	0.27	−3.64	−2.80	e	O
	1248	7.1	35.1	0.21	−2.63	−2.63	e	O
	1232	7.5	0.0	0.20	−2.42	−2.35	e	O
	1248	8.5	35.0	0.19	−2.45	−2.45	e	O
	1232	8.8	10.1	0.20	−2.76	−2.30	e	O
	1232	12.4	25.1	0.20	−2.86	−2.01	e	O
860	A1248	1.44	25.1	0.35	−1.76	−2.17	e	O
	1248	3.0	35.1	0.28	−1.75	−1.73	e	O
	1232	3.8	25.3	—	−2.45	−1.60	e	O
				Poly(vinyl Acetate)				
240	DEP	2.3	0.0	0.32	−3.66	−3.21	e	O
	DEP	3.4	0.0	0.30	−3.43	−2.98	e	O
	A1248	4.3	25.0	0.31	−2.65	−3.06	e	O

[a] A = Aroclor, DEP = diethyl phthalate.
[b] N = new apparatus (after references 5-7), O = old (before).
[c] Data of D. J. Massa.[6,7]
[d] Reduced from measurements at two or more temperatures.
[e] Reported previously.

TABLE III
Crossover Parameter Δ_x and Nominal Terminal Relaxation Time
(Polystyrenes)

$M \times 10^{-3}$	Solvent	$c \times 10^2$, g/ml	Temp, °C	Δ_x	log τ_1	log τ_1/η_s	App.[a]
267	A1232	24.3	25.0	2.05	−1.59	−0.66	N
	1232	28.1	25.0	2.35	−1.22	−0.29	N
	1232	34.6	24.9	2.85	−0.65	0.28	N
860	A1248	7.0	34.8	1.36	—	—	O
	1232	9.0	40.1	2.06	−1.88	−0.82	O
	1232	11.4	40.0	2.54	−1.54	−0.62	O

[a] N = new apparatus (after references 5–7), O = old (before).

$A_G cRT/M(\eta - \eta_s)^2$. (This quantity has previously[2-4] been denoted by S'/S^2, but it seems desirable to reserve the latter designation for theoretical calculations and use j^0_{eR} for experimentally determined values; $j^0_{eR} = J_e{}^0[\eta/(\eta - \eta_s)]^2 cRT/M$.) At the lowest concentration, $j^0_{eR} = 0.16$, less than the minimum of 0.206 predictable by the usual bead-spring theories with variable hydrodynamic interaction, and all the values are less than the Rouse prediction of 0.400.

To characterize the high-concentration crossover, its width on the logarithmic scale, Δ_x, is given in Table III for several solutions. Although this does not have a simple theoretical interpretation, it is a rough measure of the number of entanglement points per molecule; it increases with c (approximately a linear function of log c with slope 5.3) and with M.

DISCUSSION

Terminal Relaxation Times

In the normal coordinate theories of linear viscoelastic properties, or any theory involving discrete contributions associated with discrete relaxation times, an important parameter is the terminal or longest relaxation time τ_1 characterizing the slowest mode of motion. In particular, it is of interest to determine whether τ_1 is proportional to the solvent viscosity η_s.

If each contribution to the shear modulus G_i is associated with a relaxation time τ_i, the constant A_G is given by $\sum G_i\tau_i^2$, and $\eta - \eta_s = \sum G_i\tau_i$, independently of any molecular theory. It follows that

$$\tau_1 = \frac{A_G}{\eta - \eta_s} \frac{\sum G_i(\tau_i/\tau_1)}{\sum G_i(\tau_i/\tau_1)^2} \tag{1}$$

so τ_1 can be determined from measurements at low frequencies—the same information[2] that furnishes $J_e{}^0$—provided the ratio of sums is known. For the Rouse, Zimm, or Tschoegl theories, all G_i are equal, and the ratio (often[2] denoted by S/S') varies only from 1.52 for vanishing hydrodynamic interaction to 2.05 for dominant hydrodynamic interaction. The Graes-

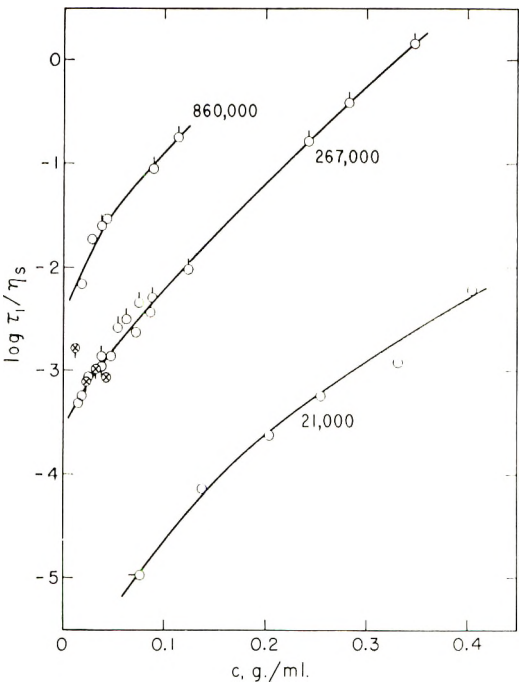

Fig. 4. Logarithm of ratio of nominal terminal relaxation time to solvent viscosity, plotted against concentration for polystyrenes with different molecular weights as indicated and for poly(vinyl acetate) (⊗,⊗) with M = 240,000. Code to solvents same as in Fig. 3, except (-O) is in A1254.

sley theory for entangled polymers[21] specifies this ratio as 2.00. The Rouse value of 1.52 for S/S' has been used to calculate nominal terminal relaxation times for the solutions listed in Table II, and the Graessley value of 2.00 for those in Table III which are subject to entanglement coupling as evidenced by the crossover Δ_r. Values of log τ_1/η_s are also given in the Tables.

It is implicit in the bead-spring molecular theories with no account of internal viscosity that the frictional resistance to motion is determined solely by the environment and therefore that the terminal relaxation time in very dilute solution is proportional to the solvent viscosity. This relation has been confirmed recently by data extrapolated to infinite dilution.[16] Even in moderately concentrated solution, if $\eta - \eta_s$ is approximately proportional to η_s, τ_1 should be proportional also. The solvents employed here have viscosities ranging over more than a factor of 500; there are only a few cases of matching concentrations in different solvents, but the proportionality of τ_1 to η_s can be tested by plotting τ_1/η_s against c to see if all points fall on a single curve for each molecular weight. This is found to be the case approximately for each of the polystyrenes, as shown in Figure 4. Exact conformance is not expected, since even in a single solvent the temperature dependences of η_s and $\eta - \eta_s$ are not the

same. However, τ_1 is evidently roughly proportional to η_s. The points for the poly(vinyl acetate) fall close to those for the polystyrene with nearly the same molecular weight.

The dependence of τ_1 on polymer concentration and molecular weight is also of great interest. Another characteristic time constant τ_0 obtained from the dependence of non-Newtonian viscosity on shear rate,[22] which according to the Graessley theory[23] should be closely related to τ_1, has been found to be proportional to $\eta M/c$ when entanglement is not present and to η/c^2 when entanglement dominates.[23,24] The present data allow us to make an analogous examination of τ_1. According to the modified Rouse theory,[19] when $\eta \gg \eta_s$, $\tau_1 cT/\eta M$ should be a constant equal to $6/\pi^2 R$.

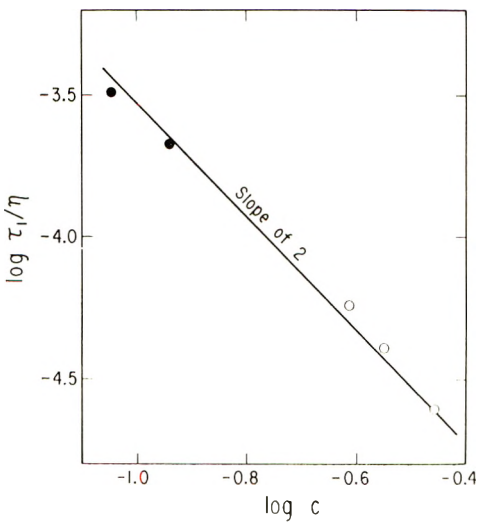

Fig. 5. Logarithmic plot of τ_1/η against concentration: (○) M = 267,000 (new apparatus); (●) M = 860,000 (old apparatus).

Averaging the data of Table II for M = 267,000 in the concentration range from 0.04 to 0.12 g/ml gives $\log(\tau_1 cT/\eta M) = -8.17$, and for M = 860,000, -8.13; whereas $\log(6/\pi^2 R) = -8.13$, so the proportionality to $\eta M/c$ is confirmed with the factor predicted by the Rouse theory. The values of τ_1 in Table III, where entanglement is present, are proportional to η/c^2 without a factor of M as illustrated in Figure 5. Thus the behavior of τ_1 parallels that of τ_0, although the data are too sparse for a detailed analysis. From the Graessley relation[21] $\tau_1 c^2/\eta = 3.575\, M_e \rho/RT$, where M_e is the average molecular weight between entanglements in the undiluted polymer, the data of Figure 5 give M_e = 20,000, a reasonable value.

The regimes where τ_1 is proportional to $\eta M/c$ and to η/c^2 respectively correspond to those where the steady-state compliance is proportional to M/c and to $1/c^2$ respectively, as observed by several investigators.[23–26]

Anomalies for Low Molecular Weights

In undiluted polystyrene above the glass transition temperature, various departures from the predictions of the Rouse theory have been reported for low molecular weights.[27,28] For $M < 10{,}000$, J_e^0 is abnormally low, and the viscoelastic properties have a different time or frequency dependence, reflecting the paucity of submolecules in the Rouse sense. Even for M up to 50,000, there is an anomalous temperature dependence[27] of J_e^0. Evidently, the presence of diluent causes anomalously low values of J_e^0 to appear at higher molecular weights than in the undiluted polymer, since in Table II j_{eR}^0 is smaller than the Rouse value of 0.40 when $M = 21{,}000$ and $c \leqq 0.4$ g/ml. It is reasonable that the presence of diluent should enhance the tendency of the molecule to move as a unit without internal configurational adjustments, but no attempt is made to interpret these observations in terms of molecular theory at present.

Theory of the Plateau Zone

Several modifications[21,29–32] of the Rouse theory have been introduced to account in terms of entanglement for the plateau zone in undiluted polymers or concentrated solutions, where G' changes slowly with frequency and $G'' < G'$, as in Figure 2. But they all reduce to a frequency dependence of the Rouse form at high frequencies so that G' and $G'' - \omega\eta_s$ merge with a common slope of $^1/_2$ on a logarithmic plot without the second crossover illustrated at the two highest concentrations in Figure 2. They cannot describe a transition zone where $G'' - \omega\eta_s > G'$ because the Rouse theory itself is deficient in this respect.

Yamamoto and Tanaka[33] have shown that the general shape of the two upper pairs of curves in Figure 2 can be represented by a relaxation spectrum H with the Zimm form (*i.e.*, H proportional to $\tau^{-2/3}$ in the transition zone) grafted on to a box distribution[34] in which H is a constant over a range of time scale corresponding to the pleateau zone, following the theory of Hayashi.[35] However, the box distribution is not an accurate representation of H in the plateau zone, which is never exactly flat and often exhibits a minimum. Also, it is doubtful whether the Zimm form should be applicable in concentrated solution, since the value of j_{eR}^0 from viscoelastic measurements[2–4] and also from considerably more precise flow birefringence measurements[34,35] is 0.40 in concentrated solution, corresponding to vanishing hydrodynamic interaction (Rouse form), if the effects of entanglements are not dominant.

The frequency dependences of G' and G'' in concentrated solution can be represented quite well[9] by grafting a sequence of Zimm normal modes at higher frequencies on to a sequence of Rouse normal modes at lower frequencies:

$$\begin{aligned} \mathbf{G}^* &= G' + iG'' \\ &= \frac{cRT}{M}\left\{\sum_{p=1}^{P}\left[\frac{i\omega\tau_p}{1+i\omega\tau_p}\right]_{\mathrm{R}} + \sum_{p=1}^{N}\left[\frac{i\omega\tau_p}{1+i\omega\tau_p}\right]_{\mathrm{Z}}\right\} \end{aligned} \tag{2}$$

where the subscripts R and Z define the sequences of relaxation times in the Rouse and Zimm theories, respectively. Thus, in the Rouse sequence, $p = 1, 2, 3 \ldots$ correspond to τ_1, $\tau_1/4$, $\tau_1/9$, ... with τ_1 specified by eq. (1) as listed in Table III. The sequence runs until $\tau_p < \tau_1'$, where τ_1' corresponds to the high-frequency or short-time end of the plateau zone, estimated somewhat arbitrarily from G'' or H; in some cases one term is sufficient. The Zimm sequence then starts with τ_1' and follows the relaxation time sequences prescribed for dominant hydrodynamic interaction; the result is insensitive to the value of N if this is reasonably high. This treatment, like that of Yamamoto and Tanaka, suffers from the questionable applicability of dominant hydrodynamic inter-

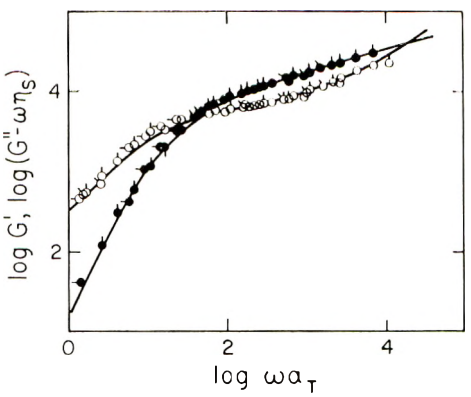

Fig. 6. Logarithmic plots of $G'' - \omega\eta_s$ (○) and G' (●) against reduced frequency for polystyrene, M = 860,000 c = 0.114 g/ml, reduced to 25°C from measurements in A1232 (◔,◕) at 10.0°C, (◔,◕) 25.2°C, and (○,●) 40.2°C; (——) calculated from eq. (2) with $\log \tau_1 = -1.19$ and $\log \tau_1' = -2.40$.

action in concentrated solutions. However, it conforms rather well to the observed frequency dependence of G' and G'' as illustrated in Figure 6. Probably a combination of the entanglement network spectrum of Graessley[21] with a sequence of Zimm relaxation times would be equally satisfactory.

An interesting consequence of the combined series, eq. (2), is the prediction of values of the characteristic ratio S'/S^2 which can be higher than the Rouse value of 0.40 if the Rouse sequence is quite short (especially if there is only one Rouse term). Such figures have been observed; with increasing concentration, j^0_{eR} starts from the Zimm value of 0.206 and actually passes through a maximum before approaching the 0.40 specified for vanishing hydrodynamic interaction. This behavior is clearly deduced from flow birefringence measurements[36,37] and was also apparent, though less conclusively, in viscoelastic measurements.[3,4,26] It has also been pointed out by Janeschitz-Kriegl[37] that combination of two Rouse sequences of relaxation times can produce a maximum in S'/S^2, higher than 0.4, as a function of concentration.

This work was supported in part by Grant GM-10135 from the U.S. Public Health Service. We are indebted to Professor John L. Schrag and Dr. Dennis J. Massa for valuable advice.

References

1. J. E. Frederick, N. W. Tschoegl, and J. D. Ferry, *J. Phys. Chem.*, **68**, 1974 (1964).
2. L. A. Holmes, K. Ninomiya, and J. D. Ferry, *J. Phys. Chem.*, **70**, 2714 (1966).
3. L. A. Holmes and J. D. Ferry, in *Macromolecular Chemistry, Tokyo-Kyoto 1966* (*J. Polym. Sci. C*, **23**), I. Sakurada and S. Okamura, Eds., Interscience, New York 1968, p. 291.
4. S. Kusamizu, L. A. Holmes, A. A. Moore, and J. D. Ferry, *Trans. Soc. Rheol.*, **12**, 559 (1968).
5. D. J. Massa and J. L. Schrag, *J. Polym. Sci.*, in press.
6. D. J. Massa, Ph.D. Thesis, University of Wisconsin, 1970.
7. D. J. Massa, J. L. Schrag, and J. D. Ferry, *Macromolecules*, **4**, 210 (1971).
8. J. E. Frederick, Ph.D. Thesis, University of Wisconsin, 1964.
9. L. A. Holmes, Ph.D. Thesis, University of Wisconsin, 1968.
10. M. H. Birnboim and J. D. Ferry, *J. Appl. Phys.*, **32**, 2305 (1961).
11. N. W. Tschoegl and J. D. Ferry, *Kolloid-Z.*, **189**, 37 (1963).
12. J. E. Frederick and J. D. Ferry, *J. Phys. Chem.*, **69**, 346 (1965).
13. A. Sakanishi and H. Tanaka, *J. Phys. Soc. Japan*, **24**, 222 (1968).
14. A. Sakanishi, *J. Chem. Phys.*, **48**, 3850 (1968).
15. H. Tanaka and A. Sakanishi, *Kobunshi*, **17**, 954 (1968).
16. R. M. Johnson, J. L. Schrag, and J. D. Ferry, *Polym. J. (Japan)*, **1**, 748 (1970).
17. P. E. Rouse, Jr., *J. Chem. Phys.*, **21**, 1272 (1953).
18. B. H. Zimm, *J. Chem. Phys.*, **24**, 269 (1956).
19. J. D. Ferry, *Viscoelastic Properties of Polymers*, 2nd ed., Wiley, New York, 1970, Chap. 13.
20. M. Kurata and W. H. Stockmayer, *Adv. Polym. Sci.*, **3**, 196 (1963).
21. W. W. Graessley, *J. Chem. Phys.*, **54**, 5143 (1971).
22. W. W. Graessley, *J. Chem. Phys.*, **47**, 1942 (1967).
23. W. W. Graessley and L. Segal, *Macromolecules*, **2**, 49 (1969).
24. W. W. Graessley, R. L. Hazleton, and L. R. Lindeman, *Trans. Soc. Rheol.*, **11**, 267 (1967).
25. M. Kurata, K. Osaki, and M. Tamura, *Bull. Inst. Chem. Res. Kyoto Univ.*, **46**, 87 (1968).
26. Y. Einaga, K. Osaki, M. Kurata, and M. Tamura, *Macromolecules*, **4**, 87 (1971).
27. D. J. Plazek and M. O'Rourke, *J. Polym. Sci. A-2*, **9**, 209 (1971).
28. N. J. Mills and A. Nevin, *J. Polym. Sci. A-2*, **9**, 267 (1971).
29. J. D. Ferry, R. F. Landel, and M. L. Williams, *J. Appl. Phys.*, **26**, 359 (1955).
30. F. Bueche, *J. Appl. Phys.*, **26**, 738 (1955).
31. R. S. Marvin and H. Oser, *J. Res. Nat. Bur. Stand.*, **66B**, 171 (1962).
32. A. J. Chompff and W. Prins, *J. Chem. Phys.*, **48**, 235 (1968).
33. M. Yamamoto and H. Tanaka, *J. Macromol. Sci.*, **B1**, 199 (1967).
34. A. V. Tobolsky, *Properties and Structure of Polymers*, Wiley, New York, 1960.
35. S. Hayashi, *J. Phys. Soc., Japan*, **19**, 101, 2306 (1964).
36. V. Daum and J. L. S. Wales, *J. Polym. Sci. B*, **7**, 459 (1969).
37. H. Janeschitz-Kriegl, *Adv. Polym. Sci.*, **6**, 170 (1969).

Received April 28, 1971

JOURNAL OF POLYMER SCIENCE: PART A-2 VOL. 9, 2023–2032 (1971)

Piezoelectricity in Oriented Films of Poly(γ-benzyl-L-Glutamate)

TOSHIYOSHI KONAGA* and EIICHI FUKADA, *The Institute of Physical and Chemical Research, Wako, Saitama, 351, Japan*

Synopsis

Oriented films of poly(γ-benzyl L-glutamate) (PBLG) were prepared by two methods. Films of PBLG cast from chloroform solutions were elongated by rolling at 70°C. A solution of PBLG in methylene bromide was placed in a magnetic field of about 7000 gauss and the solvent was slowly evaporated for a few days until an oriented film was obtained. The real and imaginary components of the complex piezoelectric strain-constant $d_{25}^* = d_{25}' - jd_{25}''$ were determined over the temperature range from −180°C to +180°C at a frequency of 20 Hz. The constants showed dispersions at about 20°C and about 100°C, where dynamic viscoelastic dispersions were also observed. Degree of crystallinity X_c and degree of orientation Π_a of crystallites were determined from x-ray diffraction diagrams. The product $X_c\Pi_a$ and the value of d_{25}' at room temperature were found to be linearly related, and both showed a maximum at an elongation ratio of 1.5 (the ratio of the final to initial length) for roll-oriented films and at an initial solution concentration of 15% by weight for magnetically oriented films. The largest values of d_{25}' were approximately 2×10^{-12} and 4×10^{-12} coulomb/newton, respectively, at room temperature.

INTRODUCTION

Piezoelectric effects have been reported in various kinds of biopolymers.[1] Piezoelectric properties and their temperature dependence in oriented films of poly(γ-methyl L-glutamate) have recently been investigated in detail.[2] Poly(γ-benzyl L-glutamate) (PBLG) is one of the best known synthetic polypeptides with the α-helical molecular conformation. Fairly large piezoelectric effects have been observed in oriented films of this polymer. The present paper describes temperature dispersions of complex piezoelectric constants of PBLG and the dependence of the piezoelectric constants on crystallinity and orientation of crystallites.

EXPERIMENTAL

Poly(γ-benzyl L-glutamate) with an average molecular weight of 320,000 was obtained from Pilot Chemicals Co. Watertown Mass. Oriented films of this polymer were prepared by two different methods.

* On leave from: Department of Chemistry, Gakushuin University, Mejiro, Tokyo.

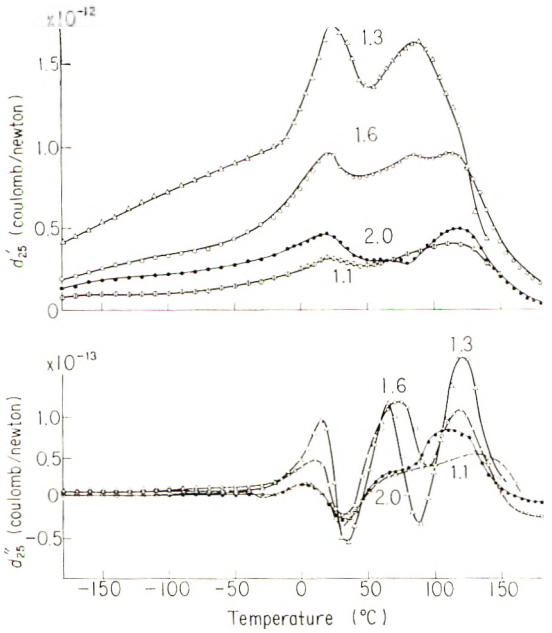

Fig. 1. Piezoelectric temperature dispersions for roll-oriented films of poly(γ-benzyl-L-glutamate) at the elongation ratios indicated.

Mechanically Oriented Films

PBLG was dissolved in chloroform to a concentration of 9% by weight. The solution was spread over the surface of a flat Teflon plate, and the solvent was allowed to evaporate until a film of PBLG was obtained. The cast film was desiccated under vacuum and elongated by rolling to 1.1 to 2.5 times the original length at a temperature of 70°C. After elongation the film was heat treated for about 15 min at 180°C. No shrinkage of film was observed during the heat treatment. X-ray studies revealed that the molecular axis was oriented in the direction of elongation.

Magnetically Oriented Films

It has been reported that molecules of PBLG orient in the direction of a magnetic field when dissolved in certain liquid-crystal-forming solvents such as methylene bromide (CH_2Br_2).[3,4] Solutions of PBLG in CH_2Br_2 with concentrations from 6 to 30% by weight were prepared. About 1 cc of the solution was placed in a cubical glass vessel 15 mm on a side and left at room temperature for about a week, until the PBLG molecules attained the liquid crystalline state. The glass vessel was then placed in the gap between two poles of a permanent magnet. The strength of the magnetic field was about 7000 gauss. The glass lid was slightly shifted in order to evaporate the solvent very slowly during a period of

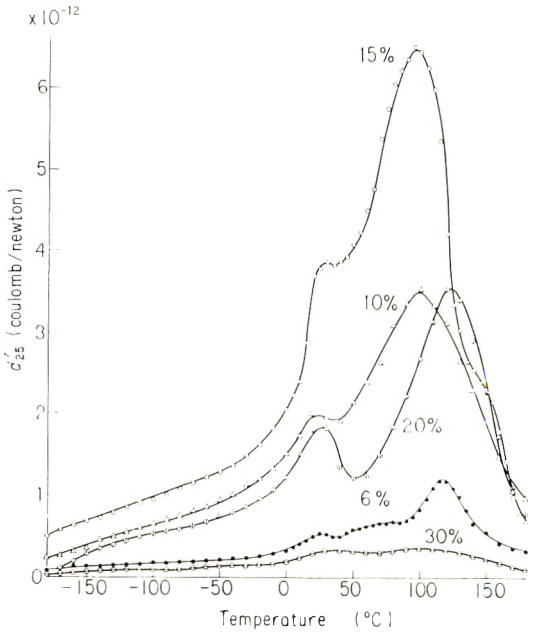

Fig. 2. Temperature dependence of the real component d_{25}' of the complex piezoelectric strain-constant for magnetically oriented films of poly(γ-benzyl L-glutamate). The figures indicate initial concentration of PBLG in methylene bromide solutions: magnetic field of 7000 gauss.

1 to 2 days. Films cast under the magnetic field were evacuated for about 12 hr at a temperature of about 120°C.

Small rectangular strips were cut out of either mechanically or magnetically oriented PBLG films at a direction 45° to the orientation axis. (so that tensile force would produce shear in the film plane[1,2]). The length of the sample was 10 to 12 mm, the width 5 to 8 mm, and the thickness 0.15 to 0.35 mm. Very thin square brass foils were joined to both surfaces of the films as electrodes with a dilute alcoholic solution of shellac.

Complex piezoelectric constants $d_{25}^* = d_{25}' - jd_{25}''$ for oriented films were determined at a frequency of 20 Hz in the temperature range from −180°C to 180°C by means of the apparatus described in the previous paper.[2] The assignment of coordinates is also the same as that employed previously.[2] A shear stress in the xz plane, i.e., the film plane, produces a polarization in the y axis, which is normal to the film surface.

As described later, the piezoelectric effect in oriented proteins[1] and synthetic polypeptides[2] is caused only by shear. When a shear stress is applied to the plane in which the orientation axis of crystallites lies, a polarization is produced in the direction normal to the plane. This is a consequence of the piezoelectricity being due to uniaxially oriented crystallites which exhibit classical piezoelectricity.

Wide-angle x-ray diffraction patterns of oriented films were obtained with Cu-Kα radiation, incident normal to the plane of the films. The sharp diffraction peaks due to crystalline regions were graphically separated from the broad diffraction band due to amorphous regions. From the ratio of area of crystalline diffraction to total area of diffraction, the degree of crystallinity X_c was calculated.

At the diffraction angle for $(1\bar{1}0)$ reflections (where $2\theta \approx 7°$) the variation of the diffraction intensity with the azimuthal angle over a 180° range was also measured by rotating the film in the plane of its surface. From a half-width angle $\Delta\varphi$ in the curve of diffraction intensity against azimuthal angle φ, the degree of orientation Π_α for an axis of crystallites, which should be in the same direction as that of the α-helix axis of the molecules, was estimated from a formula $\Pi_\alpha = (180 - \Delta\varphi)/180$.

RESULTS

Variations with temperature of piezoelectric strain constants d_{25}' and d_{25}'' for mechanically oriented films of PBLG are illustrated in Figure 1. The units of d_{25}' are the MKS units (coulomb/newton), which may be transformed to the cgs esu system by multiplying by 3×10^4. It is

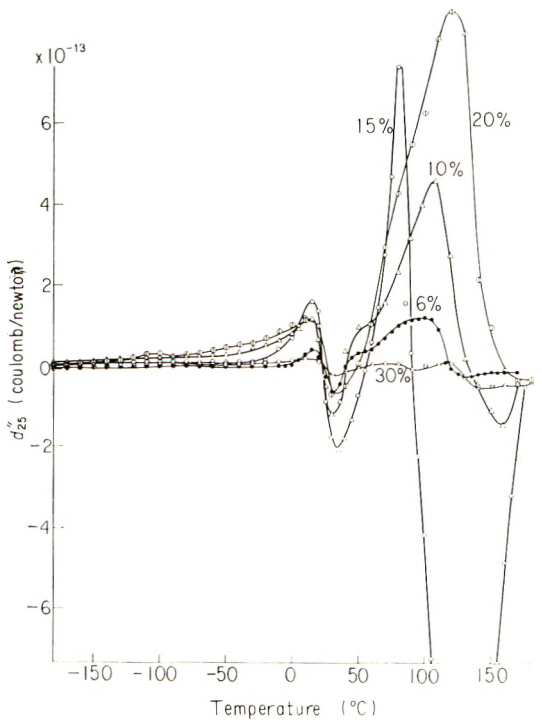

Fig. 3. Temperature dependence of the imaginary component d_{25}'' of the complex piezoelectric strain-constant for magnetically oriented films of poly(γ-benzyl L-glutamate). The figures indicate initial concentration of PBLG.

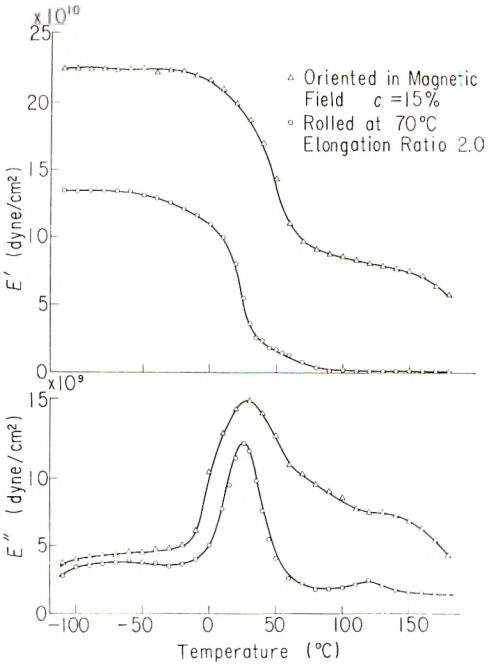

Fig. 4. Real and imaginary components E' and E'' of dynamic elastic modulus for magnetically oriented and roll elongated films of poly(γ-benzyl L-glutamate).

seen from Figure 1 that the value of d_{25}' increases with elongation until an elongation ratio of 1.3 is reached. Further elongation reduces the value of d_{25}'. As described later, strong elongation causes the disruption of crystallites and hence a decrease in d_{25}'.

The temperature variations of d_{25}' and d_{25}'' for magnetically oriented films of PBLG are shown in Figures 2 and 3. The value of d_{25}' increases with increasing initial concentration of PBLG in CH_2Br_2 up to 15% and then decreases with the further increase of the initial concentration. The films magnetically oriented with an initial concentration of 15% show a piezoelectric constant d_{25}' twice as large as the d_{11} constant of an x-cut quartz crystal (2×10^{-12} coulomb/newton). At 100°C, d_{25}' amounts to nearly 7×10^{-12} coulomb/newton.

In Figures 1 and 2, peaks in d_{25}' are seen at about 20°C and around 100°C, corresponding to an inflection at the same temperature between a maximum and a minimum in d_{25}''. The shape of the curves for the temperature dependence of d_{25}' and d_{25}'' is very similar to that observed for poly(γ-methyl L-glutamate).[2]

The dynamic elastic modulus and loss modulus were determined as functions of temperature by means of a viscoelastorecorder developed in our laboratory.[5] The frequency of measurement was 30 Hz and the elastic modulus in the direction of elongation of the film was determined. Figure 4 illustrates the results for a film oriented in a magnetic field from

an initial solution concentration of 15% by weight and for a film elongated by rolling to about twice its original length at 70°C. Maxima in E'' are seen at about −80, 20, and 120°C. The positions of temperature for the latter two maxima are the same as those for piezoelectric dispersions shown in Figures 1–3.

DISCUSSION

A theory for piezoelectric dispersion in semicrystalline polymers has been reported.[2,6] Piezoelectric polarization produced under an external stress is proportional to the mechanical strain of the crystallites which are piezoelectric. Viscoelastic properties of noncrystalline regions surrounding the crystallites have a large influence on the strain of the crystallites. Mechanical relaxation in noncrystalline regions connected effectively in parallel with crystalline regions produces an increase in strain or polarization of the crystallites with a rise of temperature. The phase of the resulting alternating polarization lags behind the externally applied alternating stress. On the other hand, mechanical relaxation in noncrystalline regions connected effectively in series with crystalline regions produces a decrease of strain or polarization of the crystallites with a rise of temperature. The phase of the resulting alternating polarization leads the externally applied alternating stress. Therefore, with increasing temperature, d_{25}' shows a maximum at a certain temperature, where d_{25}'' changes phase from lagging to leading.

The piezoelectric dispersions observed for PBLG at about 20 and 100°C are in good accord with the theoretical predictions. Initiation of some molecular motions in noncrystalline regions should take place at these temperatures. Similar to the results for PMLG,[2] the dispersion at about 20°C can be ascribed to the onset of thermal motions of side chains of the α-helical molecules in noncrystalline regions. The dispersion at about 100°C is presumably due to the onset of thermal brownian motion of nonhelical molecules which form the noncrystalline regions.

Figure 4 illustrates the temperature variations of dynamic elastic modulus E' and loss modulus E'' for mechanically and magnetically oriented films. Maxima in E'' are seen at about −80, 20, and 120°C. The last two peaks indicate the side-chain dispersion and primary dispersion in amorphous regions, respectively; and they are located at the same temperatures as the piezoelectric dispersions. The peak in E'' at about −80°C seems to be due to small-scale vibration of molecular chains. It is noticeable that the elastic modulus of the magnetically oriented film is double that of the mechanically oriented film.

The degree of crystallinity X_c and the degree of orientation of crystallites Π_α, determined by x-ray diffraction, are plotted against elongation ratio in Fig. 5 for roll-oriented films. Although Π_α increases with increasing elongation, X_c decreases, probably because of the destruction of crystallites at very high extension of the films. It is anticipated that the

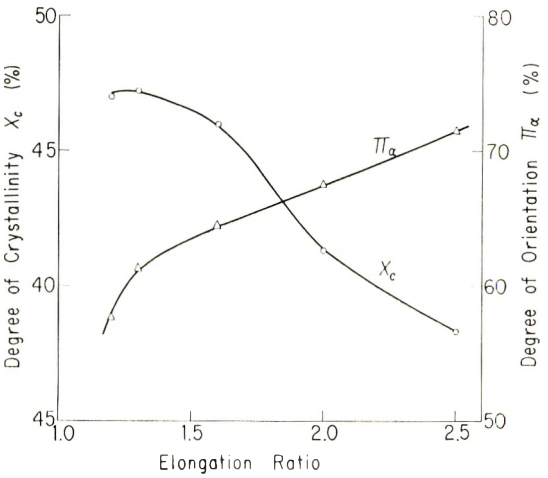

Fig. 5. Variation with elongation ratio of the degree of crystallinity and the degree of orientation of crystallities in roll-elongated films.

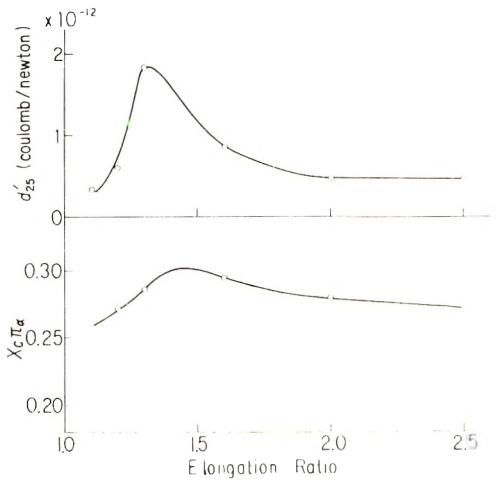

Fig. 6. Piezoelectric strain-constant d_{25}' and the product $X_c\Pi_\alpha$ plotted against elongation ratio.

magnitude of the piezoelectric constant should be proportional to the product $X_c\Pi_\alpha$. Therefore, $X_c\Pi_\alpha$ and the piezoelectric constant d_{25}' at room temperature have been plotted against the elongation ratio in Figure 6. Maxima of d_{25}' and $X_c\Pi_\alpha$ appear at the same elongation ratio of about 1.5.

If the initial concentrations of solutions placed in the magnetic field were different, X_c and Π_α were quite different. Figure 7 shows X_c and Π_α of the films plotted against the initial concentration. Both quantities decrease at high concentration. The reason for these effects on the magnetic orientation of PBLG solutions is not certain, but plausible explana-

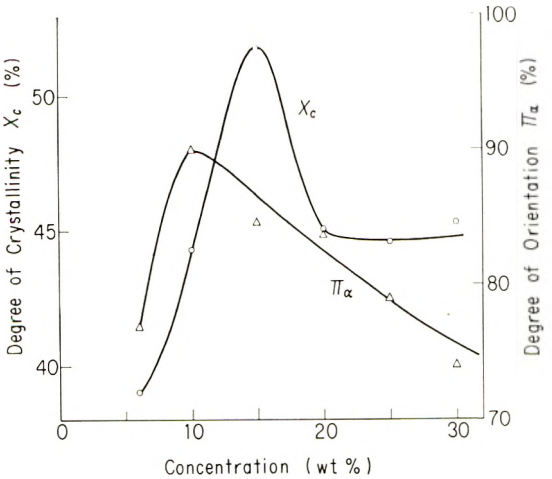

Fig. 7. The degree of crystallinity and the degree of orientation of crystallities for magnetically oriented films plotted against initial concentration of PBLG in the solution placed in a magnetic field.

tions can be offered. It is known that PBLG molecules form liquid crystals in concentrated solutions[7,8] and that these liquid crystals can be oriented in a magnetic field.[3,4,12] If the initial concentration is very high, the number of liquid crystals or of crystalline nuclei which may grow to larger crystallites during solidification is large. This situation would lead to a smaller degree of crystallinity for the resulting polycrystalline film. The high viscosity of concentrated solutions may also hinder orientation of liquid crystals in the magnetic field during solidification. The products $X_c\Pi_\alpha$ and the value of d_{25}' at room temperature are plotted against the initial concentration in Figure 8. The maxima of $X_c\Pi_\alpha$ and d_{25}' are seen at the same concentration of about 15%. From the results in Figures 6 and 8 it is observed that d_{25}' and $X_c\Pi_\alpha$ are nearly proportional.

Piezoelectricity in oriented proteins and synthetic polypeptides is generated by the piezoelectric polarization of crystallites of polymers.[1,2] The observed polarization is the statistical sum of the polarizations of a large number of uniaxially oriented crystallites. The symmetry of crystals of PBLG is thought to be nearly hexagonal.[9] If the polar axis of the helical molecules is oriented in the same direction in the crystal, the symmetry of the crystal would be approximately hexagonal polar C_6, and the piezoelectric tensor would acquire the form:[10]

$$\begin{matrix} 0 & 0 & 0 & d_{14} & d_{15} & 0 \\ 0 & 0 & 0 & d_{15} & -d_{14} & 0 \\ d_{31} & d_{31} & d_{33} & 0 & 0 & 0 \end{matrix} \qquad (1)$$

where the 3-axis is the direction of orientation of the molecules, and the 1 and 2 axes are perpendicular to it. On the other hand, if the polar axis of the helical molecules is distributed at random in the crystal, the sym-

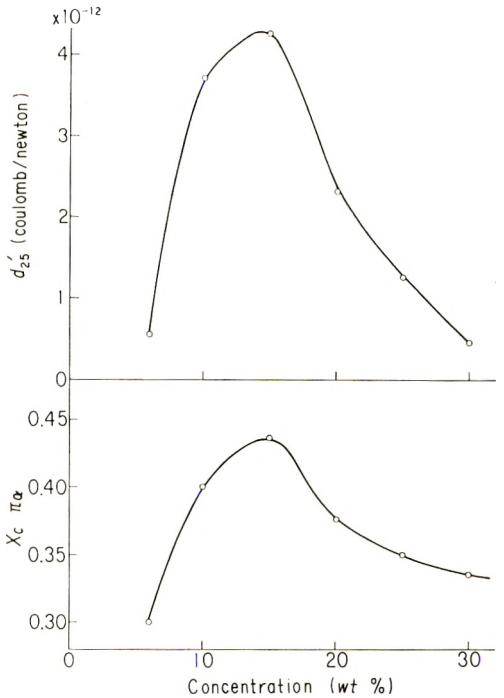

Fig. 8. Piezoelectric strain constant d_{25}' and the product $X_c\Pi_\alpha$ plotted against the initial concentration of PBLG.

metry of the crystal is approximately hexagonal holoaxial D_6, and the piezoelectric tensor is:[10]

$$\begin{matrix} 0 & 0 & 0 & d_{14} & 0 & 0 \\ 0 & 0 & 0 & 0 & -d_{14} & 0 \\ 0 & 0 & 0 & 0 & 0 & 0 \end{matrix} \tag{2}$$

In the film specimens, in which the crystallites are uniaxially oriented, it is most probable that the positive sense of the long axis of the crystallites is randomly distributed. Therefore, whether the symmetry of the single crystal is polar or nonpolar, the symmetry of the assembly of the crystallites is represented by D_∞. This symmetry is usually found in uniaxially elongated fibrous polymers. For the system with the symmetry D_∞, the piezoelectric tensor is:[1,10]

$$\begin{matrix} 0 & 0 & 0 & d_{14}^* & 0 & 0 \\ 0 & 0 & 0 & 0 & d_{25}^* & 0 \\ 0 & 0 & 0 & 0 & 0 & 0 \end{matrix} \tag{3}$$

where the 3-axis is the direction of orientation of the crystallites. The relation $-d_{14}^* = d_{25}^*$ holds.

Although the uniaxial orientation of crystallites has been demonstrated by x-ray studies for elongated and magnetically oriented films of PBLG,[9,12]

the polarity of the orientation of the crystallites can not be determined by such studies. However, a nonpolar orientation of crystallites is most plausible for mechanically elongated films of PBLG. We therefore assume the piezoelectric tensor (3) for the oriented film of PBLG. The 3-axis is assigned in the direction of elongation, the 2-axis normal to the plane of the film and the 1-axis in the plane of the film. The polarization in the 2-axis is experimentally determined when a shear stress is applied in the 1–3 plane. Thus d_{25}* can be determined.

If magnetic orientation produces parallel orientation of polar axis of crystallites, there is a possibility that the tensor form (1) is correct. It is not possible, however, to measure the piezoelectric constants other than d_{25}* for the film specimens.

It has been shown theoretically that the piezoelectric constant d_{25}* observable in uniaxially oriented films is represented by[11]

$$d_{25}^* = KX_c\Pi_\alpha d_{25}$$

where K is a temperature-dependent constant which varies with the viscoelastic and dielectric properties of the polymer and $d_{25} = -d_{14}$ is the piezoelectric constant for the single crystal of PBLG. The results presented in this paper indicate qualitatively that the piezoelectric constant is proportional to the product of the degree of crystallinity X_c and the degree of orientation of crystallites Π_α.

In conclusion, shear-type piezoelectricity has been demonstrated in oriented films of PBLG. The piezoelectric strain-constant d_{25}* for magnetically oriented films is larger than that for mechanically oriented ones. The magnitude of d_{25}' is proportional to the product of the degree of crystallinity and the degree of orientation of the crystallites. The characteristic dispersions of d_{25}' and d_{25}'' have been observed at temperatures where side-chain relaxation and primary relaxation, respectively, take place.

References

1. E. Fukada, *Biorheology*, **5**, 199 (1968).
2. M. Date, S. Takashita, and E. Fukada, *J. Polym. Sci. A-2*, **8**, 61 (1970).
3. S. Sobajima, *J. Phys. Soc. Japan*, **23**, 1070 (1967).
4. Y. Go, S. Ejiri, and E. Fukada, *Biochim. Biophys. Acta*, **175**, 454 (1969).
5. M. Date and E. Fukada, *Repts. Progr. Polym. Phys. Japan*, **7**, 183 (1964).
6. E. Fukada and M. Date, *Polym. J.*, **1**, 410 (1970).
7. C. Robinson, J. C. Ward, and R. B. Beevers, *Discussions Faraday Soc.*, **25**, 29 (1958).
8. C. Robinson, *Tetrahedron*, **13**, 219 (1961).
9. A. Elliott, *Poly-α-Amino Acids*, G. D. Fasman, Ed., Dekker, New York, 1967, p. 33.
10. W. G. Cady, *Piezoelectricity*, Dover, New York, 1964, p. 190.
11. T. Furukawa and E. Fukada, *Repts. Progr. Polym. Phys. Japan*, **12**, 401 (1969).
12. E. T. Samulski and V. Tobolsky, *Macromolecules*, **1**, 555 (1968).

Received February 10, 1971
Revised May 13, 1971

JOURNAL OF POLYMER SCIENCE: PART A-2 VOL. 9, 2033–2042 (1971)

NMR Observations of Drawn Polymers. IX. Chain Mobilization and Water Mobility in Nylon 66

H. G. OLF and A. PETERLIN, *Camille Dreyfus Laboratory, Research Triangle Institute, Research Triangle Park, North Carolina 27709*

Synopsis

Wide-line NMR spectra of nylon 66 fibers have been obtained at different alignment angles between the fiber axis and the magnetic field, at varying water contents (H_2O and D_2O), and at different temperatures. At 28°C the spectrum of the dry fibers consists of a nearly structureless broad line. At water regains of 1.4% by weight (dry basis) and higher a sharp line appears which originates from highly mobile water molecules. The width of this line decreases with increasing water content, implying an increase of water mobility. Moreover, the width is a function of the alignment angle; this shows that the water is not reorienting isotropically owing to specific water–polymer interaction. The amount of mobile water is always smaller than the amount of water absorbed. At water contents close to saturation, a mobile polymer line appears with a width intermediate between the broad line (immobile polymer) and the sharp water line. This line, most clearly observed at an alignment angle of 0°, is due to a shift of the α_a process to lower temperatures in the presence of water. A similar line is observed in the dry fibers at 120°C. It is shown that the α_a process decreases the NMR second moment only slightly. The shift of the high temperature drop in second moment to lower temperatures in the presence of water is therefore interpreted as due to a shift of the α_c process, and not of the α_a process, to lower temperatures.

INTRODUCTION

Nuclear magnetic resonance (NMR) studies of the structure and mobility of water absorbed in solid polymers have greatly benefited from the use of fiber specimens as shown, for example, by the work of Berendsen et al.[1,2] and Dehl et al.[3,4] Specific interactions between water and the polymer can, in favorable cases, be discovered by a careful study of the NMR spectrum as a function of the fiber-field angle. The present paper reports work of this kind on nylon 66 fibers with varying water content. Some novel aspects concerning the behavior of both water and polymer are presented. NMR studies of unoriented nylon–water systems have already appeared in the literature.[5–10]

EXPERIMENTAL

The nylon 66 fibers used in this work have already been used in a previous NMR study,[11] where a detailed description of this material can be found. A Varian DP-60 spectrometer was used for the proton wide-line

TABLE I
Water Regain of the Nylon 66 Fibers at Different Relative Humidities at 28°C and NMR Second Moment at Alignment Angles 0°, 45°, and 90°

Relative humidity, %	Water regain, g of water/ 100 g dry nylon 66	Second moment, G^2		
		$\gamma = 0°$	$\gamma = 45°$	$\gamma = 90°$
0	0.0	16.8 ± 0.5	11.2 ± 0.5	14.9 ± 0.5
2	—	16.8	11.5	14.5
10	0.4	17.2	11.5	14.8
20	0.7	17.0	11.0	14.8
33	1.4	17.0	11.0	14.8
53	2.6	16.8	10.8	14.7
75	4.3	16.7	10.4	14.3
80	4.8	16.5	10.0	14.1
91	6.2	16.4	9.7	14.0
100	—	16.5	9.5	14.2

NMR work. Calibration and evaluation procedures and steps taken to prevent saturation are described elsewhere.[11,12]

Most of the NMR experiments described herein were done at 28°C. The fibers were inserted into an opening cut in a Teflon rod sample holder so that the fiber axis was perpendicular to the rod axis. By turning the rod around its axis the fiber axis could be set at any alignment angle γ with respect to the magnetic field. The angle was read on a goniometer. Sample and sample holder were enclosed in a glass tube which could be attached to a vacuum system for equilibration with water vapor of different relative humidities at 28°C. Dry samples were prepared by keeping the fibers in a vacuum at 100°C for one week. The relative humidities and the corresponding water regain of the fibers are given in Table I. The influence on the NMR spectrum of different amounts of water absorbed by the fibers was studied as a function of the alignment angle γ (fiber-field angle).

The NMR second moment has been determined as a function of temperature in dry and wet nylon 66 fibers at an alignment angle of 90°. The results differ slightly from those obtained by Woodward et al.[6] on unoriented nylon 66 and will be reported here mainly because they lead to a different interpretation in terms of polymer mobility.

RESULTS AND DISCUSSION

Angle Dependence

Shape of Spectra. Proton absorption spectra of the nylon 66 fibers are shown in Figure 1 in the first derivative form obtained experimentally. They were taken at values of the alignment angle of 0°, 45°, and 90°, respectively, and at the indicated relative humidities. The spectrum of the dry fibers is changed considerably upon addition of water. The most obvious effect of adding water is the appearance of a narrow line. This

line is believed to arise from protons on highly mobile water molecules in the sample. Not shown in Figure 1 are the spectra obtained at relative humidities between 20% and 0%. These spectra did not show a narrow line but only a slight change in shape as compared with the spectrum of the dry fibers. This implies that water is so tightly bound at these levels of water content that its mobility is severely restricted.

It is apparent from Figure 1 that at relative humidities of 75% and 91% in addition to the broad polymer line and the sharp water line, a line of intermediate width has emerged. This line is more clearly distinguished at the alignment angle 0° than at 45° and 90°. That it does not originate from water but from mobilized polymer segments is concluded for the following two reasons. First, the broad polymer line decreases slightly in intensity as would be expected if the polymer chain segments mobilized by the water no longer contribute to it. Second, a fiber sample exposed to D_2O at 91% RH showed a line identical to that produced by H_2O. Since D_2O does not contribute to the proton absorption, of course, it is clear that this line represents polymeric protons. (Prior to this experiment the accessible amide protons were exchanged with D to prevent formation of HDO.) This line will be called the mobile polymer line.

It is believed that the mobile polymer line is the NMR manifestation of the chain segmental motion involved in the α_a process, which is sometimes called the "glass transition" of nylon 66. In dry nylon 66, the α_a process occurs at approximately 100°C[14] (5×10^4 Hz) as indicated by a pronounced narrowing of the NMR spectrum,[11,15] for example. Water is known to act as a plasticizer, shifting the process to lower temperatures.[14] Woodward et al.[16] have reported a shift of the α_a process as observed by dynamic-mechanical techniques from 100°C in dry nylon 66 to about 5°C in nylon 66 saturated with water, at frequencies around 700 Hz. This shows that under the conditions of temperature (28°C), relative humidity (91%) and frequency (10^4 to 10^5 Hz) employed here the α_a process may well be expected to be activated.

Much discussion has been devoted to the existence of a frequency–humidity superposition in dynamic-mechanical data on nylon 66.[17–22] In the context of the present experiments, this idea can be stated as follows. If the mobile polymer line observed at 28°C in the presence of water does indeed correspond to the α_a process in nylon 66, then it should be possible to observe a very similar line with dry nylon 66 at some elevated temperature. This is actually the case as is illustrated in Figure 2. A comparison is made between the spectrum of the nylon 66 fibers at 28°C, containing water, and the spectrum of dry fibers at 120°C. Although the spectra are by no means identical, the similarity of the mobile polymer lines in both spectra is apparent.

Another feature of the spectra in Figure 2 which deserves some comment is that broad line is considerably narrower at 120°C than at 28°C. This is attributed to motion in crystalline regions (the α_c process) which has recently been discussed.[11,23]

Width and Intensity of the Narrow Line. The width of the narrow water line strongly depends on the amount of water absorbed by the fibers, as shown in Figure 3. The linewidth is defined in the insert in Figure 3, showing the narrow water line at 75% RH on an expanded field scale compared to that used in Figures 1 and 2. The smaller the linewidth, the higher the water mobility, in general.

The mass of mobile water per 100 g of dry nylon 66 is plotted in Figure 4 as a function of the water content. This mass fraction was calculated from the ratio of the area under the narrow absorption line to the area

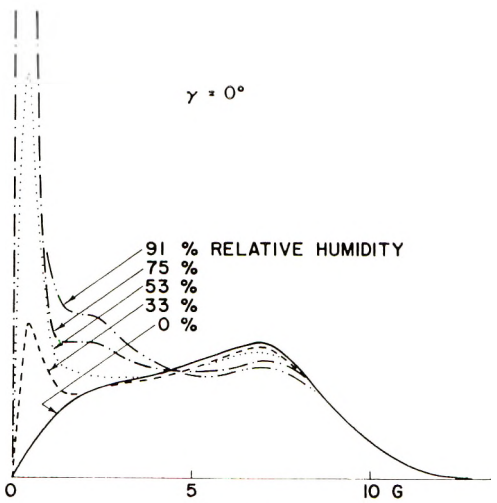

(*a*)

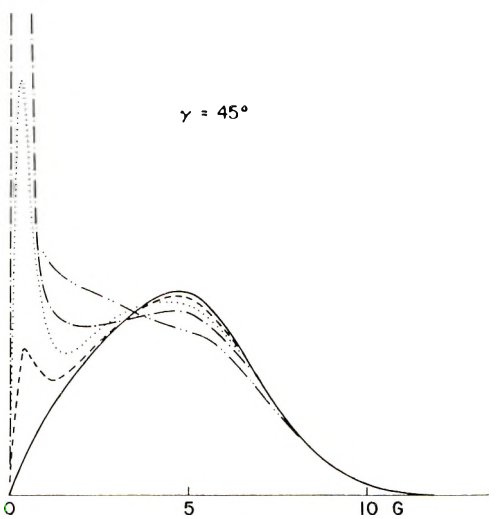

(*b*)

Fig. 1 (*continued*)

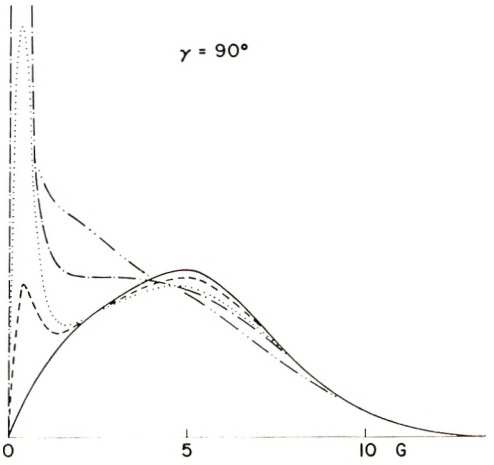

(c)

Fig. 1 First-derivative NMR absorption (in arbitary units) versus the magnetic field from the center of resonance (in gauss). The nylon 66 fibers, equilibrated with water vapor at the indicated relative humidities, were set at alignment angles γ of the fiber axis with respect to the magnetic field of 0°, 45°, and 90°. Since the spectra are symmetric with respect to the origin, only one-half of each trace is shown.

under the whole spectrum, that ratio being the fraction of mobile hydrogens in the sample. (The area under the absorption line is equal to the first moment of the derivative spectrum.) As has already been mentioned, there is no separate sharp line below 20% RH. At low regain values the amount of mobile water is considerably smaller than the total amount of water absorbed by the fibers. The hypothetical case where the two are equal is represented by the broken line in Figure 4. At higher regain values

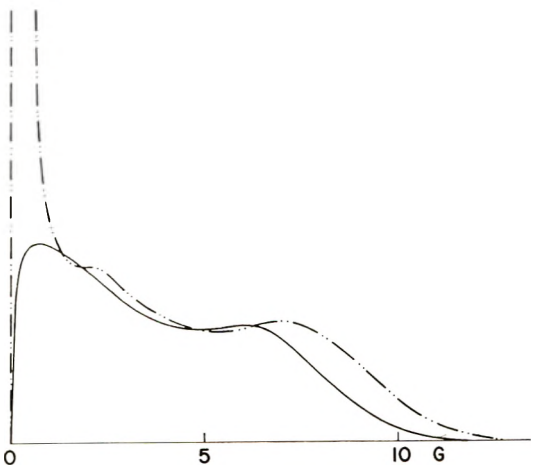

Fig. 2. Comparison of two spectra of nylon 66 fibers, taken at alignment angle 0° under the following conditions: (- · ·) 28°C, 91% RH; (—) 120°C, dry sample.

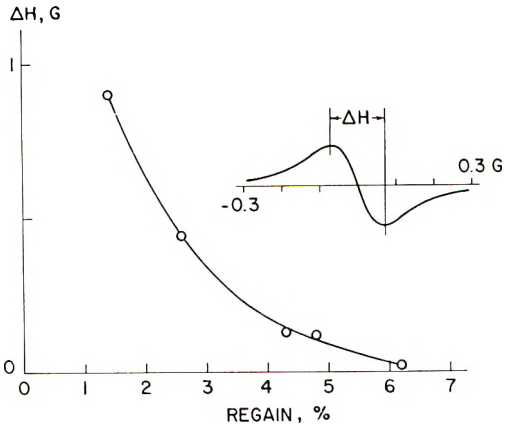

Fig. 3. Width ΔH of the sharp line as a function of water regain (g of water/100 g of dry polymer). The linewidth is defined in the insert (see text).

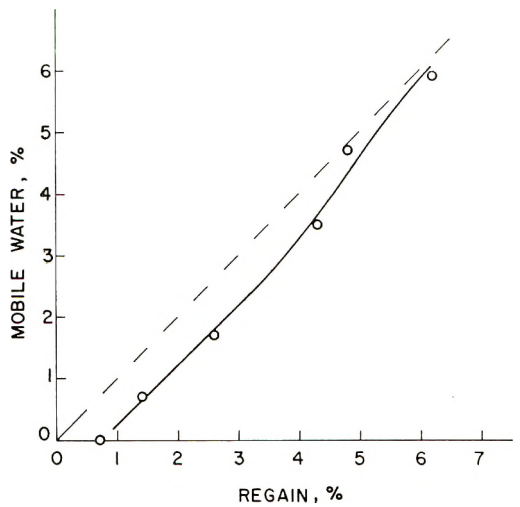

Fig. 4. Amount of mobile water (g/100 g of dry nylon 66) as a function of water regain g/100 g of dry nylon 66. The broken line would apply if all the absorbed water were highly mobile (see text).

the experimental points seem to approach this line, indicating that newly added water mobilizes some of the water which remained immobile at smaller water regains. The fraction of mobile water is not considered accurate enough to allow determination of the amount of "bound" or immobile water by taking the difference between the amount of absorbed and of mobile water.

It was noted that the width of the narrow water line depends on the alignment angle. At relative humidities around 53%, conditions were most favorable to determine this anisotropy. The measurements appear in Figure 5. There is a variation of the linewidth of about 25%, with a mini-

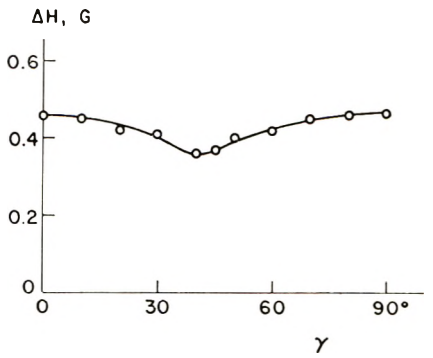

Fig. 5. Dependence of the width of the sharp line on the alignment angle γ at 53% relative humidity.

mum width at an alignment angle of approximately 40°. This angle dependence implies that the water molecules do not reorient isotropically. Rather they prefer certain orientations with respect to the fiber axis over other orientations on a time average. This preference is thought to be dictated by the specific water–polymer interaction[3,4] which probably consists mainly of hydrogen bonds between water and the peptide groups of the nylon.

If the principal axis of anisotropy of the reorienting water molecules were along the fiber axis, then ΔH would be expected to vary according to $|3\cos^2\gamma - 1|$. The angle dependence in Figure 5 clearly does not conform to this, indicating that the principal axis of anisotropy is at an angle with respect to the fiber axis.

Temperature and Moisture Dependence of Second Moment

Spectra were obtained between −200°C and +200°C with dry fibers and with fibers saturated with D_2O at room temperature; as mentioned earlier, the alignment angle was 90°. The second moments of these spectra appear in Figure 6 as a function of temperature. As is now well established,[6,11] the second moment of the dry sample decreases in essentially two stages with rising temperature: the first stage begins at about −120°C and encompasses the decrease in second moment up to approximately 80°C; this decrease has been attributed to chain segmental motion in noncrystalline regions,[11,24] called the γ process. The second stage is the high temperature decrease in second moment starting at about 90°C. This is caused mainly, but not exclusively, by chain segmental motion in the crystalline regions, termed the α_c process;[11,23] the small contribution to this decrease from the α_a process[11] will be discussed below.

The second moments of the D_2O-saturated fibers were determined by ignoring the sharp line which arises from a small amount of H_2O and HDO formed by deuterium exchange of the amide hydrogen. These second moments, therefore, essentially represent the polymer. The curve of second moment versus temperature for the wet fiber is seen to differ from

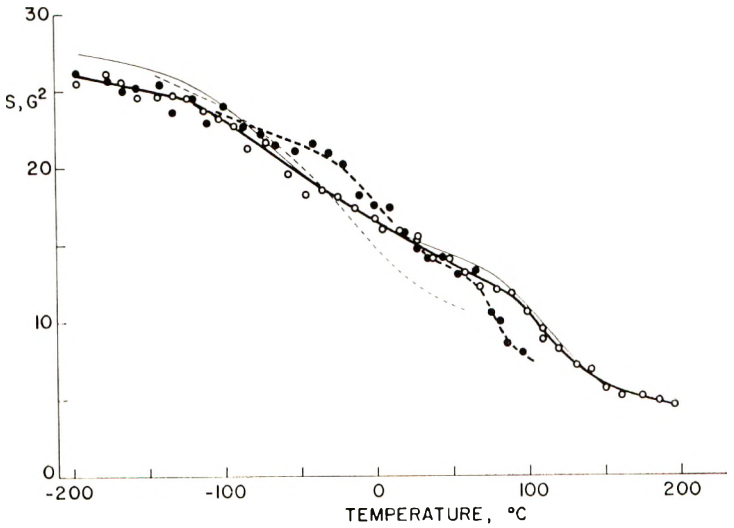

Fig. 6. Second moment S as a function of temperature for nylon 66 fibers at the alignment angle 90°: (○)dry fiber; (●) fiber saturated with D_2O; (—) data[6] on an unoriented, dry (deuterated) sample; (- - - - - - -) sample[6] with D_2O.

that of the dry fiber, running above it at temperatures around −40°C and falling below it at high temperatures. An interpretation of these differences will be given below in terms of the various mechanisms of chain segmental motion in the polymer.

Also shown in Figure 6, by the thin lines, are results taken from the work of Woodward et al.[6] The general features of the curve corresponding to a dry sample, indicated by the thin continuous curve, are similar to the present results. As the data of Woodward et al. were obtained with an unoriented bulk sample, they ought to fall well below the curve for the fiber at an alignment angle of 90°.[11] That they are actually above that curve may be due to saturation.[25] The temperature dependence of the second moment observed here for wet nylon 66 differs slightly but characteristically from that observed by Woodward et al.[6]

In agreement with Woodward et al.[6,26] and Kolařík et al.,[27] the present data show that the drop in second moment at low temperatures, which is due to the γ process, is smaller at first in the wet than in the dry sample. In keeping with the interpretation given by these authors we attribute this effect to immobile water which presumably hinders polymer chain mobility in noncrystalline regions. At temperatures above −75°C[10] the water becomes increasingly mobile, as shown by the appearance of a sharp water line, enabling the polymer to gain in mobility and causing the second moment to fall toward the curve of the dry polymer.

It has been pointed out by Woodward et al.[6] that about half the decrease in second moment occurring in the dry polymer at high temperatures (second stage) appears to be shifted to lower temperatures in the wet sample

(compare the thin curves in Fig. 6). This was attributed to the shift of the α_a process to lower temperatures. The present data suggest a somewhat different interpretation. Although it is agreed that water does shift the α_a process to lower temperatures, the fiber data in Figure 6 indicate that the second moment around 28°C is little affected by this. This point is further supported by the second-moment data in Table I. The fibers saturated with H_2O show an average drop in second moment of only about 1 G^2 as compared with the dry sample. This is in agreement with the value for fibers saturated with D_2O (Fig. 6), but at variance with the thin broken line[6] in Figure 6.

It should not be surprising that the second moment is so insensitive (Table I) to the α_a process, i.e., the emergence of the mobile polymer line at high water contents (Fig. 1). It must be remembered that the NMR second moment is proportional to the third moment of the first derivative line;[28] this implies that the outer wings of the broad line have the predominant influence and that the central portion, including the mobile polymer line, has a comparatively small influence on the second moment.

Since the decrease associated with the α_a process is seen to be small, most of the decrease occurring at 90°C and above must be due to the α_c process in both dry and wet nylon 66. The results in Figure 6 imply that water also shifts the α_c process to lower temperatures, in seeming contradiction to the often stated fact that water enters the noncrystalline regions of nylon 66 but not the crystalline regions. It should be noted, however, that this observation is in good agreement with Brill's X-ray data;[29] he found that the transition to the pseudohexagonal phase in nylon 66, which is believed to be intimately connected with the α_c process,[11,23] occurs at temperatures 20°C lower in the presence of water. This compares favorably with the shift of approximately 25°C observed in Figure 6.

Exactly how water affects the chain segmental motion in crystalline regions remains a matter of conjecture.

The authors are grateful to the Camille and Henry Dreyfus Foundation for the generous support of this work and Dr. G. W. Sovereign of the Chemstrand Research Center at Durham, N. C., for supplying the nylon 66 fibers.

References

1. H. J. C. Berendsen, Thesis, University of Groningen, Holland, 1962.
2. H. J. C. Berendsen and C. Migchelsen, *Ann. N. Y. Acad. Sci.*, **125**, 365 (1965).
3. R. E. Dehl, *J. Chem. Phys.*, **48**, 831 (1968).
4. R. E. Dehl and C. A. J. Hoeve, *J. Chem. Phys.*, **50**, 3245 (1969).
5. J. G. Powles and J. A. E. Kail, *Trans. Faraday Soc.*, **55**, 1996 (1959).
6. A. E. Woodward, R. E. Glick, J. A. Sauer, and R. P. Gupta, *J. Polym. Sci.*, **45**, 367 (1960).
7. K.-H. Illers and R. Kosfeld, *Makromol. Chem.*, **42**, 44 (1960).
8. R. P. Gupta, *J. Phys. Chem.*, **65**, 1128 (1961).
9. Y. Sekita and K. Kawasaki, *Repts. Progr. Polym. Phys. Japan*, **7**, 283 (1964).
10. R. E. Glick and R. C. Phillips, *J. Polym. Sci. A*, **3**, 1885 (1965).
11. H. G. Olf and A. Peterlin, *J. Polym. Sci. A-2*, **9**, 1449 (1971).

12. H. G. Olf and A. Peterlin, *J. Appl. Phys.*, **35**, 3108 (1964).
13. H. G. Olf and A. Peterlin, *Kolloid-Z., Z. Polym.*, **215**, 97 (1967).
14. N. G. McCrum, B. E. Read, and G. Williams, *Anelastic and Dielectric Effects in Polymeric Solids*, Wiley, London–New York–Sydney, 1967.
15. W. P. Slichter, *J. Appl. Phys.*, **26**, 1099 (1955).
16. A. E. Woodward, J. M. Crissman, and J. A. Sauer, *J. Polym. Sci.*, **44**, 23 (1960).
17. B. A. Dunell and J. M. R. Quistwater, *J. Chem. Phys.*, **29**, 450 (1958).
18. J. M. R. Quistwater and B. A. Dunell, *J. Appl. Polym. Sci.*, **1**, 267 (1959).
19. F. L. Warburton, J. F. P. James, and S. Hother-Lushington, *Brit. J. Appl. Phys.*, **12**, 230 (1961).
20. S. Onogi, K. Sasaguri, T. Adachi, and S. Ogihara, *J. Polym. Sci.*, **58**, 1 (1962).
21. M. L. Williams and M. F. Bender, *J. Appl. Phys.*, **36**, 3044 (1965).
22. W. H. Howard and M. L. Williams, *Text. Res. J.*, **36**, 691 (1966).
23. H. G. Olf, *J. Polym. Sci. A-2*, in press.
24. K. Schmieder and K. A. Wolf, *Kolloid-Z.*, **134**, 149 (1953).
25. E. R. Andrew, *Nuclear Magnetic Resonance*, Cambridge Univ. Press, 1958.
26. C. W. Deeley, A. E. Woodward, and J. A. Sauer, *J. Appl. Phys.*, **28**, 1124 (1957).
27. J. Kolařík and J. Janáček, in *Macromolecular Chemistry, Prague 1965* (*J. Polym. Sci. C*, **16**), O. Wichterle and B. Sedláček, Eds., Interscience, New York, 1967, p. 441.
28. J. G. Powles, *Polymer*, **1**, 219 (1960).
29. R. Brill, *J. Prakt. Chem.*, **161**, 49 (1943).

Received April 12, 1971
Revised May 18, 1971

JOURNAL OF POLYMER SCIENCE: PART A-2 VOL. 9, 2043–2060 (1971)

Growth and Morphology of Single Crystals of Linear Aliphatic Polyesters

T. KANAMOTO and K. TANAKA, *Department of Chemistry, Faculty of Science, Science University of Tokyo, Kagurazaka, Shinjuku-ku, Tokyo, Japan,* and H. NAGAI, *Material Laboratory, Furukawa Electric Co., Ltd., Yokohama Electric Wire and Cable Works, Nishi-ku, Yokohama, 220, Japan*

Synopsis

In order to elucidate the relations between morphological habits and chemical structure of polymers, poly(ethylene sebacate), poly(hexamethylene sebacate) and poly(decamethylene 1,16-hexadecanedicarboxylate) were crystallized from dilute solutions in n-hexanol, isoamyl acetate etc., and were studied with the electron microscopy and x-ray diffraction. The crystal structures of these polyesters are tentatively determined. Morphological "regularity" and "simplicity" of the single crystals are correlated with the chemical structure of the polymers. The crystallization conditions under which "regular" and "simple" single crystals are obtained are relaxed with increase of methylene sequence length in chemical repeat unit. The Bragg extinction bands in the single crystals of poly(hexamethylene sebacate) and poly(decamethylene 1,16-hexadecanedicarboxylate) suggest nonplanar nature of these crystals. The molecular chains in the poly(ethylene sebacate) single crystal are inclined from the normal of the basal plane; the fold surface corresponds to the (001) plane.

INTRODUCTION

Since the discovery of single crystals of polyethylene,[1–3] those formed by a large variety of polymers have been studied. It is well known that certain kinds of polymers, such as polyesters and polyamides crystallize generally in less regular habits than polyethylene and polyoxymethylene.[4,5]

Only a few studies[6–8] have reported on single crystals of linear aliphatic polyesters. Mnynku et al.[6] studied the morphology of oligomeric polyesters ($\bar{M}_n$, 2000–3000) from 1,10-decanediol (and 1,20-dodecanediol) and various dibasic acids. The crystals precipitated by cooling the solutions were rhombic or hexagonal, and the fold period was equivalent to the chemical repeat unit. Gumargaliyeva et al.[8] studied the annealing of single crystals of poly(hexamethylene sebacate) and poly(eicosamethylene dodecanedicarboxylate) and reported that the fold period and density increased with heat treatment.

The $+O-(CH_2)_x-O-CO-(CH_2)_y-CO+_n$ polyesters are particularly interesting polymers for elucidating relations between chemical structure and physical properties. First, the methylene sequence length can be varied easily. Second, the molecular packing in the crystalline state is

similar to that of polyethylene;[9–12] and third, the crystal structure, in contrast to that of polyethylene, shows anistropy, due to the ester groups, in a plane nearly perpendicular to the molecular chain.

The purpose of the present work is to investigate the morphological habits of solution-grown crystals of linear aliphatic polyesters with a variety of chemical repeat units, specifically of single crystals of poly(ethylene sebacate), poly(hexamethylene sebacate), and poly(decamethylene 1,16-hexadecanedicarboxylate) and to illustrate the relations between the chemical structure of the polymers and the morphological regularity of the single crystals. Hereafter, these polymers are referred to as 2–8, 6–8, and 10–16 polyesters, respectively.

EXPERIMENTAL

Preparation and Characterization of Polyesters

Polyesters were prepared according to Carother's method:[13]

$$\mathrm{H{-}O{-}(CH_2)_x{-}O{-}H + R{-}O{-}CO{-}(CH_2)_y{-}CO{-}O{-}R \xrightarrow[\text{or } Zn(CH_3COO)_2]{ZnCl_2} {+}O{-}(CH_2)_x{-}O{-}CO{-}(CH_2)_y{-}CO{+}_n}$$

where R = —H or —CH_3 (denoted as x-y polyester).

After the reaction, the polymers were purified by repeated precipitation. Number-average molecular weights ($\bar{M}_n$) were estimated by vapor-pressure osmometry. Melting points of bulk polymers were determined by dilatometry. To estimate the effect of solvents, cloud (T_{cloud}) and dissolution (T_d) temperatures were also observed visually at a cooling or heating rate of approximately 1°C/30 min. The results of these characterizations are given in Table I.

TABLE I
Characterization of the Bulk and Single Crystals of Polyesters

Polymer	$\bar{M}_n$	Bulk T_m, °C	Crystals in solvent		
			Solvent[a]	T_{cloud}, °C	T_d, °C
2–8 polyester	13,000	81	i-AA	43.5	54.5
+O—$(CH_2)_2$—O—CO—$(CH_2)_8$—CO+$_n$			*n*-H	59	65.5
			i-B	61	66
6–8 polyester	12,000	78.0	i-AA	30.5	40.5
+O—$(CH_2)_6$—O—CO—$(CH_2)_8$—CO+$_n$			*n*-H	46	57
10–16 polyester	13,000	92.7	i-AA	52	63.5
+O—$(CH_2)_{10}$—O—CO—$(CH_2)_{16}$—CO+$_n$			*n*-H	66.5	70.5

[a] i-AA, *n*-H and i-B represent isoamyl acetate, *n*-hexanol, and isobutanol, respectively.

Solution Crystallization

Crystallizations were carried out as follows from isoamyl acetate and *n*-hexanol solvents: (1) slow cooling of dilute solutions at the rate of

1°C/30 min from 10°C above the dissolution temperature, (2) isothermal crystallization of solutions held for 20–40 hr at a fixed temperature and then filtered at that temperature to prevent additional crystallization during further cooling.

Electron Microscopy and X-Ray Diffraction

Electron microscopic observations were carried out with a Hitachi HU-10 type electron microscope. Crystals were shadowed with germanium. Gold was used to calibrate the diffraction spots. Wide-angle x-ray diffraction photographs of stretched fibers and oriented mats of single crystals were obtained by cylindrical and flat plate cameras with Ni-filtered CuKα radiation. Small-angle x-ray scattering was also measured. A Rigaku Denki D-8C type x-ray diffraction instrument and accessories were used.

RESULTS AND DISCUSSION

Crystal Structures of 2–8, 6–8 and 10–16 Polyesters

Crystal structures of linear aliphatic polyesters have been studied by Fuller et al.,[9–11] and recently, detailed analyses have been reported on some of the polyesters by Turner-Jones et al.[12] and Chatani et al.[14] However, few studies have been reported on the polyesters used in the present study.

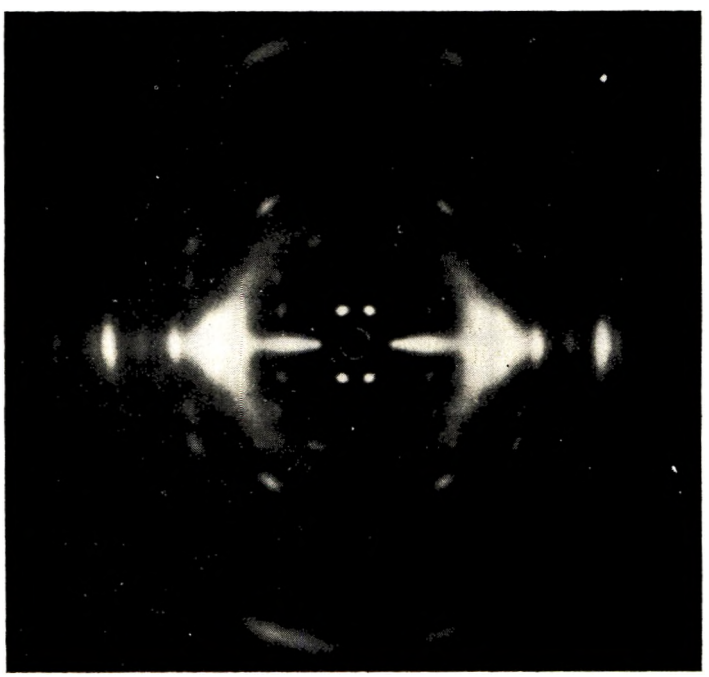

Fig. 1. X-Ray fiber photograph of 2–8 polyester.

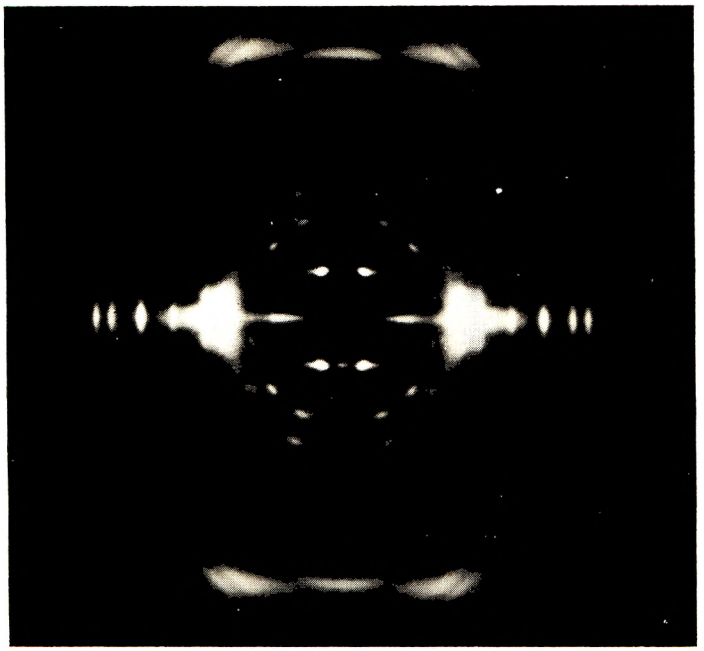

Fig. 2. X-Ray fiber photograph of 6–8 polyester. Weak streaks are observed along the layer lines. Note some weak reflections suggesting the presence of a different modification (for example, the reflection on the meridian of the second layer).

The x-ray fiber photographs of the 2–8 and 6–8 polyesters are shown in Figures 1 and 2 respectively. The unit cell and space group of the 2–8 polyester were determined from the 49 spots in the photograph. Although the x-ray diffraction pattern of the 6–8 polyester shows very weak streaks along the layer lines, except on the equator, and a few weak reflections suggesting an orthorhombic modification, the substantial spots were indexed with the monoclinic structure. The space group of the 2–8 polyester is $P2_1/a$, for which the absence are; $(h0l)$ when h is odd and $(0k0)$ when k is odd. This is in agreement with 2–4 and 2–6 polyesters.[12] By comparing the observed density with the calculated one, it is certain that two chains penetrate into a unit cell (2–8 polyester, $d_{obs.} = 1.173$, $d_{calc.} = 1.227$ g/cm.^{3}; 6–8 polyester, $d_{obs.} = 1.114$, $d_{calc.} = 1.151$ g/cm^3). The unit cell parameters obtained are shown in Table II. The table indicates that the chains are of planar zigzag conformation as reported for aliphatic polyesters. Furthermore the difference of around 0.5 Å in the observed and calculated fiber periods may be ascribed to distortion in the ethylene glycol unit.[9,11,12]

Information on the crystal structure of the 10–16 polyester was obtained from electron diffraction on single crystals (Fig. 3) and x-ray diffraction from oriented mats of single crystals (Fig. 4), because of the lesser drawability of this material. Assuming a monoclinic cell with polyethylene type molecular packing, the unit cell parameters of the 10–16 polyester were determined as $a \sin\beta = 4.96$ Å ($a = 5.47$ Å), $b = 7.38$ Å, $c = 37$ Å and ($\beta =$

TABLE II
Crystallographic Data

Polymer	Unit cell parameters						Chain conformation	Reference
	a, Å	$a \sin \beta$, Å	b, Å	c, Å (fiber axis)	c_{calc}, Å	β		
2–2 Polyester	7.60		10.75	8.30	9.65		T_3GT_3G	14
2–4 Polyester	5.47	5.02	7.23	11.72	12.20	113.5°	T[b]	12
2–6 Polyester	5.51	5.01	7.25	14.28	14.74	114.5°	T[b]	12
2–8 Polyester	5.52	5.00	7.30	16.65	17.29	115°	T[b]	15
	5.58	5.04	7.31	16.76		115.5	T[b]	This work
6–8 Polyester	5.52	5.00	7.40	22.15	22.36	115°	T	This work
10–8 Polyester	5.66	5.0	7.4	27.1	27.45	62°	T	10
10–16 Polyester	5.47	4.96	7.38	37	37.65	115°	T	This work
Polyethylene	7.40		4.95	2.55			T	16

[a] Calculated on the basis of planar zigzag chain conformation.
[b] These ethylene glycol polyesters take on a skew-form in the glycol portions.

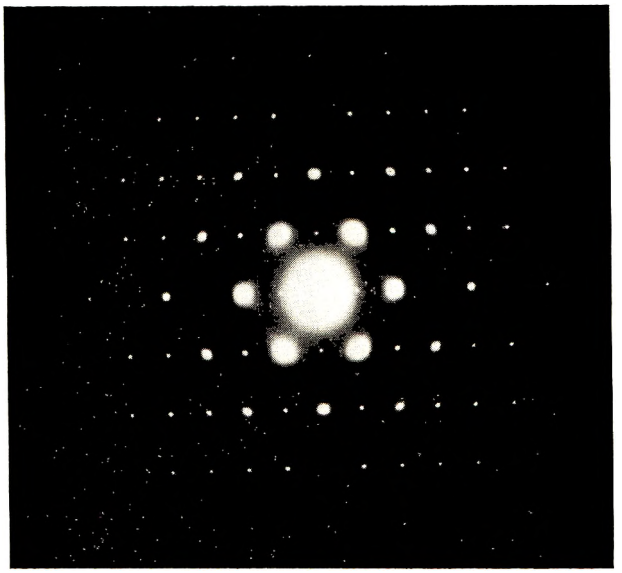

Fig. 3. Selected-area electron diffraction pattern of a single crystal of 10–16 polyester.

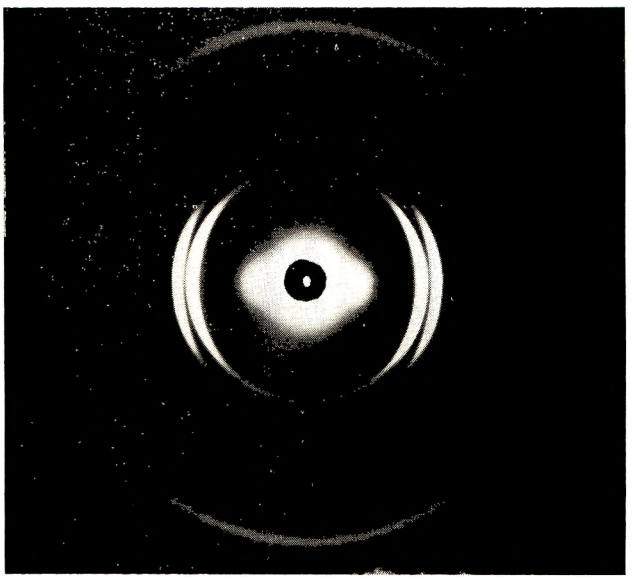

Fig. 4. X-Ray diffraction pattern of 10–16 polyester single crystal mats obtained with the beam parallel to the mat surface (which is horizontal in the present mounting).

115°). These results and others on some of the linear aliphatic polyesters are summarized in Table II.

Morphology of Single Crystals

2–8 Polyester. The morphology of single crystals reflects the crystallographic symmetry of the unit cells; for example, single crystals of linear

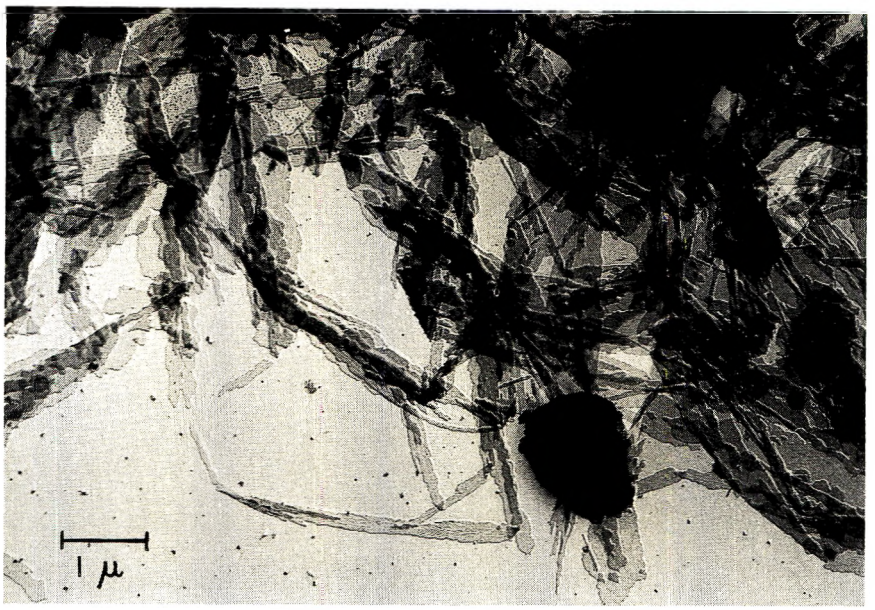

Fig. 5. 2–8 Polyester crystals grown from 0.005 wt-% solution in *n*-hexanol at 57°C (2°C below T_{cloud}). Note marked striations in the ribbons.

polyethylene show smooth faces well defined by (110) and (100) planes, sharp corners, distinct fold sectors, and hollow pyramidal structure.[4] Crystals which possess these characteristics are designated below as "regular" crystals, and those of monolayers alone or with slight overgrowths as "simple" crystals.

Figure 5 shows an electron micrograph of crystals formed isothermally near the cloud temperature (T_c = 57°C, 2°C below T_{cloud}) from a solution 0.005 wt-% in *n*-hexanol. Similar crystals were obtained from isoamyl acetate solution at the same degree of supercooling. Those crystallized near T_{cloud} are ribbonlike lamellae extended along the *a*-axis, 1–3 μ wide and about 100 Å thick. Other morphological features are the irregular growth faces and the marked striations running along the longer dinension (the *a* axis) of the crystals (Figs. 5 and 6). Although the origin of these striations is not clear, they are quite similar to those found in single crystals and in two dimensional spherulites of poly(ethylene terephthalate).[17] Figure 6 shows the complex crystals precipitated by slow cooling of an isoamyl acetate solution. They are similar to those in Figure 5, but well-defined faces, (110), are observed in some regions of the crystals (labeled by the arrow in Fig. 6).

As is shown in Figure 7, fairly "simple" crystals could be grown from solutions in isoamyl acetate, *n*-hexanol, and isobutanol. However, the number of such crystals were very few and their dimensions were very small. Fairly "regular" crystals were also formed through spiral growth, (Fig. 8). They are surrounded by (110) and (010) growth faces reflecting

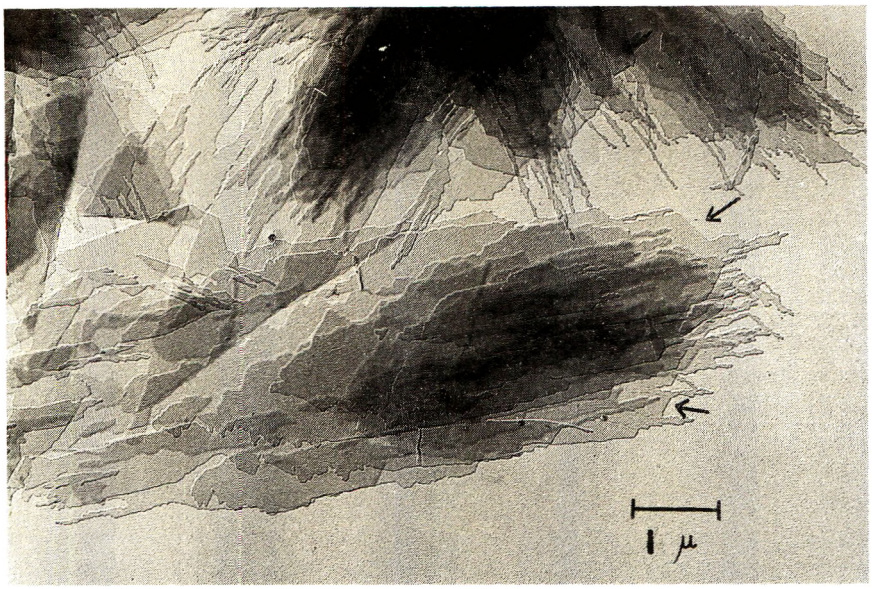

Fig. 6. 2–8 polyester crystals precipitated by slow cooling of 0.005 wt-% solution in isoamyl acetate. The (110) faces are observed in some portions (shown by the arrows).

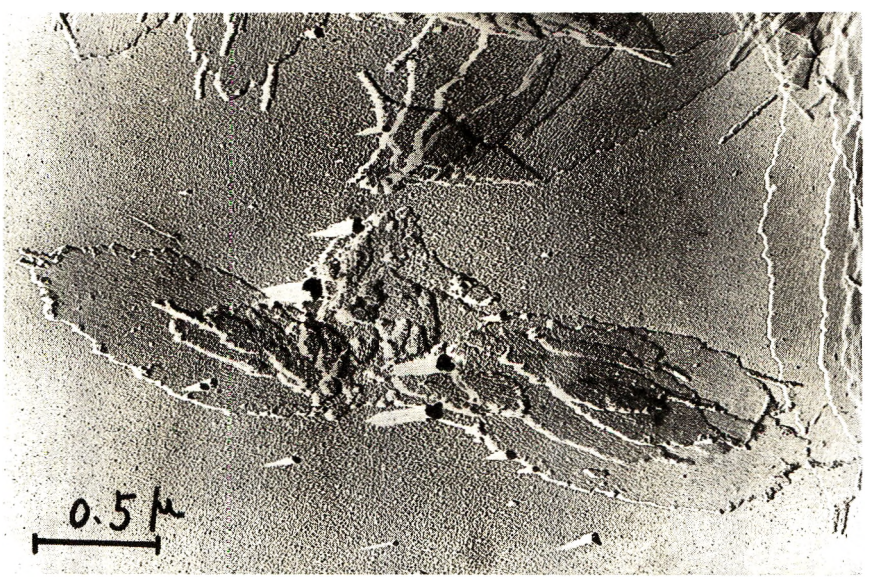

Fig. 7. Elliptical crystals of 2–8 polyester grown from 0.05 wt-% solution in isoamyl acetate at T_c = 30°C (13°C below T_{cloud}). Very few of these relatively simple crystals appear in the electron microscope field.

Fig. 8. Well defined crystals of 2–8 polyester formed through spiral growth on the mother crystal. Note that the dimensions of such well-defined crystals are very small, ($\leq 0.5\,\mu$).

the crystallographic symmetry. The size of such crystals was also very small ($\leq 0.5\ \mu$). They seem to grow at intermediate supercooling in poor solvents such as *n*-hexanol and isobutanol (Table I).

Although various solvents (polar and nonpolar, such as isoamyl acetate, *n*-butanol, *tert*-butanol, isobutanol, *n*-hexanol, and mixtures of nonpolar solvents), concentrations, and crystallization conditions (slow cooling, isothermal crystallization, and seeded nucleation[18]) were tried, attempts to precipitate simple and regular single crystals of large size were not successful. In general the crystals grow into two-dimensional spherulites or ribbonlike lamellae with the longer axis corresponding to the *a* axis and with curved or rough faces. However, in a few cases, fairly "simple" elliptical lamellae (Fig. 7), and very small "regular" crystals formed by spiral growth on the mother crystals (Fig. 8) were observed.

Electron and X-Ray Diffraction of 2–8 Polyester Single Crystals. Electron diffraction patterns of crystals of various morphologies were essentially the same (Fig. 9). The main features are (1) the (020) reflection is very strong and all others weak, and (2) in addition to low order (*hk*0) reflections, that with $d = 4.44$ Å is observed inside the (110) reflection. This suggests a tilting of molecules from the normal to the basal plane in the (020) plane. The spacing $d = 4.44$ Å is substantially identical with $d_{11\bar{1}}^{\text{calc}} = 4.42$ Å. If the fold surface of the crystals is assumed to be the (001) palne, the diffraction effect can be understood as follows. (1) an angle of 4°50′ between the (11$\bar{1}$) plane and the incident beam (parallel to the normal of the

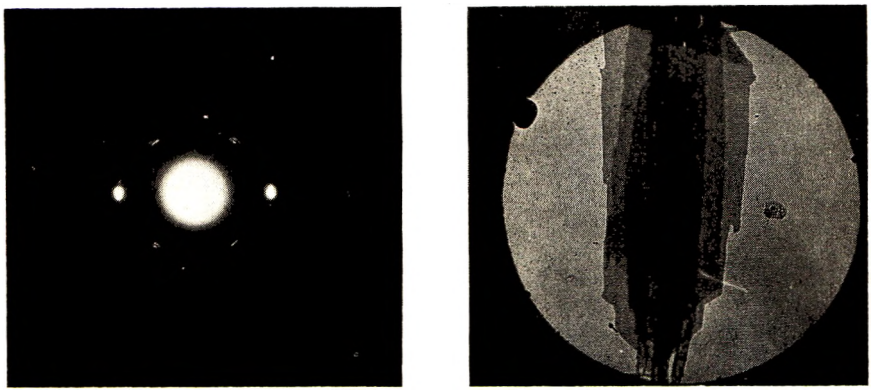

Fig. 9. Selected-area electron diffraction pattern of 2-8 polyester crystal. The pattern corresponds to the reflections from the circular portion in the photograph. Note the four weak reflections from planes with $l \neq 0$. All others are $(hk0)$. The (020) reflections are very strong and all others are very weak. These facts indicate that the molecules are inclined from the normal of the basal plane in (020) plane.

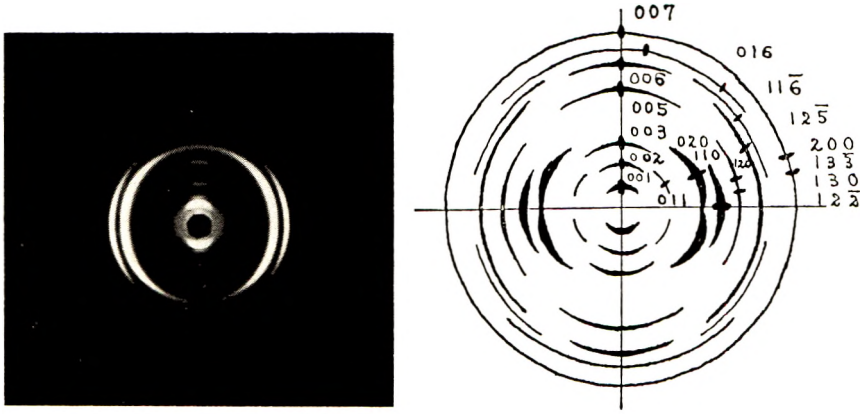

(*a*) (*b*)

Fig. 10. (*a*) X-Ray diffraction pattern of sedimented mat of 2-8 polyester single crystals (x-ray beam parallel to the mat surface, which is horizontal in the present mounting), and (*b*) scale drawing of the pattern. The points in the quadrant represent the calculated positions when the (001) plane is the basal plane of the crystals which lie parallel to the mat surface.

basal plane) might be sufficient to satisfy the Bragg condition for $(11\bar{1})$ planes relaxed by the extension of the reciprocal lattice point due to the thickness of the crystals[19] (80 Å), and (2) the molecules are inclined from the normal of the fold surface (basal plane) in the (010) planes, and accordingly only the (020) reflectiln is strong.

In order to obtain additional information on the orientation of molecules, an x-ray diffraction study was carried out. Figure 10 shows the x-ray diffraction pattern of a sedimented mat with the incident beam parallel to the surface of the mat. Although the orientation is inherently broad, the maxima of the reflections may be distinguished. All the (00*l*) reflections

have their maxima on the meridian and the (020) reflections, on the equator; however, the (110) and (011) reflections diverge from the equator by 22° and 28°, respectively. The small-angle reflection on the meridian (along the normal to the mat) indicates that the lamellae orient with basal plane parallel to the mat surface.

If the (001) planes are parallel to the mat surface, the splitting of the (hkl) reflections from the equator, ϕ_{hkl}, is given by,

$$\sin \phi_{hkl} = \frac{d_{001} d_{hkl}}{\cos \theta_{hkl}} \left\{ \frac{h \cos (180° - \beta)}{ac \sin^2 \beta} + \frac{l}{c^2 \sin^2 \beta} \right\}$$

where d_{001} and d_{hkl} are the spacings of the (001) and (hkl) plane respectively, and θ_{hkl} is the Bragg angle. The calculations of splitting, $\phi_{00l} = 90°$, $\phi_{020} = 0°$, $\phi_{110} = 21°21'$ and $\phi_{011} = 26°$, are in good agreement with the observed values, $\phi_{00l} = 90°$, $\phi_{020} = 0°$, $\phi_{110} = 22°$ and $\phi_{011} = 28°$. These facts indicate that the fold surface of the crystals is the (001) plane, in accordance with the result from electron diffraction. The situation is similar to that reported on several polyamides and poly(ethylene adipate).[20]

Kawai et al.[21] and Holdsworth et al.,[22] have reported that in polyethylene, complex and irregular crystals were formed when the number of alkyl-branches increased. Kawai et al. have attributed the effect to the irregular folds perturbed by the branches rejected from the crystal lattice. Ltoz et al.[23,24] studied single crystals of copolymers composed of one poly(ethylene oxide) and one polystyrene block. They found that the crystal platelets consisted of chain-folded poly(ethylene oxide) portions sandwiched between amorphous polystyrene portions; these block copolymers could crystallize in a regular habit reflecting the crystallographic symmetry even if the crystals were wrapped in amorphous layers.

On the other hand, although the 2–8 polyester generally crystallizes in less regular habits, the fold surface seems to be fairly regular because it corresponds to the (001) plane. The crystallization pattern of this polymer may be ascribed not to irregularity of chain molecules introduced by side-reaction during polymerization, but to the crystallization mechanism related to the chemical structure. The effect of methylene sequence length in polymer molecules on morphological habit will be described further for 6–8 and 10–16 polyesters.

6–8 Polyester. Gumargalieva et al.[8] studied the annealing behavior of 6-8 polyester single-crystals precipitated from ethanol solution. The crystals reported were very small (ca. 1 μ) and hexagonal with heavy overgrowth and irregular edges. Insolubility of the polymer ($\bar{M}_n = 12{,}000$) in ethanol in our experiments suggests that the material used in their study was of low molecular weight.

Figure 11 shows typical single crystals precipitated from a 0.005 wt-% solution in n-hexanol at $T_c = 44°C$ (2°C below T_{cloud}). These hexagonal crystals are outlined by (110) and (100) growth faces and are 80 Å thick. On comparing the morphology of these large single-crystals (10–20 μ) with those of 2–8 polyester crystals, it is clear that the former exhibit smoother

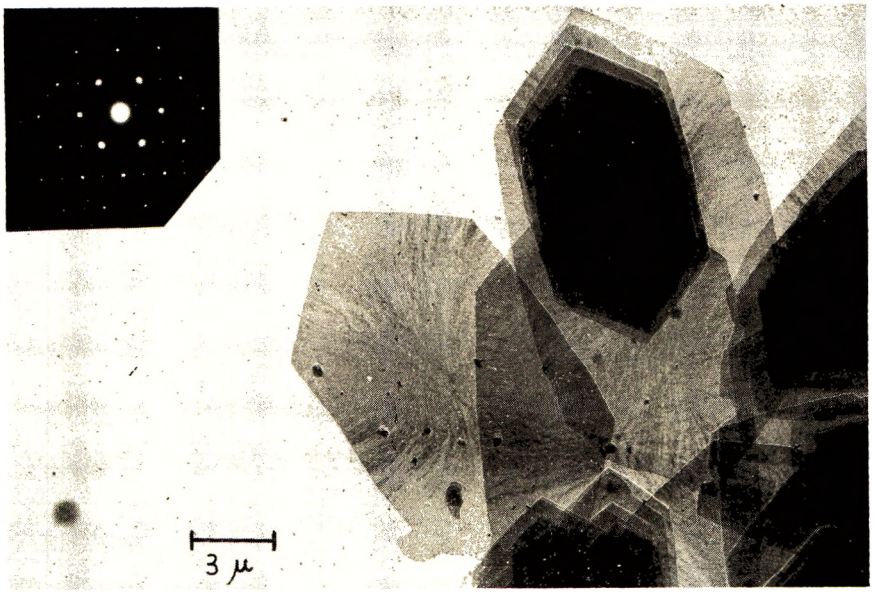

(a)

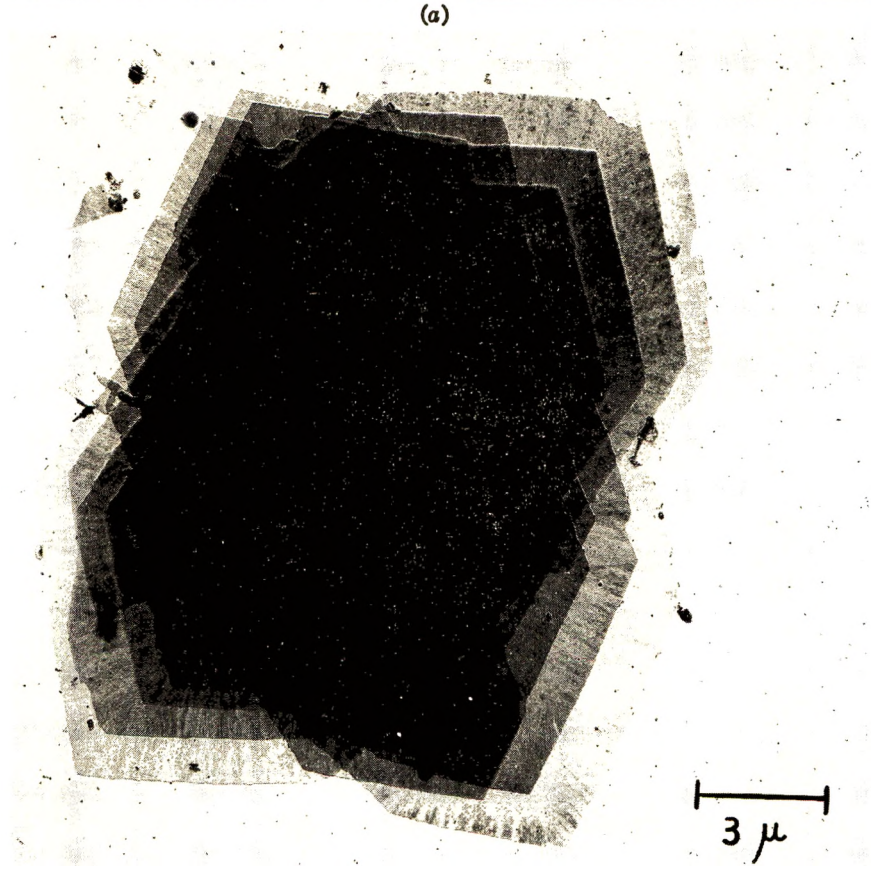

(b)

Fig. 11. Single crystals of 6–8 polyester grown from 0.005 wt-% solution in *n*-hexanol at 44°C (2°C below T_{cloud}). The Bragg extinction bands running perpendicular to the growth planes are more regular in the twinned crystals (*b*), than in the monolayers (*a*).

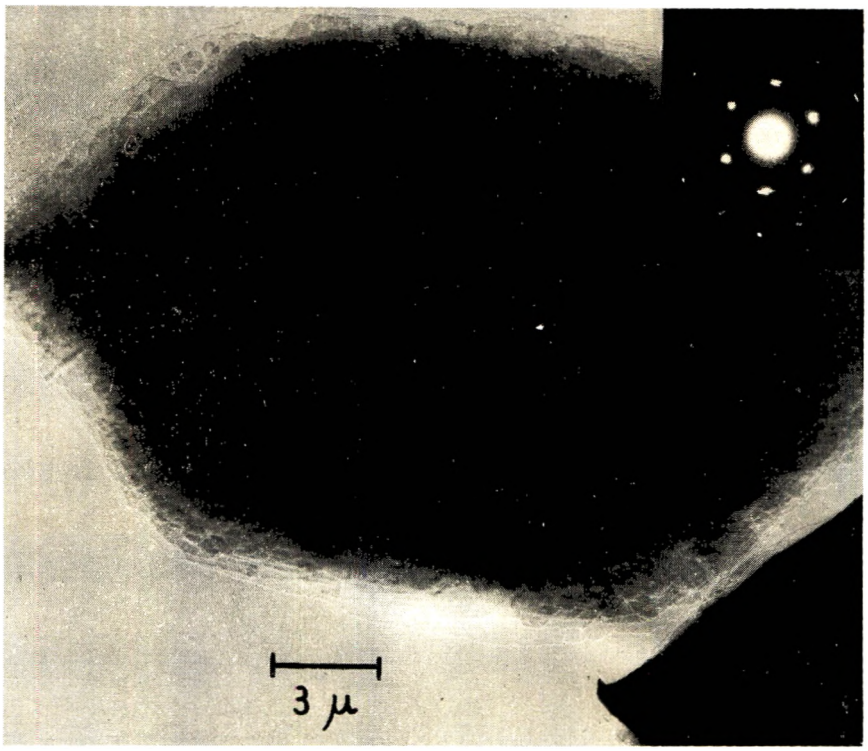

Fig. 12. 6–8 polyester crystal precipitated from isoamyl acetate solution by slow cooling, and a selected-area electron diffraction pattern from thinner portion of the crystal.

faces and sharper corners than the latter. The Bragg extinction bands in Figure 11 are approximately perpendicular to the corresponding growth faces in both the (110) and (010) fold sectors. They are less regular, and hence the fold sector boundaries are not so apparent as in the 10–16 polyester single crystals shown in Figure 13 (below). Some differences in the extinction bands for the twinned crystals (Fig. 11*b*) and the monolayers (Fig. 11*a*) are significant, and may be interpreted as due to the nonplanar structure of the crystals. Furthermore, the appearance of such Bragg extinction bands suggests nonplanarity of the 6–8 polyester single crystals.

The crystals grown from isoamyl acetate solutions were in general thickened by heavy overgrowths (Fig. 12), and no simple and regular crystals were observed with the crystallization conditions employed.

The electron diffraction pattern shown in Figure 11*a* is simple; it shows up to five orders of (*hk*0) reflections and no reflections from planes with $l \neq 0$. This indicates that the molecular chains in the 6–8 polyester crystals are nearly perpendicular to the basal plane, a finding which is supported by x-ray diffraction studies on single crystal mats.

10–16 Polyester. This polymer crystallizes in "simple" and "regular" habits under the various crystallization conditions.

The single crystals shown in Figure 13 were obtained by immersing a hot isoamyl acetate solution in a bath regulated at 40°C (12°C below T_{cloud}) for 8 hr and then cooling to room temperature. In the photograph, lozenge and truncated lozenge crystals are observed. This suggests that the crystallization was not isothermal. The true lozenges show regular extinction bands running along the ⟨310⟩ direction (the direction corresponding to ⟨130⟩ in polyethylene). The extinction pattern indicates that two diagonals of the true lozenge correspond to fold sector boundaries. As was suggested by Reneker et al.[25] and Bassett et al.[26,27] in their studies on habit features in polyethylene single-crystals, the extinction bands may be as-

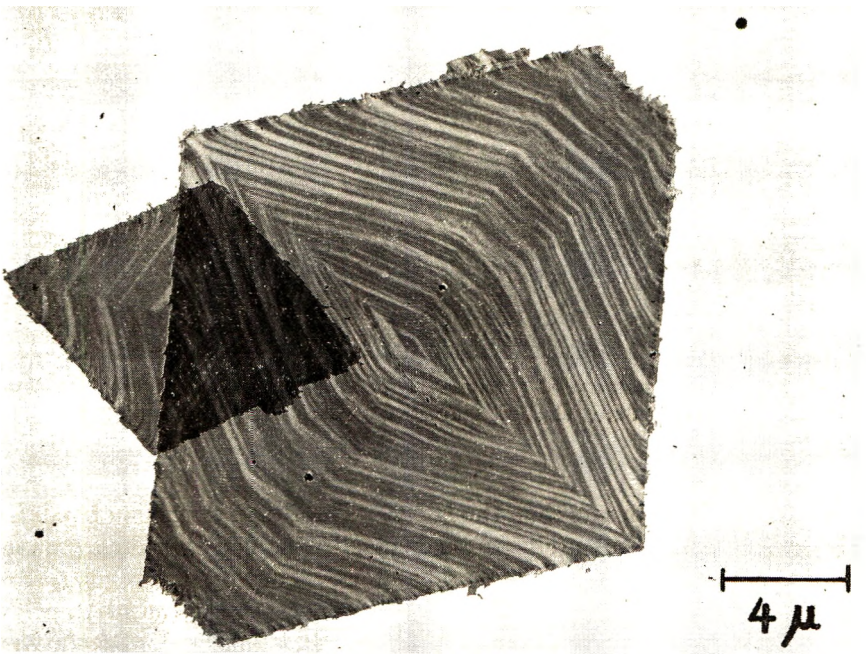

Fig. 13. Single crystals of 10–16 polyester. Two types of crystal are observed; lozenges and truncated lozenges. The thin border of the crystals is believed to have grown during cooling.

sociated with the collapse of the pyramidal crystals during sedimentation onto the substrate. Although these crystals are surrounded by thin ragged borders, the thicker lamellae show smooth growth faces, sharp corners, distinct fold sectors, and hollow pyramidal structure.

In Figure 14 is shown a large hexagonal crystal (40–50 μ), 120 Å thick, grown from isoamyl acetate solution at 50°C (2°C below T_{cloud}) and its electron diffraction pattern. This type of crystal, outlined by (110) and (010) growth faces, is very similar to high-temperature polyethylene single crystals.[28] They also show diffraction contrast but the extinction pattern is different from those observed with true lozenges of the 10–16 polyester, the

6–8 polyester, and high-temperature polyethylene crystals. Although the extinction bands are irregular in the (010) fold secotrs, they orient parallel to the a-axis (which corresponds to the b-axis of polyethylene) throughout the crystal. Central pleats were sometimes observed in monolayer single-crystals (Fig. 14). As was confirmed in polyethylene single crystals,[29,30] polymer molecules deposit on growth faces with folding along the (010) planes in the (010) fold sectors and along the (110) planes in the (110) sectors. Hence, the crystal may be expected to collapse more smoothly along (010) planes in the (010) sectors than in the (110) sectors. Contrary to the above expectation, the extinction bands become more irregular in the (010) fold

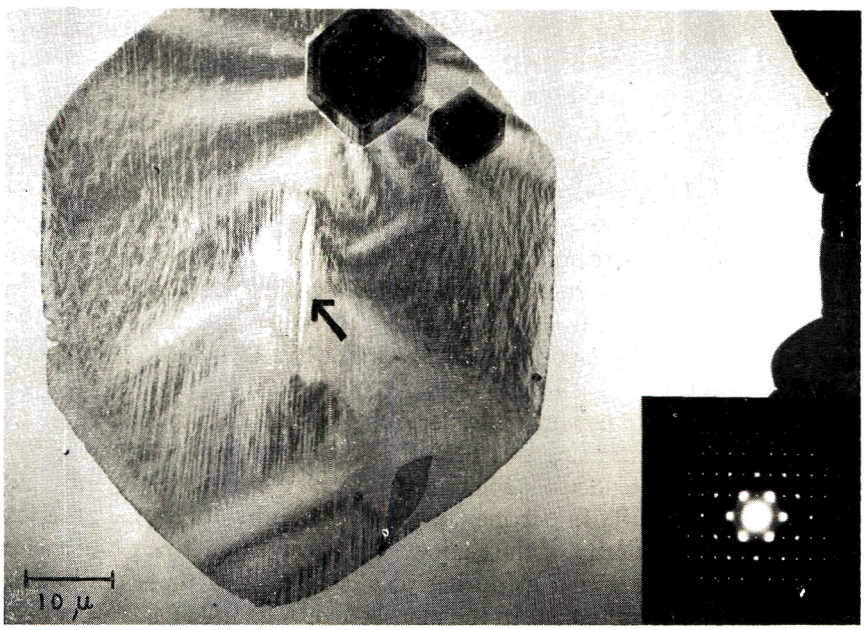

Fig. 14. A large hexagonal single crystal of 10–16 polyester grown from isoamyl acetate solution at 50°C (2°C below T'_{cloud}). The Bragg extinction bands are parallel to the a-axis throughout the crystal but staggered in the (010) sectors. A pleat lies parallel to the extinction bands at the center of the crystal (shown by the arrow).

sectors. Further study is needed for detailed analysis of these bands and pleats in relation to the spatial nature. Nevertheless, there is clear evidence for the nonplanar nature of the high temperature form of 10–16 polyester single crystals.

Electron diffraction patterns from lozenges and truncated lozenges are identical and show ($hk0$) reflections up to eight orders and no reflections from planes with $l \neq 0$, (Fig. 14). Although Bragg extinction bands were observed in both types of single crystals, the electron diffraction pattern suggests that the molecular chains are perpendicular to the basal plane of the single crystals after collapse. This is consistent with the result deduced from the x-ray diffraction of single-crystal mats.

Relation between Chemical Structure and Habit Features in Single Crystals

In summary of the above results and discussion, the 2–8 polyester crystallizes generally into two-dimensional spherulites or ribbonlike lamellae, (Figs. 5 and 6). Simple and elongated ellipsoids, (Fig. 7), and very small daughter crystals ($< 0.5\ \mu$), well-defined with low index planes (Fig. 8), were also formed, but the number of such crystals was very small. Although various polar and nonpolar solvents were employed, no simple and regular crystals of large size were formed under the crystallization conditions employed here. The 6–8 polyester crystallizes from *n*-hexanol solution near the cloud temperature into simple and fairly regular single crystals of hexagonal outline, defined with low index planes. A nonplanar structure for these single crystals is suggested by the Bragg extinction bands. In the crystallization of the 10–16 polyester, which possesses the longest methylene sequences in both glycol and acid portions, conditions under which "regular" and "simple" single crystals are formed are further relaxed. For instance, true lozenges and hexagonal single crystals of large size (10–50 μ) with smooth faces, sharp corners, distinct fold sectors, and pyramidal structure, were precipitated from isoamyl acetate solutions in the temperature range from T_{cloud} to 15° below T_{cloud}. Table III summarizes some habit features of the single crystals of 2–8,6–8, and 10–16 polyesters.

The morphology of polyethylene single crystals has been found to become less regular with increasing numbers of alkyl branches in the chains.[21,22] Livingston,[5] who extended the relation to polymers generally, suggests that the degree of regularity in polymer single-crystals provides a good criterion for judging the regularity of the chains. However, there is no evidence for production of chain branches during polymerization of these polyesters. Hence, the marked difference in the morphological habits of single crystals of linear aliphatic polyesters formed from monomers of different length must be ascribed to properties inherent in the methylene sequence length in the chemical repeat units.

The x-ray and electron diffraction studies on the orientation of the molecules in the single crystals show: (1) in crystals of 2–8 polyester, the molecules are inclined from the normal of the basal plane; (2) in 6–8 and 10–16 polyester single crystals, however, the molecules are approximately perpendicular to the basal plane.

In 2–8 polyester crystals the results indicate that the (001) plane corresponds to the fold surface. The similarity of habit in the true lozenge crystals of 10–16 polyester and polyethylene crystals, which have a [(314)(110)] fold surface,[26,27] suggests that the fold surface of the former is not the (001) plane. To elucidate the fold surface geometry of 6–8 and 10–16 polyester single crystals is more complex, because the resultant basal planes after collapse are closely correlated with the mode of collapse and the original spatial structure.

TABLE III
Characteristic habits of the single crystals of 2–8, 6–8, and 10–16 Polyesters

Polymer	General crystal shape	Fraction of monolayers (at $T_c = T_{cloud} - 2°C$)	Crystal[b] dimension of regular crystal, μ	Overgrowth	Degree of perfection of crystals[a]			Spatial structure
					Smoothness[b] of growth faces	Sharpness[b] of corners	Distinctness of fold sectors	
2–8 polyester	Spherulitic or ribbonlike	0	<0.5	Always (heavy)	3	2–3	3	Planar
6–8 polyester	Hexagonal	~1/5	<20	Very often	2	2	2	Nonplanar
10–16 polyester	Lozenge or hexagonal	~4/5	<50	Sometimes	1–2	1–2	1	Hollow pyramidal and nonplanar

[a] 1, 2, 3, represent degree of perfection , in decreasing order.
[b] As Keith et al.[31] observed, single crystals of a given polymer show a tendency to lose their regularity and simplicity with increasing size.

The authors wish to thank Dr. K. Nakagawa for helpful suggestions, Prof. M. Takeda for continuing interest and encouragement, and Mr. S. Shibata for help with the electron microscopy.

References

1. A. Keller, *Phil. Mag.*, **2**, 1171 (1957).
2. E. W. Fisher, *Z. Naturforsch.*, **12b**, 753 (1957).
3. P. H. Till, Jr., *J. Polym. Sci.*, **24**, 301 (1957).
4. P. H. Geil, *Polymer Single Crystals*, Interscience, New York, 1963.
5. H. K. Livingston, *Macromolecules*, **2**, 98 (1969).
6. Yu. Y. Mnynku, E. M. Belavtseva, and A. I. Kitaigorodski, *Dokl. Akad. Nauk SSSR*, **133**, 1132 (1960).
7. N. Hirai, N. Toyama, Y. Ogawa, and A. Yonamine, paper presented at the 18th Annual Meeting, Chemical Society of Japan, Osaka, Japan, 1965; *Proceedings*, p. 252.
8. K. Z. Gumargaliyeva and E. M. Belavtseva, *Polym. Sci. USSR*, **8**, 1769 (1967).
9. C. S. Fuller and C. L. Erickson, *J. Amer. Chem. Soc.*, **59**, 341 (1937).
10. C. S. Fuller and C. J. Frosch, *J. Amer. Chem. Soc.*, **61**, 2575 (1939).
11. C. S. Fuller and C. J. Frosch, *J. Phys. Chem.*, **43**, 323 (1939).
12. A. Turner-Jones and C. W. Bunn, *Acta Cryst.*, **15**, 105 (1962).
13. W. H. Carothers and J. A. Arvin, *J. Amer. Chem. Soc.*, **51**, 2560 (1929).
14. Y. Chatani, A. Ueda, K. Suehiro, and H. Tadokoro, paper presented at the 20th Annual Meeting, Chemical Society of Japan, Tokyo, Japan, 1967.
15. S. Y. Hobbs and F. W. Billmeyer, Jr., *J. Polym. Sci. A-2*, **7**, 1119 (1969).
16. C. W. Bunn, *Trans. Faraday Soc.*, **35**, 482 (1939).
17. Y. Yamashita, *J. Polym. Sci. A*, **3**, 81 (1965).
18. D. J. Blundell, A. Keller, and A. L. Kovacs, *J. Polym. Sci. B*, **4**, 481 (1966).
19. A. W. Agar, F. C. Frank, and A. Keller, *Phil. Mag.*, **4**, 32 (1959).
20. K. Monobe, A. Kawaguchi, and N. Hirai, paper preseted at the International Symposium on Macromolecular Chemistry, Tokyo-Kyoto, Japan, 1966.
21. T. Kawai, K. Ujihara, and H. Maeda, *Kolloid-Z.*, **132**, 87 (1970).
22. P. J. Holdsworth and A. Keller, *J. Polym. Sci. B*, **5**, 605 (1967).
23. B. Lotz and A. J. Kovacs, *Kolloid-Z.*, **209**, 97 (1966).
24. B. Lotz, A. J. Kovacs, G. A. Bassett,and A. Keller, *Kolloid-Z.*, **209**, 115 (1966).
25. D. H. Reneker and P. H. Geil, *J. Appl. Phys.*, **31**, 1916 (1960).
26. D. C. Bassett and A. Keller, *Phil. Mag.*, **6**, 345 (1961).
27. D. C. Bassett, F. C. Frank, and A. Keller, *Phil. Mag.*, **8**, 1739 (1963).
28. T. Kawai and A. Keller, *Phil. Mag.*, **11**, 1165 (1965).
29. D. C. Bassett, F. C. Frank, and A. Keller, *Phil. Mag.*, **8**, 1753 (1963).
30. M. I. Bank and S. Krimm, *J. Polym. Sci. A-2*, **8**, 1785 (1969).
31. H. S. Keith, *J. Polym. Sci. A-2*, **2**, 4339(1964).

Received March 5, 1971

JOURNAL OF POLYMER SCIENCE: PART A-2 VOL. 9, 2061-2080 (1971)

Fractionation of Linear Polyethylene during Bulk Crystallization under High Pressure*

J. L. KARDOS, H.-M. LI, and K. A. HUCKSHOLD, *Department of Chemical Engineering, Washington University, St. Louis, Missouri 63130*

Synopsis

Two linear polyethylene fractions (M_n, 11,260 and 100,000) and mixtures of these fractions have been isothermally crystallized from the melt under pressures up to 3000 atm. Characterization of individually crystallized fractions with transmission electron microscopy indicates that pressure can be used to produce a crystallite whose thickness is a measure of the chain length within it. Although the high molecular weight fraction yields spherulites containing individually varying lamellae thicknesses, the maximum thickness of each lamella is a measure of the chain length within it. Both electron micrographs and differential thermal analysis results show that crystallization of homogeneous mixtures of the high and low molecular weight fractions under high pressure results in a distinct fractionation and segregation according to molecular weight.

INTRODUCTION

Almost all characteristic bulk properties of crystallizable polymers depend on the structure of the crystallites and the nature of the interaction between them. Both the crystallite size and perfection and the nature of the intercrystallite regions depend on the mechanism by which individual polymer chains crystallize from what is often referred to as a bulk, spaghetti-like melt. Much is now known about the crystallization mechanism in the case of dilute polymer solutions,[1] but extrapolation of these results to the bulk situation is, at best, risky. Thus, in attempts to interpret the properties of bulk crystalline polymers by elucidating the nature of their solid state, considerable controversy has emerged concerning the molecular nature of the crystallites and the mechanism by which they form. Specifically, the question of how much molecular weight fractionation and segregation can occur during bulk crystallization is still largely unanswered and is the subject of this paper.

In the case of crystallization from dilute solution, fractionation has been predicted from theoretical considerations by Kawai[2] and demonstrated experimentally by Kawai and Keller.[3] Kinetic crystallization theory, as presented by Hoffman,[4] predicts fractionation during bulk crystallization, but conclusive experimental proof is lacking in the literature. This is not

* Presented in part at the Dallas Meeting of the American Physical Society, High Polymers Division, March 1970.

too surprising when one considers the morphology of bulk-crystallized polymers. The crystallites in most cases are lamellae of 100–500 Å thickness, which contain highly folded chains. Thus, high or even relatively low molecular weight chains will crystallize in a folded conformation to form lamellae which look much the same in the electron microscope and possess nearly the same physical properties. To be sure, there are differences in melting points between high and low molecular weight samples, but unless the molecular weights differ by an order of magnitude or more, such differences are not large enough to allow distinction between the melting of lamellae containing short folded chains and those containing long folded chains in the same sample.

When the molecular weight is low enough, normal crystallization conditions can produce crystallites which apparently contain completely extended chains. Anderson[5,6] has isothermally crystallized various narrow, low molecular weight fractions of linear polyethylene. In looking at the individual fractions, he found that for isothermal crystallization at rather low supercoolings those fractions with molecular weights below 12,000 crystallized in an extended-chain conformation while above 12,000, folded-chain crystallites were formed. Both types of conformation were found in an isothermally crystallized sample of whole polymer, indicating that some fractionation of low molecular weight polymer had occurred during crystallization. Other evidence for fractionation during spherulitic crystallization from the melt comes from the work of Keith and Padden,[7] who demonstrated that both stereoirregular molecules (e.g. atactic polypropylene) and low molecular weight chains [poly(ethylene oxide)] are preferentially rejected by growing crystals of polyethylene. Although this evidence does not directly illustrate the phenomenon of fractionation of short polyethylene molecules from long ones, it does demonstrate the mobility available to molecules in a crystallizing melt.

Using infrared spectroscopy, Bank and Krimm[8] have recently analyzed mixtures of two fractions, one of which was deuterated. They attributed observed doublet formation in certain bands to aggregation of similar molecular weight species.

With the discovery that high pressure can be used to cause even high molecular weight polyethylene chains to crystallize in an extended conformation,[9] the possibility of examining melt-crystallized polyethylene for fractionation effects was greatly enhanced. A review of pressure crystallization of polyethylene has been presented recently by Wunderlich and Davidson.[10] It is now generally accepted beyond reasonable doubt[9,11] that the polyethylene chains in extended-chain lamellae are parallel to the striations found upon fracture of the lamellae. Thus, it is possible for the lamella thickness to be an indicator of the lengths of molecules comprising the lamella. In their initial work on pressure-crystallized polyethylene, Geil et al.[9] pointed out that the average extended-chain thickness agreed reasonably well with the number-average molecular length and suggested that molecular fractionation might have occurred. The same suggestion was made

later by Kardos et al.[12] from a study of pressure-crystallized linear and branched polyethylenes, in which the average extended-chain thickness was found to increase with increasing average molecular weight. It has also been shown by Prime and Wunderlich[13] that for a range of pressure-crystallized, linear polyethylene fractions, as well as whole polymer, the lamella thickness distribution exactly matches the molecular length distribution up to a molecular weight of 10,000. Above weights of 10,000, the lamella thickness increased with increasing molecular weight, although the thickness was considerably less than the molecular length at high molecular weights.

The objectives of the work reported and discussed here were to determine to what degree the extended-chain lamella thickness is a measure of the molecular lengths therein and to determine whether or not significant fractionation and segregation can occur during crystallization at high pressure. Two narrow, linear polyethylene fractions and mixtures of these fractions were isothermally crystallized from the melt under pressures up to 3000 atm. The specimens were subsequently characterized with transmission electron microscopy and differential thermal analysis.

EXPERIMENTAL

Materials and Sample Preparation

Two narrow molecular weight fractions of linear polyethylene having viscosity-average molecular weights of 100,000 ($\bar{M}_w/\bar{M}_n = 1.5$) and 11,260 ($\bar{M}_w/\bar{M}_n = 1.2$) were used in this study. The fractions were prepared from Ziegler-type whole polymer by the large-scale elution fractionation technique of Kenyon et al.[14]

The two fractions, high molecular weight (HMW) and low molecular weight (LMW), were combined in three proportions to yield samples containing 25%, 50%, and 75% by weight of LMW polymer. A sufficient quantity of each mixture was dissolved completely in boiling xylene to form a homogeneous solution containing less than 5% polyethylene by weight. After thorough mixing, the boiling solution was poured into a large quantity of methanol at Dry Ice temperature. The instantaneously formed precipitate was filtered and then dried under high vacuum at room temperature. Mass balances indicated that all but trace quantities (<0.1%) of polymer were recovered from the solution as a dried precipitate. At this point it was essential to show that no significant fractionation took place during the quench-precipitation step of the mixtures. In light of the speed with which the polymer precipitated (ca. 1 sec), there is no *a priori* reason for expecting any significant fractionation and segregation to occur. However this point was checked by DTA analysis which showed one broad melting peak for the precipitated mixtures. Mechanical mixtures of the fractions after they were individually precipitated under the same conditions as the mixtures yielded doublet peaks or peaks with strong shoulders.

Samples of both the mixtures and pure fractions were ground into powder. Those samples not amenable to grinding were chopped into very small pieces. A small quantity (0.1%) of antioxidant (Santenox R, Monsanto Co.) was then mixed into each sample. The samples were subsequently cold-molded at temperatures below 80°C to form cylinders $^5/_{16}$ in. in diameter and $^1/_4$ in. high. Great care was taken not to crystallize or anneal the sample during the molding stage. Differential thermal analysis of the samples before and after molding showed no change due to this step. After molding, the samples were wrapped with one layer of aluminum foil and encapsulated with a thin layer of silicone rubber (RTV-112, General Electric) prior to insertion in the pressure vessel. This technique provides an oil-tight seal at temperatures up to 200°C under pressures up to 3000 atm for 3 days.

Apparatus and Crystallization Procedure

The pressure apparatus used in this investigation was that described by Barlow[15] with the exception that a different pressure vessel design was used. Briefly, the system uses a high-pressure hydraulic pump and an intensifier to generate hydrostatic pressures up to 50,000 psi in a motor oil-kerosene fluid which is fed directly to the pressure vessel containing the sample.

In this work, the pressure vessel shown in Figure 1, consists of a high-pressure, line filter assembly, with the filter removed, and a thermocouple assembly both produced by the American Instrument Company as standard items of high pressure equipment. The thermocouple assembly is installed

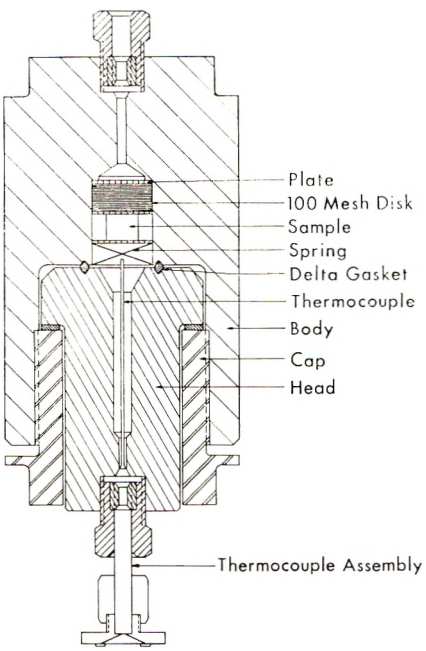

Fig. 1. Pressure vessel and thermocouple assembly.

in the head opening of the filter with the high pressure tubing connected to the filter bottom. Although the thermocouple was not in the sample itself, the temperature at the center axis of the vessel and near the sample closely approximated the sample temperature since there was a negligible temperature gradient in the axial direction. The vessel was placed in a silicone oil bath with temperature fluctuations less than ±0.5°C. The hydrostatic pressure was measured with Bourdon tube gages. Minute leaks in the system and the thermal-pressure effect due to room temperature fluctuations limited the pressure constancy of the system for a 24-hr run to ± 10 atm up to 3000 atm.

The pressure vessel was loaded as shown in Figure 1, care being taken to bleed all air from the system. In a given crystallization experiment, the sample was heated at atmospheric pressure to the crystallization temperature T_x, chosen to yield a specific supercooling under the desired crystallization pressure. The desired T_x was determined using the melting point of the fractions crystallized by slow-cooling at atmospheric pressure and the change in melting point with pressure reported by Baer and Kardos.[16] After 1 hr at T_x to ensure complete melting and temperature equilibrium, the pressure was rapidly raised to the desired value and the crystallization carried out under constant pressure and essentially constant temperature.

The onset of crystallization was detected by an initial drop in pressure and the increased pumping needed to keep the pressure constant. In all cases, the sample was observed to begin to crystallize at T_x. Following sufficient time for crystallization (up to 72 hr), the sample was cooled slowly at 2°C/hr until it was well below normal atmospheric crystallization temperatures, after which it was rapidly cooled to room temperature and the pressure released.

Samples of individual fractions were isothermally crystallized at atmospheric pressure using an oil bath with temperature regulation to ±0.5°C. Mixtures of fractions were crystallized at atmospheric pressure by slow cooling at less than 1°C per minute.

Sample Characterization

Two-stage, cellulose acetate/platinum–carbon replicas of sample fracture surfaces were made for examination with a Hitachi HU-IIB electron microscope. All but the pure LMW samples were fractured in liquid nitrogen. Over 100 lamellae were measured for each fracture surface. Lamellae with surfaces noticeably tilted from the plane of the photograph were not included in the analysis. In the HMW and mixture samples, the thickness of any one lamella near its visible origin, particularly those growing from spherulite centers or from points of impingement, varied occasionally by a factor of over two. In those cases the maximum thickness was used in the average thickness calculations. With the above qualifications, a number-average thickness was calculated for each fracture surface.

Differential thermal analysis (DTA) was performed on 5-mg samples by using a DuPont Model 900 unit with a heating rate of 10°C/minute. The

samples were prepared by grinding or chopping the bulk specimens into a coarse powder.

Viscosity measurements were made before and after crystallization to check on the possibility of degradation during the melting and crystallization. No change in molecular weight was indicated.

RESULTS

Individual Fractions

When the linear polyethylene fractions were isothermally crystallized individually from the melt at low degrees of supercooling and under sufficiently high pressure, their entire fracture surfaces were occupied by extended-chain lamellae of fairly regular thickness. The observed average thickness of these lamellae, the DTA melting points, and the crystallization conditions used are summarized in Table I. The calculated fully extended chain lengths for each fraction are included for comparison. Also included are Anderson's results for atmospheric crystallization of a LMW fraction.[5] The supercooling values should be viewed as only approximate since the pressure-melting point data were determined for whole polymer. No correction has been made for superheating effects on the melting points.

A typical fracture surface from a LMW sample crystallized at 1000 atm is shown in the electron micrograph of Figure 2. The lamella thicknesses are very uniform and yield an average thickness of 1000 Å, which agrees closely with the calculated value of 1020 Å for fully extended chains. Great care was taken to avoid counting tilted lamellae which can cause a large underestimation of thickness for these very thin lamellae. Anderson has acknowledged this as a possible cause of the discrepancy between his observed and calculated thickness values.[5] Although increasing the crystallization pressure from 1 to 1000 atm causes the lamellae to thicken slightly, raising the pressure further to 2000 atm has no effect on the average lamella thickness. Thus, the critical pressure for formation of completely extended chains in LMW fractions under the crystallization conditions employed here is less than 1000 atm. The two-degree difference in melting point between the 1000 and 2000-atm samples can easily be attributed to differences in crystallite perfection and/or differences in superheating which are known to occur during melting of extended-chain crystals.[17]

Specimens of the HMW fraction were crystallized isothermally at both 2000 and 3000 atm. The 2000-atm sample was ductile and hard to break under liquid nitrogen. It is presumed to be made up primarily of folded-chain crystallites, since the drawn, fibrillar fracture surface and the melting point were the same as found for crystallization under atmospheric pressure.

A representative fracture surface from the HMW sample crystallized at 3000 atm is shown in Figure 3. Thick, extended-chain lamellae are present with an average maximum thickness of 8950 Å which again agrees closely with the fully extended chain length of 9050 Å for this fraction.

TABLE I
Characterization of Individual Polyethylene Fractions Crystallized under Various Conditions

Sample molecular weight	Crystallization conditions				DTA melting point, °C	Average lamella thickness Å	Calculated fully extended chain length, Å
	Pressure, atm	Crystallization temperature, T_x, °C	Supercooling, C°	Time, hr			
10,000[a]	1	128	8	72	136	700	906
11,260	1	125	7	30	132	870	1020
11,260	1000	161	6	72	134	1000	1020
11,260	2000	181	6	28	136	1000	1020
100,000	1	130	8	72	138	—	—
100,000	2000	175	12	72	139	—	—
100,000	3000	187	18	72	146	8950[b]	9050

[a] Data of Anderson.[5]
[b] Average maximum thickness.

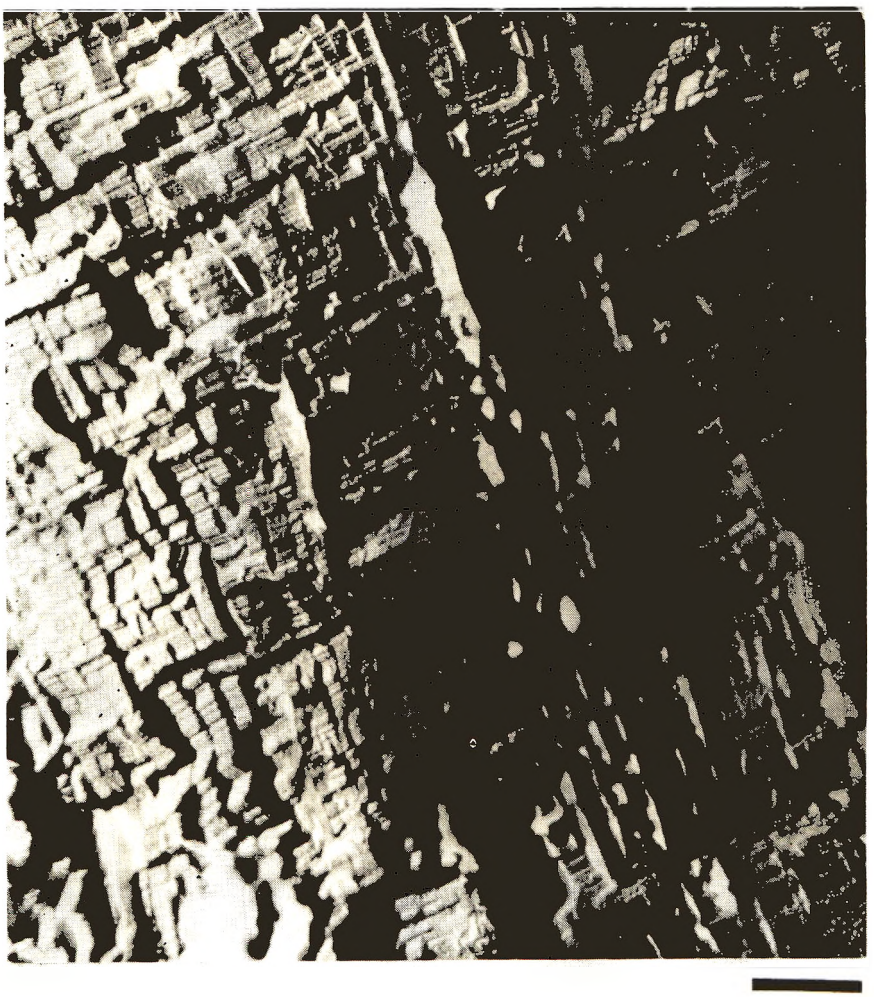

Fig. 2. Fracture surface from LMW fraction of linear polyethylene crystallized at 1000 atm. The scale bar represents 0.5 μ.

The critical pressure for formation of extended-chain lamellae in the HMW fraction therefore lies somewhere between 2000 and 3000 atm. The DTA melting points (Table I) also reflect this change in morphology. The samples crystallized at 1 and 2000 atm have nearly the same melting point while the 3000-atm specimen exhibits a much higher value due to increased perfection and superheating of thick, extended-chain crystals.

It is obvious in Figure 3 that many of the lamellae thicken considerably as they grow away from spherulite centers or impingement points. For these lamellae, the maximum thickness was used in the averaging. Since it is known that almost all the molecules have nearly the same length in this narrow HMW fraction and the maximum thickness for each lamella corresponds nearly to that length, some folding must still occur in the thin

Fig. 3. Fracture surface from HMW fraction of linear polyethylene crystallized at 3000 atm. Note the dark fibrils indicative of folded-chain or imperfectly crystallized material. Points of lamella termination and impingement are designated by arrows. The scale bar represents 1 μ.

regions of the lamellae. Such folding is necessary because of spatial constraints from neighboring lamellae growing from the same nucleus or impinging from nearby. Several dark fibrils, which are indicative of folded-chain lamellae or imperfectly crystallized material, are present on the fracture surface of Figure 3. No fibrils were observed on the LMW surfaces. Although some folding necessarily occurs, the lamella thickness in these regions is still two orders of magnitude larger than the 100 Å, folded-chain thicknesses found in atmospherically crystallized samples.

In studying pressure-crystallized, linear whole polyethylene, Wunderlich and Melillo[18] have shown that extended-chain lamellae have a habit of impingement which, instead of forming a regular spherulite, yields a more irregular arrangement of lamellae. Depending on the geometry of ap-

proach, impingement of two growing lamellae may lead either to termination of growth of one lamella leaving the other one unaffected, or to interpenetration of the two lamellae. The same phenomena characterize extended-chain growth of the HMW fraction and are visible in Figure 3 (see arrows).

Mixtures of Fractions

From the above results it is clear that a pressure (and temperature) range exists in which the LMW fraction crystallizes in an extended-chain morphology while the HMW fraction yields folded-chain lamellae. Furthermore, at 3000 atm the maximum thickness of the extended-chain lamellae of the HMW fraction is roughly 10 times that for the LMW fraction. With these facts as incentive, several homogeneous mixtures of the fractions were prepared and crystallized under various pressures in order to look for fractionation and segregation effects. The sample compositions, crystallization conditions, DTA melting points, and observed lamella thicknesses are summarized in Table II.

Three different mixtures of the two fractions were crystallized at 2000 atm. Figure 4 shows a fracture surface from a sample containing 25% HMW material. Close examination clearly reveals rows of thin extended-chain lamellae running primarily from left to right in the photomicrograph. The average thickness of these lamellae is about 1000 Å where it can be measured. Some small regions exhibit a mottled fracture-surface which is characteristic of a folded-chain morphology (see upper left of micrograph). Even where the extended-chain lamellae are visible, their boundaries are not clear and are often marked by black fibrous material which can be attributed to folded-chain, HMW material drawn during fracture. Thus, two distinct morphologies are visible, with the thin extended-chain lamellae constituting the major fraction of the sample.

Two distinct morphologies are observable again in the 50% HMW sample crystallized at 2000 atm whose fracture surface is illustrated in Figure 5. Fewer extended-chain lamellae are present than in the 25% HMW sample, and their boundaries are again not as clear as those of the pure LMW sample. Several parallel lamellae, which are visible in the lower right center of Figure 5, have an average thickness of 970 Å; again the agreement with the fully extended chain length of 1020 Å is quite good.

When the HMW concentration rises to 75%, the fracture surface shown in Figure 6 is distinguishable from those of the other two mixtures. Almost the entire surface is now occupied by drawn material. Close scrutiny reveals only a few thin extended-chain lamellae (see center-right of micrograph). Their average thickness is about 700 Å; however, the drawn surface makes accurate measurements nearly impossible.

When the crystallization pressure is increased to 3000 atm for the mixture compositions described above, two groups of extended-chain lamellae with distinctly different thickness ranges can be observed. A low magnification micrograph of a fracture surface from a 25% HMW sample is shown

TABLE II
Characterization of Mixtures of Polyethylene Fractions Crystallized under Various Conditions

Sample composition[a]	Crystallization conditions: Pressure, atm	Crystallization conditions: Crystallization temperature T_x, °C	Crystallization conditions: Supercooling, C°	Crystallization conditions: Time, hr	DTA melting points, °C	Average lamella thickness, Å
25% HMW,	1	Slow cool	—	—	133	—
75% LMW	2000	176	12	72	137	1000
	3000	193	12	72	136, 139, 142	870, 8300[b]
50% HMW,	1	Slow cool	—	—	134	—
50% LMW	2000	176	12	72	137	970
	3000	193	12	72	137, 144	900, 8700[b]
75% HMW,	1	Slow cool	—	—	136	—
25% LMW	2000	176	12	72	139	700

[a] LMW = low molecular weight, M_η = 11,260; HMW = high molecular weight, M_η = 100,000.
[b] Average maximum thickness.

Fig. 4. Fracture surface from a mixture containing 25% HMW material crystallized at 2000 atm. Note the large number of thin, extended-chain lamellae (middle) and the smaller, folded-chain drawn areas (top and bottom). The scale bar represents 1 μ.

in Figure 7. Many comparatively thin lamellae, with an average thickness of about 870 Å, are distinguishable along with a few thick lamellae. The fracture surfaces from samples containing 50% HMW polymer are similar to Figure 7 except for the presence of more thick, extended-chain lamellae.

As in the pure LMW sample, many of the thin extended-chain lamellae in Figure 7 have crystallized nearly parallel to one another. This is more clearly seen in the higher magnification view of Figure 8. Wunderlich and Melillo[18] have suggested that secondary nucleation on an already-formed crystal surface may yield many stacks of parallel lamellae. There are in fact several instances in Figure 7 where thin extended-chain lamellae appear to have nucleated and grown from thick extended-chain lamellae. One

Fig. 5. Fracture surface from a mixture containing 50% HMW material crystallized at 2000 atm. Several parallel thin lamellae are visible (lower right and center). The scale bar designates 1 μ.

implication from such behavior is that the HMW material crystallized first in thick lamellae, extruding the LMW polymer melt aside as growth proceeded. Since the supercooling was much lower for the LMW polymer, it then crystallized at a later time or perhaps even during the slow cooling step.

The central region of an especially well-formed spherulite of thick lamellae is shown in Figure 9 and is similar to those described by Wunderlich and Melillo.[18] Many lamellae have nucleated at what appears to be one,

Fig. 6. Drawn fracture surface from a mixture containing 75 w% HMW material crystallized at 2000 atm. Only a few thin, extended-chain lamellae are visible (center right). The scale bar designates 1 μ.

short extended-chain lamella. As growth proceeds radially, the lamellae thicken until at a point less than 5μ from the center many of them achieve a maximum thickness corresponding to the molecular length of the HMW fraction. Those that do not achieve the maximum possible thickness are usually constrained on one or both sides by maximum-thickness lamellae. As the lamellae splay apart, one can also locate regions (right-center of Figure 9) where thin extended-chain lamellae have formed presumably from segregated LMW material.

Figure 10 shows DTA scans of the mixtures crystallized at 3000 atm along with scans of the pressure-crystallized pure fractions for comparison. In

Fig 7. Fracture surface from a mixture containing 25 w% HMW material crystallized at 3000 atm. Both thick and thin extended-chain lamellae are present. The scale bar designates 1 μ.

the 50% HMW sample, two peaks are clearly visible at 136°C and 144°C, respectively; they agree very closely with the melting peaks of 136°C and 146°C for the respective pure LMW and pure HMW extended-chain crystals. Moreover, the two peaks from the mixture sample have nearly equal intensities, which implies that the two groups of extended-chain lamellae with distinctly different thicknesses have crystallized in nearly equal amounts. The scan for the 25% HMW mixture is more complex. Two resolvable peaks and a strong shoulder are visible. The low-temperature peak at 136°C corresponds to the melting peak of the pure LMW fraction, but the other peak (139°C) and shoulder (142°C) are significantly below the pure HMW melting peak.

DTA scans of the mixtures crystallized at 2000 atm showed only one peak in the 137–139°C range (Table II), even though the micrographs show

Fig. 8. High magnification view of a portion of Figure 7 showing many thin extended-chain lamellae which have crystallized nearly parallel. The scale bar designates 0.1 μ.

two distinct morphologies. This is not surprising, since the melting peaks for the two pure fractions crystallized at 2000 atm are only 3° apart (Table I). The single mixture peak is broader than those for either of the pure fractions and rises from 137°C to 139°C as the HMW concentration increases from 25 to 75%.

DISCUSSION

The results from the individual narrow-fraction experiments indicate that for a given supercooling and molecular weight, there is a critical pressure, and thus temperature, above which extended-chain crystals form whose thickness is a measure of the molecular lengths within the crystal. As the molecular weight increases, supercoolings being equal, the critical pressure and temperature increase, and spatial constraints during crystal growth make it more and more difficult for the lamellae to achieve the maximum

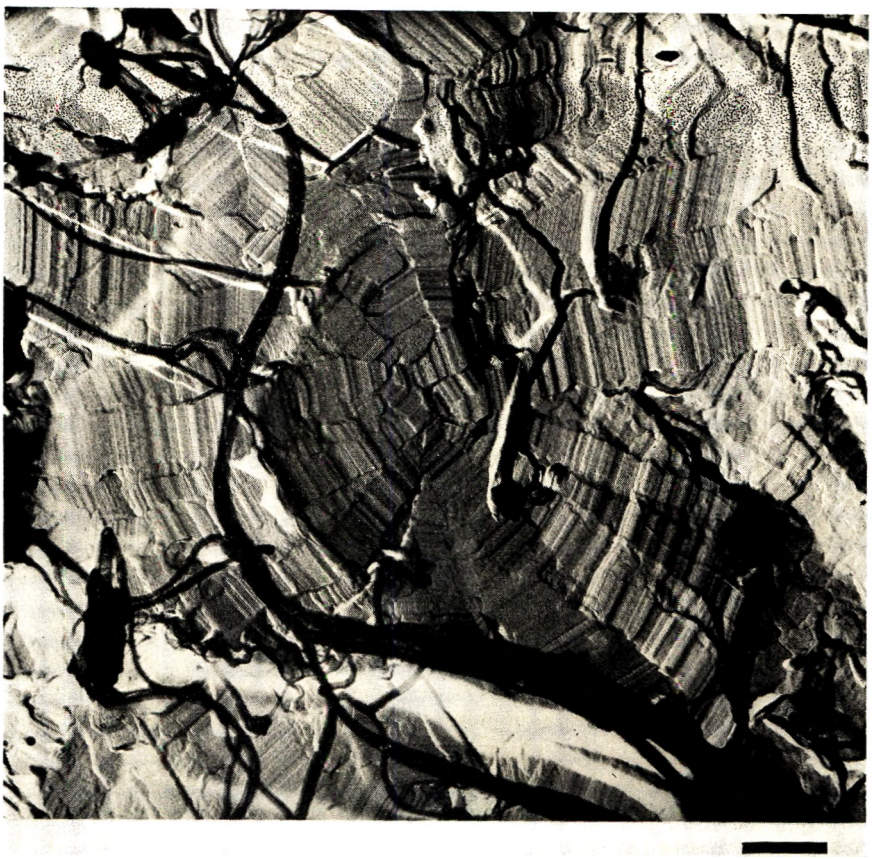

Fig. 9. A spherulite center on the fracture surface of a mixture containing 25% HMW material crystallized at 3000 atm. Many of the lamellae have nucleated at the center on what appears to be a short, extended-chain crystal. The scale bar designates 1 μ.

thickness corresponding to fully extended molecules. Nonetheless, for narrow fractions having molecular weights up to 100,000, extended-chain crystals with thicknesses corresponding to the average polymer chain length can be grown under pressure.

The electron micrographs of the mixture samples provide sound evidence that fractionation and segregation have occurred during high-pressure crystallization. Both the 2000- and 3000-atm fracture surfaces indicate that as the concentration of LMW polymer in the mixture increases, the number of thin, LMW extended-chain lamellae increases. In the 3000-atm samples, the percentage of the surface area occupied by the small or large-thickness lamellae does not correspond exactly to the percentage composition of the mixture; but in any one micrograph these two values differ by not more than $\pm 15\%$. One might expect this variation, since any one fracture surface may have arisen from preferential crack propagation through more of one lamella type than the other. A statistically accurate percentage would require analysis of many more fracture surfaces for each sample.

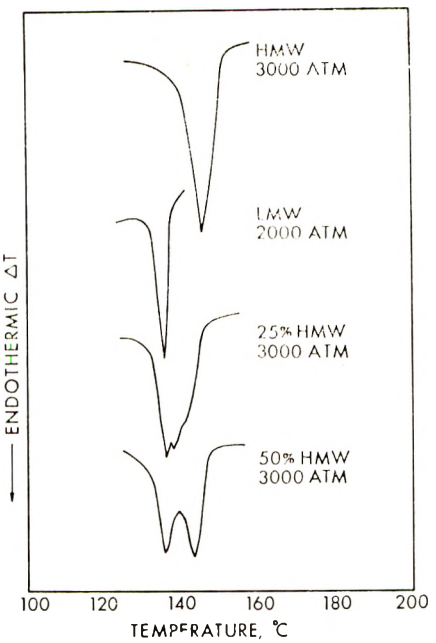

Fig. 10. DTA scans showing the atmospheric melting behavior of mixtures crystallized at 3000 atm along with scans of pressure-crystallized pure fractions. The heating rate was 10°C/min.

For the LMW-rich samples crystallized at 2000 atm, fracture surfaces showed more thin extended-chain lamellae than would be expected if all the LMW material of the mixture crystallized as thin extended-chain lamellae. This anomaly most likely arises from the fracture propagating preferentially through the more brittle extended-chain lamellae and not from degradation since none occurred. In the samples of low LMW concentration, the HMW material was highly drawn on fracture and could easily have masked LMW extended-chain lamellae. This would explain why fewer of the LMW extended-chain crystals were seen in these samples than one might expect if all the LMW polymer crystallized as thin extended-chain lamellae.

The DTA scans of the 3000-atm mixture samples provide additional evidence of fractionation and segregation during crystallization under high pressure. In light of the microscopy results, the 50% LMW scan shows that very nearly half the sample has crystallized as thick extended-chain crystals which superheat considerably even at a heating rate of 10°C/min, while the other half has crystallized as thin extended-chain crystals. The complex scan of the 25% HMW sample is a bit difficult to reconcile with the interpretation of the 50% HMW scan. The low-temperature peak at 136°C corresponds to the melting of thin LMW extended-chain lamellae which are clearly visible in the micrographs. The high-temperature shoulder (142°C) probably represents melting of the thick extended-chain lamel-

lac, also seen in the micrographs, which contain mostly HMW material The shoulder is about 4°C below the melting point of the pure HMW fraction. Such a depression could easily arise from incorporation of only a few LMW chains in the HMW crystals, which would act as defects and cause less superheating to occur. The mid-temperature peak at 139°C may be made up of "mixed" crystals, as defined by Prime and Wunderlich,[13,19] which consist of a solid solution of LMW and HMW molecules. In addition to a lower superheating tendency, these crystals will melt 2–3°C lower than pure equilibrium extended-chain crystals of the same thickness.[19] In addition, the LMW component exerts a diluent effect which could depress the melting point by more than 1°C[19] for the molecular weight involved here. Close examination of the electron micrographs (Fig. 7) reveals an occasional lamella whose thickness is uniformly about half of the maximum possible thickness for the HMW material. Such lamellae are not found on the pure HMW fracture surfaces. While these lamellae may be "mixed" crystals, they are also present in the 50% HMW sample which yielded only two DTA peaks. In any event DTA appears to detect three types of crystals in the 25% HMW sample while only two distinct species seem to be present in the 50% HMW sample. One might expect the number of solid solution or "mixed" crystals to depend on component concentration; additional experiments are needed to clarify this point.

The micrographs and DTA scans leave no doubt that fractionation and segregation have occurred during high pressure crystallization of the mixture samples. In some cases, the fractionation may not have been entirely complete, but in all cases it occurs to a very large degree. This results in an eutectic-like mixture of LMW crystals containing fully extended chains and HMW crystals which can contain both fully extended chains and folded chains. Our results are in accord with those of Prime and Wunderlich[13] who showed close agreement between molecular weight distribution and crystal thickness distribution up to molecular weights of about 10,000 for fractions of intermediate polydispersity.

Finally, the mechanism by which extended-chain crystals form from the melt under pressure deserves some comment. On the basis of pressure-annealing experiments on solution-crystallized polyethylene, Rees and Bassett[20] have proposed that thinner, folded-chain lamellae are initially formed and thicken under pressure with time into extended-chain lamellae. On the other hand, Gruner *et al.*[21] have concluded from pressure-annealing experiments that a regular, well-formed, folded-chain crystal cannot be an intermediate in the growth of extended-chain crystals from the melt. Calvert and Uhlmann have also recently concluded[22] that crystallization from the melt under high pressure results in the direct formation of extended-chain crystals. Although our results do not directly distinguish between formation mechanisms, our observations in the light of recent work[21,22] seem to support the latter two contentions, namely that solid-state thickening of folded-chain lamellae is not an ingredient in the formation of extended-chain crystals from the melt under pressure. On the fracture surfaces of

the individually crystallized fractions, many extended-chain lamellae extend uniformly for lateral distances of 10–20 μ or longer. Had these lamellae formed by thickening of relatively perfect folded-chain lamellae, conservation of mass dictates that each lamella would have had to break up into pieces of much smaller breadth, much as polymer single crystals do on annealing.[1] No evidence for this was seen. Furthermore, the fact that thick extended-chain crystals superheat considerably along with the demonstration by Prime et al.[17] that extended-chain crystals melt in a direction perpendicular to the chain axes means there are few major discontinuities along the lateral directions of the lamellae. Again, this would not be expected for lamellae formed by a thickening mechanism.

We are grateful to Dr. A. Kenyon of the Monsanto Company for supplying us with the polyethylene fractions and stabilizer. This research was supported in part by the National Science Foundation (Grant No. GY-5807).

References

1. P. H. Geil, *Polymer Single Crystals*, Interscience, New York, 1963.
2. T. Kawai, *J. Polym. Sci. B*, **3**, 83 (1965).
3. T. Kawai and A. Keller, *J. Polym. Sci. B*, **2**, 333 (1964).
4. J. D. Hoffman, *SPE Trans.*, **4**, 315 (1964).
5. F. R. Anderson, *J. Appl. Phys.*, **35**, 64 (1964).
6. F. R. Anderson, in *Analysis and Fractionation of Polymers* (*J. Polym. Sci. C*, **8**), J. Mitchell, Jr., and F. W. Billmeyer, Eds., Interscience, New York, 1965, p. 275.
7. H. D. Keith and F. J. Padden, Jr., *J. Appl. Phys.*, **35**, 1270 (1964).
8. M. I. Bank and S. Krimm, *J. Polym. Sci. B*, **8**, 143 (1970).
9. P. H. Geil, F. R. Anderson, B. Wunderlich, and T. Arakawa, *J. Polym. Sci. A*, **2**, 3707 (1964).
10. B. Wunderlich and T. Davidson, *J. Polym. Sci. A-2*, **7**, 2043 (1969).
11. B. Wunderlich, *J. Polym. Sci. B*, **5**, 7 (1967).
12. J. L. Kardos, E. Baer, P. H. Geil, and J. L. Koenig, *Kolloid-Z. Z. Polym.*, **204**, 1 (1965).
13. R. B. Prime and B. Wunderlich, *J. Polym. Sci. A-2*, **7**, 2061 (1969).
14. A. S. Kenyon, I. O. Salyer, J. E. Kurz, and D. R. Brown, in *Analysis and Fractionation of Polymers* (*J. Polym. Sci. C*, **8**), J. Mitchell, Jr., and F. W. Billmeyer, Eds., Interscience, New York, 1965, p. 205.
15. J. Barlow, Ph.D. Thesis, Univ. Wisconsin, 1969.
16. E. Baer and J. L. Kardos, *J. Polym. Sci. A*, **3**, 2827 (1965).
17. R. B. Prime, B. Wunderlich, and L. Melillo, *J. Polym. Sci. A-2*, **7**, 2091 (1969).
18. B. Wunderlich and L. Melillo, *Makromol. Chem.*, **118**, 250 (1968).
19. R. B. Prime and B. Wunderlich, *J. Polym. Sci. A-2*, **7**, 2073 (1969).
20. D. V. Rees and D. C. Bassett, *J. Polym. Sci. B*, **7**, 273 (1969).
21. C. L. Gruner, B. Wunderlich, and R. C. Bopp, *J. Polym. Sci. A-2*, **7**, 2099 (1969).
22. P. D. Calvert and D. R. Uhlmann, *J. Polym. Sci. B*, **8**, 165 (1970).

Received October 5, 1970
Revised May 24, 1971

JOURNAL OF POLYMER SCIENCE: PART A-2 VOL. 9, 2081–2093 (1971)

Terephthalamide–Nylon Single Crystals Isolated from Dilute Solutions of Hexafluoro-2,2-propandiol

H. K. LIVINGSTON and R. L. GREGORY, *Department of Chemistry, Wayne State University, Detroit, Michigan 48202*

Synopsis

Terephthalamide nylons with two to five carbon atoms in the aliphatic portion of the chain have been crystallized from aqueous solutions of hexafluoro-2,2-propandiol. The 3T and 4T nylons in particular form rodlike crystals. Indications are that these are bundles of cylindrical structures about 50 nm in diameter. Electron diffraction shows the symmetry to be C_{2v}. Films of the nylons were drawn with great difficulty. The x-ray diffraction on the films is consistent with a monoclinic structure, though the crystal structure could not be positively established. There is some evidence for a polymer chain alignment perpendicular to the long axis of the rods.

INTRODUCTION

The formation of polymer single crystals of sharp outline and maximum dimension of 10 μ or more has only been observed with polymers of regular structure,[1] i.e., polymers in which there are no chiral chain atoms or only chiral chain atoms in which all such have the same stereochemistry. The apparent exception of certain block copolymers[2,3] proves on examination to apply only to those copolymers in which there are large blocks of regular structure.

The polyamides are ordinarily polymers of regular structure, since the common synthetic methods do not lead to branching or side reactions and the common intermediates contain no chiral atoms. Yet of the 88 aliphatic polyamides whose synthesis we find[4] reported in the literature, only nylons 6, 66, 610, and 612 are known to form single crystals. Platelets or lamellae of good size and sharp outline form on cooling solutions of nylon in glycerol[5] or water,[6] water under pressure at 170°C serving as the solvent in the latter case. No examples of aromatic nylons forming single crystals are known.

The remarkable solvent properties of fluoroketone hydrates for polymers were discovered by Middleton and Lindsey.[7] They reported that hexafluoro-2,2-propandiol and other substances with closely related structures would dissolve difficulty soluble polymers such as nylon. At about the same time and from the same laboratory, Longworth[8] reported that hexafluoro-2,2-propandiol formed strong hydrogen bonds with polypeptides such as silk fibroin but did not degrade the polymers as much as other strong

hydrogen-bonding solvents did. It appeared that the formation of nylon single crystals from dilute solution might be brought about without ever heating the nylon if aqueous hexafluoro-2,2-propandiol were the solvent used. This was actually accomplished[9] with nylon 610, but the crystals were long and narrow, with an appearance unlike any previously reported. They appeared much more compact and rod-like than the nylon sheaves first reported by Keller[10] and later studied in detail by Dreyfuss and Keller.[11]

In the present work, the new solvent was used with a series of nylons that are harder to dissolve than the aliphatic nylons. It was hoped in this way to extend the knowledge of polymer single crystals into a new class of polymers. These, according to our ideas,[1] should form single crystals because of their good structural regularity but would require an excellent solvent to accomplish this result.

EXPERIMENTAL PROCEDURE

Synthesis of Nylons

The series of nylons was prepared by interfacial condensation following essentially the procedure described by Shashoua and Eareckson.[12] A 1-qt Waring Blendor was used, and the batch size was adjusted accordingly. The reaction ingredients were added at about 30°C and a temperature rise of 5°C throughout the 5 minute reaction time was normal. Terephthaloyl chloride reacted with ethylenediamine or its homologs to form 2T, 3T, 4T or 5T nylon.

The product was collected on a coarse sintered-glass filter over vacuum, boiled twice (5 min each time) in approximately 300 ml distilled water, and recovered on a coarse glass filter. The product was then either oven-dried at 110°C for 1 hr or dried in a vacuum desiccator over a period of days. The carbon to nitrogen ratios, which would be independent of the water content, agree within 1–2% of predicted values, which is on the same order as the reproducibility of the method. On the basis of the hydrogen analysis it appears that the polymers usually contained on the order of 3% water.

Infrared spectra were run both on films cast from trifluoroacetic acid solutions and on potassium bromide pellets. The general character of the spectra is in keeping with that of a polyamide containing a 1,4-disubstituted benzene ring.

Inherent viscosities were run on solutions of the polyamides in concentrated sulfuric acid. Shashoua and Eareckson[12] reported molecular weights of 15,800–23,700. Our inherent viscosity results indicated molecular weights that were within 12% of their values.

Crystallization

The solutions of nylon were made without heating by stirring 0.06 g nylon in 10 ml of commercial hexafluoro-2,2-propandiol solution, which is

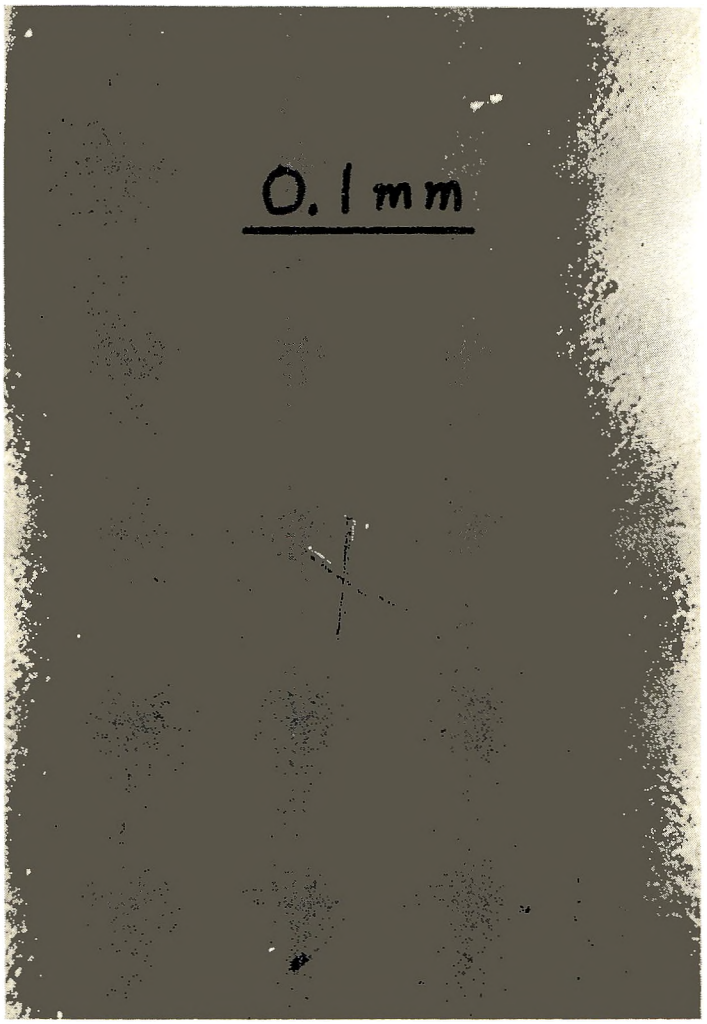

Fig. 1. Light photomicrograph showing 4T nylon crystals.

supplied as $(CF_3)_2CO \cdot {}^3/_2H_2O$. The solutions were then filtered through a medium-grade sintered-glass filter. The filtered solutions were titrated with distilled water till cloudy, then boiled until the solutions were only very slightly cloudy. These turbid solutions were allowed to stand, loosely capped, for periods ranging from days to weeks. During this period samples were taken and examined by light microscopy for the presence of crystals. The concentration of nylon gradually increased throughout this period because of solvent loss.

5T Nylon under our experimental conditions formed only spherulites. Small rodlike objects were obtained from 2T nylon. 4T Nylon gave needle-shaped crystals but also much amorphous material (Fig. 1). It was 3T nylon that most often gave us electron photomicrographs with

well-formed, rodlike crystals free from globs or spherulites. We will therefore devote the balance of our discussion of single crystals to a description of the results obtained with 3T and 4T nylons.

Preparation of Samples for Observations

Light photomicrographs were made of the crystals in suspension and after drying on glass slides. An example of results obtained with a polarizing light microscope is given in Figures 2 and 3. As in Figure 1, this 4T nylon sample contains amorphous as well as crystalline material, but the use of polarized light shows clearly that the needles are crystalline.

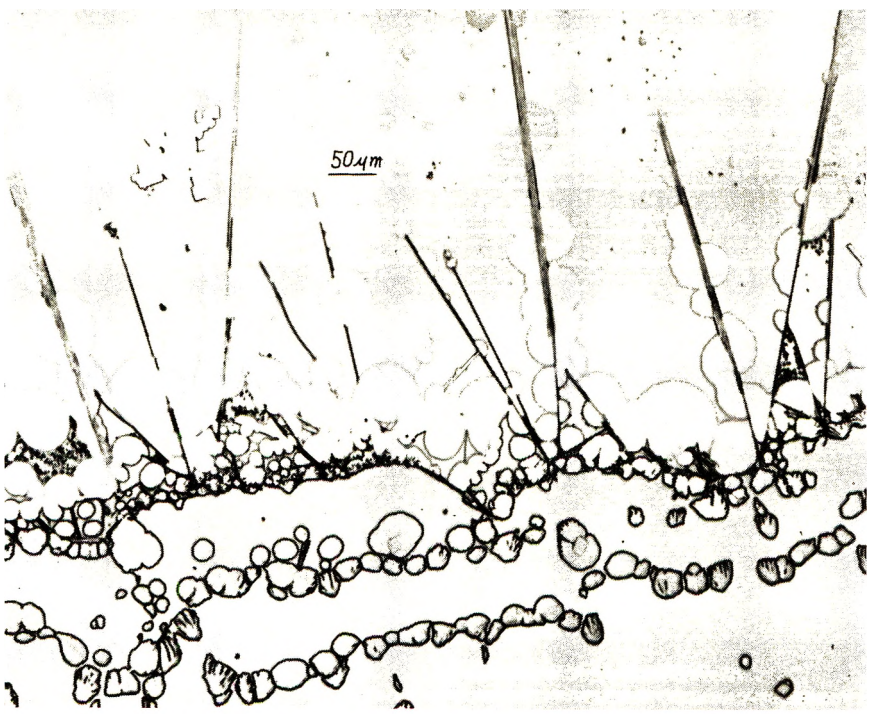

Fig. 2. Photograph of 4T nylon crystals in a polarizing light microscope set for slight polarization.

When there was evidence from the light microscope that crystals had been formed, a drop of the solution was placed on a prepared electron microscope grid and examined in an electron microscope. Where conditions were optimum for crystallization, conditions for observation of the crystals were good; however, where crystallization was minimal, the crystals would usually be imbedded in a relatively thick residue of amorphous nylon film, and detail was visible only in selected areas.

Fig. 3. Photograph of 4T nylon crystals in a polarizing light microscope; polarization set for almost complete extinction.

RESULTS

Electron Microscopy

Keller[10] reported in some detail on the difficulties of carrying out electron microscopy with nylon 610, which is degraded by the electron beam so rapidly that electron diffraction spots fade before the microscopist's eyes. We have had similar experiences with the terephthalamide nylons. Like Keller, we conclude that the best recourse is to work fast with high beam intensity. To obtain electron diffraction patterns we set the microscope for diffraction, photograph the pattern as fast as possible, then switch to the viewing mode and photograph the object that produced the diffraction pattern. We used RCA model EML and EMU electron microscopes at 50 kV and the Hitachi model HU125A at 75 and 100 kV. The results were as follows.

(1) Length-to-thickness ratios as high as 200:1 were observed. The ratio of width to thickness was generally about 1:1.

(2) The thickness of the rodlike objects observed was almost always in the range of 25–60 nm.

(3) The tips of the crystals were in steps (Fig. 4), rather like the appearance of the end of a bundle of rods of differing length (Fig. 5).

Fig. 4. Electron photomicrograph of 3T nylon crystals at high magnification.

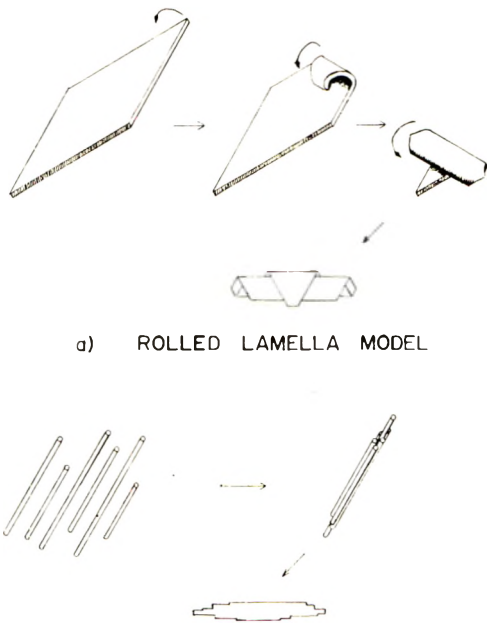

Fig. 5. Schematic representation of two models leading to rodlike crystals.

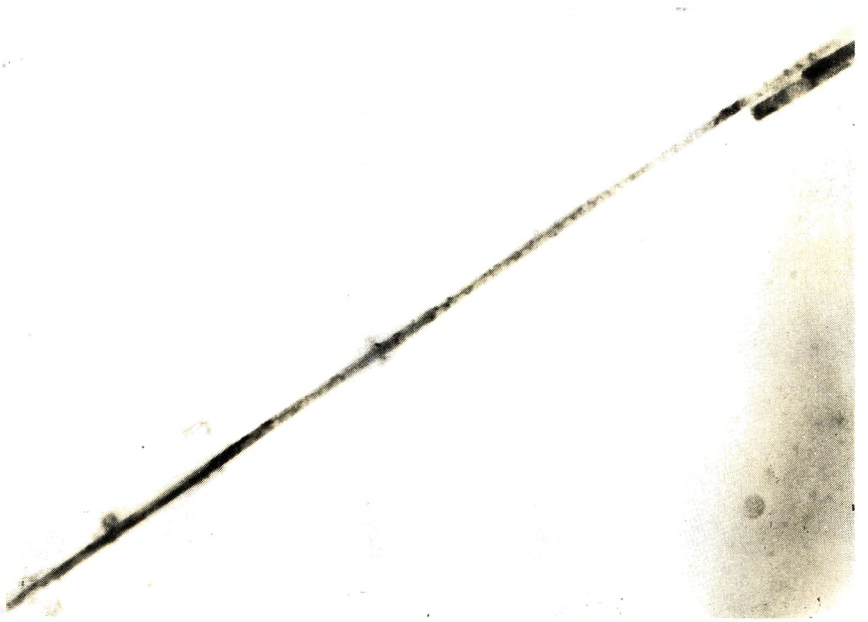

Fig. 6. Electron photomicrograph in bright field transmission (3T nylon) 45,000×.

(4) The dimensions involved in these steps were measured with a tilting-stage electron microscope. This was done by taking a stereo pair of photographs of a crystal cluster. The rotation angle was 5° and was sufficient to cause a displacement of one fiber end with respect to the other. From the magnification it was possible to calculate that the edge of one crystal fiber lay 300–400 Å above the edge of one below it.

(5) The rods are sometimes striped (Fig. 4). In some respects this appearance is remarkably similar to that reported by Colson and Reneker[13] for polyoxymethylene crystals. They ascribed the stripes to bend contours (Bragg lines) which in their case resulted from flexing of the crystals under the influence of the electron beam.

(6) Electron dark-field microscopy indicates that the rods are made up of two or more acicular crystals. Figures 6 and 7 are bright-field and dark-field transmission photomicrographs of the same 3T crystal. Note that no part of the crystal in Figure 7 is bright along its entire length. This indicates that the orientation is changing, either through bending or twisting. In the section where the crystal is bright only half the cross section has such an orientation as to give a bright image at any area along the length of the crystal. It is at least possible that this particular crystal is made up of two parallel fibers (or twins) whose orientations are not identical but are not greatly different.

(7) Electron diffraction shows that the 3T nylon rods, in the normally observed orientation in which they lie lengthwise along the grid, give a pattern with C_{2v} symmetry (Fig. 8). The monoclinic and triclinic systems are typical of polyamide systems[14] and this observation rules out the

triclinic. The row of diffraction spots is at 30° to the long axis of the diffracting crystal, which was the longer of the two crystals in the figure.

(8) The d spacings observed for various 3T nylon single crystals in electron diffraction are given in Table I. These can be reconciled with the bundled fiber model (Fig. 5*b*) more easily than with the rolled lamella model (Fig. 5*a*). The smallest selected area used in the diffractions was about 1 μ wide. An electron beam this wide, in passing through a rolled lamellar crystal with a width on the order of 0.5 μ, would be exposed to all possible orientations of the crystal lattice about the central axis. Therefore, one would expect to see a pattern similar to a rotation pattern with all possible reflections. The distribution of the reflections would depend

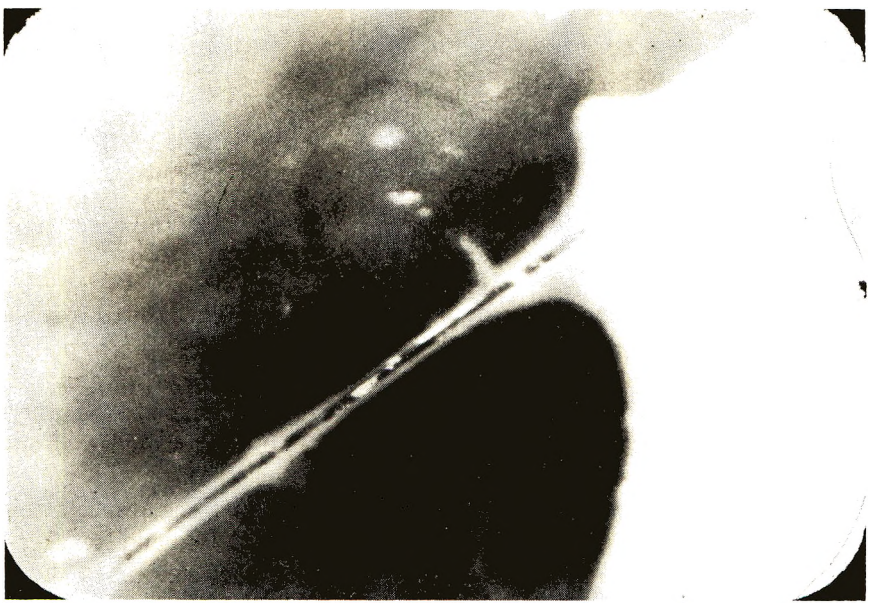

Fig. 7. Same field and magnification as Figure 6; dark field image.

on how the axis of the rolled lamella was aligned with respect to the crystal axes. In one limiting case the rolling would occur parallel to a crystallographic axis. The pattern observed would then be a typical "fiber pattern" with all reflections occurring on layer lines related to levels in the reciprocal lattice. As the angle the roll direction makes with the nearest crystallographic axis increased, the number of d spacings would decrease, but would still be large because the roll direction cannot form a large angle with all three crystallographic axes.

Dreyfuss and Keller,[11] working with lath-shaped single crystals of 66 nylon, observed both spots and broad arcs in their diffraction pattern. We never observe arcs. This leads us to believe that our single crystals are closer to the limiting case of bundled fibers (Fig. 5*b*), in which all fibers in the bundle have a similar crystallographic orientation.

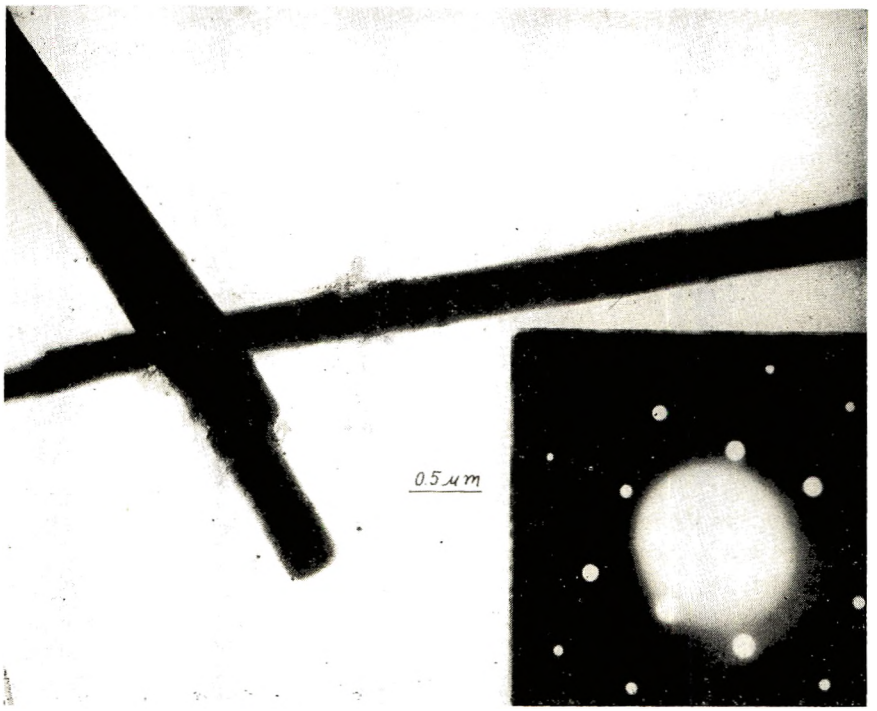

Fig. 8. Electron photomicrograph of 3T nylon with the electron diffraction pattern obtained from a selected area of one of the two crystals.

As shown in Table I, most of the diffraction spots observed correspond to d spacings that are either near 3.0 Å or between 5.9 and 6.8 Å. The interpretation of these experimental observations and considerations of orientation and folding will be discussed later, after the consideration of the crystal structure of the terephthalamides in the next section.

TABLE I
Observed d Spacings, Electron Diffraction[a]

d spacing, Å	No. of times observed
1.8–2.0	1
2.1–2.3	7
2.3–2.5	2
2.7–3.3	34
3.4–3.5	7
4.0–4.2	1
4.3–4.5	2
5.6–5.8	4
5.9–6.0	4
6.1–6.3	7
6.4–6.8	10

[a] From all of the 36 photographs of electron diffraction (24 different crystals) taken for 3T nylon.

Crystal Structure of Terephthalamide Nylons

The published literature gives no help to the electron microscopist who wishes to reach conclusions concerning the folding of terephthalamide nylon chains in single crystals. The crystal structure of these nylons has not been reported. These are high-melting nylons, and the usual methods of melt-spinning and drawing to get a fiber for x-ray diffraction and structure determination will not work. We have tried by the following methods to obtain fibers or films for x-ray diffraction measurements: fiber-drawing from melts in air or controlled atmospheres, injection of a stream of sulfuric acid solution into water, fiber-drawing from a viscous solution of polymer in trifluoroacetic acid, and casting films from solutions in aqueous hexafluoro-2,2-propandiol or trifluoroacetic acid. Only two methods were satisfactory. Fibers and films were obtained from trifluoroacetic acid. The fibers could not be stretched in air at room or elevated temperatures nor in steam or boiling water. The films, however, could be placed on the Kofler hot-stage of a microscope and drawn when the temperature was in the range empirically established as being suitable.

The detailed procedure of sample preparation was as follows: Nylon 3T or 5T was dissolved in trifluoroacetic acid to form a viscous solution which was cast to form a film 30 μ thick which was air-dried, oven-dried (100°C), boiled in distilled water (the water was changed several times), and then allowed to stand in distilled water for 12 hr. This treatment was necessary to remove residual solvent, but after treatment the films were free of the infrared absorption at 1760 and 2400–2500 cm^{-1} that characterized the films as cast. The strip was drawn down (necking occurred just as in nylon 6) at 320–340°C for 5T nylon or at 250–350°C for 3T nylon. The maximum elongation achieved was 375%.

The x-ray diffraction of the films was observed by using a Siemens unit with V-filtered chromium Kα radiation produced at 30 kV and 14 milliamperes and recorded with a flat-film Laue transmission camera. This equipment was also used with oriented fibers of nylon 6 and gave average spacings (three determinations) within 0.1 Å of the b spacing and 0.5 Å of the a and c spacings given by Bunn and co-workers.[15]

Films of 3T and 5T nylon both gave three distinct reflections spread over arcs of about 45°. The strongest reflection was axial (corresponding to 13.3 Å for 5T; 11.4 Å for 3T); there was also a weak axial reflection that we measured to be for 6.6 and 5.5 Å, respectively, which was probably half the strong reflection distance. An equatorial reflection, diffuse and difficult to measure, we indexed at approximately 4.3 Å, 5T giving a value 3% less than 3T.

These results are far less satisfactory than those obtained by Bunn and co-workers with highly oriented specimens and careful densitometry of photographic records, using aliphatic nylons[15] and terephthalate polyesters.[16] However, they can be used by reference to the Bunn results and to our general knowledge of polymer structure to reach conclusions that would not be possible if we had no x-ray diffraction data at all.

We offer the following assumptions concerning the crystal structure of 3T and 5T nylons. (1) The stretching of the films causes the polymer chain to orient along the direction of stretch. (2) The polymer chains crystallize in the extended-chain conformation. (3) Hydrogen bonding between chains, which Trifan and Terenzi[17] have shown to be nearly complete in all the nylons examined by them, is also nearly complete in these nylons. We observed in our films the strong infrared absorption at 3300 cm^{-1} that is considered to be the best evidence of hydrogen bonding. (4) The H-N-C=O bonds lie in a plane. (5) The unit cell length is not uncommonly large. (The consequence of this assumption is that rotations at each successive chemically equivalent linkage must be equal in angle and direction).

Within this framework, we have built models of 3T nylon and carried out calculations for 14 combinations of the crystallographically allowed rotation axes. The only one that meets our assumptions and has a density that can correspond to the measured density of 3T nylon (1.31 g/cc) is that with two chemical repeat units and a 2_1 axis along the polymer chain. The calculated density for this model is 1.58 g/cc, indicating that the observed density is 83% of theory. For nylon 6 the observed density is 88% of that calculated for the known crystal structure.

Calculations of unit cell dimensions, using the 2_1 model and the bond distances and angles found in the standard reference[18] (which distances and angles give a long unit cell dimension within 0.2 Å of the Bunn value for nylons 6 and 66 and within 0.6 Å of the Bunn value for 2T polyester) indicates that the unit cell lengths should be 12.1 Å for 3T and 14.6 Å for 5T nylon. Our values are 95% and 91% of the calculated values. Packing of Stuart-Briegleb models can be used to estimate the other dimensions. If we assume the benzene rings are 45° out of the plane containing the chains, as they are in 2T polyester,[16] there should be a unit-cell dimension of about 5 Å (compared to the observed 4.3 Å). The monoclinic angle β should be near 90°. Thus we get some correspondence between the 2_1 model and the observed x-ray diffraction pattern, though it is far from perfect.

Comparison of X-Ray and Electron Diffraction

Turning to the electron diffraction data, we observe that the 3T nylon crystals that we studied are monoclinic (Fig. 8), which is consistent with the 2_1 model used above. Furthermore the model indicates a near-perfect alignment of the benzene rings with the 102 and $\bar{1}02$ planes. This gives a predicted spacing of 2.9 Å, in reasonable agreement with the most frequent d spacings from electron diffraction (Table I).

The other significant observation from the electron diffraction data is the occurrence of spacings of 5.6–6.0 Å in 20% of the photographs (Table I) and spacings of 6.2–6.8 Å in 47%. The former corresponds to the 5.7 Å spacing calculated for the 020 plane of 3T nylon (from the 11.4 Å spacing observed in x-ray diffraction, see previous section). The latter

is close to the spacing of 6.5 Å calculated for the 022 plane of the 2_1 model mentioned in the previous section. It was observed for three different crystals that the electron diffraction spots corresponding to 6.5 Å were in a line at about 30° to the long axis of the nylon rod. If the nylon is folded so that the unit cells are generally perpendicular to the long axis of the rodlike single crystals, it would be expected that these planes would frequently be nearly parallel to the beam direction. This could reduce the intensity of diffraction so that the spots would not be detected for these orientations, and therefore not be seen in all, or even most, of the single crystals. Without a better set of x-ray diffraction data, it is not possible to reach any more positive conclusions.

DISCUSSION

Terephthalamide nylon crystals from hexafluoropropandiol solution are long and narrow, quite different in appearance from the lamellae and sheaves reported for aliphatic nylon single crystals prepared with conventional solvents. We have presented evidence to indicate that our crystals form bundles of rods, not rolled lamellae. We should stress that our experiments differ in three important respects from those of experimenters who obtained nylon lamellae: (1) we used aromatic polyamides not previously studied by electron microscopy and electron diffraction; (2) these polyamides were made by interfacial polymerization and had never been subjected to temperatures above 115°C nor to any mechanical working other than the shear used to maintain the dispersion in which they were polymerized; (3) while the crystals were formed from dilute solution, the usual procedure of heating above the polymer melting point and then crystallizing on slow cooling was not followed. Instead, the driving force for crystallization was the increase in polymer concentration on evaporation.

We believe that this last difference is the most significant. Nakajima et al.[19] have cited reasons why the solvent can be expected to have a significant effect on the morphological form of polymer crystals formed from solution and have presented experimental evidence for polyethylene crystals that supports their ideas.

With regard to crystal structure and x-ray diffraction, we have noted that reflections corresponding to 5.5 and 11.4 Å in 3T nylon films are in reasonable agreement with a plausible monoclinic crystal structure. The structure was based on molecular models and a comparison of known and calculated densities.

Electron diffraction data indicate that the crystals are not triclinic and therefore are presumably monoclinic. Spacings near 5.5 Å are observed but infrequently in electron diffraction, indicating that the long axis of the unit cell is generally parallel to the electron beam. This is the result to be expected if the rodlike crystals have the polymer chains folded so that the chain axis is perpendicular to the long axis of the rod.

The assistance of Mr. Kenneth R. Mikel of the Wayne State University Medical School and Mr. Conrad Herald of Bendix Corporation (Southfield, Michigan), who participated in the electron microscopy, is gratefully acknowledged.

References

1. H. K. Livingston, *Macromolecules* **2,** 98 (1969).
2. B. Lotz, A. J. Kovacs, G. A. Bassett, and A. Keller, *Kolloid-Z. Z. Polym.*, **209,** 115 (1966).
3. G. Hinrichsen, E. W. Fischer, and G. Wegner, *Ber. Bunsenges. Phys. Chem.* **74,** 832 (1970).
4. H. K. Livingston, M. S. Sioshansi, and M. D. Glick, *J. Macromol. Sci. C*, in press.
5. P. H. Geil, *Nylon Single Crystals*, Interscience, New York, 1963.
6. E. Nagai and M. Ogawa, *J. Polym. Sci. B*, **3,** 295 (1965).
7. W. J. Middleton and R. V. Lindsey, *J. Amer. Chem. Soc.*, **86,** 4498 (1964).
8. R. Longworth, *Nature*, **203,** 295 (1964).
9. H. K. Livingston, in *The Meaning of Crystallinity in Polymers* (*J. Polym. Sci. C*, **18**), F. P. Price, Ed., Interscience, New York, 1967, p. 105.
10. A. Keller, *J. Polym. Sci.*, **36,** 361 (1959).
11. P. Dreyfuss and A. Keller, *J. Macromol. Sci.*, **B4,** 811 (1970).
12. V. E. Shashoua and W. M. Eareckson, *J. Polym. Sci.*, **40,** 343 (1959).
13. J. P. Colson and D. H. Reneker, *J. Appl. Phys.*, **41,** 4296 (1970).
14. Y. Kinoshita, *Makromol. Chem.*, **33,** 1 (1959).
15. D. R. Holmes, C. W. Bunn, and D. J. Smith, *J. Polym. Sci.*, **17,** 159 (1955).
16. R. Daubeney, C. W. Bunn, and C. J. Brown, *Proc. Roy. Soc.* (London) **226A,** 531 (1954).
17. D. S. Trifan and J. F. Terezi, *J. Polym. Sci.*, **28,** 443 (1958).
18. *Tables of Interatomic Distances*, Chemical Society, London, 1958 and 1959.
19. A. Nakajima, F. Hamada, S. Hayaski, and T. Sumida, *Kolloid Z.Z. Polym.*, **222,** 10 (1968).

Received October 27, 1970
Revised May 13, 1971

NOTES

Mechanical Dispersions of Crystalline Poly(vinyl Fluoride)

Schmieder and Wolf[1] reported the mechanical dispersions of poly(vinyl fluoride) (PVF); Ishida and Yamafuji,[2] its dielectric dispersions; and Reddish[3] discussed the interrelations between the two types of dispersions. These investigations were concerned with the assignment of α_a and β absorptions associated, respectively, with micro-Brownian motion and the local twisting motion of the chain in the amorphous region.

In the present investigation the thermal molecular motion in crystalline PVF was studied by the viscoelastic method. An α_c absorption related to the molecular motion in the crystalline phase of single-crystal mats was found.

Dalvor 720, a crystalline PVF (Diamond Alkali Co.) was used throughout this work. This polymer is a homopolymer of vinyl fluoride according to elemental analysis. Its intrinsic viscosity in dimethylformamide (DMF) was determined as 0.81 at 120°C,[4] and the concentration of head-to-tail structure was estimated to be 75% according to the nuclear magnetic resonance method of Wilson.[5]

Single crystals were prepared according to the method of Takayanagi and Matsuo[6] by isothermal crystallization at 40, 50, and 60°C from a solution 0.1% by weight in DMF, followed by filtration through a glass filter, drying under vacuum at room temperature, and pressing into single-crystal mats. Wide-angle x-ray diffraction indicated that the molecular chains in the crystals were slightly oriented perpendicular to the mat surface. For comparison, a bulk film obtained by quenching from 230°C to 0°C was also examined. The viscoelastic measurements were made with a Vibron DDV-II[6] apparatus at a frequency of 110 Hz and a heating rate of about 1°C/min.

Figure 1 shows the temperature dependence of the dynamic storage modulus E' and the loss tangent tan δ for these specimens. Dominant tan δ peaks are obtained at temperatures near 150°C for all the single-crystal mats, and they shift to higher temperature with increasing crystallization temperature. This behavior is consistent with the data on single crystal mats of linear polyethylene reported by Takayanagi and Matsuo.[6] The peaks at the highest temperature (α_c) of the mats in the figure are considered to be associated with the molecular motion in the crystalline phase. On the other hand, the bulk specimen exhibits its dominant absorption at about 80°C. It cannot be definitely determined whether this absorption should be assigned to the α_a or the α_c absorption, because the degree of crystallinity (as estimated from DSC data by using the heat of fusion of 1.8 kcal/mole reported by Sapper[7]) was about 35% for the bulk specimen and about 45% for the single-crystal specimens, and simultaneously the melting point was determined to be about 217°C for each specimens.

In general, β absorptions associated with the local twisting motion of molecular chains have been observed in PVF over a wide temperature range below 0°C by both viscoelastic and dielectric measurements.[1–3] For our bulk specimen, however, at least two absorptions were observed in the same temperature range. The low-temperature absorption seems to be of the same type as those of the single-crystal mats, but the high-temperature absorption is not. From a knowledge of both the mechanical loss and fine structure for crystalline polymers, it seems reasonable to assign the low-temperature loss to the $\beta(A)$ process associated with a local twisting motion in the amorphous region, and the high-temperature absorption to a $\beta(C)$ loss due to defects in the crystal.

For each of the single-crystal mats, two absorptions are observed between the α_c and β absorptions. One peak at about 50°C probably corresponds to the α_a absorption in

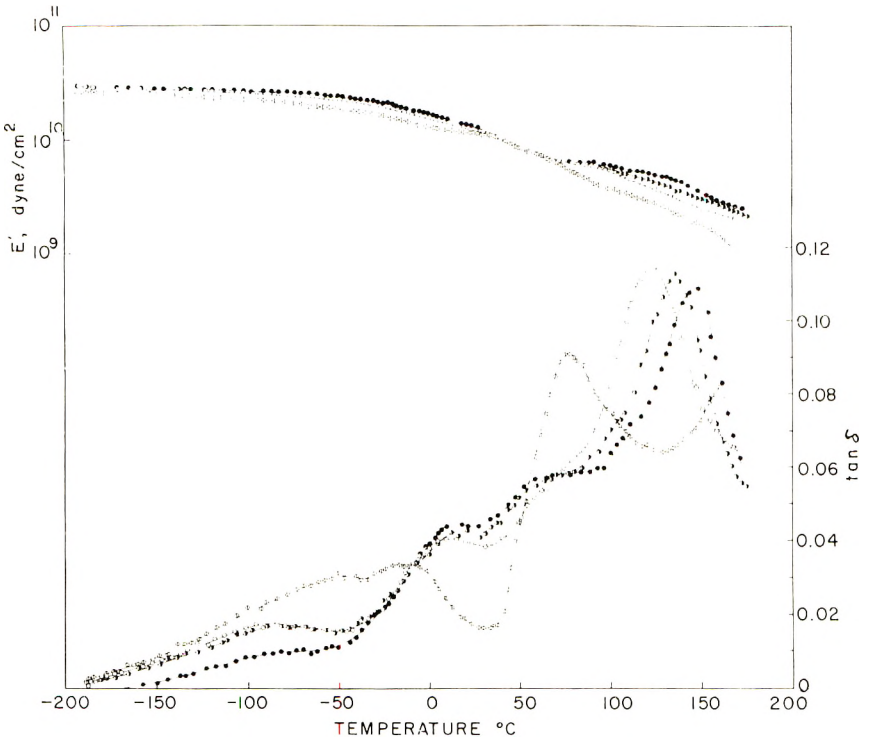

Fig. 1. Temperature dependence of dynamic storage modulus and loss tangent measured at 110 Hz for single-crystal mats crystallized at (○) 40°C, (◑) 50°C, and (●) 60°C and (◐) for a bulk specimen.

view of its temperature location and the fact that tan δ is lower than it is for the bulk-crystallized material. The other peak at about 20°C might be due to the $\beta(C)$ absorption on the basis of a simple three-phase model, involving a perfect crystal region, a defect region, and an amorphous region. It is reasonable to consider that the $\beta(A)$ loss due to the local twisting motion in the amorphous region appears in a definite temperature range almost independently of thermal and mechanical history, but for the $\beta(C)$ process in the defect region, the temperature location varies widely, reflecting the complex fine structure.[8] No crystal modification was observed by x-ray method.

This short report describes only an initial investigation of the mechanical dispersions of crystalline PVF using viscoelastic measurement. More extensive investigations are needed to establish the relations between these dispersions and molecular motion in crystalline PVF.

References

1. K. Schmieder and K. Wolf, *Kolloid Z.*, **134,** 149 (1953).
2. Y. Ishida and K. Yamafuji, *Kolloid Z. Z. Polym.*, **200,** 50 (1964).
3. W. Reddish, *Pure Appl. Chem.*, **5,** 723 (1962).
4. M. L. Wallach and M. A. Kabayama, *J. Polym. Sci. A-1,* **4,** 2667 (1966).
5. C. W. Wilson, *J. Polym. Sci. A,* **1,** 1305 (1963).
6. M. Takayanagi and T. Matsuo, *J. Macromol. Sci.-Phys.*, **B1,** 407 (1967).

7. D. Sapper, *J. Polym. Sci.*, **43**, 383 (1960).
8. M. Takayanagi and N. Kawasaki, *J. Macromol. Sci.-Phys.*, **B1**, 741 (1967).

Nobuhiro Kawasaki
Tsutomu Hashimoto

Toyo Soda Manufacturing Co., Ltd.
Central Research Laboratory
Tonda, Shin-nanyo-shi, Yamaguchi-ken,
Japan

Received January 26, 1971
Revised April 26, 1971

Effects of a Static Electric Field upon Dielectric Properties of Poly-ε-caprolactam

Introduction

In the preceding paper[1] we reported that a drastic decrease of ϵ' and ϵ'', the real and imaginary parts of the complex dielectric constant at lower frequencies, results when a static electric field is applied to poly(vinylidene fluoride) and poly(vinyl fluoride). This has made it possible to measure unambiguously the highest temperature relaxation. This method was applied to poly-ε-caprolactam.

Polyamides give anomalously large values of ϵ' and ϵ'' in the low-frequency region at high temperatures. This phenomenon has been studied by many authors. Yager and Baker[2] ascribed the conduction and the low-frequency dielectric loss to amide protons in the amide linkage. McCall and Anderson[3] observed that the dc conductivity was greatly reduced if the amide hydrogens were replaced by methyl groups and gave experimental support to the view that amide protons act as current carriers. From the pressure dependence of dc conductivity, Saito[4] concluded that the conduction process is ionic.

On the other hand, Eley and Spivey[5] suggested that above the glass temperature, protonic charge carriers are generated by self-ionization of the amide group, while below the glass temperature the conduction arises from electrons. Seanor[6] also suggested that at temperatures above 120°C the conduction in nylon 66 involves transport of both protons and electrons, whereas at lower temperatures it is electronic, and further, on the basis of measurements of the volume of gas evolved, that the proton carriers are amide protons. Baird et al.[7] concluded that the main cause of low frequency dielectric relaxation could well be electrons, because the dc conductivities of polyamides with amide protons and polyamides without amide protons did not differ greatly. This result cast doubt on the view of the amide protons as coming from hydrogen bonds. Further, the role of electrons in very low frequency region also was unclear.

The change of dielectric behavior of poly-ε-caprolactam caused by the application of a static electric field led us to the conclusion that the dielectric behavior at low frequencies is mainly due to impurity ions; that is, protons and hydroxyl ions from bound water.

Experimental

Poly-ε-caprolactam supplied by Unitika Co. Ltd. was used. The average molecular weight was 17,000, as measured by the viscosity method. Specimens for dielectric measurement were prepared by molding. Their thickness and density were 0.2 mm and 1.183 g/cm^3. By means of a differential scanning calorimeter, the melting point and the glass transition temperature were determined to be about 210°C and 75°C, respectively. After the specimen had been kept at room temperature at a pressure of 10^{-2} mm Hg for three days, the surfaces of the specimen were sputtered with silver or gold to form electrodes. Dielectric measurements were carried out by the mutual inductance bridge, which accommodates three terminal electrodes.[8] In order to avoid the effect of humidity, the specimen was placed in a sealed cell. The design of the cell has been described elsewhere[9] in detail. After a static electric field had been applied to a specimen at constant temperature for a certain period, the field was removed and dielectric measurements were carried out without delay. The change of dielectric properties on drying at 156°C and 10^{-2} mm Hg was also measured.

Results

When a static field was applied to a specimen, a drastic decrease of ϵ' and ϵ'' occurred. The decrease was more significant at lower frequencies, as is the case with poly(vinylidene fluoride).[1]

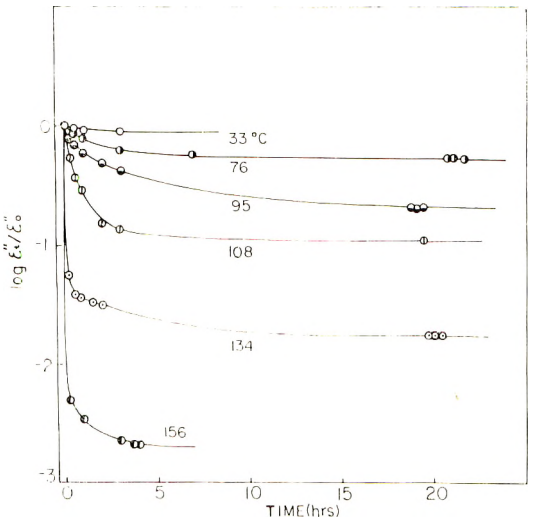

Fig. 1. Change of ϵ'' at 1 kHz with time; applied static field 12 kV/cm, silver electrodes.

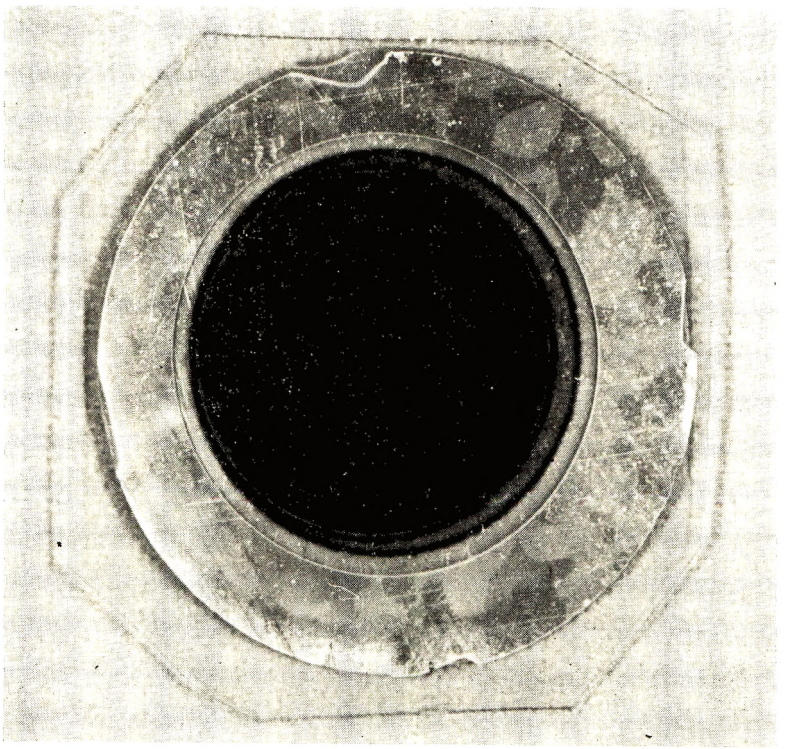

Fig. 2. Photograph of silver electrode surface after a static field of 28 kV/cm had been applied at 156°C for two days.

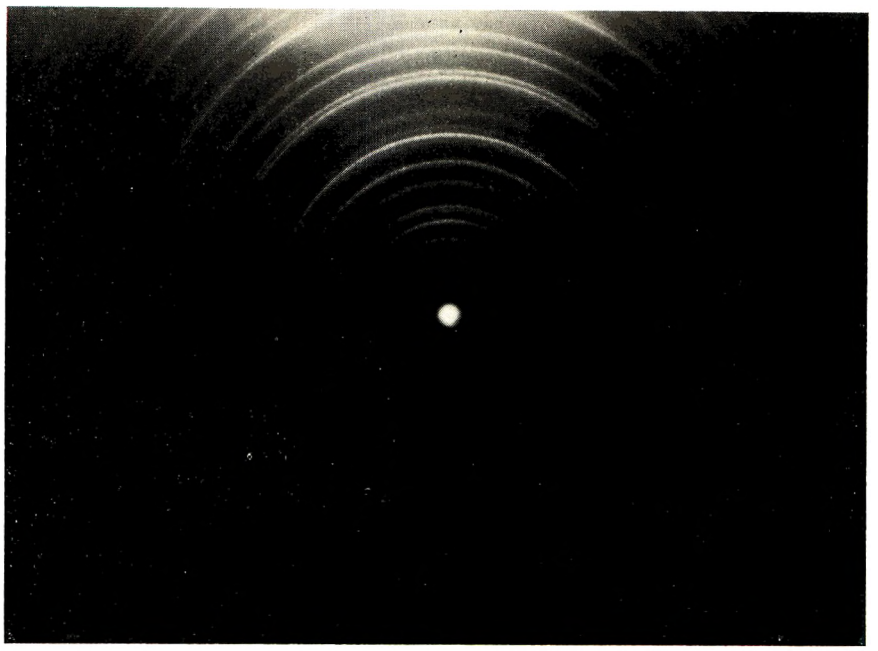

Fig. 3. Electron diffraction pattern from the blackened electrode surface shown in Figure 2.

The change of ϵ'' with time at a fixed frequency is shown in Figure 1 for a specimen with silver electrodes. The change of ϵ' with time was similar. The change was more rapid at higher temperatures. Above the glass transition temperature, the decrease of ϵ'' was especially rapid. When the value of ϵ'' reached an asymptotic value, the specimen was taken out of the cell. The color of the guarded electrode was found to have changed. While the change was hardly observable below 76°C, the silver darkened slightly at 95°C; and, as is shown in Figure 2, the guarded electrode became black at 156°C. The guard electrode and the unguarded electrode remained unchanged in appearance.

In the application of the static field, the polarity of the guarded electrode was positive. Therefore, the change of the color can be interpreted as follows. The bound water, which cannot be removed by heating under vacuum, is electrolyzed by the static field and oxygen generated at the positive electrode causes oxidation of the silver. If this assumption is correct, hydrogen, instead of oxygen, will be generated,[4] and the silver oxide will be reduced to silver when the applied field is reversed. In fact, the black surface did revert to its original color on reversal of the polarity.

The identification of silver oxide was carried out by electron diffraction. Since silver oxide is not a conductor, electrons accumulate and a diffraction pattern cannot be obtained in the usual way. We adopted the following procedure to overcome this difficulty. After gold was sputtered on the surface of the specimens, silver was sputtered on the gold layer. The gold layer remains conductive, even if the silver layer is oxidized. Such a device eliminated the difficulty. The electron diffraction pattern of the blackened layer is shown in Figure 3. The pattern is that of silver oxide.

On the basis of the above results, it was decided to sputter gold rather than silver on the surfaces of a specimen to form electrodes. While the specimen with gold electrodes was dried at 156°C and 10^{-2} mm Hg in the cell, the changes in ϵ' and ϵ'' were measured, as shown in Figure 4. The decrease of ϵ' or ϵ'' is not due to crystallization but to drying,

since the specimen had been previously annealed at 156°C for a few days. Then the effect of the static field was studied. After the field was applied and the value of ϵ' or ϵ'' reached an asymptotic value, the field was removed and the specimen was kept at the same temperature. However, ϵ' or ϵ'' did not recover to the original value, as is shown in Figure 4. This behavior suggests electrolysis of the bound water due to the ionic conduction. It is, therefore, concluded that the anomalously large values of ϵ' and ϵ'' at lower frequencies are mainly ascribable to protons and hydroxyl ions from bound water.

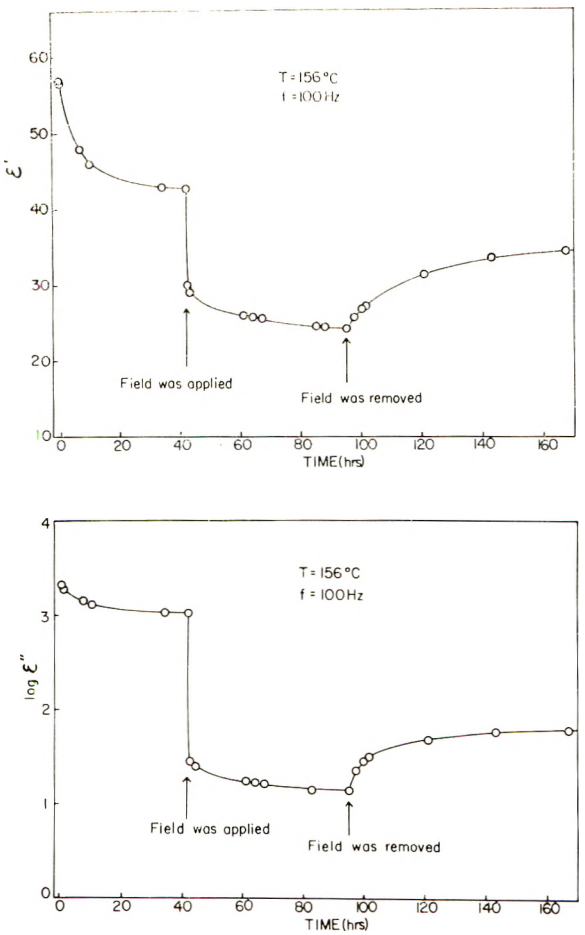

Fig. 4. Change of ϵ' and ϵ'' at 100 Hz with time. The specimen was dried at 156°C under a vacuum of 10^{-2} mm Hg for 42 hr before application of static field of 28 kV/cm for 53 hr; gold electrodes.

Application of 25 kV/cm at 156°C for three days revealed the dielectric absorption, as is shown in Figure 5. By comparison with viscoelastic measurements on poly-ε-caprolactam carried out by Takayanagi,[10] this dielectric absorption was assigned to the α_a absorption due to the segmental motion in the amorphous region. These results indicate that bound water in solid polymers, which cannot be taken out by heating under vacuum, can be removed by applying a dc field.

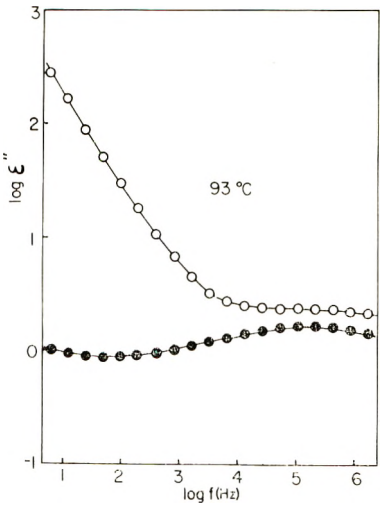

Fig 5. Effect of static electric field upon the frequency dependence of ϵ' and ϵ'' of poly(ε-caprolactam) at 93°C (○) before and (●) after application of 28 kV/cm static field at 156°C for three days; gold electrodes.

We wish to thank Dr. R. Oshima for the electron diffraction pattern. We are also indebted to Prof. S. Seki for the use of the DSC apparatus and to Mr. K. Hazama of Unitika Co. Ltd. for supplying the polymer.

References

1. S. Osaki, S. Uemura, and Y. Ishida, *J. Polym. Sci., A-2*, **9**, 585 (1971).
2. W. A. Yager and W. O. Baker, *J. Amer. Chem. Soc.*, **64**, 2171 (1942).
3. D. W. McCall and E. W. Anderson, *J. Chem. Phys.*, **32**, 237 (1960).
4. S. Saito, *Repts. Progr. Polym. Phys. Japan*, **12**, 411 (1969).
5. D. D. Eley and D. I. Spivey, *Trans. Faraday Soc.*, **57**, 2280 (1961).
6. D. A. Seanor, *J. Polym. Sci. A-2*, **6**, 463 (1968).
7. M. E. Baird, G. T. Goldsworth, and C. J. Creasey, *J. Polym. Sci. B*, **6**, 737 (1968).
8. R. H. Cole and P. M. Gross Jr., *Rev. Sci. Instr.*, **20**, 252 (1949).
9. Y. Ishida, M. Yoshino, M. Takayanagi, and F. Irie, *J. Appl. Polym. Sci.*, **2**, 227 (1959).
10. M. Takayanagi, *Mem. Fac. Eng. Kyushu Univ.*, **23**, 1 (1963).

Shigeyoshi Osaki
Shinsaku Uemura
Yōichi Ishida

Department of Polymer Science
Faculty of Science
Osaka University
Toyonaka, Osaka, Japan 560

Received January 26, 1971
Revised May 10, 1971

Small-Angle Light Scattering by an Anisotropic Cylinder

From the linearity of Maxwell's equations, a linear dependence can be derived for the components of a scattered electromagnetic field on those of the incident field. Let us introduce a system of coordinates in which the components of the incident and scattered radiation are defined in such a manner that the plane ZY is taken as the (Fig. 1) plane containing both incident and scattered beams (the scattering plane). The scattering particle is located at the origin 0 of the coordinate system. Hence for the Mueller matrix $\mathbf{F}$, which linearly transforms the Stokes parameters of incident and scattered radiation, $\mathbf{S}$ and $\mathbf{S}'$, we can write[1]

$$\mathbf{S}' = \mathbf{F}\mathbf{S} \tag{1}$$

Stokes parameters for incident and scattered radiation are defined in terms of the components of the electric field, E_l and E_r, as column vectors

$$\mathbf{S} = (I, Q, U, V),$$

$$\mathbf{S}' = (I', Q', U', V')$$

where

$$I = \langle E_l E_l^* + E_r E_r^* \rangle,$$

$$Q = \langle E_l E_l^* - E_r E_r^* \rangle,$$

$$U = \langle E_l E_r^* + E_r E_l^* \rangle,$$

$$V = \langle i(E_l E_r^* - E_r E_l^*) \rangle$$

The angular brackets denote time averages, and, as usual, the asterisk denotes a complex conjugate. The quantities I', Q', U', V' are formed analogously from E'_l and E'_r. In the matrix $\mathbf{F}$ there are 16 coefficients, among which nine relations must exist.[1] To attain a further decrease in the number of coefficients, the symmetry properties of the particle and the Helmholtz reciprocity theorem can be made use of. If we employ the

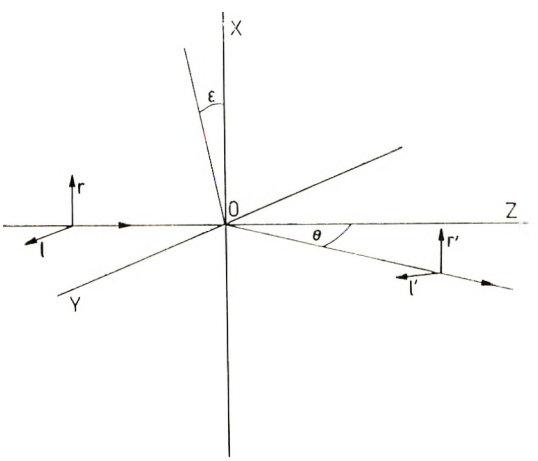

Fig. 1. A pair of unit vectors (r,l) and (r',l'), reflecting the state of polarization of the incident and scattered radiation. The plane YZ is the scattering plane, the angle θ in this plane is the scattering angle. The angle ϵ in the plane XY is the angle formed by the axis of the cylinder and a perpendicular to the scattering plane, i.e., the X axis.

matrix formulation of this principle,[2,3] the final form of the matrix **F** can be written as follows:

$$\mathbf{F} = \begin{bmatrix} (1/2)(M_1 + M_2 + 2M_3) & (1/2)(M_2 - M_1) & S_{23} - S_{31} & -D_{23} + D_{31} \\ (1/2)(M_2 - M_1) & (1/2)(M_1 + M_2 - 2M_3) & S_{23} + S_{31} & -D_{23} - D_{31} \\ -S_{23} + S_{31} & -S_{23} - S_{13} & S_{12} - M_3 & -D_{21} \\ -D_{23} + D_{31} & -D_{23} - D_{31} & D_{21} & S_{12} + M_3 \end{bmatrix} \tag{2}$$

where

$$\begin{aligned} M_k &= A_k A_k^* \\ S_{kj} = S_{jk} &= (1/2)(A_j A_k^* + A_k A_j^*) \\ -D_{kj} = D_{jk} &= (i/2)(A_j A_k^* - A_k A_j^*) \end{aligned} \tag{3}$$

are real numbers obtained from the elements of the 2×2 amplitude matrix **A**. Together, the relations

$$S_{jk}^2 + D_{jk}^2 = M_j M_k \qquad j, k = 1, 2, 3, 4$$

the elements of the matrix **F** yield quantities that can be expressed by means of six constants, in accordance with the formulation of the principle of reciprocity for the amplitude matrix.[1] Thus the form of the matrix representation considerably simplifies the application of the principle of reciprocity, allowing us to reduce substantially the number of coefficients in the Mueller matrix.

Let us start with matrix (2) in the system of coordinates in Figure 1. If the polarizability tensor of the particle under investigation is diagonal in a system of coordinates which arises from the system in Fig. 1 by anticlockwise rotation about the Z axis by an angle ϵ, the matrix **F** is given[1] by

$$\mathbf{F}_\epsilon = \mathbf{R}(-2\epsilon)\mathbf{F}\mathbf{R}(2\epsilon) \tag{4}$$

where $\mathbf{R}(2\epsilon)$ is a matrix for the rotation. If we denote the elements of matrix (2) by a_{jk} and write it in the form

$$\mathbf{F} = \begin{bmatrix} a_{11} & a_{12} & a_{13} & a_{14} \\ a_{12} & a_{22} & a_{23} & a_{24} \\ -a_{13} & -a_{23} & a_{33} & a_{34} \\ a_{14} & a_{24} & -a_{34} & a_{44} \end{bmatrix} \tag{5}$$

we obtain, by substituting into eq. (4), the expression

$$\mathbf{F}_\epsilon = \begin{bmatrix} a_{11} & a_{12}C_2 - a_{13}S_2 & a_{12}S_2 + a_{13}C_2 & a_{14} \\ a_{12}C_2 + a_{13}S_2 & a_{22}C_2^2 + a_{33}S_2^2 & a_{23} + (a_{22} - a_{33})S_2C_2 & a_{24}C_2 - a_{34}S_2 \\ a_{12}S_2 - a_{13}C_2 & -a_{23} + (a_{22} - a_{33})S_2C_2 & a_{22}S_2^2 + a_{33}C_2^2 & a_{24}S_2 + a_{34}C_2 \\ a_{14} & a_{24}C_2 + a_{34}S_2 & a_{24}S_2 - a_{34}C_2 & a_{14} \end{bmatrix} \tag{6}$$

in which

$$\begin{aligned} C_2 &= \cos 2\epsilon \\ S_2 &= \sin 2\epsilon \end{aligned}$$

If the object under investigation is a cylinder having longitudinal polarizability α_l and polarizability α_r in the direction of the radius of the cylinder, that is, a body having rotational symmetry of the ellipsoid of polarizability located in the plane XY and having

the axis of the cylinder forming an angle ϵ with the perpendicular to the scattering plane, then eq. (6) can be simplified by substituting $A_2 = \alpha_l$, $A_1 = \alpha_r$, $A_3 = A_4 = 0$ in eq. (3), and from there in eq. (6), where the corresponding values from eq. (2) have been substituted for a_{ik}. This yields[1] for $\mathbf{F}_\epsilon$

$$\mathbf{F}_\epsilon = p^2 \begin{bmatrix} (1/2)(\alpha_l^2+\alpha_r^2) & (1/2)(\alpha_l^2-\alpha_r^2)\cos 2\epsilon & (1/2)(\alpha_l^2-\alpha_r^2)\sin 2\epsilon & 0 \\ (1/2)(\alpha_l^2-\alpha_r^2)\cos 2\epsilon & (1/2)[\alpha_l^2+\alpha_r^2-(\Delta\alpha)^2\sin^2 2\epsilon] & (1/2)(\Delta\alpha)^2\cos 2\epsilon \sin 2\epsilon & 0 \\ (1/2)(\alpha_l^2-\alpha_r^2)\sin 2\epsilon & (1/2)(\Delta\alpha)^2\cos 2\epsilon\sin 2\epsilon & \alpha_l\alpha_r+(1/2)(\Delta\alpha)^2\sin^2 2\epsilon & 0 \\ 0 & 0 & 0 & \alpha_l\alpha_r \end{bmatrix}, \tag{7}$$

where $p^2 = \kappa F^2(x)E^2(y)$, κ being a constant; $F(x) = (2/x)J_1(x)$, J_1 denoting Bessel's function of the first kind, order 1, and $E(y) = (\pi/2y)^{1/2}J_{1/2}(y)$, $J_{1/2}$ denoting Bessel's function of the first kind, order 1/2. Arguments of the function are

$$x = 2ka \sin (\theta/2)[(1 - \cos^2 (\theta/2)\cos^2 (\gamma - \epsilon)]^{1/2}$$

and

$$y = kl \sin (\theta/2) \cos (\theta/2) \cos (\gamma - \epsilon)$$

where $k = 2\pi/\lambda$, λ is the wavelength of light in the scattering medium, $2a$ is the diameter of the cylinder, and l is its length. The angle γ determines the distribution of the intensity of the scattered light in a plane perpendicular to the primary beam; it is measured clockwise from the perpendicular to the scattering plane if we look in the direction of the incident beam (in the direction of the Z axis). The angle ϵ is in the plane XY, formed by the axis of the cylinder with the perpendicular to the scattering plane; $\Delta\alpha$ denotes the difference $\alpha_l - \alpha_r$; θ is the scattering angle. The relation for the matrix $\mathbf{F}_\epsilon$ in this form holds for small angles of scattering, for which it can be assumed that $\cos\theta = 1$, and also for cylinders fulfilling the conditions of the Rayleigh-Gans approximation.[1] With the aid of eq. (1), in which the matrix $\mathbf{F}$ is determined by eq. (7), it is possible to determine the light scattering by an anisotropic cylinder having an arbitrary orientation of polarizers in the small-angle approximation. The explicit relationships for the components are as follows:

$$\begin{aligned} H_H &= (p^2/2)\{(1/2)(\alpha_l^2 + \alpha_r^2) + (\alpha_l^2 - \alpha_r^2)\cos 2\epsilon + (1/2)[\alpha_l^2 + \alpha_r^2 - (\Delta\alpha)^2 \sin^2 2\epsilon]\} \\ H_V &= (p^2/4)(\alpha_l - \alpha_r)^2 \sin^2 2\epsilon = V_H \\ V_V &= (p^2/2)\{(1/2)(\alpha_l^2 + \alpha_r^2) - (\alpha_l^2 - \alpha_r^2)\cos 2\epsilon + (1/2)[\alpha_l^2 + \alpha_r^2 - (\Delta\alpha)^2 \sin^2 2\epsilon]\} \end{aligned} \tag{8}$$

$$\begin{aligned} H_U &= (p^2/2)[(1/2)(\alpha_l^2 + \alpha_r^2) + (1/2)(\alpha_l^2 - \alpha_r^2)\cos 2\epsilon] \\ V_U &= (p^2/2)[(1/2)(\alpha_l^2 + \alpha_r^2) - (1/2)(\alpha_l^2 - \alpha_r^2)\cos 2\epsilon] \end{aligned}$$

The above relations can be compared with those obtained for the transmission of light through an oriented nylon fiber,[5] since the transmission measurements can be regarded as measurements of the light intensity in angles passing through the input aperture of the photometer used for intensity measurements.[6] In this way, physical content can be assigned to phenomenological coefficients. It may be noted that it is convenient in experiments to place a fiber in a light-scattering experiment so that $\epsilon = 0$. This arrangement gives $V_H = H_V = 0$, $H_H = 2H_U = p^2\alpha_l^2$, and $V_V = 2V_U = p^2\alpha_r^2$.

The results obtained are in agreement with the phenomenological study by Tewarson[5] on the transmission of light through an oriented nylon fiber and allow a quantitative evaluation of small-angle scattering.

References

1. H. C. van de Hulst, *Light Scattering by Small Particles*, Wiley, New York–London, 1957.

2. Z. Sekera, *J. Opt. Soc. Amer.*, **56**, 1732 (1966).

3. S. P. Tewarson and Vachaspati, *Kolloid-Z. Z. Polym.*, **213**, 131 (1966).

4. W. A. Shurcliff, *Polarized Light: Production and Use*, Harvard Univ. Press, Cambridge, Mass., 1962.

5. S. P. Tewarson, *Kolloid-Z. Z. Polym.*, **229**, 132 (1969).

6. S. Clough, M. B. Rhodes, and R. S. Stein, in *The Meaning of Crystallinity in Polymers* (*J. Polym. Sci. C*, **18**), F. P. Price, Ed., Interscience, New York, 1966, p. 1.

Jaroslav Holoubek

Institute of Macromolecular Chemistry
Czechoslovak Academy of Sciences
Prague 6, Czechoslovakia

Received December 14, 1970
Revised April 5, 1971

INFORMATION FOR CONTRIBUTORS

This *Journal* Does Not Carry a Page Charge for Contributions

1. Manuscripts should be submitted to H. Mark, Polytechnic Institute of Brooklyn, 333 Jay Street, Brooklyn, New York 11201, or for Part A-1 (Polymer Chemistry) to C. G. Overberger, Department of Chemistry, University of Michigan, Ann Arbor, Michigan 48104, or for Part A-2 (Polymer Physics) to T. G. Fox, Mellon Institute, Pittsburgh, Pennsylvania 15213. Address all other correspondence to Periodicals Division, Interscience Publishers, John Wiley & Sons, Inc., 605 Third Avenue, New York, New York 10016.
2. It is the preference of the Editors that papers be published in the English language. However, if the author desires that his paper be published in French or German, it is necessary that a particularly complete and comprehensive English synopsis be furnished.
3. Manuscripts should be submitted in triplicate (one *original*, two carbon copies), typed *double space* throughout and on one side of each sheet only, on a *heavy* grade of paper with margins of at least one inch on all sides.
4. A short synopsis (maximum length 200 words) is required for papers in Parts A-1 and A-2. No synopsis is published for Part B or for "Notes" in Parts A. This synopsis should be carefully prepared, for it is automatically the source of most abstracts. The Synopsis should be a summary of the entire paper; not the conclusions alone.
5. The paper should be reasonably subdivided into sections and, if necessary, subsections. Please refer to any issue of this *Journal* for examples.
6. The references should be numbered consecutively in the order of their appearance and should be complete, including authors' initials and—for unpublished lectures or symposia—the title of the paper, the date, and the name of the sponsoring society. Please compile references on a separate sheet at the end of the manuscript. Abbreviations of journal titles should conform to the practices of *Chemical Abstracts*.
7. Please supply numbers and titles for all tables. All table columns should have an explanatory heading.
8. It is particularly important that all figures be submitted in a form suitable for reproduction. Good glossy photographs are required for halftone reproductions. For line drawings (graphs, etc.), the figures must be drawn clearly with India ink on heavy white paper, Bristol board, drawing linen, or coordinate paper with a very light blue background. The India ink lettering of graphs must be large, clear, and "open" so that letters and numbers do not fill in when reduced for publication. It is the usual practice to submit drawings that are twice the size of the final engravings; the maximum final size of figures for this *Journal* is $4^1/_2 \times 7^1/_2$ inches.
   It is the author's responsibility to obtain written permission to reproduce material which has appeared in another publication.
   If in doubt about the preparation of illustrations suitable for reproduction, please consult the publisher at the address given above in paragraph *1* and ask for a sample drawing.
9. Please supply legends for all figures and compile these on a separate sheet.
10. Authors are cautioned to type—wherever possible—all mathematical and chemical symbols, equations, and formulas. If these must be handwritten, please print clearly and leave ample space above and below for printer's marks; please use only ink. All Greek or unusual symbols should be identified in the margin the first time they are used. Please distinguish in the margins of the manuscript between capital and small letters of the alphabet wherever confusion may arise (e.g., k, K, κ). Please underline with a wavy line all vector quantities. Use fractional exponents to avoid root signs.
    The nomenclature sponsored by the International Union of Chemistry is requested for chemical compounds. Abbreviations should follow the American Chemical Society *Handbook for Authors*. Chemical bonds should be correctly placed, and

double bonds clearly indicated. Valence is to be indicated by superscript plus and minus signs.

11. Authors will receive 50 reprints of their articles without charge. Additional reprints can be ordered and purchased by filling out the form attached to the galley proof. Page proofs will not be supplied.
12. No manuscript will be returned following publication unless a request for return is made when the manuscript is originally submitted.

Manuscripts and illustrations not conforming to the style of the *Journal* will be returned to the author for reworking, thus delaying their appearance.

The *Journal of Polymer Science* publishes results of fundamental research in all areas of high polymer chemistry and physics. The *Journal* is selective in accepting contributions on the basis of merit and originality. It is not intended as a repository for unevaluated data. Preference is given to contributions that offer new or more comprehensive concepts, interpretations, experimental approaches, and results. Part A-1 *Polymer Chemistry* is devoted to studies in general polymer chemistry and physical organic chemistry. Contributions in physics and physical chemistry appear in Part A-2 *Polymer Physics*. Contributions may be submitted as full-length papers or as "Notes." Notes are ordinarily to be considered as complete publications of limited scope.

Three copies of every manuscript are required. They may be submitted directly to the editor: For Part A-1, to C. G. Overberger, Department of Chemistry, University of Michigan, Ann Arbor, Michigan 48104; and for Part A-2, to T. G Fox, Mellon Institute, Pittsburgh, Pennsylvania 15213. Three copies of a short but comprehensive synopsis are required with every paper; no synopsis is needed for notes. Books for review may also be sent to the appropriate editor. Alternatively, manuscripts may be submitted through the Editorial Office, c/o H. Mark, Polytechnic Institute of Brooklyn, 333 Jay Street, Brooklyn, New York 11201. All other correspondence is to be addressed to Periodicals Division, Interscience Publishers, a Division of John Wiley & Sons, Inc., 605 Third Avenue, New York, New York 10016.

Detailed instructions on preparation of manuscripts are given frequently in Parts A-1 and A-2 and may also be obtained from the publisher.

POLYMER SCIENCE AND MATERIALS

Edited by Arthur V. Tobolsky, *Princeton University, and* Herman F. Mark, *Dean Emeritus, Polytechnic Institute of Brooklyn*

A stimulating approach to the fundamentals coupled with clearly written specialized discussions, *Polymer Science and Materials* guides the reader through the science and technology of this increasingly important area of organic and physical chemistry. The editors treat the topics under discussion as aspects of a developing science, stressing the potential for creative research in its various disciplines.

Tentative Contents and Contributors:

Polymer Molecules—*H. Mark* and *A. V. Tobolsky*. Molecular Weight and Molecular Weight Distribution—*S. Siggia* and *H. Mark*. Conformations of Polymer Molecules—*A. Peterlin*. Thermodynamics of Polymer Solutions—*A. V. Tobolsky* and *I. Yannas*. Hydrodynamics of Polymer Solutions and Melts—*A. V. Tobolsky*. Phase Transitions and Vitrification—*A. Bondi* and *A. V. Tobolsky*. The Mesomorphic State: Liquid and Plastic Crystals—*D. B. Dupre, E. T. Samulski,* and *A. V. Tobolsky*. Crystallinity in Polymers—*R. S. Stein* and *A. V. Tobolsky*. Rubber Elasticity—*A. V. Tobolsky*. Viscoelastic Properties of Polymers—*A. V. Tobolsky*. Strength of Polymers—*H. Mark*. Diffusion Through Polymers—*A. F. Stancell*. Science of Rubbers—*A. N. Gent*. The Science of Plastics—*R. D. Deanim*. Science of Fibers—*L. Rebenfeld*. Equilibrium Polymerization—*A. V. Tobolsky*. Index.

1971 150 illus. 432 pages $21.50

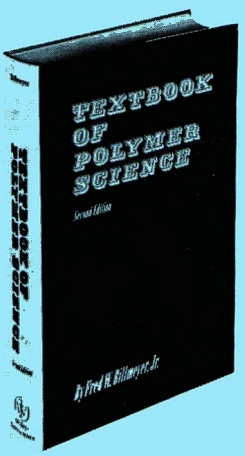

TEXTBOOK OF POLYMER SCIENCE

Second Edition

By Fred W. Billmeyer, Jr.,

Rensselaer Polytechnic Institute

Textbook of Polymer Science was originally published in 1962 to keep pace with the rapid developments in the field. This new **Second Edition** has been completely revised and enlarged to incorporate the latest advances in the theory and practice of all major phases of polymer science, engineering, and technology.

Part I. An introduction to concepts and characteristics of macromolecules, Part I now includes material on solubility parameters, free-volume theories of polymer solution thermodynamics, gel-permeation chromatography, vapor-phase osmometry, and scanning electron microscopy.

Part II. The advances gained from new data on the crystalline nature of polymers are now treated in a thorough discussion of the structure and properties of bulk polymers.

Part III. The format and content of Part III, concerned with polymerization kinetics, have been revised to include recent advances and new references, as well as further data and explanations of recently discovered processes.

Part IV. The material on commercially important polymers has been rearranged, and now includes information on aromatic heterochain, heterocyclic, ladder, and inorganic polymers.

Part V. The comprehensive discussion of polymer processing in Part V now includes many new references for plastics, fiber, and elastomer technology.

1971 152 illus. 598 pages $15.95

WILEY-INTERSCIENCE

a division of JOHN WILEY & SONS, Inc. 605 Third Avenue, New York, New York 10016
In Canada: 22 Worcester Road, Rexdale, Ontario